

**DESIGN OF FIBRE REINFORCED CONCRETE  
SLABS-ON-GRADE AND PAVEMENTS**

*A THESIS*

*SUBMITTED BY*

**SUNITHA K NAYAR**

*for the award of the degree*

*of*

**DOCTOR OF PHILOSOPHY**



**BUILDING TECHNOLOGY AND CONSTRUCTION MANAGEMENT DIVISION  
DEPARTMENT OF CIVIL ENGINEERING  
INDIAN INSTITUTE OF TECHNOLOGY  
CHENNAI 600 036**

**APRIL 2016**

**Dedicated to**  
*Ever Loving Memories of*  
**My Father**

## **THESIS CERTIFICATE**

This is to certify that the thesis entitled “**DESIGN OF FIBRE REINFORCED CONCRETE SLABS-ON-GRADE AND PAVEMENTS**” submitted by **Sunitha K Nayar** to the Indian Institute of Technology Madras for the award of the degree of **Doctor of Philosophy** is a bonafide record of research work carried out by her under my supervision. The contents of this thesis, in full or in parts, have not been submitted to any other Institute or University for the award of any degree or diploma.

Chennai 600 036  
Date:

**Prof. Ravindra Gettu**  
(Research Guide)  
Professor  
Department of Civil Engineering  
Indian Institute of Technology Madras

## **ACKNOWLEDGEMENTS**

I wish to express heartfelt gratitude to my guide Prof. Ravindra Gettu for making the journey of my doctoral thesis research a thoroughly enjoyable one in addition to being productive. I shall be indebted to him for the long hours of patient listening he gave me, however trivial my queries were. His persistence for perfection led me to understand that excellence is a habit and not a virtue. Integrating analytical skills with practical and experimental knowledge is one of his greatest qualities that one can emulate. His profound ability to give easily adoptable solutions to problems, be it analytical or practical, reflecting his deep fundamental knowledge has inspired me immensely. In the various trying situations I have faced, both in academic and personal fronts, during my tenure as a research scholar, he has been my pillar of strength and mentor. I wish to thank him for having let me learn from mistakes and for arousing me from every bout of ignorance and arrogance I had, as a young learner. I thank God almighty for having given me the opportunity to work under his guidance, leading me on a path of self-discovery, by being a part of this high quality research community.

I am thankful to Prof. Manu Santhanam for his encouragement and the various valuable inputs given adding insight on many aspects of my research, in the capacity of my teacher as well as doctoral committee member. I am very grateful to Dr. Radhakrishna Pillai for his relentless support and suggestions that have helped me improve my technical writing skills and presentation skills in addition to the technical inputs given by him. I wish to thank Prof. K Ramamurthy for having given me right directions for the progress of my work as a doctoral committee member. I take this opportunity to thank all other the faculty members of the Building Technology and Construction Management Division, Prof. K Ananthanarayanan, Prof. K N Satyanarayana, Prof. Koshy Varghese, Dr. Ashwin Mahalingam, Dr. Benny Raphael and Dr. Sivakumar Palaniappan for their support and encouragement.

I am extremely grateful to Prof. A Veeraraghavan for his valuable inputs and words of wisdom given to me during various stages of my research. I also thank Dr. J Muralikrishnan for his constant support and encouragement and technical advice for my research.

It gives me immense pleasure in thanking Prof. Surendra P Shah, Distinguished Professor, IIT Madras, and Prof. V S Gopalaratnam, Professor, University of Missouri, Columbia, for their

timely suggestions, during their visits to IIT Madras, which has resulted in throwing open many arenas in my research work.

I extend my sincere thanks to the Head of the Civil Engineering Department, Prof. Meher Prasad and former heads, Prof. S Rajagopal and Prof. S R Gandhi, for all the administrative support extended to me for carrying out this work. I thank my doctoral committee members Dr. Susy Varughese and Dr. M S Sivakumar for their suggestions during different stages of my work.

I gratefully acknowledge the partial financial support through the Women Scientist Scheme A of the Ministry of Science & Technology, Govt. of India (ref. SR/WOS-A/Et-1007/2015 (G)) during the completion of this Ph.D thesis.

I wish to thank Dr. K Srinivas Reddy, Professor, Department of Mechanical Engineering for his valuable suggestions and support to use the laboratory facilities. I acknowledge the support and help given by Dr. Sachin Gunthe, EWRE Division, in planning an experimental programme.

I am deeply indebted to my dear friend Dr. C Jayasree, for leading the way for me to reach the current stature in my life. I will always be thankful for all her support, encouragement and timely advices during different stages of my research.

The support extended to me by the staff of concrete lab has been a key point to the success of my thesis work. I wish to profoundly thank Mrs. Malarvizhi for her help and support. I thank Mr Soundarapandian, Mr. Murthy, Mr. Subramaniam and Mr. Krishnan for their immense help in carrying out the experimental work. I also thank all the support staff of the lab. I wish to acknowledge the help given to me in carrying out the experiments by all the project associates and intern students who have worked with me. A special thanks to Mr Murali and all the staff of the Department Workshop for their help in all fabrication work. I am thankful to the staff of the Civil Engineering Department office, BTCM office and Department Computer facility for their cooperation.

I acknowledge the support of fibre suppliers, A-Fibres, Bekaert Industries India, Nina Concrete Systems, Stewols, Saint Gobain Seva and Owens Corning for having provided the fibres used in this study.

I thank the help of my friends Mr. Ajay Krishnan, Engineering Unit IIT Madras, Mr. Navneet Narayan, Bekaert Industries, and Mr. Sree Krishnan C, L&T, in carrying out this work. All my fellow research scholars, Dr. Dhanya, Pinky, Sujatha, Anitha, Sakthivel, Karmugil, Stefie, Siraj, Muthukumar, Siva, Murugan, Jeevan Jacob, Dr. Geetha, Dr. Elson, Dr. Prakash, Dr. Ganesh and many others, who have been a constant source of encouragement, have helped in making my tenure here a remarkable experience. I thank all of them for having taught me the importance of collaborative work.

I would not have been able to conduct this research work with such ardour if not for the whole hearted support I have received from my family. I thank my mother for having been my support and for taking responsibility of my kids and home, which enabled me to work with free mind. I believe that it is the encouragement and optimism of my husband, Dr. Santhosh, that has made it possible for me to achieve this degree of success and I thank him immensely for it. I wish to specially thank my daughter Mydhili and son Arjun for having put up with my busy schedule. I wish to thank my cousin Devika, my sister and all other family members who have made me what I am today.

Finally, I thank God and my father (Late Mr. V Kesavan Nayar) for all the opportunities and success I have attained in life.



## ABSTRACT

Use of fibre reinforced concrete in applications such as slabs-on-grade and pavements will ensure competency in terms of crack resistance leading to systems with minimum maintenance. In order to enable the adoption of FRC in such applications, it is imperative to develop comprehensive guidelines that address different facets of the slab behavior. The use of appropriate material parameters will result in better optimization of design by translating the enhanced performance of FRC. The current study aims at providing a design methodology for FRC slabs-on-grade and pavements, which incorporates suitable material parameters and include various failure conditions.

The design is based upon inelastic analysis techniques since the presence of fibres impart sufficient rotation capacity to the slabs. The methodologies use a toughness based material parameter, the equivalent flexural strength  $f_{e,150}$ , to quantify the crack resisting potential in the design expressions. Unnotched beam tests and the post-cracking response thus obtained were used for creating a database of flexural toughness and also to study the suitability of fibres for the specified application. The toughness test was performed with various fibres incorporated in concrete as part of this work. The tests and evaluation of toughness parameters have been done as per ASTM 1609, ACI 544 2R and JSCE-SF4. The types of fibres used include steel fibres (hooked-ended and undulated, with various length to depth ratios) and amorphous metallic fibres, in varying dosages. Hybrid mixes with two types of fibres used in the test programme were also tested to investigate a possible synergistic behaviour due to the fibre combination. The results indicate that the performance of concrete with the same dosage of different fibres will vary based on the material, shape and size of fibres. Consequently, arbitrarily specifying a dosage applicable to all fibre brands in design/contractual specifications could be unconservative, and the specification of a minimum required  $f_{e,150}$  should be done. The experience gained from the test programme resulted in a pre-normative guideline for flexural toughness characterization as the applicability of the tests have been verified for FRC with most types of fibres available in Indian market. The test configuration, test procedure and reporting methods are described in the guidelines, which have been the basis for the Indian Concrete

Institute Technical Recommendation ICI TC/01.1 (2014)-Test Method for the Flexural Strength and Flexural Toughness Parameters of Fibre Reinforced Concrete.

The design methodology developed for FRC slabs-on-grade based on inelastic analysis addresses various failure patterns, depending on the dimensions and end conditions of the slab. The design expressions are developed based on the yield line analysis for different types of loads at various positions. The interaction between the subgrade and slab is incorporated in the design using the radius of relative stiffness obtained from the Winkler foundation assumption for the subgrade. The design expressions lead to performance requirements in terms of equivalent flexural strength for a minimum thickness and chosen grade of concrete, by using appropriate limiting moment equation based on the assumed collapse condition. Since the presence of fibres impair crack growth and also impart sufficient rotation capacity, the collapse condition is chosen as the appearance of crack at the top of the slab. The design methodology includes various failure patterns due to loading and integrates stresses due to temperature variation and restraint to shrinkage in the strength requirement while calculating the required equivalent flexural strength.

The design methodology developed for FRC pavements tackles the critical conditions causing pavement failure based on the dimensions of the slab since the design approach depends on the curling characteristics of the slab. Through a dimension check, the governing failure mechanism is categorized into elastic (in cases where the pavements are susceptible to curling, resulting in loss of contact of slab with subbase and fatigue failure) and inelastic. For the failure conditions where inelastic design is suitable, an approach similar to slab-on-grade design is adopted for the limiting moment calculations. However, since pavement failures are more likely to be caused by fatigue, response of the material to repetitive cyclic loading is incorporated in the limiting moment expression by the use of strength reduction factors. The design also includes a fatigue damage-accumulation check, thereby ensuring the required performance of the pavement throughout the design life.

Keywords: Fibre reinforced concrete, flexural toughness, inelastic analysis, fatigue, slabs-on-grade, pavement.

# TABLE OF CONTENTS

<b>ACKNOWLEDGEMENTS</b>	<b>1</b>
<b>ABSTRACT</b>	<b>5</b>
<b>LIST OF TABLES</b>	<b>13</b>
<b>LIST OF FIGURES</b>	<b>17</b>
<b>1 INTRODUCTION</b>	<b>21</b>
1.1 Background	21
1.2 Objectives and scope	22
1.3 Structure of the thesis	24
<b>2 LITERATURE REVIEW</b>	<b>27</b>
2.1 General	27
2.2 Role of fibres with respect to applications of FRC	27
2.3 Types of fibres and their action	28
2.4 Characterization techniques for FRC	29
2.4.1 On flexural toughness testing of FRC	30
2.5 Application of FRC in slabs-on-grade	36
2.5.1 Design challenges for slabs-on-grade	36
2.5.2 Existing approaches in the design of slabs-on-grade	37
2.5.3 Existing design methods for FRC slabs-on-grade	44
2.5.4 Numerical methods for design of FRC slabs-on-grade	48
2.6 Pavement design	50
2.6.1 Existing design methods for rigid pavements	50

2.6.2	Existing design methods for FRC pavements .....	53
2.6.3	Fatigue modeling .....	54
2.6.4	Fatigue models for plain and fibre reinforced concrete .....	55
2.7	Summary .....	59
<b>3</b>	<b>EXPERIMENTAL PROGRAMME .....</b>	<b>61</b>
3.1	Introduction .....	61
3.2	Flexural toughness test setup and test procedure .....	61
3.2.1	Deflection measurement .....	61
3.2.2	Test control parameters.....	64
3.3	Materials used .....	65
3.3.1	Cement .....	65
3.3.2	Fly ash.....	66
3.3.3	Fine aggregates .....	67
3.3.4	Coarse aggregates .....	67
3.3.5	Fibres.....	68
3.3.6	Superplasticizer.....	69
3.4	Mix proportions.....	69
3.5	Preparation of specimens .....	70
3.6	Summary .....	71
<b>4</b>	<b>CHARACTERIZATION OF CONCRETES WITH CONVENTIONAL FIBRES .....</b>	<b>73</b>
4.1	Introduction .....	73
4.2	Steel fibre details .....	74
4.3	Results and discussions .....	74
4.3.1	Fresh properties.....	74

4.3.2	Compressive strength.....	75
4.3.3	Flexural behaviour .....	77
4.3.4	Determination of the flexural toughness parameters .....	79
4.3.5	Implications of the variations in the toughness parameters for design.....	83
4.4	Guidelines for flexural toughness characterization.....	86
4.5	Characterization of FRC with glass fibres as per the suggested testing guidelines .....	87
4.5.1	Fresh properties.....	88
4.5.2	Compressive strength.....	88
4.5.3	Flexural behavior .....	88
4.5.4	Flexural toughness evaluation.....	89
4.6	Summary .....	91
<b>5</b>	<b>CHARACTERIZATION OF CONCRETES WITH HYBRID COMBINATION OF AMORPHOUS METALLIC AND STEEL FIBRES .....</b>	<b>95</b>
5.1	Introduction .....	95
5.2	Amorphous metallic fibres .....	96
5.3	Experimental programme.....	98
5.4	Results and discussions .....	99
5.5	Synergistic behaviour and its implications.....	104
5.6	Summary .....	108
<b>6</b>	<b>DESIGN METHODOLOGY FOR FIBRE REINFORCED CONCRETE SLABS-ON-GRADE .....</b>	<b>109</b>
6.1	Introduction .....	109
6.2	Critical factors to be considered in design of slabs-on-grade .....	109

6.2.1	External actions (wheel loads, rack loadings, line loads, etc.) .....	109
6.2.2	Thermal and shrinkage stresses .....	110
6.2.3	Fatigue stresses .....	110
6.2.4	Impact loading .....	111
6.3	Limitations of existing approaches to the design of FRC slabs-on-grade.....	111
6.4	Design philosophy.....	112
6.4.1	Failure pattern .....	112
6.5	Considerations for the choice of joint spacing and slab dimensions.....	115
6.6	Moment capacity based on equivalent flexural strength.....	116
6.6.1	Limiting moment capacity estimate.....	116
6.6.2	Using equivalent flexural strength instead of the equivalent flexural strength ratio.....	116
6.6.3	Justification for deflection limit of $l_s/150$ .....	118
6.6.4	Design equations.....	122
6.6.5	Summary of the design expressions.....	127
6.7	Validation of design equations in terms of load-carrying capacity.....	132
6.8	Design for thermal stresses .....	135
6.9	Design for shrinkage stresses .....	136
6.10	Design check .....	137
6.11	Parametric study for the suggested method.....	138
6.11.1	Parametric study 1 – Influence of load magnitude on the design solutions.....	138
6.11.2	Parametric study 2 – Influence of thickness of slab on the design solutions.....	139
6.11.3	Parametric study 3 - Influence of the material parameters on the design.....	141
6.12	Design example.....	145
6.13	Comparison of the suggested method with existing design methods. ....	147

6.14	Design framework and summary .....	153
<b>7</b>	<b>DESIGN METHODOLOGY FOR PAVEMENTS .....</b>	<b>161</b>
7.1	Introduction .....	161
7.2	Failure patterns and conditions in rigid pavements.....	161
7.2.1	Case 1: Curling of slab is significant leading to the loss of contact with the subgrade .....	163
7.2.2	Case 2: Curling of the slab is completely neutralized by self-weight and there is no loss of contact with the sub-grade .....	164
7.3	Fatigue based design .....	165
7.4	Proposed design method for FRC pavements .....	166
7.4.1	Determination of fatigue reduction factors .....	167
7.4.2	Thermal stresses.....	168
7.4.3	Shrinkage stress .....	170
7.4.4	Design steps .....	170
7.4.5	Fatigue damage check.....	171
7.5	Design example .....	171
7.6	Parametric study.....	174
7.7	Comparison with existing design methods.....	176
7.8	Design framework .....	179
7.9	Case studies .....	184
7.9.1	Compilation of trial stretches laid in the IIT Madras Campus.....	184
7.9.2	Details of Trial stretch 4 .....	186
7.9.3	Trial stretch 3 .....	189
7.9.4	Trial stretch 5 .....	190
7.9.5	Trial stretch 6-8.....	190

7.9.6	Trial stretch 9 .....	190
7.9.7	Comparison with the design.....	191
7.10	Conclusions .....	193
<b>8</b>	<b>CONCLUSIONS AND SCOPE FOR FUTURE WORK.....</b>	<b>195</b>
8.1	General conclusions .....	195
8.2	Specific conclusions.....	197
8.2.1	Flexural behaviour of FRC with different fibres and fibre combinations .....	197
8.2.2	Inelastic design method for FRC slabs-on-grade.....	198
8.2.3	Design methodology developed for FRC pavements .....	199
8.3	Recommendations for future work.....	200
<b>9</b>	<b>REFERENCES .....</b>	<b>203</b>
	<b>APPENDIX A .....</b>	<b>221</b>
	<b>APPENDIX B .....</b>	<b>231</b>
	<b>APPENDIX C .....</b>	<b>233</b>
	<b>APPENDIX D .....</b>	<b>237</b>
	<b>APPENDIX E .....</b>	<b>261</b>
	<b>PUBLICATIONS BASED ON THE THESIS .....</b>	<b>263</b>

## LIST OF TABLES

Table 2.1 Types of fibres generally used in FRC .....	29
.Table 3.1 Physical properties of PPC (Results obtained in the laboratory).....	65
Table 3.2 Chemical composition of the PPC used.....	66
Table 3.3. Physical properties of Class F fly ash used.....	66
Table 3.4. Chemical composition of fly ash used.....	66
Table 3.5 Physical properties of fine aggregates used.....	67
Table 3.6 Physical properties of coarse aggregates .....	68
Table 3.7 Fibres used for FRC characterization with relevant properties .....	69
Table 3.8 Mix proportions used.....	70
Table 4.1 Details of the type of steel fibres used.....	75
Table 4.2 Fresh properties and compressive strengths of the different FRC mixes with conventional steel fibres .....	76
Table 4.3 Flexural strengths and equivalent flexural strengths of FRC with steel fibres.....	81
Table 4.4 Mean residual strengths .....	83
Table 4.5 Variability in the flexural toughness parameters .....	85
Table 4.6 Details of the glass fibres used (properties as reported by the manufacturer).....	87
Table 4.7 Mix designations and details of various GFRC used including fresh concrete properties and compressive strength (mean±std. deviation).....	87
Table 4.8 Flexural strengths and equivalent flexural strengths of FRC with glass fibres .....	90

Table 4.9 Residual flexural strengths of FRC with glass fibres. ....	90
Table 4.10 Variability in the flexural toughness parameters for glass fibre reinforced concrete. ....	91
Table 5.1 Fibres used and their properties (as given by the manufacturers) .....	96
Table 5.2 .Concrete designation and fibre dosages.....	99
Table 5.3 Fresh concrete properties and compressive strengths (mean $\pm$ std. deviation).....	100
Table 5.4 Flexural toughness parameters (means and coefficients of variation).....	104
Table 5.5 Comparison of toughness parameters obtained from test results and estimated using the rule of mixtures .....	105
Table 6.1. Toughness parameters of FRC having similar area under the load – deflection curve .....	118
Table 6.2 Toughness parameters of mixes having misrepresentation of post-peak capacity .....	118
Table 6.3 Parameters from the tests by Alani et al. (2012).....	121
Table 6.4. Design expressions for each loading case as per the suggested method .....	128
Table 6.5 Parameters from the tests by Belletti et al. (2008).....	132
Table 6.6 Parameters from Shentu et al. (1997) .....	134
Table 6.7 Parameters from the tests of Falkner and Teutsch (1993) .....	135
Table 6.8 Values of constant A to be used in Eqn. 6.32 for various load cases .....	137
Table 6.9 Results of parametric study of suggested method with load as variable .....	139
Table 6.9 Variation of minimum required slab thickness with flexural strength for edge-loading of single point load.....	143

Table 6.10 Variation of minimum required slab thickness with equivalent flexural strength for edge-loading of single point load.....	143
Table 6.12 Details of design trial 1 .....	144
Table 6.13 Details of design trial 2.....	144
Table 6.14 Design input.....	145
Table 6.15 Assumed and derived design parameters.....	146
Table 6.16 Curling stresses due to temperature differential .....	146
Table 6.17 Final design for the case study.....	147
Table 6.18 Details of the design parameters for each method used for numerical comparison .	148
Table 6.19 Parameters used in the design trials for comparison of methods (mean and characteristic values).....	149
Table 6.20 Minimum fibre dosage required for 80 kN tyre load.....	150
Table 6.21 Design parameters for the comparison study of required dosages .....	151
Table 6.22 Design solutions as per each method for case 1 (load 100 kN constant).....	151
Table 6.23 Design solutions as per each method for case 2 (thickness 150 mm constant) .....	152
Table 7.1 Results of the temperature differential testing on model slabs (avg. of two cycles)..	169
Table 7.2 Axle load spectrum .....	172
Table 7.3 Values of X and Y used .....	173
Table 7.4 Fatigue damage analysis for the load spectrum .....	174
Table 7.5 Final design solution.....	174

Table 7.6 Results of the parametric study of the design methodology.....	175
Table 7.7 Material parameters used for the design trial for comparison .....	177
Table 7.8 Details of trial stretches of FRC pavements laid within IIT Madras campus until November 2015.....	185
Table 7.9 Assessment of the design as per the suggested method for trial stretches in IIT Madras .....	192

## LIST OF FIGURES

Figure 2.1 Square panel testing as per EFNARC-EVS-EN 14488-5.....	31
Figure 2.2 Testing configuration for third point loaded unnotched beam .....	33
Figure 2.3 Testing configuration for centre point loaded notched beam .....	33
Figure 2.4 Determination of $T_{e,n}$ .....	35
Figure 2.5 Moment distribution and crack development in concrete ground supported slab during the initial cracking phase .....	40
Figure 2.6 Moment distribution and crack pattern at collapse.....	41
Figure 2.7 Assumed collapse condition .....	43
Figure 2.8 Scheme of the slab-on-grade stiffness assumption.....	44
Figure 2.9 Fatigue models (S-N) for FRC under flexure with steel fibre dosage of 0.5% in comparison with the model for plain concrete suggested in IRC 58:2010 .....	57
Figure 2.10 Comparison of generalised fatigue models (S-N) for FRC with that of a model for plain concrete .....	57
Figure 2.11 Fatigue models (S-N) for FRC under flexural loading on pre-cracked specimens ...	58
Figure 3.1 Flexural toughness test setup.....	62
Figure 3.2 Schematic diagrams of flexural toughness setup.....	63
Figure 3.3 Screen shot of the software interface with the test in progress: (a) stable test; (b) unstable response. ....	65

Figure 3.4 Grain size distribution of fine aggregates.....	67
Figure 3.5 Grain size distributions of 10 mm down and 20 mm down aggregates .....	68
Figure 4.1 Typical load deflection curves for M35 concrete with different types and dosages of steel fibres .....	79
Figure 4.2 Crack pattern after the end of the beam test: (a) larger damaged area in concrete with SFC fibres and (b) single major crack in concrete with SFB fibres .....	80
Figure 4.3 Typical load-deflection curves for M35 concrete with different dosages of glass fibres (a) up to 300 $\mu\text{m}$ deflection (b) up to 2000 $\mu\text{m}$ deflection .....	89
Figure 5.1 XRD spectra of AMF and SF .....	97
Figure 5.2 Fibres as received. ....	98
Figure 5.3 Fibres after 4 weeks of immersion in 3.5 % NaCl solution.....	98
Figure 5.4 Typical curves for the different concretes shown (a) upto 250 $\mu\text{m}$ deflection, and (b) upto 3000 $\mu\text{m}$ deflection. ....	101
Figure 5.5 Typical curves of different mixtures including hybrid mixtures (a) upto 200 $\mu\text{m}$ deflection, and (b) upto 3000 $\mu\text{m}$ deflection.....	102
Figure 5.6 Comparison of fibre contributions to the load deflection behavior for (a)10 $\text{kg}/\text{m}^3$ of AMF and (b) 20 $\text{kg}/\text{m}^3$ of AMF.....	106
Figure 5.7 Estimated curve and band of measured load deflection curves (a) for SF15AMF10 mix (b) for SF15AMF20 mix.....	107
Figure 6.1 D-cracking at the edges .....	113
Figure 6.2 Crack initiation and appearance of radial yield lines .....	114

Figure 6.3 Collapse condition: appearance of radial yield lines .....	114
Figure 6.4 Yield line pattern for slabs-on-grade with free edges .....	114
Figure 6.5 Load deflection curves of FRC with two fibres having comparable areas under curve .....	117
Figure 6.6 Relation between the crack rotation and the slab geometry at collapse .....	119
Figure 6.7 Minimum required thickness for 80 kN load on FRC with four types of steel fibres	140
Figure 6.8 Variation of minimum required dosage of SFB fibre with thickness for different load .....	141
Figure 6.9 Comparison of allowable loads for different slab thickness as calculated using different design methods.....	150
Figure 6.10 Comparison of required dosage for varying thickness .....	152
Figure 6.11 Comparison of required dosages for varying load .....	153
Figure 7.1 Cracking pattern in pavements (a) bottom-up cracking due to downward curling during day time (b) top-down cracking due to upward curling during night time .....	162
Figure 7.2 Formation of transverse yield lines on a slab with low width and high slenderness.	165
Figure 7.3 Fatigue reduction factors from S-N curves .....	168
Figure 7.4 Variation of minimum required thickness with subgrade modulus for slab of M35 grade concrete having different dosages of hooked ended steel fibres.....	176
Figure 7.5 Comparison of design solutions for FRC with 10 kg/m <sup>3</sup> of steel fibres.....	178
Figure 7.6 Comparison of design solutions for FRC with 20 kg/m <sup>3</sup> of steel fibres.....	178

Figure 7.7 Fatigue models for first crack strength used in the three design methods in the comparative study .....	179
Figure 7.8 Prepared surface of the existing pavement to receive the new concrete (a) leveled surface, (b) HDPE sheet on the prepared surface .....	186
Figure 7.9 Concrete being poured and spread on the prepared surface .....	187
Figure 7.10 Screed vibration and manual screeding .....	187
Figure 7.11 Power trowelling of freshly laid concrete surface .....	187
Figure 7.12 Wire brush finishing for final surface texturing .....	188
Figure 7.13 Curing of pavement surface by ponding .....	188
Figure 7.14 Saw cutting of grooves .....	188
Figure 7.15 Crack occurred within 48 hours after casting during the second phase .....	189
Figure 7.16 Trial stretch 3.....	190

# 1 INTRODUCTION

## 1.1 Background

In tune with the current trend in concrete technology to emphasise performance rather than strength alone, fibre reinforced concrete (FRC) is being widely adopted in the Indian construction industry. In terms of performance enhancement, the addition of fibres in concrete imparts pseudo-ductility to an otherwise brittle matrix with the consequent behaviour supporting larger deflections. Though the incorporation of fibres in many applications is restricted to providing supplementary reinforcement, fibres are used as the primary and/or the only reinforcement of concrete, in applications such as in slabs-on-grade and pavements, and in shotcreting of tunnel linings. The effective exploitation of the crack resisting potential of FRC by the inclusion of appropriate material parameters in design methodologies is a necessity for these applications, where relatively lower dosages of fibres may be employed as "stand-alone" reinforcement. Currently, many design guidelines are available for design of FRC slabs-on-grade and pavements, in addition to those provided by manufacturers. However, detailed guidelines that address all critical parameters for the design of FRC slabs-on-grade and pavements are lacking, in spite of useful documents, such as the FHWA Research Report (FHWA- ICT-08-016), Concrete Society Guidelines (TR34) and ACI reports (ACI 360 R) (Roesler et al. 2006, TR 34:2003, 2013, ACI 360R:2010). Taking into account the requirements of flooring and pavement design, it is appropriate to develop techniques for roads/floors that last long with minimum maintenance. This is all the more relevant in India, where there is no national test standard for the fibres or fibre reinforced concrete and no comprehensive national design code for concrete floors.

In this context, the goal of this doctoral work is to develop and propose, for possible preparation of design codes, a comprehensive methodology for the design of FRC pavements/slabs-on-grade incorporating inelastic design techniques and specific material characteristics. The final expected outcome of this thesis is to improve the understanding of the industry about the intricacies of inelastic design as suitable for FRC and to provide a database on relevant material properties of typical FRC mixes used in India.

## 1.2 Objectives and scope

The present thesis has two facets, namely the material characterization and development of design methodology. Based on these two broad perspectives, the specific objectives are:

- To identify significant material parameters of FRC that can be used to formulate the design methodology for slabs-on-grade and pavements
- To characterize typical concretes with different types of fibres available in Indian market and propose a pre-normative guideline for characterization of significant properties of FRC.
- To develop guidelines for the design and construction of FRC slabs-on-grade.
- To develop guidelines for the design and construction of FRC pavements.

The scope of the work is limited to the following components in the experimental study

- Grade of concrete used is M35, with the mix having Class F Fly ash as supplementary cementitious material
- The fibres used in the study include macrofibres of steel and microfibres of amorphous metal.
- The volume fraction of fibres used in the study varies from 0.2 % to 0.6 %.
- The flexural toughness testing has been performed on unnotched prism specimens under four point bending.

The review of the state-of-the-art with regard to mechanical characterization and design of FRC was done. The implication of adopting the fibres and its suitability, as suggested in literature, was assessed and a detailed database of the different test methods and related properties, so as to categorize the material parameters based on applications, was compiled. Since the work aims at developing design guidelines and procedures, a detailed survey of existing standards was carried out to understand the various approaches used in the design of FRC elements. The knowledge base obtained from these reviews was used to shortlist materials (components, target properties), test and design procedures.

Based on the literature, significant material properties for characterizing FRC to suit the intended application were identified as flexural strength and flexural toughness, and a detailed test programme was conducted to obtain these parameters. The programme was also intended to develop a pre-normative guideline for characterization of FRC for the suggested applications.

Based on the review and understanding of the general failure conditions for slabs-on-grade design, strategies for each condition were evolved and relevant inelastic analysis methods were identified. The analytical models from the corresponding methods were suitably modified to incorporate significant material parameters and formulate the design expressions for each load type, load position, end condition and dimensions of the slab. The material database from the experimental programme was used as an input in the design methodology to generate design solutions. In order to validate the developed methodology for slabs-on-grade, the solutions as per the design were compared with results reported in literature, based on either experimental or numerical model studies. The comparison was done in terms of maximum allowable loads in comparison to the collapse loads reported in the literature with same loading conditions and material parameters.

Considering the possible modes of failure of pavements with respect to the types of load, load repetitions and environmental effects, different design strategies have been developed and corresponding solutions suggested. The required fatigue based design models and serviceability checks were devised to be incorporated in pavement design since the expected failure mode is due to fatigue loading. Similar to the slabs-on-grade design, the material database was used as an input in the design method to generate design solutions. For validating the pavement design methodology, a comparison was done with the performance of trial stretches laid within IIT Madras campus with FRC. The adequateness of the design was checked based on the required thickness as per design meeting the current condition of the pavements. Parametric studies for various design variables were also done to understand their influence on the solutions obtained. A comparison of the design solutions as per the suggested methods with those obtained as per existing design procedures was also done to assess the methodologies.

### **1.3 Structure of the thesis**

The research strategy that was followed in order to achieve the objectives specified and the results obtained are described in the following chapters of the thesis.

Chapter 2 has a review of relevant literature in conjunction with the study and the conclusions are categorized based on the various phases of the work. The significant characterization techniques for FRC have been presented with emphasis on flexural toughness testing. A detailed review of the various design strategies existing for concrete slabs-on-grade, followed by the discussion of the inelastic design methodologies for FRC slabs-on-grade, is presented. The later part of the Chapter covers a discussion of design methodologies for rigid and FRC pavement designs. A review of the existing studies of flexural fatigue behaviour of FRC is also presented in the same chapter.

Chapter 3 describes the experimental programme used for the characterization of FRC in the study. After a detailed description of the test setup, and related issues, the chapter has a description of the materials used, mix proportioning and specimen preparation.

Chapter 4 has a detailed discussion of the results of the characterization of FRC with steel fibres. The load-deflection curves lead to specific conclusions regarding the comparative performance of FRC with each type of fibre. The results are presented, followed by a discussion of the influence of fibre type and dosage on the flexural toughness parameters and the variability in the results for various mixes. The chapter also presents the guidelines formulated for flexural toughness testing.

In Chapter 5, the results of the flexural toughness tests on FRC with hybrid combination of amorphous metallic and steel fibres have been presented. The initial part of the chapter has a discussion on the amorphous metallic fibre and its properties. The discussion brings out the advantage of using a hybrid combination in FRC mixes for performance enhancement.

The development of the design methodology for FRC slabs-on-grade using the inelastic analysis by the yield line theory is presented in Chapter 6. The design philosophy is described for various slabs conditions, leading to design expressions and checks required. The chapter also includes the validation of the methodology and a parametric study. The design framework is

summarised, followed by a comparison of the suggested method with existing design methods relevant to the current work.

Chapter 7 details the suggested design methodology for FRC pavements giving emphasis to various possible failure loading combinations. The discussion gives an insight to the difference in approach to be used for pavement design owing to the influence of temperature and fatigue induced stresses. The design framework, parametric study and comparison with existing methods of design are also presented. The chapter closes with a discussion of case studies with a comparison of design solutions as per the suggested method.

The conclusions drawn from the research work are summarized and presented in Chapter 8 including the scope for further research.

In the final section of the thesis, four appendices are presented with data obtained from experimental programme. Appendices A-C consist of load-deflection curves of all the mixes used in the characterization programme. Appendix D has the description and results of tests conducted to determine the temperature differentials on model slabs under various diurnal environmental conditions. Appendix E consists of the equations reproduced from IRC 58:2010, to be used in design calculations of FRC pavements as per the suggested method.



## 2 LITERATURE REVIEW

### 2.1 General

In recent times, there has been a major shift in the demand in the construction industry, from high strength materials to high performance materials. Consequently, concrete, being a heterogeneous material, has been modified in components and proportions to tailor its performance to requirements of various applications. High performance concrete with significant improvements over traditional concrete in terms of strength, durability, ductility, flowability, etc., has been developed by incorporating various ingredients like chemical and mineral admixtures and fibres economically. This study specifically pertains to fibre reinforced concrete (FRC) addressing its mechanical performance and applications.

### 2.2 Role of fibres with respect to applications of FRC

Reinforcing concrete with fibres is an established technique for improving the mechanical performance of cracked concrete. The improvement in performance due to fibre addition to concrete is prominently translated in terms of toughness, crack control, impact resistance and fatigue characteristics of the concrete (Swamy 1992, Balaguru and Shah 1992, Mindess et al. 1994, Gopalaratnam and Gettu 1995, Cachim 1999, Zerbino et al. 2006, Thomas and Ramaswamy 2007, Sivakumar and Santhanam 2007, Dattatreya et al. 2008, Ganesan et al. 2008, Kumar and Prasad 2008). The studies on the use of different types of fibres and hybrid fibre combinations have demonstrated performance enhancement in both plastic and hardened states of concrete (Sivakumar and Santhanam 2007, Ravi and Prakash 2008, Bharathkumar et al. 2008, Jain and Singh 2014, Nayar et al. 2014). It is important to note that fibres are not generally expected to increase the tensile, flexural or compressive strength of the concrete. Nevertheless, experimental studies could show a slight increase in the strength when fibres are added, which can be attributed to the more controlled (i.e., less brittle) nature of failure of the FRC during testing, and other factors related to the casting and testing. Such observations should not be used to decrease the cement content or increase the water content of the concrete used in the structural application under the assumption that the fibres increase the concrete strength.

The applications where fibres are used as supplementary reinforcement are those where the requirements of ductility are significantly high, such as seismic design of beam-column joints (Olariu et al. 1992, Bayasi and Gebman 2002, Abbas et al. 2014, Sharma et al. 2015) or as supplementary shear reinforcement (Narayanan and Darwish 1987, Kwak et al. 2002, Meda et al. 2005, Kim et al. 2012, Jain and Singh 2014, Soltanzadeh et al. 2015). The applications where fibres are used as stand-alone reinforcement are those where the serviceability requirements in terms of crack widths and deflections are less stringent, such as floorings, slabs-on-grade, pavements, tunnel-linings, etc. In the fibre-reinforced concrete (FRC) used in flooring, slabs-on-grade and pavements, the appropriate incorporation of fibres provides adequate post-cracking load-carrying capacity due to stress transfer by the fibres across the crack and the moment redistribution occurring after the first crack, though the first cracking strength itself is not generally enhanced (Beckett 1991, Falkner et al. 1995, Elsaigh et al. 2005, Elsaigh 2007, Altoubat et al. 2008).

### **2.3 Types of fibres and their action**

Incorporating fibres in concrete ensures competence in terms of crack control and associated ductility for an otherwise brittle matrix. From existing studies it is clear that the scale of influence of fibres in the cracking behaviour is twofold; at the material level (before crack localisation) and at the structure level (after crack localisation) (Rossi 1992, Shah et al. 1996). If the fibre action is fully activated at the stage prior to propagation of major cracks, it will result in substantial increase in the tensile strength or peak load, since the fibres delay damage localisation. However, if the action of fibres is restricted to after crack localisation notable improvement in toughness will be obtained since the fibres will cause stress transfer across the crack after the macro-cracks have coalesced (Shah et al. 1996). The former situation mostly arises when the fibres are of lower dimensions (microfibres) and are in sufficient quantity so as to bridge the micro-cracks whereas with the longer fibres (macrofibres) and with lower dosages, the latter condition is encountered. In order to identify the phase of crack propagation where a particular fibre becomes mobilized and manifests its potential, the flexural toughness test maybe used, as it captures the influence of fibres in the matrix since the pre-cracking and post-cracking load deflection behaviour efficiently translates the crack bridging efficiency.

The classification of fibres as micro and macro has been based on fibre diameter: micro, when the diameter of fibres < 0.3 mm and diameter higher than 0.3 mm as macro (EN 14889-2:2006). This classification is purely based on dimensions and does not relate to the performance since a microfiber could also provide significant toughness if used in appropriate quantities (Banthia and Mindess 2012). The fibres also vary in materials and are listed in Table 2.1.

Table 2.1 Types of fibres generally used in FRC

Microfibres	Steel, Polypropylene, Polyester, Poly Acrylic Nitrate, Carbon, Glass, Nylon, Amorphous metal, etc.
Macrofibres	Steel, Polypropylene, Glass, Basalt

Since the fibre composites have variations in magnitude of the significant properties based on the type of fibre, the quantity and the matrix itself, it is important that the selection of fibre for an application is done with caution (Rossi 1992, Nayar et al. 2014). Mechanical characterization suiting the intended application is the most common method of fibre selection (Barragan et al. 2000). In this context, it is essential to characterize (i.e., objectively quantify) the parameters that can represent the post-cracking strength or energy dissipation capacity of FRC so as to be included in the relevant design methodologies (Falkner et al. 1995, TR 34:2003, Elsaigh 2007, ACI 360 R-10, TR 34:2013). Such parameters, classified as toughness parameters, need to be obtained experimentally for the FRC intended to be used in the specific application.

#### 2.4 Characterization techniques for FRC

Toughness parameters have been defined on the basis of tests conducted under compression, direct tension and flexure (Gopalaratnam and Gettu 1995). The stress-strain response under compression reflects the toughening effect of the fibres with a more progressive drop in the post-peak load-carrying capacity, which is more evident in higher strength concretes that have a sharply descending post-peak stress-strain curve. However, toughness is rarely characterized under compression or shear due to the difficulty in obtaining a stable post-peak stress-strain curve and due to the lack of application in normal design formulations (Barragan et al. 2006). There are exceptions that use compression tests of cylinders, such as the Japanese JSCE-SF5 (1984) recommendation and the Spanish Barcelona test (UNE 83515), which has been used for quality control of FRC for tunnel segments (JSCE SF4 Part III 1984, Molins et al. 2009). The characterization of toughness under uniaxial tension is probably most significant since it reflects

the crack bridging effect of the fibres (Wang et al. 1990, Barragan et al. 2000, RILEM TC 162-TDF 2000, Barr et al. 2003, Barragan et al. 2003). However, it is extremely difficult to perform the test due to problems such as the complicated setup needed, the possible failure of the specimen at the grips and the challenges in maintaining stable control just after the peak. It is well established that FRC under shear fails in a more ductile manner due to toughening (Barragan et al. 2000, 2006). However, it is not common to characterize toughness parameters through shear tests due to difficulty in conducting appropriate tests and in correlating them to design problems. Consequently, flexural testing is most widely recommended and favoured for toughness characterization as it is relatively easy to perform and it seems to simulate more realistic conditions of loading, especially in applications such as slabs and tunnel linings (ACI 544.2R-89, Gopalaratanam and Gettu 1995, TR 34:2003, EN 14488-3, ACI 544 2R-2009). Moreover, advances in testing have led to better understanding of the fracture behaviour and effects of specimen size and geometry (Gopalaratnam and Gettu 1995).

#### **2.4.1 On flexural toughness testing of FRC**

Generally, toughness measures under flexure are obtained from the load-deflection curve of the specimen until a specified deflection. The specimen can be a prism, similar to that used widely for determining the modulus of rupture of concrete, a notched prism or a panel (either square or round).

Panel testing for the determination of load-deflection response of FRC is used extensively for shotcrete or sprayed concrete, and is specified in EFNARC 371 FTC and EN 14488-5 (square panel) and ASTM C1550-08 (round panel). This test configuration reflects better the response required in concrete linings to resist point loads (due to anchors or loose rocks). In the EFNARC test, the  $600 \times 600 \times 100$  mm FRC panel is tested under deflection control by applying load over a  $100 \times 100$  mm area at the centre and supporting the slab on a rigid frame spanning  $500 \times 500$  mm as shown in Figure 2.1. The load-deflection curve is obtained up to a deflection of 30 mm and used to obtain an energy-based toughness parameter. More recently, ASTM C1550-08 has specified the testing of centrally-loaded round panels. The panel tests seem to represent better the behavior of FRC structural members due to the biaxial response and the possibility of stress redistribution. Also, the scatter of the toughness values obtained from panel testing is much lower than that of beam tests (Parmentier et al. 2008, Vandewalle et al. 2008). However,

the panel test is not popular for non-shotcrete applications due to practical difficulties in fabrication, loading and in avoiding extraneous deformations.



Figure 2.1 Square panel testing as per EFNARC-EVS-EN 14488-5

The ASTM Standard C 1399 uses the residual strength of a pre-cracked beam. The FRC prism is loaded until crack initiation (i.e., the beam attains a deflection of 0.25 to 0.5 mm) along with a steel plate that prevents the beam from breaking completely even through the testing is done in load control. The plate is subsequently removed after the specimen and the beam is reloaded to obtain residual load-deflection curve. Load values at specified deflections are used to calculate the average residual strength of the beam. Though this standard allows the use of more common testing machines that work with load or piston control, the residual strengths obtained have not yet been correlated with the more conventional toughness parameters or used in design equations (Banthia and Mindess 2004).

Two classes of parameters have been commonly obtained using the flexure test, namely, the flexural strength and the toughness. The flexural strength is generally related to the maximum load or the load at a certain displacement or point in the load-deflection curve that denotes the appearance of the first crack or nonlinearity in the response. The flexural toughness parameters

are generally related to the area under the load-deflection curve or a post-peak load, as seen in standards such as ACI 544-2R, ASTM C 1399, ASTM C 1609, EFNARC 14488, EN 14651, German DBV code, ISO 13270, JSCE-SF4, and RILEM TC 162 recommendations for toughness characterization (Gettu et al. 2000). Though there are similarities in the concepts, test procedures and toughness calculations used, each standard has marked differences in the methodology adopted. The testing configurations often differ in specimen dimensions, loading conditions, rate of loading, position and frequency of deflection measurement, limiting deflection and toughness calculations. It is of concern to note that there is no Indian Standard yet on the testing and toughness characterization of FRC, even though it is urgently needed for design. Therefore, a discussion and comparison of different approaches are presented here, leading to the proposal of a test procedure that seems most appropriate for the Indian context.

As mentioned earlier, the two configurations advocated for the flexural testing of beams are the third-point loading (or four-point bending) and the centre-point loading (or three-point bending) configurations (see Figure 2.2 and 2.3). Most of the current FRC standards (e.g., ASTM 1609) use the unnotched beam under third-point loading due to advantages such as the availability of moulds and test setup (i.e., same as those used for flexural strength or modulus of rupture), and the ability to generally obtain stable tests with relatively inexpensive equipment. Nevertheless, the test may be difficult to control in cases where the concrete strength is high (making the response very brittle) and the fibre efficiency is low. The notched specimen test is gaining acceptance as it is suitable for toughness characterization, as well as more rational analysis with fracture mechanics (Gopalaratnam and Gettu 1995, Jamet et al. 1995, Gettu et al. 1998, RILEM TC 162-TDF 2003, EN 14651 2005). Such tests can be controlled using the crack mouth opening displacement (CMOD) giving reliable test data for practically all types of concrete. Nevertheless, the test configuration, shown in Figure 2.3, requires sophisticated equipment for cutting the notch, for accurately measuring the crack width and for the closed-loop control of the test (Gettu et al. 1996). Moreover, there is some debate on whether there is higher scatter in the data from notched beam tests, in addition to having significantly higher post-peak size effect, than the more conventional four-point bending tests of unnotched specimens (Gettu et al. 1998, Saldivar 1999, Parmentier et al. 2008, Vandewalle et al. 2008, Merretz et al. 2011).

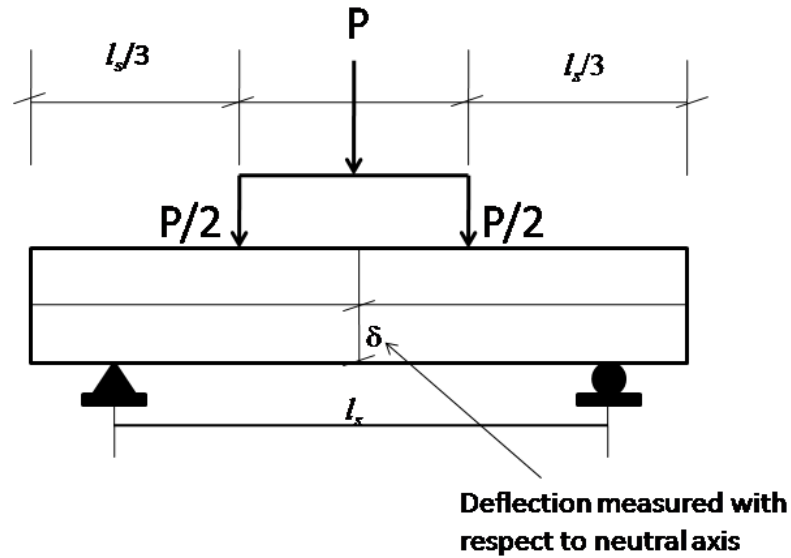


Figure 2.2 Testing configuration for third point loaded unnotched beam

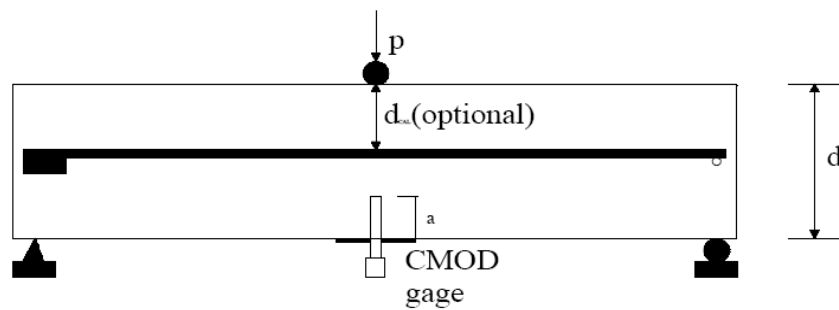


Figure 2.3 Testing configuration for centre point loaded notched beam

The philosophies involved in the definition of toughness parameters based on the load-deflection curve obtained from the unnotched beam test are found to vary among the different recommendations/standards. The toughness parameters that have been dealt with can be put into three categories (Gopalaratanam and Gettu 1995). Firstly, toughness has been defined simply as the area under the load-deflection curve until a certain displacement limit, say 1/300th or 1/150th of the span. Secondly, the area under the curve until a certain limit has been divided by the area under the first crack (signifying normalization with respect to the toughness of plain concrete) to obtain a non-dimensional toughness index (ASTM C 1018, ACI 544-2R). However, this has been largely discontinued due to the ambiguities involved in such definitions (Chen et al. 1994, Trottier and Banthia 1994, Barr et al. 1996, Nataraja et al. 2000, Jain and Singh 2014). Thirdly,

there are sets of strength-based parameters, which are now widely accepted, where the formula for the modulus of rupture based on the simple beam theory is used to obtain equivalent or residual flexural strengths. For the third-point loading configuration of a simply supported beam (see Figure 2.2), the general equation is:

$$f_{x,n} = \frac{P_{x,n} \times l_s}{bd^2} \quad (2.1)$$

where  $l_s$ ,  $b$  and  $d$  are the span, width and depth of the beam, respectively;  $n$  denotes the deflection limit at which the toughness parameter is defined (normally taken as a prescribed deflection, say 3 mm, or multiple of the span, say  $l_s/150$ ); and  $P_{x,n}$  is the load at the deflection limit or the average (equivalent) load up to the deflection limit.  $f_{x,n}$  is designated as the residual or equivalent flexural strength depending on whether the load  $P_{x,n}$  considered in the calculation is the residual load or the average load, respectively. Note that the deflection limit of 3 mm, which is commonly used, seems to have been chosen arbitrarily with no relation to serviceability conditions (Tatnall 2006).

In the case of the equivalent flexural strength  $f_{e,n}$  (ASTM 1609, JSCE SF4, ACI 544), the average load  $P_{e,n}$  is obtained as:

$$P_{e,n} = \frac{T_{e,n}}{\delta_n} \quad (2.2)$$

yielding,

$$f_{e,n} = \frac{P_{e,n} \times l_s}{bd^2} \quad (2.3)$$

where  $T_{e,n}$  is the area under the load deflection curve upto the deflection  $\delta_n = l_s/n$  (as shown in Figure 2.4); normally,  $n = 150$  or  $300$ .

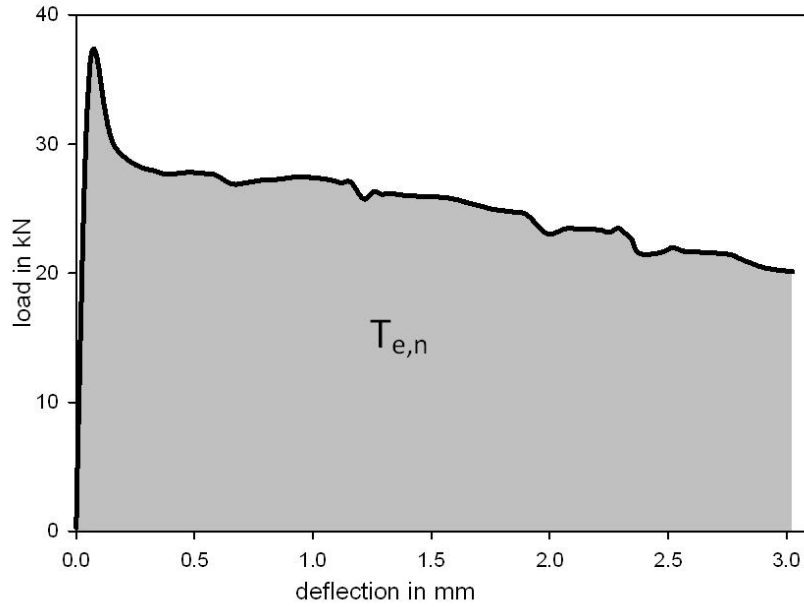


Figure 2.4 Determination of  $T_{e,n}$

There is a non-dimensional strength-based index, namely the equivalent flexural strength ratio, which is used in some design codes and recommendations, given as:

$$R_{e,n} = \frac{150T_{e,n}}{f_{ct}bd^2} \times 100\% \quad \text{or} \quad R_{e,n} = \frac{f_{e,n}}{f_{ct}} \times 100\% \quad (2.4)$$

where,  $f_{ct}$  is the flexural strength of the concrete referring mainly to the value obtained using the first-peak load of the FRC specimen in Equation. 2.1 or the maximum load obtained from testing a plain concrete specimen. The index  $R_{e,n}$  is used in the Concrete Society TR34 guidelines for the design of slabs-on-grade with  $n = 150$  and the test done as per the JSCE SF4 standard. This toughness index can be taken as an estimate of the fraction of the flexural strength retained by the FRC after cracking. However, when this is used as the only FRC parameter in design, the interaction between the fibres and the matrix is ignored due to the implicit assumption that the toughness index will be the same in all the concretes of the same compressive strength grade when a certain dosage and type of fibre are used. This index also becomes unreliable when the fibre incorporation alters the first cracking response of the concrete, i.e., the flexural strength.

## **2.5 Application of FRC in slabs-on-grade**

As discussed in Section 2.2, the performance enhancement of concrete due to the addition of fibres can be most beneficially exploited in applications such as floorings, slabs-on-grade and pavements. However, these systems are complicated to handle in design since the interface interactions and material modelling are critical in obtaining realistic solutions. Design methods have to make approximations at different stages of analysis and design to arrive at optimum solutions, which has been illustrated in further discussions.

### **2.5.1 Design challenges for slabs-on-grade**

Slabs-on-grade can be considered as systems in which the behaviour is dictated by the interaction between the constructed layer, supporting layer and loading. Thus, any analysis technique has to essentially predict the response of the system considering the dependency of these three factors. Based on different models assumed for the material, subbase, interface, load distributions, temperature variation, etc., in the analysis, the accuracy of the response prediction varies. The design methodologies based on each of the analysis philosophies would result in solutions that are optimized differently depending upon the efficiency of the model used to capture the behavior. It is necessary that an analysis takes into account the character of a material in the most advantageous way, so as to obtain the most economical design. This is especially so in applications of pseudo-ductile materials, like fibre reinforced concrete (FRC), due to the softening characteristics and the improved performance characteristics especially in the post cracking regime.

In general, the use of reinforcement in slabs-on-grade is specified for handling thermal and shrinkage stresses, whereas the stresses due to external loading is usually handled in design by providing an adequate thickness of the concrete slab, with the exception of continuously reinforced concrete pavements (Meyerhof 1962, AASHTO 1993, Ringo and Anderson 1996, IRC 58 1998, Huang 2004, Knapton 2005, Delatte 2014). In commonly used design methods, the thickness calculation is based on elastic techniques and the slab thickness is determined for the un-cracked state of concrete. Consequently, the resulting thickness is considerably high for the common loading conditions (Knapton 2005). It is worthwhile to introspect whether the service condition of slab could be extended to a state of allowable cracking for such applications, since

the slab-on-grade may still be suitable as far as serviceability requirements are concerned (Cachim 1999, TR 34: 2003, 2013). For better understanding, a review of the existing analysis and design techniques relevant to slabs-on-grade with emphasis on FRC slabs-on-grade has been done and is presented below.

## **2.5.2 Existing approaches in the design of slabs-on-grade**

### ***2.5.2.1 General assumptions***

Due to the complexity of the actual problem, most of the existing design techniques adopt several assumptions for the slab behaviour. The two common assumptions are that the slab can be considered as either an elastic layer (i.e., the load-response behaviour is governed by linear elastic theory) or as an elastic plate whereby plate bending theory is applicable (Westergaard 1945, Losberg 1961, Meyerhoff 1962). In addition, there are two major approximations for the subgrade or the supporting layer: an elastic solid and a dense liquid (resilient subgrade).

### ***2.5.2.2 Subgrade approximations***

The effect of subbase behaviour on the slab response has been studied extensively and reported. The deflection of the slab is related to the subgrade pressure and, with respect to design, depends upon the subgrade assumption. There are two commonly adopted approximations for the subgrade behaviour as mentioned earlier. In the first approach, the subgrade is simulated by a dense liquid (Winkler foundation), which assumes that the stresses at any point are independent of stresses at other points and are proportional to the degree of depression (Westergaard 1945, Losberg 1961, Meyerhof 1962, Cachim 1999, Elsaigh et al. 2005, Ionides 2006). The soil is characterized by the resilient constant  $k = p_s/w$ , where  $k$  is the modulus of soil reaction, representing the stiffness of the subgrade,  $p_s$  is the soil reaction pressure and  $w$  is the deformation of the soil at a point. The approximation allows the modelling of the subgrade as a series of elastic springs attached to the slab. There have been extensions of the Winkler model to bring in more realistic solutions, such as the Pasternak model that introduces a term to account for shear interaction between the Winkler springs and the soil pressure as  $p_s = kw - G \nabla^2 w$ , where  $G$  is the coefficient representing the shear interactions and  $\nabla$  is the Laplace operator (Ionides 2006).

The second approach is that of an elastic solid, which assumes that the stresses produced by the load at a point are not independent, i.e., the deflection is continuous and extends over infinite area. The subgrade simulated as an elastic solid is, however, more realistic compared to the resilient subgrade assumption since it considers that the subgrade is an elastic, isotropic and homogeneous body of semi-infinite extent (Losberg 1961, Meyerhof 1962, Cachim 1999, Elsaigh et al. 2005). The Boussinesq solution is the most popular model for the elastic solid assumption (Ionnides 2006).

From all the existing solutions, it can be deduced that the design using Winkler approximation and the elastic solid approximation may form the upper and lower bounds of representing the soil-structure interactions. The Pasternak approach lies between these two limit solutions and has been adopted mostly in numerical solutions, like finite element analysis (Ionnides 2006). Since the current study of FRC slabs-on-grade utilizes the reserve ductility of the concrete, an upper-bound solution, such as the Winkler approximation, is considered suitable.

The concept of radius of relative stiffness was introduced by Westergaard in his classical elastic theory for slabs-on-grade, and represents the interaction and influence of the subgrade and slab with respect to the bending behaviour for the resilient subgrade approximation. Practically, the radius of relative stiffness,  $l$ , represents the distance from loading point in the slab to the point of contraflexure in the moment distribution along a yield line for a single point load (TR34 2003), as in Figure 2.5.

In the case of resilient subgrade, the radius of relative stiffness is calculated as

$$l = \left[ \frac{Eh^3}{12(1-\mu^2)k} \right]^{1/4} \quad (2.5)$$

where  $E$  is the modulus of elasticity of concrete,  $\mu$  is the Poisson's ratio of concrete and  $h$  is the thickness of the slab.

### ***2.5.2.3 Elastic methods for slabs-on-grade design***

The earliest works on slabs-on-grade have been based on the Westergaard's analysis, where the slab is approximated as an elastic plate on a resilient subgrade. The basic differential

equation  $D\nabla^2\nabla^2w = q - p$  has been solved for the three different positions of loading, for single wheel load, and the expressions for deflections and stresses have been obtained. Subsequently, these formulae have been modified by Westergaard himself and also by other experts in this area, such as Ionnides and Pickett by modifying the idealizations and approximations to offer more realistic values for stresses and deflections (Yoder and Witczak 1975, Ionnides 2006, Huang 2004). As an example the formulae for an interior loading case as given by Westergaard are shown below:

Interior loading case:

$$\sigma = \frac{0.316P}{h^2} \left[ 4 \log_{10} \left( \frac{l}{b} \right) + 1.069 \right], \text{ where } \begin{cases} b = \sqrt{1.6a^2 + h^2} - 0.675h, \text{ for } a < 1.724h \\ b = a, \text{ for } a \gg h \end{cases} \quad (2.6)$$

and  $a$  is the contact radius of the load.

Similarly, equations have been obtained for deflections and moments under the wheel loads at each of the critical positions. These equations have been widely used in thickness design for rigid concrete pavements and slab-on-grade including the Indian Pavement Design Code, IRC 58. However, it has been observed by many subsequent researchers that the assumption of the concrete slab to be elastic results in the highly conservative estimation of strains and deflections at failure loads, even for plain concrete sections, resulting in highly uneconomical thickness (Meyerhof 1962, Ionnides 2006). Further, the limitation that the concrete has to be un-cracked results in very thick concrete slabs owing to the low tensile strength of concrete (Losberg 1961, Meyerhoff 1962). Moreover, near the failure load, an ultimate strength analysis is considered to result in better estimation of the behavior of the inelastic concrete slab, and consequently more economical designs (Meyerhoff 1962, Ghosh and Dinakaran 1970, Baumann 1983).

#### ***2.5.2.4 Ultimate strength methods for slab-on-grade***

More realistic values for stresses and deflections have been obtained using inelastic theories, as in the rigid-plastic slab on elastic subgrade analysis, where the maximum load is estimated from ultimate strength analysis, which is explained below (Losberg 1961, Meyerhoff 1962, Baumann and Weisberg 1983, Rao and Singh 1986).

The initial stage of moment distribution on a concrete slab on soil due a concentrated load is shown schematically in Figure 2.5. As seen from the diagram, there is initially considerably high moment under the load, which is the maximum positive moment and a more moderate negative wave at a section away from the load. Once the bending stresses below the load become equal to the flexural strength of the concrete, the slab cracks at the bottom and develops radial tensile cracks. Further, the crack opens and extends, during which the maximum positive moment (along the crack) will become equal to the plastic moment capacity of the concrete  $M_p$ . As the sections of the slab between the radial cracks are rotating along the radial yield lines, the negative bending stresses along a circumferential section of the slab become equal to the flexural strength of the concrete and a circumferential crack is formed as shown in Figure 2.6 (Losberg 1961, Meyerhof 1962, TR 34 2003). As discussed earlier, plain concrete slab design using the criterion of no tensile cracking for positive moment results in greater thickness of slab. At the same time it has been theoretically found that the thicker the slab, higher will be the maximum moment (Losberg, 1978). Therefore, an analysis of the slab considering the circumferential cracking as the collapse condition is considered to give better estimates of collapse load and deflections. Throughout the analysis, one significant assumption is that the slab is in continuous contact with the subgrade (Losberg 1961, Meyerhof 1962).

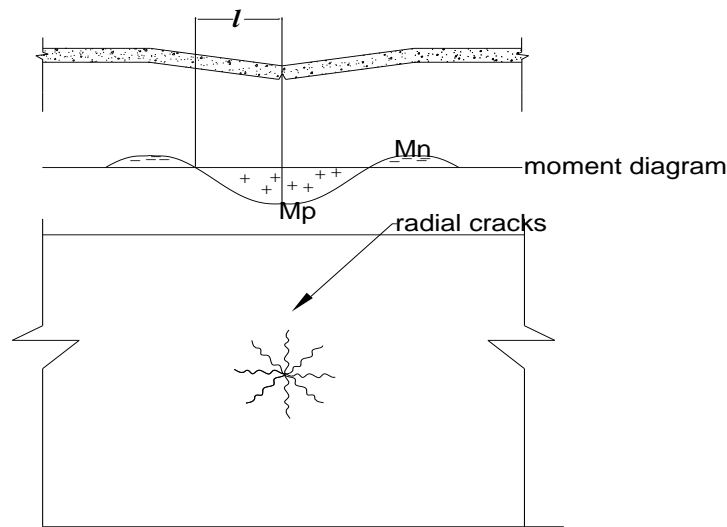


Figure 2.5 Moment distribution and crack development in concrete ground supported slab during the initial cracking phase

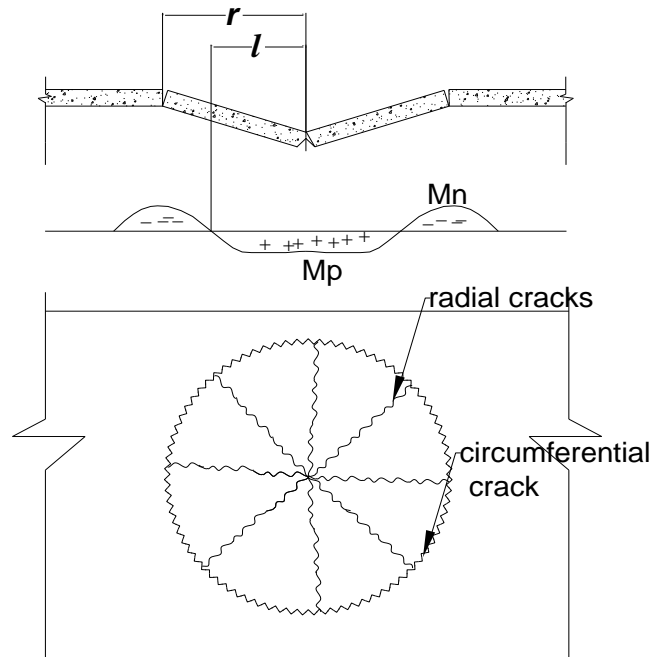


Figure 2.6 Moment distribution and crack pattern at collapse

The analysis assumes the slab to be a thin, rigid, ideally plastic infinite slab of uniform thickness and the moment estimate at collapse is based on yield line analysis. The solutions have been obtained for both unreinforced and reinforced concrete slabs. The design considers that radial yield lines are formed at the bottom of the slab, once the slab cracks, and the plastic moment capacity is imparted by the yield capacity of the reinforcement (for a reinforced concrete slab) (Losberg 1961, Meyerhof 1962, TR34 2003). Subsequently, when the circumferential stresses (as discussed in the earlier paragraph) reach the flexural strength, circumferential yield lines appear. The collapse condition assumed for the design is that of the crack appearing at the top of the slab along these circumferential yield lines. Thus, the negative moment capacity is still the elastic moment carrying capacity of concrete related to the flexural strength of concrete. The solution is obtained using the moment and the shear equilibrium equations. For ultimate load design, using yield-line analysis, which is extensively used in slabs-on-grade applications, the design equations by Meyerhof and Losberg are widely used. In Meyerhof's method, the shear equilibrium equation is simplified in the analysis and the soil pressure is assumed only as a

function of the vertical displacement and is not related to the geometry of the yield section, as opposed to the Losberg's yield line analysis.

In the yield line analysis of Losberg, the author resorts to the elastic theory for soil pressure calculations, as it is dependent on the deformation of the slab and the elastic properties of the soil and cannot be calculated in yield line theory. This is justified as only the loaded portion of the slab is in the plastic stage and this zone is small in comparison to the whole slab, which is considered to be still in the elastic state. Thus, the soil can be assumed to be elastic especially if the slab is relatively thin. Accordingly, soil pressure distribution curves developed based on elastic theories for the infinite elastic slab on elastic subgrade assumption have been used for the calculation of subgrade pressure for the yield line analysis (Losberg 1961), making the shear equilibrium equation more accurate in comparison to the Meyerhof's analysis.

From the collapse condition, the limiting moment of resistance of the slab is calculated as  $M_o = M_n + M_p$  as shown in Figure 2.7. Accordingly, the relationship between the yielding moments for different loading cases is obtained as:

$$\frac{M_n + M_p}{P} = f\left(\frac{c}{l}\right) \quad (2.7)$$

where  $P$  is the load,  $c$  is the load distribution radius and  $l$  is the elastic rigidity radius or radius of relative stiffness.

It is of interest to note here that leading fibre manufacturers, like Bekaert, have developed design software based on the Losberg yield line analysis (DRAMIX DRAPRO) for SFRC slabs-on-grade. This is based on the assumption that the moment redistribution at the ultimate state for SFRC is similar to that of reinforced concrete.

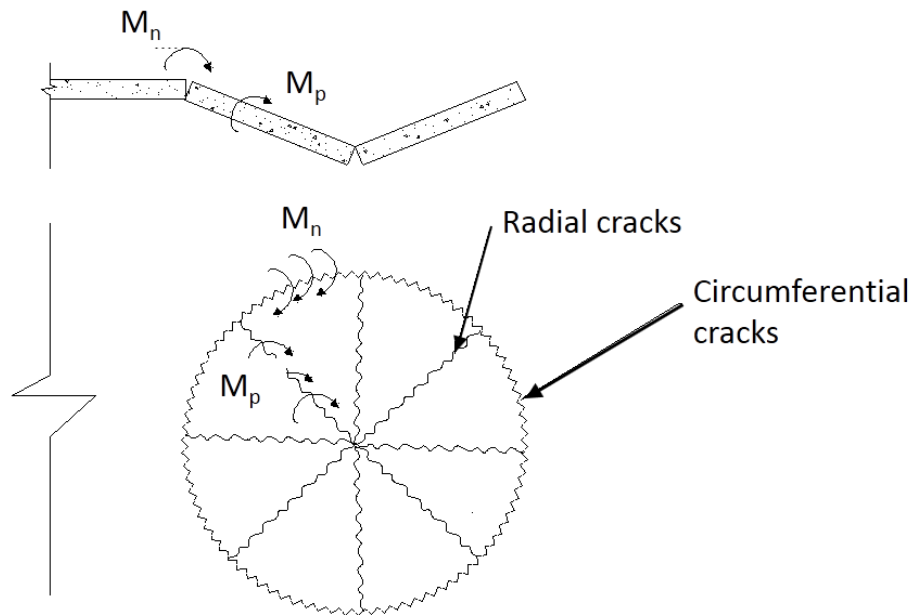


Figure 2.7 Assumed collapse condition

Extensions of the yield line method, like the virtual work method used by Baumann and Weisberg (1983) and the lower bound limit analysis by Rao and Singh (1986), are other approaches available for slab-on-grade design that are less conservative when compared to Losberg's analysis (Baumann and Weisberg 1983, Rao and Singh 1986). Yield-line analysis by the principle of virtual work has been used for the design of FRC slabs-on-grade as the formulations allow the incorporation of different end conditions, which in turn affects the failure pattern (Baumann and Weisberg 1983, Irving 1999, Meda 2003). However, in the virtual work based yield line analysis, prediction of the deflection at collapse is necessary as it forms part of the term accounting for the external work done since the soil pressure is directly proportional to the deflection. This has been often approximated by superposing the effect due to soil alone and due to the slab without support (which is easier to predict) since the stiffness of the two systems can be modeled. The method assumes the total collapse load of the slab supported by the soil to be the sum of the load carrying capacity of the unsupported slab and that of the soil for the same deflection. This has been illustrated in the Figure 2.8 where the collapse load  $P_u$  is obtained as:

$$P_u = P_c + K\Delta \quad (2.8)$$

where  $P_c$  is the collapse load of the unsupported slab,  $K$  is the stiffness of supporting soil. From this relation the  $\Delta$  term is obtained and substituted in the virtual work equation and thereby yield-line solutions are obtained.

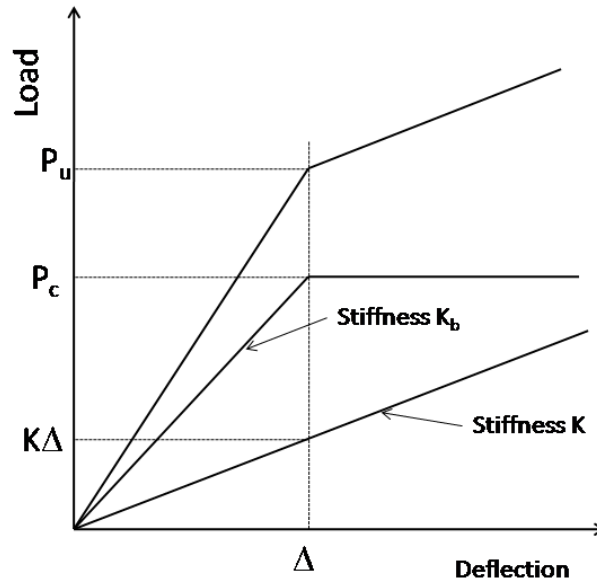


Figure 2.8 Scheme of the slab-on-grade stiffness assumption

### 2.5.3 Existing design methods for FRC slabs-on-grade

As discussed earlier, the majority of the existing design codes and recommendations for fibre reinforced concrete slabs-on-grade/pavements advocate inelastic techniques for static loading design (Westergaard 1945, Baumann and Weisberg 1983, Rao and Singh 1986, Falkner 1995, Elsaigh et al. 2005, Altoubat 2008, Roesler 2008, TR34 2003, 2013). Guidelines for design and construction of FRC slabs-on-grade have been specified by the Concrete Society in 2003 and 2013. In the earlier version of the TR34 (2003) guideline, the design methodology essentially adopts the ultimate load analysis by Meyerhof using the flexural strength ratio  $R_{e,150}$  as the toughness parameter in the material model. The  $R_{e,150}$  value is used to calculate the residual positive bending moment at collapse as:

$$M_p = \frac{f_{ctk,fl}}{\gamma_c} (R_{e,150}) \left[ \frac{h^2}{6} \right] \quad (2.9)$$

and, since the fibres do not affect the (first) cracking stress, the negative moment capacity is obtained as:

$$M_n = \frac{f_{ctk,fl}}{\gamma_c} \left[ \frac{h^2}{6} \right] \quad (2.10)$$

where,  $f_{ctk,fl}$  is the characteristic flexural strength at peak load,  $h$  is the thickness of slab, and  $\gamma_c$  is the partial safety factor. The limit moment of resistance is consequently:

$$M_o = (M_n + M_p) = (1 + R_{e,3}) \frac{f_{ctk,fl}}{\gamma_c} \left[ \frac{h^2}{6} \right] \quad (2.11)$$

The TR-34 2003 design procedure suggests that a dosage and thickness be suitably assumed so as to obtain the design moment (Equation 2.11) to be more than the actual moment due to load. The ACI 360 R also adopts the same method in its design guidelines. In both standards, to obtain the theoretical collapse moment due to applied load, Meyerhof's expressions, as suggested for various cases of loading, are adopted. A value of 1.5 has been suggested for the material safety factor in these guidelines.

However, in the recent revision of Concrete Society Guideline (2013) there has been a major change in the design philosophy, which is now based on the stress-strain model for FRC proposed by RILEM TC 162 TDF. The residual strengths at 0.5 mm ( $f_{r1}$ ) and 3.5 mm ( $f_{r4}$ ), obtained from the notched beam test, are adopted as the material characteristics. The model assumes the tensile stress at tip of the crack ( $\sigma_{r1}$ ) and at the crack face ( $\sigma_{r4}$ ) as functions of  $f_{r1}$  and  $f_{r4}$ , respectively, based on the stress distribution in the cross-section, as proposed in RILEM TC 162 TDF:

$$\sigma_{r1} = 0.45 f_{r1} \quad (2.12)$$

$$\sigma_{r4} = 0.37 f_{r4} \quad (2.13)$$

Using these stress functions, the moment capacity is calculated using the strain compatibility and equilibrium of forces at ultimate limit state. The residual positive moment is obtained as:

$$M_p = \frac{h^2}{\gamma_m} (0.29 \sigma_{r4} + 0.16 \sigma_{r1}) \quad (2.14)$$

whereas the negative moment of resistance from the uncracked moment capacity is obtained as:

$$M_n = \frac{f_{ct} h^2}{\gamma_m 6} \quad (2.15)$$

where  $f_{ct}$  = flexural tensile strength of concrete. The material safety factor  $\gamma_m$  suggested is 1.5.

An alternate approach is to provide the strength required to resist the stress under design load, as in the DBV recommendations, allowing the slab to be in uncracked and cracked states (Gettu et al. 2000, Jansson et al. 2008). In the uncracked state, the stresses are not allowed to exceed the flexural tensile strength of concrete. In the cracked state, the internal forces are calculated considering a reduced stiffness along the crack cross section and full stiffness is assumed between the cracks. The stresses obtained should be lower than the equivalent flexural strength of the SFRC. The design considering the uncracked slab is governed by:

$$K_N \frac{N_u}{A_o} + \frac{M_u}{W_o} \leq cal\beta_{BZ} \quad (2.16)$$

where  $K_N$  is a load factor, taken as 2.0 for tensile force and 1.0 for compressive force,  $N_u$  is the axial force in the ultimate state (due to temperature of shrinkage stresses),  $M_u$  is the bending moment in the ultimate state,  $A_o$  is the cross sectional area of the steel fibre,  $W_o$  is the section modulus of the steel fibre slab and  $cal\beta_{BZ}$  is the flexural tensile strength of the concrete. For design, considering cracked concrete, the energy absorption capacity of SFRC is included in addition to the changed stiffness of the cracked section:

$$K_N \frac{N_u}{A_o} + \frac{M_u}{W_o} \leq nom\beta_{BZ} \quad (2.17)$$

where  $nom\beta_{BZ}$  is the design equivalent flexural strength of SFRC in the post-cracking region calculated from the energy absorption capacity up to  $l_s/150$  mm deflection (Gettu et al. 2000).

Experimental studies on fibre reinforced concrete slabs to understand the effect of usage of fibres, by comparing their performance with plain concrete slabs, have shown that the complete load-deflection behavior can be divided into three regions: (a) corresponding to the elastic deformation, (b) formation of small radial cracks in slab centre finally spreading to slab edge and (c) the redistribution of stresses until the slab fails, resulting in a rapid increase in deflection and ultimate failure either by punching or crushing of the subbase (Falkner 1995). It is understood that the fibres do not have an influence on the first crack load. However, the ultimate failure

loads are found to be higher by up to 30 - 60% and the key parameters governing the ultimate failure loads are found to be the subbase reaction, fibre type and its dosage (Beckett 1991, Falkner 1995, Roesler et al. 2006).

Consequently, the design methodology proposed by Falkner (1995) states that the design is governed by two limit states: the limit state of cracking and the ultimate failure state, and that the enhanced failure load is a function of the equivalent flexural strength ratio of concrete. Accordingly, the ultimate failure load is obtained as a modified form of Westergaard's equation:

$$F_u' = F_R' \left[ 1 + \left( \frac{k}{E_c d^3} \right)^{1/4} W \frac{\sqrt{A}}{d} \right] \left( 1 + \frac{equf_f}{f_f} \right) \quad (2.18)$$

where  $F_u'$  = theoretical failure load (N),  $F_R'$  = theoretical cracking load (N) (obtained from Westergaard's equations),  $E_c$  = Young's modulus of concrete,  $k$  = modulus of subgrade reaction,  $A$  = area of loading plate,  $d$  = slab depth,  $W$  = width of ground slab,  $equf_f$  = equivalent flexural strength of SFRC,  $f_f$  = flexural strength of concrete. The ratio of  $equf_f$  to  $f_f$  is same as the equivalent flexural strength ratio  $R_{e,150}$  as defined in JSCE SF4, ASTM C 1609 and ICI TC/01.1.

Comparative studies of the performance of plain and fibre reinforced concrete slabs have also indicated a relation between the thickness of plain concrete slab ( $h_p$ ) and SFRC slab ( $h_f$ ) as:

$$h_f = \frac{h_p}{\sqrt{(1 + R_{e,150})}} \quad (2.19)$$

Using this equation for the thickness design, a reduction of about 20% in slab thickness was obtained with 30kg/m<sup>3</sup> of fibres by Elsaigh et al. (2005), and was validated through the testing of full scale FRC pavements under in-service traffic loading. A similar approach was adopted previously by the Indian Road Congress in the recommendations for pavement design with SFRC in IRC SP-46 (1994), where the thickness of SFRC slab is given as:

$$h_{sfrc} = h_{pcc} \sqrt{\frac{f_{pcc}}{f_{sfrc}}} \quad (2.20)$$

where  $f_{pcc}$  is the design flexural strength of PCC, and  $f_{sfrc}$  is the design flexural strength of SFRC. It is to be noted that the term "design flexural strength" was not well defined in IRC. If the value of design flexural strength is considered to be:

$$(I+R_{e,150})f_{ct} \quad (2.21)$$

then the expression would be similar to the moment formula by TR 34 (2003) and also the thickness formula by Elsaigh et al. (2005). However, this term can be misleading, as it is well established that the addition of fibres does not normally enhance the flexural strength of concrete. It is to be clearly understood that the enhancement term  $(I+R_{e,150})$  is a consequence of the development of ultimate strength analysis of the slab-on-grade, and is related to the fact that the collapse condition is the first crack appearance at the top. Therefore, the use of the term design flexural strength to correlate the thickness of a plain concrete slab to that of an FRC slab is undesirable.

Similarly, another design technique based on modulus of rupture (MOR) suggests the use of  $R_{e,150}$  as the increment in the MOR value for FRC as

$$MOR' = MOR(I+R_{e,150}) \quad (2.22)$$

where  $MOR'$  is denoted as the effective flexural strength of concrete containing fibres that reflects the increase in the FRC slab flexural capacity over plain concrete. Thereby, the cracking load is obtained as:

$$F_{cr,fibre} = F_{cr,plain}(I+R_{e,150}) \quad (2.23)$$

The comparison of small scale toughness testing results to the large scale slab results for several fibres have been used to validate the effective MOR approaches (Altoubat et al. 2008).

#### **2.5.4 Numerical methods for design of FRC slabs-on-grade**

Numerical modelling and simulation of FRC slabs-on-grade are being studied extensively, taking advantage of advanced material modelling techniques and computing facilities. Such modelling of FRC slabs-on-grade generally incorporates modified constitutive behaviour in available finite element analysis procedures (FEA), which involves inelastic design approaches (Belletti et al. 2001, Belletti et al. 2008, Soranakom et al. 2008, Jafarifar et al. 2009). Most techniques use different constitutive laws for modelling the uncracked and cracked concrete regions, wherein the uncracked section is, in general, governed by the elastic stress conditions. For FRC, the constitutive laws based on strain-softening behaviour are developed using experimentally obtained material characteristics, such as load-CMOD relations, stress-strain curves (under tension and compression) (Barros and Figueiras 2001), are based on non-linear fracture

mechanics approaches (Meda and Plizzari 2004, Belleteri et al. 2008) or are based on classical mechanics using approximate post-peak behaviour models (Soranakom et al. 2008). Material models under tension (such as stress-crack opening curves) are obtained from the experimental load-CMOD curves (under flexure) by using techniques such as inverse analysis or by separate numerical analysis of the post-peak response (Barros 1999, Sousa and Gettu 2006, fib Model Code 2010). The trilinear and the bilinear tension softening models, in terms of stress-crack opening, are widely applied (Barros 1999, Barros and Figueiras 2001, Meda and Plizzari 2004, Sorelli et al. 2006).

In the modelling of FRC slabs, the isoparametric multilayered shell element with the assumption of plane stress condition for each layer is considered most suited (Barros 1999, Barros and Figueiras 2001). The concrete cracking is generally simulated as two stages/phases with separate constitutive models representing the elastic uncracked and cracked sections, as discussed above. The smeared cracked model is more commonly adopted for the FEA (Barros 1999, Barros and Figueiras 2001, Belletti et al. 2001, Belletti et al. 2008). The discrete crack concept has also been used with the slab being modelled using interface elements for the crack and other standard elements, such as 4-node tetrahedral elements, along the elastic domain (Meda and Plizzari 2004, Sorelli et al. 2006). The soil response is generally modelled using one-dimensional linear springs with no-tension assumption to simulate Winkler foundations. The soil stiffness matrix is incorporated in the structural stiffness with the soil load-deflection response generally represented by multilinear models (Barros 1999, Barros and Figueiras 2001, Belletti et al. 2001, 2008, Meda and Plizzari 2004, Sorelli et al. 2006).

The design solutions from numerical analysis have generally been validated by matching them with the experimental results of laboratory scale slabs. The extension of these methods to larger slabs has been debated since most of these models incorporate the subgrade reactions based on the Winkler foundation approach (Barros 1999, Barros and Figueiras 2001, Belletti et al. 2001, 2008, Sorelli et al. 2006, Belletti et al. 2008). Use of one-dimensional spring elements without consideration for the lateral restraint caused on slabs due to the size or the shear interaction between slab and subgrade restricts the solutions to smaller slab design, has been demonstrated from experiments.

## **2.6 Pavement design**

Improving the performance of rigid pavements requires that the material used have sufficient crack resistance, since cracking is the most critical mode of failure. Use of pseudo-ductile concrete with fibres seems to be ideally suited in order to satisfy the performance requirements of the rigid pavement. However, design methods specific to FRC pavements are few and are generally modified forms of plain concrete pavement design (Roesler 2008, IRC SP:46 2013). Another category of design methods use the equations suggested for slabs-on-grade, which is debatable since the general failure patterns of pavements rarely resemble failure in slabs-on-grade (US Army Corps, 2005) and failure is more likely to occur due to fatigue and curling. To understand better the current status of FRC pavement design, a review of the relevant design methods for rigid pavements is presented below leading to the discussion of design strategies specifically for FRC pavements.

### **2.6.1 Existing design methods for rigid pavements**

Rigid pavement design has been mostly based on empirical (PCA 1984, AASHTO 1993) or mechanistic methods (IRC 58:1988), the former being largely dependent upon the field experience of pavement performance. The recent trend has been towards mechanistic-empirical methods that integrate the performance based evaluation with the theoretical models in terms of material and structural behaviour (MEPDG 2004). The mechanistic-empirical approach brings in uncertainty using the reliability concept since the design methodology is guided by the amount of allowable cracking and probability of its occurrence (AASHTO 1993, MEPDG 2004, Roesler 2008).

In general, most design methods adopt elastic models as proposed by Westergaard (that has been discussed in Section 2.5.2.3) for determining stresses in the slab due to applied loads (Westergaard 1945, PCA 1984, IRC 58:1988, Ionnides 2006). Variations and subsequent refinement of these equations have been done but the basic analysis adopted in most of the prevailing design techniques may be attributed to Westergaard's equations though they have been proved to be highly conservative, especially at higher values of load (Losberg 1961, Meyerhof 1962). This may be due to the fact that the pavement system in its full configuration, including the subbase and subgrade behavior, load interactions and interface behavior, has high

amount of uncertainty in modeling and prediction, so resorting to a conservative analysis could be efficient. However, with modern computing facilities and better understanding of material behavior, numerical techniques, such as finite element analysis, have been widely used in pavement design (Cachim 1999, Ionnides 2006).

Curling of the slab due to thermal effects contributes to the pavement behavior two-fold. Due to curling the pavement loses contact with the subgrade and thus the slab behavior is different from the condition with contact. On the other hand, due to the self-weight resisting the curling, the slab experiences flexural stresses that would be a function of the temperature gradient in the slab (Ghosh and Dinakaran 1970, Yoder and Witczak 1975, Choubane 1995, Huang 2004, Pandey 2005). Basically, most design methods resort to reducing the effect due to curling by providing sufficient joints and joint spacing such that the thickness design is still governed by the stresses due to applied loads as curling is a function of the ratio of the width of the slab to the radius of relative stiffness (which is a function of the thickness of the slab) (Delatte 2014). The lower this ratio, less is the curling, and therefore, with proper joint spacing, the effect of curling can be significantly controlled (Ghosh and Dinakaran 1970, Huang 2004).

In addition to the effect of the magnitude of loading, a major contributor to pavement thickness design is the repetition of loads. It is inadequate that a design method addresses only the tyre (static) loading conditions, as it is well established that, in general, the failure of pavements occurs due to fatigue (Huang 2004, MEPDG 2004, Fwa 2006). Failure under fatigue may occur at stress levels much lower than the capacity of the material and is generally the governing factor in design. Fatigue could be both due to external loading or thermal loading. It is understood that a separate serviceability condition under fatigue loading has to be devised for the design to be comprehensive (Cachim 1999). Many design techniques try to address the issue of fatigue loading through the consideration of a dynamic factor converting the cyclic load to an equivalent static load (Dramix Manual 2001, di Prisco and Mauri 2004, TR34 2003, 2013, ACI 360R 2010). However, in the application of FRC to pavements, such an approach seems inadequate since it is not possible to accommodate any benefits in the performance characteristics of the material as the factor is common and not specific with respect to the material.

Since the recent approach in codes and standards for pavement design has been based on performance, damage accumulation based fatigue models have been widely adopted (Roesler et al. 2008, MEPDG 2004, IRC 58 2010). The cumulative fatigue damage (CFD) is calculated and evaluated as per the Palgren-Miner's rule as:

$$CFD = \sum \frac{n_i}{N_i} \quad (2.24)$$

where  $n_i$  is the expected number of repetitions for a load category and  $N_i$  is the allowable number of repetitions on the slab for the particular load level calculated based on the suitable fatigue model. S-N curve based fatigue models are used widely, such as in IRC 58:2010 and the PCA method etc., as given below

$$\text{For } SR \geq 0.55, \log N = 11.737 - 12.077(SR)$$

$$\text{For } 0.45 < SR < 0.55, N = \left[ \frac{4.2577}{SR - 0.435} \right]^{3.268} \quad (2.25)$$

$$\text{and for } SR \leq 0.45, N = \infty$$

where  $SR$  is the stress ratio, which is the ratio of applied stress to the maximum allowable stress. The applied stress is the expected stress in the slab due to external loading determined as per elastic analysis and the maximum allowable stress is the flexural strength of the material.

In the MEPDG design method, the fatigue model that has been developed for ACPA StreetPave has been used in which the pavement fatigue model is based on the field fatigue data. The major change was the inclusion of the probability of failure:

$$\log N = \left[ \frac{-(SR)^{-10.24} \log(1-P)}{0.0112} \right]^{0.217} \quad (2.26)$$

where  $P$  is the probability of failure, and therefore  $(1-P)$  is the probability of survival. For example, if  $P=5\%$ , then there is a 5% chance that the designed pavement fails before the specified number of years. The same model has been further modified and adopted in design proposals for FRC overlays in an FHWA document, as discussed in the next section (HIPERPAVE II).

## 2.6.2 Existing design methods for FRC pavements

In India, the design of FRC pavements is guided by IRC SP:46, which essentially uses the ultimate load design based on the circular yield-line pattern incorporating the equations suggested by Meyerhof for infinite slabs-on-grade (Meyerhof 1962, IRC SP 46:2014). The approach incorporates the post-cracking moment carrying capacity of FRC using the equivalent flexural strength ( $f_{e,nk}$ ). The method requires a fatigue check similar to that of IRC 58: 2010 for plain concrete (PCC) pavements using elastic stress based expressions (same as given in IRC 58:2010) and a modified fatigue model (S-N relation) for various ranges of stress ratios  $SR$  as given below:

$$\begin{aligned} \text{For } SR > 0.627, \log_{10} N &= \frac{0.99 - SR}{0.06189} \\ \text{For } 0.6 < SR < 0.627, N &= \left[ \frac{2.9212}{SR - 0.51} \right] \\ \text{For } SR < 0.6, N &= \infty \end{aligned} \quad (2.27)$$

Major drawback identified in this method is that, while using inelastic design equations, the design assumes the slab to be of infinite dimensions so as to allow the development of the complete circular yield line pattern, which is hardly true as such a pattern can occur only if there is contact of slab with subgrade throughout the loading history, without curling (Meyerhof 1962). The free edge boundary conditions, substantial load transfer at joints, and prevention of uplift of slab are other major factors that are assumed implicitly when the infinite slab assumption is made (Meda 2003). In addition, the fatigue damage analysis using elastic stresses and a typical S-N fatigue model may cause over-conservative design that does not take into account the improvement in the fatigue resistance of concrete due to the incorporation of fibres.

An FHWA report on design of ultra-thin white toppings (UTWT) using FRC proposes a mechanistic-empirical design based on the modified American Concrete Pavement Association (ACPA) design, which essentially utilizes reliability indices as discussed in MEPDG design procedure (Roesler et al. 2008). This allows for a certain amount of cracking in the slab thereby bringing in inelastic behavior of concrete and uses the toughness parameter (equivalent flexural strength ratio) to account for the enhanced post-cracking moment-carrying capacity of FRC. The

fatigue design uses an equation that calculates the allowable number of repetitions for a chosen level of crack, using specific material characteristics, as:

$$\log N = \left[ -\frac{SR^{-10.24} \times \log(R^*)}{0.0112} \right]^{0.217} \quad (2.28)$$

where  $N$  is the allowable number of repetitions,  $SR$  is the stress ratio,  $R^*$  is the effective reliability for an assumed percentage of cracked slabs. The material parameter is brought into the calculation through the stress ratio computation, as:

$$SR = \frac{\sigma_{applied}}{MOR(1 + R_{e,150})} \quad (2.29)$$

where  $\sigma_{applied}$  refers to the calculated stress due to loads, the denominator is denoted as the design flexural strength of FRC, wherein  $MOR$  is the modulus of rupture of the FRC and  $R_{e,150}$  is the equivalent flexural strength ratio. Both material parameters have to be obtained from flexural toughness testing on unnotched FRC specimens as per the Japanese JSCE SF4 or ASTM 1609 standards. One of the major limitations of this method is the use of a factored flexural strength to represent the flexural capacity of FRC. The use of  $(1 + R_{e,150})$  as the strength enhancement factor, can be misleading as has been discussed in Section 2.5.3, since it is well established that the addition of fibres does not normally enhance the flexural strength of concrete, at least for the commonly used fibres and fibre dosages. It has to be emphasized that the increase in moment carrying capacity is not due to an increase in flexural strength but due to the increase in the post-cracking moment carrying capacity of the SFRC slab. Therefore, the use of the term “design flexural strength of SFRC” should be avoided since it is being extended beyond the failure typology considered here.

### 2.6.3 Fatigue modeling

Though extensive studies have been done on fatigue behaviour of both plain and fibre reinforced concrete, the extent of understanding is not very comprehensive in comparison to that of metals. The further discussion deals with the possible application of available results and models to FRC pavement design.

#### **2.6.4 Fatigue models for plain and fibre reinforced concrete**

Various studies have been done on plain and fibre reinforced concrete to obtain the fatigue characteristics, which mostly consist of fatigue life predictions, creep rate etc. Such studies have been done for high or low cycle fatigue but since it is difficult to obtain any conclusive results based on a certain range of loading, the discussion hereafter would include all loading conditions, though only high cycle fatigue is of significance in pavement applications. Both empirical and analytical models are reported in literature for plain and fibre reinforced concrete. The experimentally obtained models have the drawback that the testing methods vary significantly due to the lack of standardized procedures for fatigue testing and so a comparison may not be always appropriate. However, these models are more easily adoptable than the numerical models due to their simplicity.

As mentioned, the lack of standardized procedures has resulted in the evolution of numerous testing configurations. The major differences, as per the existing literature, can be summarized to be in the type of loading, test control parameters (load or displacement), specimen shape and size, loading frequency, loading range, definition of endurance limit and the type of concrete itself (i.e., high strength, normal strength, fibre type and dosage, etc.) (Batson et al. 1972, Reinhardt and Cornelissen 1984, Oh 1991, Johnston and Zemp 1991, Chang and Chai 1995, Wei et al. 1996, Pasakova and Meyer 1997, Naaman and Hammoud 1998, Singh and Kaushik 2003, Singh et al. 2004, Germano and Plizzari 2012).

In spite of the differences, a few definite conclusions regarding the performance of FRC with reference to plain concrete can be drawn:

- The fatigue performance of FRC is better with longer or more slender fibres (i.e., with higher aspect ratio), though a definite relation with the shape of fibres could not be drawn. The improvement in fatigue performance, especially in bending, is related to the fibre volume, with more significance for low cycle loading (Batson et al. 1972, Chang and Chai 1995, Wei et al. 1996, Naaman and Hammoud 1998, Zhang et al. 1999, Lee and Barr 2004).
- The effect of the fibre addition is most significant in the second stage of crack growth during fatigue cracking (Chang and Chai 1995, Lee and Barr 2004).

- The endurance limit of FRC is in the range of 65 - 85 % of the static first-crack strength in comparison to 50 - 60% for plain concrete (with the endurance limit being defined at 2–10 million cycles) (Batson et al. 1972, Johnston and Zemp 1991, Chan and Chai 1995, Wei et al. 1996, Naaman and Hammoud 1998, Cachim 1999, Germano and Plizzari 2012).
- The incorporation of fibres results in substantial increase in deformation (crack opening) at failure reflecting the increase in toughness (Cachim 1999). Consequently, FRC has higher energy dissipation capacity than plain concrete, which is also indicated by the higher residual toughness values (in both uncracked and pre-cracked/notched specimens) (Pasakova and Meyer 1997, Lee and Barr 2004, Germano and Plizzari 2012).
- At higher fibre content and fibre aspect ratio, the stiffness of SFRC under cyclic loading increases (Chang and Chai 1995).

Many fatigue models, in terms of stress ratio – fatigue life (S-N curves), have been proposed for FRC from these experimental investigations and a comparison of these models is given in Figure 2.9, where the model predictions for flexural fatigue of unnotched or non-pre-cracked specimens with fibre volume fraction of 0.5% and the fatigue model used in IRC 58:2010 for plain concrete has been shown for the purpose of comparison. This model has been chosen since it is the most widely used fatigue model in India for plain concrete (PCC) and is comparable to other significant models in literature for plain concrete. A detail overview of the existing studies on fatigue testing is given by Lee and Barr (2004), with a generalized model proposed for fatigue life prediction based on statistical averaging (from the results of fatigue test data available in literature). This is shown along with generalized models of IRC 58:2010 for plain concrete and of IRC SP 46:2014 for FRC in Figure 2.10. From Figure 2.9 and 2.10 it can be understood that the shift of the curves towards the right for the FRC allows more load repetitions for the same stress level in comparison to PCC. Though the comparison is done only with respect to a single model for PCC, similar trends can be seen with respect to other models (Cachim 1999, Lee and Barr 2004, Niranjana 2011).

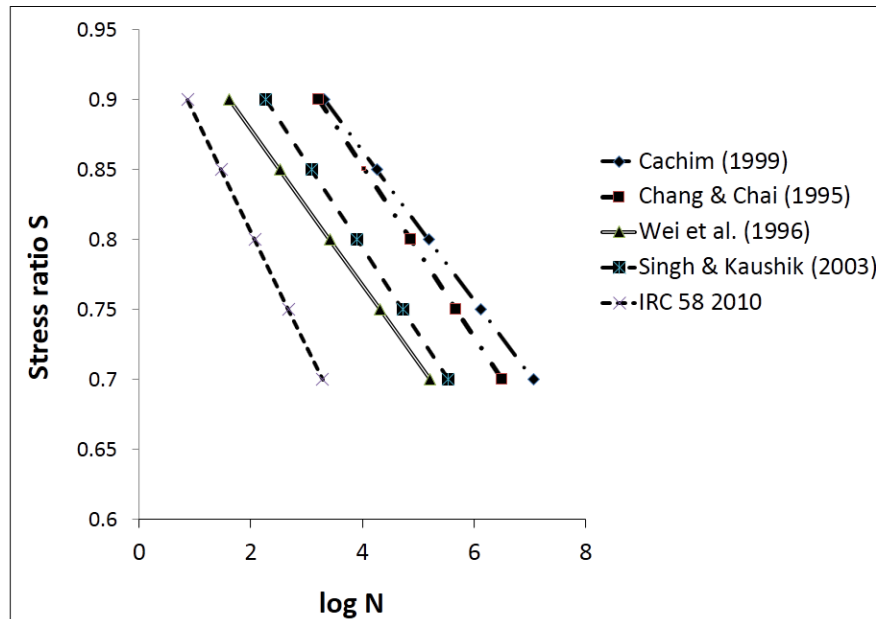


Figure 2.9 Fatigue models (S-N) for FRC under flexure with steel fibre dosage of 0.5% in comparison with the model for plain concrete suggested in IRC 58:2010

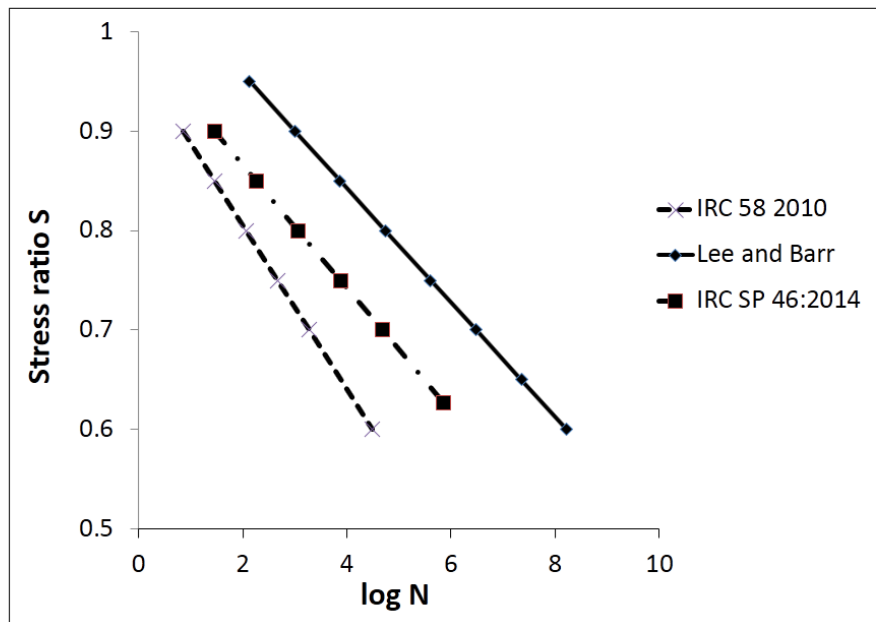


Figure 2.10 Comparison of generalised fatigue models (S-N) for FRC with that of a model for plain concrete

Since the influence of the fibres occurs mainly in the fracture process zone, a study of the effect of load cycling on un-cracked specimens may be insufficient to draw significant conclusions regarding the effect of fatigue loading on the toughness. Therefore, the data from models based on the performance of pre-cracked specimen have been presented in Figure 2.11 (Naaman and Hammoud 1998, Germano and Plizzari 2012). However, the study by Naaman and Hammoud (1998) is on high early strength concrete with higher dosages of fibres (above 1%) resulting in strain hardening type of response and so is not directly comparable to the applications being discussed here. In the tests of Germano and Plizzari (2012), fatigue behaviour corresponds to crack initiation and propagation stages, which are influenced by the toughness of the concrete. It is seen that the IRC SP:46 (2014) model, which is based on the first crack fatigue resistance of FRC, is conservative compared to the model for precracked FRC given by Germano and Plizzari (2012), at higher stress ratios.

Based on the extensive literature review and model comparisons as discussed above, it can be inferred that the addition of fibres results in the enhancement of fatigue life of concrete by about 20–25% in the pre-cracked stage. After cracking, PCC is not expected to have any further life, whereas FRC elements can endure cyclic loading at least at low stress levels for an appreciable number of cycles, due to the toughening mechanism of fibres.

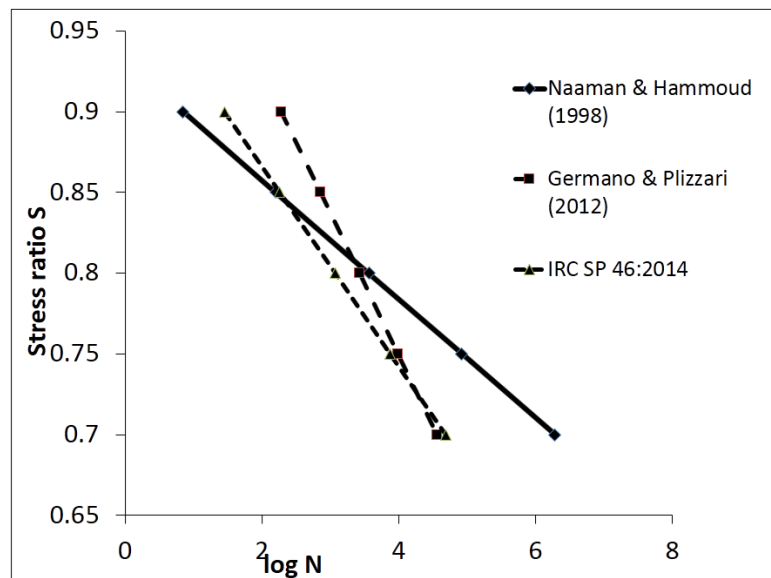


Figure 2.11 Fatigue models (S-N) for FRC under flexural loading on pre-cracked specimens

## **2.7 Summary**

This chapter discussed in detail the existing literature and the current status of characterization, application and design of FRC in the context of slabs-on-grade and pavement design. The discussion in the initial part gives an insight to the toughness characterization methods for FRC, and compares their advantages and disadvantages. The discussion aims at closing in on one particular test method and suitable test parameters for the current applications in India.

The next section discussed the design challenges and existing methodologies for slabs-on-grade. Each of the methods is critically reviewed to understand the limitations of the existing methods. In the later part of the chapter, a similar review of the current design techniques for rigid pavement and FRC pavements has been presented with emphasis on the major differences in the approaches between slab-on-grade and pavements. Since fatigue is considered a significant factor in pavement design, the fatigue response of FRC has been further explored based on the existing models available in literature. Based on a comparison of these models, an appropriate model has been identified for the material capacity evaluation in the design methodology.



## 3 EXPERIMENTAL PROGRAMME

### 3.1 Introduction

A detailed review of the existing methods of characterization for flexural toughness of fibre reinforced concrete was presented in the previous chapter. Based on these discussions it may be pointed out that, the use of the unnotched beam test and the post-cracking response thus obtained for characterizing the FRC is suitable in the present context. Further, it is expected that having a simple test method will motivate the rational choice of fibres, and probably, more efficient use of FRC in India.

Consequent to the need for creating a database and also study the suitability of fibres for the specified application, the flexural toughness test was performed with various fibres incorporated in concrete as part of this work. In this chapter, a detailed description of the experimental programme is presented. The properties of the materials used for the tests are discussed followed by the mix proportioning details.

### 3.2 Flexural toughness test setup and test procedure

The flexural toughness was assessed by the tests performed in a 1 MN closed-loop servo-controlled Controls testing system. Prisms were tested in the simply-supported configuration with a span  $l_s$  of 450 mm and loads applied at the third-points (see Figure 3.1). The test procedure generally conforms to the ICI-TC/01.1, ASTM C 1609, ACI 544-4R and JSCE SF-4 standards.

#### 3.2.1 Deflection measurement

All significant test standards specify the measurement of net deflection at the mid-span of the specimen. In order to avoid the effects of extraneous deformations (such as the local crushing and movement at the supports and loading points) and obtain sufficiently accurate results, the deflection was measured with respect to the specimen itself and with LVDT. The deflection measurement setup used was in accordance with the requirements of ASTM 1609, JSCE-SF4 and ACI 544, and consists of a yoke (or jig) that is clamped to the specimen at mid-height above the supports, as shown in Figure 3.1 and 3.2. The yoke frames were clamped to the specimen

using screw heads that ensure that the supports for the horizontal bar are fixed to the specimen while allowing for horizontal movement of the bar to accommodate the bending of the specimen. The specimen deflection was measured here with two LVDTs (of 10 mm span; accuracy of 0.001 micron) mounted on either side of the specimen, at mid-span, on the horizontal bar of the yoke. The LVDTs were placed in contact with appropriate (S-shaped) brackets glued to the top surface of the specimen. The readings of both the LVDTs were recorded and the average was taken for the calculation of the specimen deflection.



Figure 3.1 Flexural toughness test setup



### 3.2.2 Test control parameters

Most standards specify a deflection rate of 0.025 - 0.075 mm/min (i.e., 0.4 – 1.2  $\mu\text{m/s}$ ) up to the peak load (or first crack) and then a higher rate of about 0.05 to 0.2 mm/min (i.e., 0.8 – 3.3  $\mu\text{m/s}$ ). Here, the tests were performed under load control, at a constant rate of 100 N/s, up to 20% of the estimated peak load, and further under displacement control at the rate of 0.5 – 1.5  $\mu\text{m/s}$ . The switching of the control variable was done to ensure a stable initiation of the test since the small displacements at the beginning may not be significant enough for stable servo-control. In general, the peak load was obtained within 3-5 minutes, and the test was terminated when the deflection exceeds 3 mm (i.e.,  $l_s/150$ ), within 50-60 minutes of initiation. Tests on plain (unreinforced) concrete beams were performed at the displacement rate of 0.5  $\mu\text{m/s}$  since the load drop after the peak was rapid, and the tests were terminated either at complete failure of specimen or when the load dropped down to about 10 % of peak load.

The tests were performed under closed-loop control (Gettu et al. 1996) using a CONTROLS ADVANTEST controller, with a loop closure rate of 120 hz. The test parameters were the proportional gain  $k_p$  and the integral gain  $k_i$ . The  $k_p$ -values used for the test were in the range of 0.3 – 0.8 until the post peak load dropped by about 10 % of the peak load and in the range of 0.001-0.05 (varied progressively during testing) until the termination of the test (see Figure 3.3). The  $k_i$ -values were mostly maintained constant at 0.01 unless significant instability occurred (see Figure 3.3b). However, assigning control parameters for each test was based on trials and could not be decided beforehand due the uncertainty in the material behaviour. Even in the case where the control parameters were well established through trials, specimens could fail suddenly due to loss of control just after the peak load. In this work, on an average, the load deflection behaviour could be obtained until 3 mm deflection only in two-thirds of the tests. Therefore, a minimum of nine specimens were prepared for testing for each concrete to ensure that at least six reliable test results are obtained.

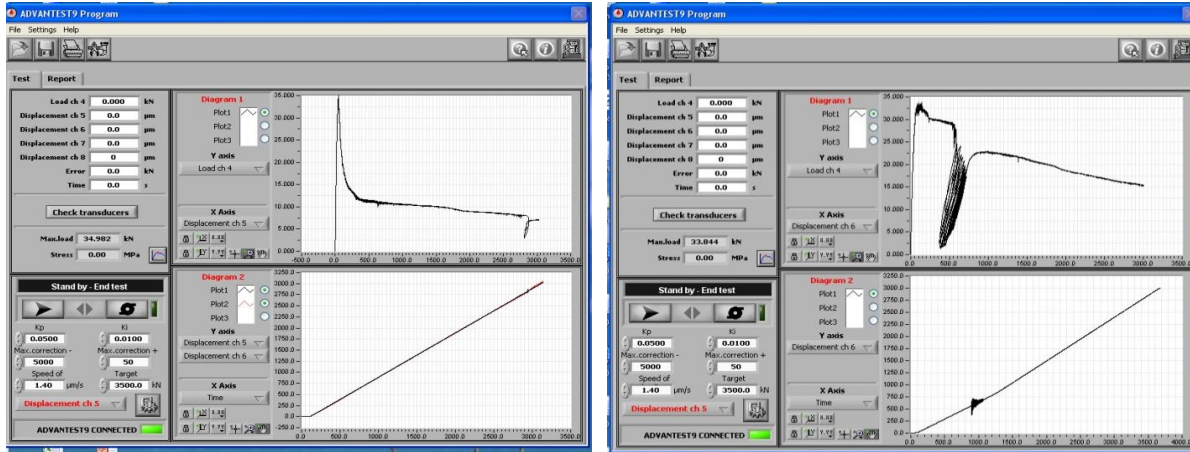


Figure 3.3 Screen shot of the software interface with the test in progress: (a) stable test; (b) unstable response.

The tests were mostly terminated after the specimen attained a deflection above 3 mm. However, in cases where there was rapid loss in load-carrying capacity in the post-cracking regime, the test was terminated when the load dropped to about 10 % of the peak load. This was done to prevent any damage to the test accessories due to sudden failure or uncontrolled crack opening.

### 3.3 Materials used

In this study, different types of fibres were incorporated in a typical M35 concrete mix. The properties of the materials used in the mixes are discussed in detail below.

#### 3.3.1 Cement

Portland pozzolana cement (PPC) conforming to IS: 1489 (2005) has been used in this work. The physical properties of cement are reported in Table 3.1 below, and the chemical composition is reported in Table 3.2.

.Table 3.1 Physical properties of PPC (Results obtained in the laboratory)

Property	Series 1 PPC
Fineness (m <sup>2</sup> /kg)	335
Initial setting time (min)	120
Final setting time (min)	282
Specific gravity (g/cm <sup>3</sup> )	2.81

Table 3.2 Chemical composition of the PPC used

Oxides	%
CaO	51.98
SiO <sub>2</sub>	26.85
MgO	0.86
Al <sub>2</sub> O <sub>3</sub>	10.78
Fe <sub>2</sub> O <sub>3</sub>	5.67
SO <sub>3</sub>	2.97
K <sub>2</sub> O	0.89

### 3.3.2 Fly ash

Fly ash was used in the mix in order to improve the flow properties of concrete and to supplement the cement. It conforms to Grade II as per IS: 3812 (1999) and may be generally termed as ASTM Class F fly ash. The physical properties of the fly ash used are shown in Table 3.3 and the chemical composition is given in Table 3.4.

Table 3.3. Physical properties of Class F fly ash used

Property	Value
Specific gravity	2.49
Blaine specific surface area (m <sup>2</sup> /kg)	330

Table 3.4. Chemical composition of fly ash used

Oxides	Amount in %
CaO	1.28
SiO <sub>2</sub>	59.32
MgO	0.61
Al <sub>2</sub> O <sub>3</sub>	29.95
Fe <sub>2</sub> O <sub>3</sub>	4.32
SO <sub>3</sub>	0.16
K <sub>2</sub> O	1.44
Na <sub>2</sub> O	0.16

### 3.3.3 Fine aggregates

Natural sand with a grain size range of 0-5 mm, corresponding to Zone 2 (see sieve analysis chart in Figure 3.4) was used conforming to IS:383 (2007), having the physical properties listed in Table 3.5.

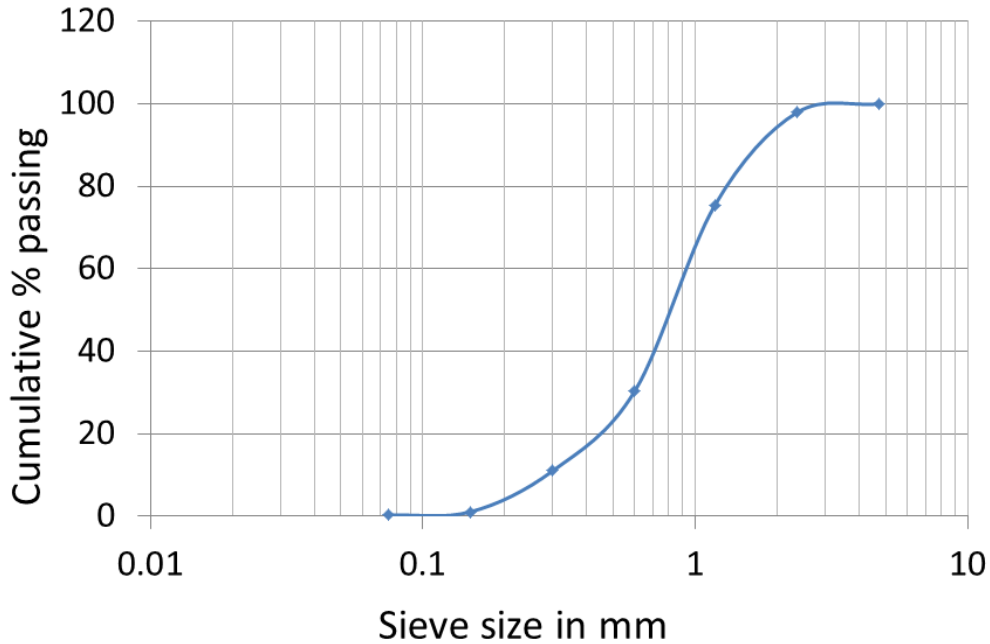


Figure 3.4 Grain size distribution of fine aggregates

Table 3.5 Physical properties of fine aggregates used

Property	Value
Water absorption ( %)	0.63
Specific gravity	2.66
Bulk Density (g/cm <sup>3</sup> )	3.99

### 3.3.4 Coarse aggregates

Crushed granite aggregates (in fractions of 5-10 mm and 10-20 mm) were used and the sieve analysis of the aggregates done as per IS:2386 -2007 (Part I); the sieve analysis curves are shown in Figure 3.5. The physical properties were determined as per IS:2386- 2007 (Part-III) and reported in Table 3.6; the aggregates conform to IS:383- 2007.

Table 3.6 Physical properties of coarse aggregates

Property	10mm	20mm
Water absorption	0.33%	0.30%
Specific gravity	2.78	2.65
Bulk density (g/cm <sup>3</sup> )	3.81	3.91

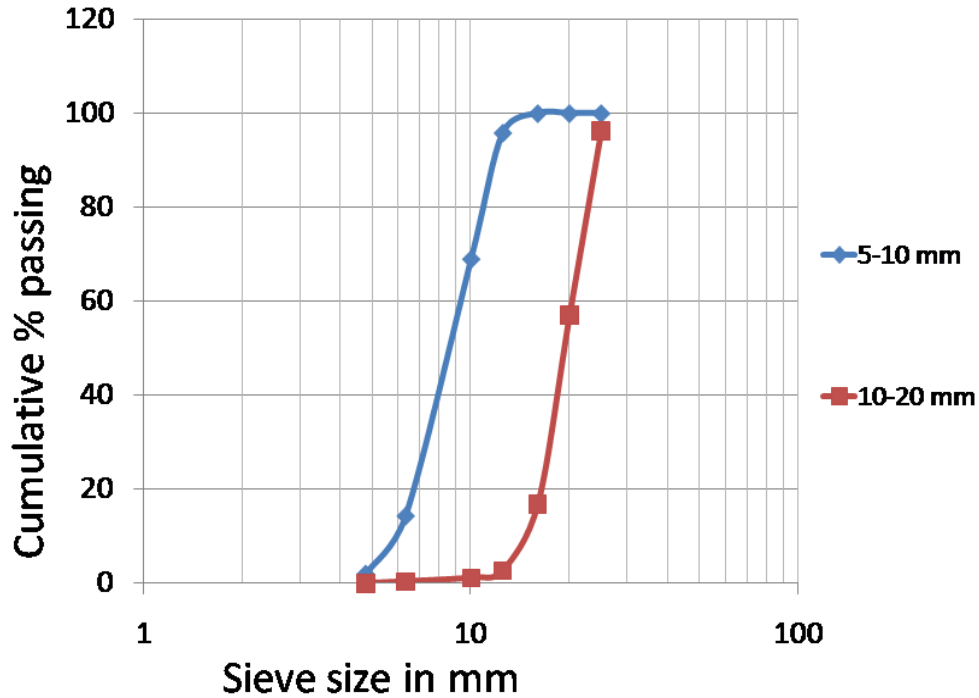


Figure 3.5 Grain size distributions of 10 mm down and 20 mm down aggregates

### 3.3.5 Fibres

Fibres varying in material, dimensions and shapes have been used in this study at different dosages, and the types of fibres and their relevant properties have been listed in the Table 3.7. The fibres include conventional metallic fibres and non-metallic fibres, which may all be categorised as macro-fibres, unconventional amorphous metallic fibres. Further details of the fibres are given in Chapters 4 and 5.

Table 3.7 Fibres used for FRC characterization with relevant properties

Fibre designation	Material of fibre	Description of the fibre	Length of fibre (mm)
SFA	Cold drawn steel wire, high yield strength	Hooked-ended flattened cross section	50
SFB		Hooked-ended, collated, round cross-section	60
SFC		Undulated, round cross-section	50
SFD	Crimped flat	Continuously deformed flat	50
GF	Glass	Monofilament	36
AMF	Amorphous metallic fibres (Fe,Cr) <sub>80</sub> P,C,Si) <sub>20</sub>	Straight flat	20

### 3.3.6 Superplasticizer

Whenever the mix required a superplasticizer to attain the required workability, BASF Glenium B233, a polycarboxylate (PCE) based product was used; the liquid product has a density of 1080 kg/m<sup>3</sup> and solid content was 33%.

### 3.4 Mix proportions

The test programme had concrete mixes of M35 grade with various fibres. The mix design was mostly done conforming to the specifications of IS 10262. However, the fine to coarse aggregate ratio used was higher (fine aggregates accounted for 40% of total aggregate content) than the recommended value (i.e., maximum 30% of total aggregate content shall be fine aggregate) as per IS 10262, in order to improve the flow characteristics. Since the introduction of fibres in concrete is expected to reduce the flowability of concrete significantly, the presence of higher fine content is required to maintain the workability (ACI 544.3R-08).

The proportions of the mix are listed in Table 3.8 considering the aggregates to be dry and water/binder ratio to be 0.5.

Table 3.8 Mix proportions used

Mix ID	Cement in kg/m <sup>3</sup>	Fly ash in kg/m <sup>3</sup>	Sand in kg/m <sup>3</sup>	5-10 mm coarse aggregates in kg/m <sup>3</sup>	10-20 mm coarse aggregates in kg/m <sup>3</sup>	Water added in kg/m <sup>3</sup>
M35	324	36	814	348	647	180

### 3.5 Preparation of specimens

The materials were weigh-batched and mixed in a vertical-axis forced-action pan mixer of 250 litre capacity. Fibres were added manually to the concrete after all the other material components (including a certain amount of superplasticizer) had been mixed together for at least 3 minutes. The concrete was mixed for at least 2 more minutes after incorporating the required dosage of fibres. When using the undulated fibres, more care had to be taken in dispersing them to ensure a uniform fibre distribution than for the hooked-ended ones.

At least nine prisms of 150 × 150 × 700 mm were cast, along with nine 150 mm cubes for each mix in two batches. While casting the prism, most of the concrete required was poured in the middle of the mould and allowed to spread to the ends; few scoops of concrete were placed at the ends to top off the mould. This method was followed so as to avoid any weak planes in the zone where failure is expected to occur during testing. The cube moulds were also filled fully in one layer. Compaction was done for all specimens by table vibration for about 15-20 seconds. It is to be noted that special care was taken to avoid excessive vibration as this could result in the settlement of fibres and segregation/non-uniformity of the concrete. The specimens were demoulded after 24 hours and maintained in a mist room (for curing) until testing. During testing, the prisms were loaded such that the direction of casting is perpendicular to the loading direction (i.e., the specimen is rotated by 90° over its longitudinal axis with respect to the casting position) in order to negate the unconservative bias on the toughness that could result from fibre settlement, if any.

### **3.6 Summary**

This chapter presented the test setup and testing details for the determination of flexural toughness. Description of the various parameters and test control has been provided. The relevant issues faced during the testing have also been discussed. This chapter is a prelude to the results and discussions of the test programme given in subsequent chapters.



## 4 CHARACTERIZATION OF CONCRETES WITH CONVENTIONAL FIBRES

### 4.1 Introduction

In the fibre-reinforced concrete (FRC) used in applications such as flooring, slabs-on-grade and pavements, the appropriate incorporation of fibres provides adequate post-cracking load-carrying capacity. In this context, it is essential to characterize (i.e., objectively quantify) the parameters that can represent the post-cracking strength or energy dissipation capacity of FRC so as to be included in the relevant design methodologies. As discussed in Chapter 2, such parameters, classified as toughness parameters, need to be obtained experimentally for the FRC intended to be used in the specific application.

The flexural toughness test methodology discussed in Chapter 2 has been applied here for the characterization of FRCs incorporating several steel fibres available in the Indian market. This study aims to draw attention to the fact that toughness testing is fundamental for characterizing FRC and fibre performance, and for fibre selection, which most often in India seems to be based on the assessment of only the compressive or flexural strength.

The test programme is intended to validate a test methodology and to develop a material database for comparison and for obtaining target values in design, in the absence of prior data from the field. In addition, the experience gained has helped prepare a pre-normative proposal for flexural toughness characterization in India so as to encourage standardization of the technology.

The chapter discusses the results of the flexural toughness tests on fibre reinforced concrete with conventional steel fibres. In this study, different types of steel fibres (see Table 4.1) were incorporated in M35 concrete (see Table 3.8) and flexural toughness testing was done. The mix proportions are given in Table 3.18 of Chapter 3. The prism specimens were prepared and tested under four point bending as described in Section 3.52 and load-deflection curves were obtained. The flexural toughness parameters studied here are those identified to be critical to the current application as discussed in Section 2.4. The discussion then leads to the suggestion of guidelines

for preparing a pre-normative proposal for the flexural toughness testing. The later part of the chapter discusses the results of tests on FRC with macro-glass fibres done as per the suggested guidelines. The results and the performance are compared with those of steel fibre concretes.

## **4.2 Steel fibre details**

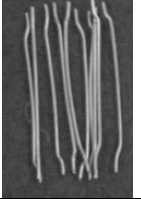
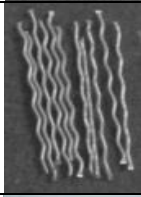
Two hooked-ended fibres SFA and SFB, with slightly different dimensions, and an undulated fibre SFC, all three made by crimping cold-drawn wires (with tensile strength  $> 1000$  MPa), were used along with an undulated fibre SFD made from crimping half-round bars of mild steel. The SFB fibre has a round cross-section whereas the others have flatter cross-sections, the dimensions of which are more difficult to measure. Also, SFB is supplied in collated form – several fibres are glued together with a water-soluble adhesive for easier handling and to avoid fibre balling during the production of the concrete. The average values and the standard deviations of the fibre dimensions have been determined by measuring about 100 fibres, in each case, and are given in Table 4.1. It can be seen that the fibre SFA is the most consistent in length whereas the fibre SFB is the most consistent in terms of the cross-section. The latter also had better shaped ends than the former.

## **4.3 Results and discussions**

### **4.3.1 Fresh properties**

The fresh concrete properties of all the FRC mixes are given in Table 4.2, along with that of the reference concrete (without fibres), M35F0. It can be seen that the unit weight in the fresh state is always in the range of  $2400 - 2550$  kg/m<sup>3</sup>, indicating that all the mixes attained comparable degrees of compaction. The uniformity of the distribution of fibres was checked by visual examination, and was found to be satisfactory in all the concretes. It was always possible to obtain the desired workability (i.e., about 100 mm slump) with minor modifications of the superplasticizer dosage.

Table 4.1 Details of the type of steel fibres used

Fibre designation	Type	Shape of fibre		Length of fibre (mm); avg. $\pm$ std. dev.)	Cross-sectional dimensions of fibre (mm); Avg. $\pm$ std. dev.	Tensile strength* of fibres (MPa)
SFA	Cold-drawn steel wire, yield strength, crimped	Hooked-ended, flattened cross-section		51 $\pm$ 0.2	width: 0.9 $\pm$ 0.05 thickness: 1.1 $\pm$ 0.3	1190
SFB		Hooked-ended, collated, round cross-section		61 $\pm$ 0.5	diameter: 0.8 $\pm$ 0.01	1225
SFC		Undulated, round cross-section		49 $\pm$ 0.2	diameter: 1.0 $\pm$ 0.2	1100
SFD	Mild steel half-wire, crimped	Undulated, crescent shaped cross-section		51 $\pm$ 0.8	width: 2.8 $\pm$ 0.5 nominal thickness: 0.75	850

\*Data given by the fibre manufacturer

### 4.3.2 Compressive strength

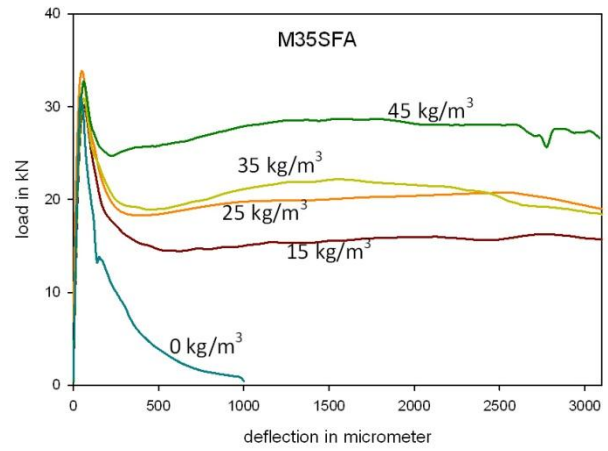
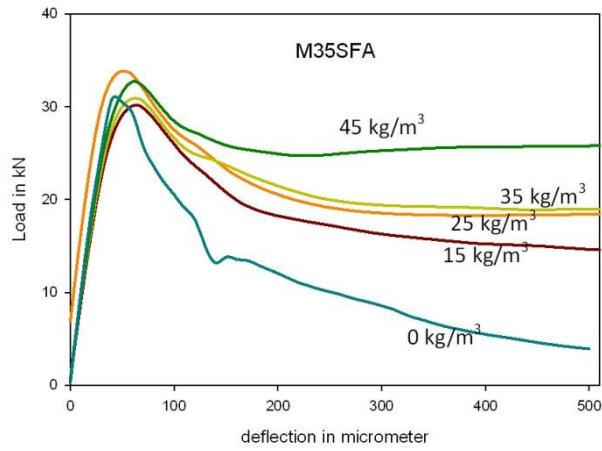
Tests were conducted on cubes to determine compressive strength at the ages of 3, 7 and 28 days using a 3 MN capacity Controls compression testing machine; a minimum of six specimens (three from each of the two batches) were tested at each age. The results reported in Table 4.2 indicate that, as expected, there is no significant change in compressive strength due to the addition of steel fibres, for the type of fibres and the dosages considered here. The evolution and variability of the compressive strength is within the usual range and is not influenced by the incorporation of fibres.

Table 4.2 Fresh properties and compressive strengths of the different FRC mixes with conventional steel fibres

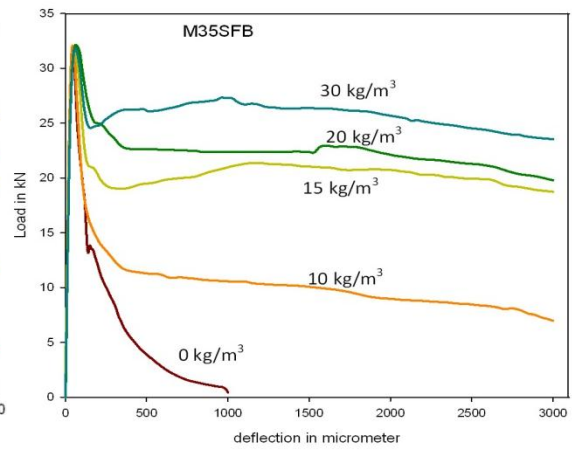
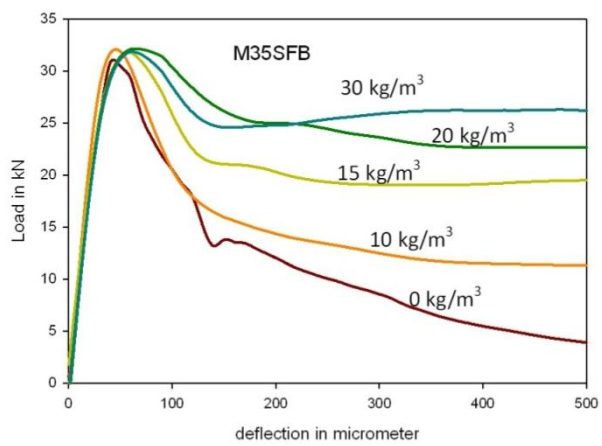
Concrete notation	Fibre	Fibre dosage (kg/m <sup>3</sup> )	Nominal volume fraction, $V_f$	Unit weight of fresh concrete (kg/m <sup>3</sup> )	Slump (mm)	Compressive strength (MPa) (mean $\pm$ standard deviation)		
						at 3 days	at 7 days	at 28 days
M35SFA45	SFA	45	0.60%	2480	85	18.6 $\pm$ 2.9	26.5 $\pm$ 2.6	41.9 $\pm$ 3.0
M35SFA35		35	0.50%	2460	90	18.3 $\pm$ 1.1	26.8 $\pm$ 1.6	43.2 $\pm$ 3.1
M35SFA25		25	0.30%	2460	110	16.4 $\pm$ 1.4	25.2 $\pm$ 3.5	42.0 $\pm$ 1.9
M35SFA15		15	0.20%	2450	95	16.7 $\pm$ 1.4	26.8 $\pm$ 1.8	41.5 $\pm$ 1.5
M35SFB30	SFB	30	0.60%	2430	110	13.7 $\pm$ 0.7	21.9 $\pm$ 0.1	41.6 $\pm$ 1.8
M35SFB20		20	0.45%	2440	100	13.7 $\pm$ 0.5	21.3 $\pm$ 1.5	40.5 $\pm$ 1.9
M35SFB15		15	0.30%	2410	130	14.2 $\pm$ 0.7	21.5 $\pm$ 0.5	40.9 $\pm$ 2.6
M35SFB10		10	0.20%	2430	90	14.8 $\pm$ 1.4	21.1 $\pm$ 1.6	39.2 $\pm$ 1.8
M35SFC45	SFC	45	0.60%	2500	115	17.3 $\pm$ 0.8	26.7 $\pm$ 3.1	43.4 $\pm$ 2.2
M35SFC35		35	0.45%	2540	100	17.6 $\pm$ 0.9	25.4 $\pm$ 0.8	44.4 $\pm$ 4.3
M35SFC25		25	0.30%	2530	120	17.4 $\pm$ 1.3	25.8 $\pm$ 1.8	44.2 $\pm$ 1.0
M35SFC15		15	0.20%	2520	90	18.6 $\pm$ 1.6	28.0 $\pm$ 0.7	44.8 $\pm$ 1.6
M35SFD45	SFD	45	0.60%	2460	120	11.2 $\pm$ 0.2	19.7 $\pm$ 0.6	42.8 $\pm$ 0.9
M35SFD35		35	0.45%	2415	115	11.3 $\pm$ 0.3	20.0 $\pm$ 0.9	40.9 $\pm$ 2.5
M35SFD25		25	0.30%	2430	110	11.6 $\pm$ 0.6	23.8 $\pm$ 1.7	42.2 $\pm$ 2.0
M35SFD15		15	0.20%	2445	100	11.9 $\pm$ 0.2	22.5 $\pm$ 0.5	39.7 $\pm$ 1.3
M35F0	-	0	0	2450	105	13.4 $\pm$ 2.1	20.2 $\pm$ 0.1	42.4 $\pm$ 4.0

### 4.3.3 Flexural behaviour

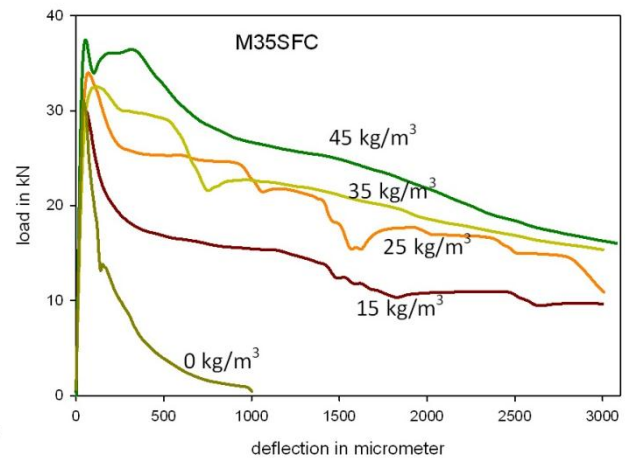
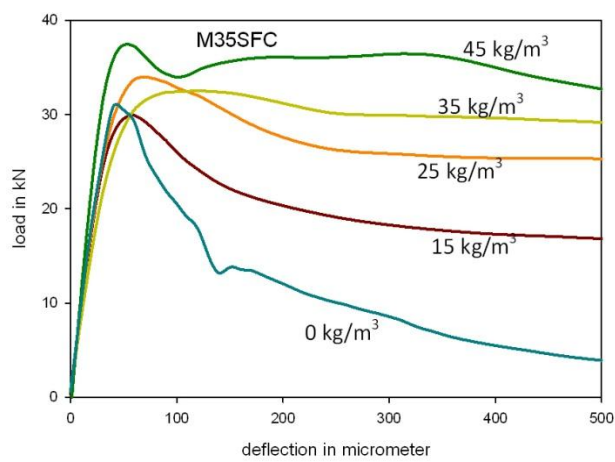
Typical load-deflection curves for the different steel fibre reinforced concretes are shown in Figures 4.1 (a-d). The curves corresponding to the individual specimens are reported in Appendix A (Figures A.1 to A.16). It can be seen in the plots given on the left of each figure (showing the behaviour up to a 500  $\mu\text{m}$ ) in Figure 4.1 that the incorporation of the hooked-ended fibres (see Figure 4.1(a) and (b)) do not influence the curve significantly until after the peak (say, until a deflection of about 150 microns). For the commonly-used steel fibres (i.e., with lengths of 50 – 60 mm and aspect ratios of 50 – 80) and the dosages considered here ( $\leq 0.6\%$ ), very few fibres come into play before and at crack initiation. Nevertheless, the peak load and the cracking response is altered by the undulated fibres (see Figure 4.1 (c) and (d)). In general, the influence of the fibres on the pre-peak mechanical response and the peak load is small. However, there is a significant effect of the fibres on the post-peak behaviour, as seen in the complete records of the load-deflection response in the plots on the right. For both the hooked-ended fibres (SFA and SFB), there is a gradual change from softening to plastic-type response, as the fibre dosage increases, especially beyond a deflection of about 500  $\mu\text{m}$ . However, by comparing Figure 4.1(a) and (b), it can be seen that the SFB fibres, which have a higher aspect ratio (i.e., length/diameter), are more efficient in increasing the toughness than the SFA fibres. In the concretes with the hooked-ended fibres, the post-peak load-carrying capacity and the area under the load deflection curve has a direct relation with the fibre dosage and aspect ratio of the fibre, as expected; higher aspect ratio and higher dosage impart more toughness to the concrete. In the case of the undulated SFC fibres (Figure 4.1(c)), the drop in load just after the peak is not as sharp as in case of the hooked-ended fibres but the response after a deflection of 500  $\mu\text{m}$  does not exhibit significant improvement with an increase in the fibre dosage. Moreover, comparison of the curves in Figure 4.1(c) with those in Figures 4.1(a) and 4.1(b) indicates that the undulated fibres are not as efficient as the hooked-ended fibres at larger deflections or crack. The behaviour of the concretes with the SFD fibres (see Figure 4.1(d)) is qualitatively similar to that of the concretes with the SFC fibres, both of which are undulated. These results reinforce the fact that straight hooked-ended fibres are more efficient than the undulated fibres in increasing the energy absorption capacity, as has been reported in literature (Soroushian and Bayasi 1991, Holschemacher and Müller 2013).



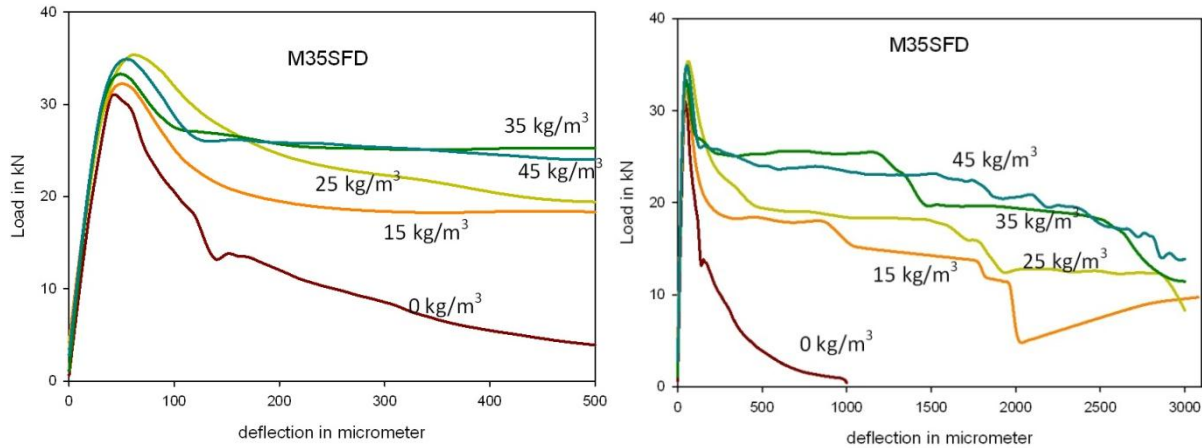
(a)



(b)



(c)



(d)

Figure 4.1 Typical load deflection curves for M35 concrete with different types and dosages of steel fibres

In general, it was seen that the waviness and the scatter in the load-deflection curve is much higher in the concretes with undulated fibres and shorter fibres than with the hooked-ended fibres. The difference between the response of the concretes reinforced with the undulated and straight hooked-ended fibres can be understood by considering how the two types of fibres act across a crack. The hooked-ended fibre deforms over the straight part, while restraining the crack opening, and then one of the ends pulls out gradually, while dissipating energy through yielding and frictional mechanisms. The undulated fibre is forced to straighten due to crack widening, and this leads to local strain in the fibre and crushing of concrete at the crack faces as seen in Figure 4.2. The latter type of fibre action does not seem to be as efficient as the former in increasing the toughness, though it could increase the flexural strength slightly. Moreover, the undulated fibres result in crack branching resulting in a larger damaged area during failure and unsteady crack propagation (which sometimes results in momentary loss of control during testing).

#### 4.3.4 Determination of the flexural toughness parameters

From the experimentally-obtained load-deflection curves two equivalent flexural strengths,  $f_{e,300}$  and  $f_{e,150}$  have been computed as described in Section 2.4.1, for the deflection limits given by  $n = 300$  and  $150$  (i.e., deflections of 1.5 and 3 mm, respectively). The mean values obtained are presented in Table 4.3, along with the mean flexural strength ( $f_{ct}$ ) found by using the peak load

and the equivalent flexural strength ratios ( $R_{e,300}$  and  $R_{e,150}$ ). The calculation have been done as discussed in Section 2.4.1 of Chapter 2. The data for the unreinforced concrete are also given at the bottom of the same table for reference.



Figure 4.2 Crack pattern after the end of the beam test: (a) larger damaged area in concrete with SFC fibres and (b) single major crack in concrete with SFB fibres

It can be seen from Table 4.3 that the flexural strength of FRC is slightly higher than that of plain concrete. However, the increase does not show any clear dependence on the fibre dosage or type, though the highest values were obtained with the undulated SFD fibre. The results reiterate the need to carry out tests on FRC for determining the flexural strength rather than using values obtained from empirical equations relating flexural strength with compressive strength or from tests of plain concrete.

The equivalent flexural strengths, i.e., the  $f_{e,n}$ -values, reflect clearly the increase in the post-peak load-carrying capacity of the FRC with an increase in dosage of the hooked-ended fibres and an increase in the aspect ratio, as expected. However, the trends are not that evident in the cases of the undulated fibres. When the results of the concretes with the SFA fibres are compared with those with the SFC fibres, both of which have similar dimensions but different shapes, it can be seen that the (former) hooked-ended fibres yield better toughening than the undulated ones, as expected. Comparison of the values of the two equivalent flexural strengths show that  $f_{e,150}$  is slightly higher than or practically equal to  $f_{e,300}$  for the hooked-ended fibres but is lower than  $f_{e,300}$  for the undulated fibres, reflecting the softening-type response of concretes with the latter fibres.

Table 4.3 Flexural strengths and equivalent flexural strengths of FRC with steel fibres

Concrete	Fibre type and dosage (kg/m <sup>3</sup> )		$f_{ct}$ (MPa)	$f_{e,300}$ (MPa)	$R_{e,300}$ (%)	$f_{e,150}$ (MPa)	$R_{e,150}$ (%)
M35SFA45	SFA	45	4.61	3.71	81	3.84	84
M35SFA35		35	4.78	3.46	73	3.45	72
M35SFA25		25	4.49	2.75	61	2.62	58
M35SFA15		15	4.40	2.31	53	2.14	49
M35SFB30	SFB	30	4.55	3.86	85	3.80	84
M35SFB20		20	4.52	3.17	71	3.19	72
M35SFB15		15	4.48	2.38	53	2.24	50
M35SFB10		10	4.51	2.05	46	1.90	42
M35SFC45	SFC	45	4.91	4.27	87	3.55	72
M35SFC35		35	4.47	2.85	64	2.44	55
M35SFC25		25	4.48	2.97	67	2.39	54
M35SFC15		15	4.68	1.86	41	1.55	34
M35SFD45	SFD	45	4.90	3.48	71	3.01	61
M35SFD35		35	4.89	2.92	60	2.48	51
M35SFD25		25	5.02	2.42	48	1.82	37
M35SFD15		15	5.11	2.46	49	2.17	43
M35F0	-		3.99	0.44	12	0.22	6

The normalized equivalent flexural strength values or the equivalent flexural strength ratios at 3 mm ( $R_{e,150}$ ) and 1.5 mm ( $R_{e,300}$ ), have been used to identify the relative strength retained after cracking; for example, in the case of M35SFB15, the  $R_{e,300}$ -value of 53% indicates that there is an average post-peak strength of about 53% of the flexural strength upto the deflection of 1.5 mm and the  $R_{e,150}$ -value of 50 % indicates that there is an average post peak strength of 50% of flexural strength upto deflection of 3 mm. Comparison of the  $R_{e,300}$ - and  $R_{e,150}$ -values gives an idea of the flatness of the post-peak curve or the retention of the post-crack load-carrying capacity; for example, in all the concretes with the hooked-ended fibres,  $R_{e,150}$  is almost the same or slightly higher than  $R_{e,300}$ , whereas in the concretes with the undulated fibres,  $R_{e,150}$  is lower than  $R_{e,300}$ , indicating a drop in load-carrying capacity as the crack widens. It can also be seen that different combinations of fibre type and dosage can have similar  $R_{e,n}$ -values,

and that different fibres at the same dosage can give different  $R_{e,n}$ -values, which has important implications for design. For example, both M35SFA35 and M35SFB20 have the same  $R_{e,150}$ -value of 72%, which means that 35 kg/m<sup>3</sup> of the SFA fibre provides similar toughness as 20 kg/m<sup>3</sup> of SFB fibre (having a higher aspect ratio).

Residual flexural strengths,  $f_{r,n}$ , were calculated for  $n = 600, 300$  and  $150$  as discussed in Section 2.4.1 at the corresponding (residual) loads. The two extreme values coincide with those specified in ASTM 1609. The mean values are presented in Table 4.4 for all the concretes tested; note that the loads corresponding to these deflections are zero for the plain concrete. The residual strengths obviously give the same trends as the load-deflection curves. They have an advantage over the equivalent strengths in that they can be used to find intermediate values of residual strengths and even estimate the equivalent strengths when the entire load-deflection curves are not available. However, as each is dependent on a single load value, small perturbations in the load-deflection curve can distort the measure of toughness, especially when the scatter in the experimental response is high. In the case of undulated fibres, it can be seen that  $f_{r,150}$  is on average less than 40% of  $f_{r,600}$  as compared to a maximum drop of 20 % for the straight hooked-ended fibres. These values confirm the inability of the undulated fibres to maintain the load-carrying capacity over large crack openings deflection when compared with the latter.

Table 4.4 Mean residual strengths

Concrete	Fibre type and dosage in kg/m <sup>3</sup>	$f_{ct}$ (MPa)	$f_{r,600}$ (MPa)	$f_{r,300}$ (MPa)	$f_{r,150}$ (MPa)
M35SFA45	SFA	45	4.61	3.48	3.69
M35SFA35		35	4.78	3.17	3.43
M35SFA25		25	4.49	2.09	2.10
M35SFA15		15	4.40	1.75	1.50
M35SFB30	SFB	30	4.55	3.65	3.66
M35SFB20		20	4.52	2.91	2.91
M35SFB15		15	4.48	2.16	2.17
M35SFB10		10	4.51	1.78	1.71
M35SFC45	SFC	45	4.91	4.21	3.01
M35SFC35		35	4.47	2.80	2.6
M35SFC25		25	4.48	2.63	2.3
M35SFC15		15	4.68	1.76	1.5
M35SFD45	SFD	45	4.90	3.38	2.96
M35SFD35		35	4.89	3.02	2.62
M35SFD25		25	5.02	2.29	1.65
M35SFD15		15	5.11	2.30	2.14

#### 4.3.5 Implications of the variations in the toughness parameters for design

In general, it can be stated that the dosage of the fibre should be such that the equivalent strength be at least 30% of the flexural strength. Practically all the cases studied here satisfy this requirement. However, the fibre type and dosage to be used in an application depends on the design requirement, which can be met by several combinations that can provide the desired toughness.

Another significant issue in design is the use of the characteristic strength. As in most civil engineering applications, we define the characteristic value as:

$$\sigma_{ch} = \sigma_m - ks \quad (4.1)$$

where  $\sigma_{ch}$  and  $\sigma_m$  are the characteristic and mean values, respectively,  $k$  is a factor that depends on the acceptable risk or confidence, and  $s$  is the standard deviation of the parameter. It has been argued that in the case of slabs and tunnel linings, the risk can be higher than 5% due to the stress redistribution capacity, low danger due to local failure and so on. However, as usual in structural design, we permit only a risk of having up to 5% of the values below the characteristic value used in design, we take the multiplier corresponding to 95% confidence, that is,  $k = 1.64$ .

Table 4.5 shows the data obtained from the tests for different toughness parameters corresponding to the deflection limit of 3 mm, along with the flexural strength, in terms of the mean and characteristic values, and coefficient of variations (CoV), each from about 6 trials. It can be seen observed that the variation of results is, in general, much lower for straight hooked-ended fibres in comparison with the undulated fibres, which is also reflected in the characteristic values. On average, the CoVs obtained here for  $f_{ct}$  range from 9% to 13%, for  $f_{e,150}$  from 13% to 21%, for  $R_{e,3}$  from 13% to 21%, and for  $f_{r,150}$  from 19% to 39%. It is evident that the toughness parameters will have higher variability than the flexural strength and much more than the compressive strength. Also, the scatter in the values of the residual strength is much higher than in the equivalent strength, which implies that the latter is a more reliable parameter than the former. Further, the lowest CoVs are for the SFB fibre (which has the least variability in the cross-section dimension) whereas the undulated fibres yield higher CoVs, especially for  $f_{r,150}$ . Note that fibres yielding higher CoVs will require relatively higher dosages to meet the characteristic toughness requirement than fibres with lower CoVs (see Equation 4.1).

Table 4.5 Variability in the flexural toughness parameters

Concrete	$f_{ct}$ (MPa)			$f_{e,150}$ (MPa)			$R_{e,3}$ %			$f_{r,150}$ (MPa)						
	mean	CoV (%)	Charact- eristic value	Mea n	CoV (%)	Charact- eristic value	mea n	CoV (%)	Charact- eristic value	mean	CoV (%)	Charact- eristic value				
M35SFA45	4.61	9	Avg = 10	3.95	3.84	6	Avg = 18	3.45	84	5	Avg = 15	78	3.59	8	Avg = 21	3.12
M35SFA35	4.78	11		3.94	3.45	18		2.43	72	17		52	2.97	19		2.06
M35SFA25	4.49	8		3.93	2.62	15		1.98	58	10		49	2.08	20		1.38
M35SFA15	4.24	13		3.35	1.87	33		0.85	44	29		23	1.56	35		0.67
M35SFB30	4.55	13	Avg = 9	3.57	3.80	16	Avg = 13	2.78	84	10	Avg = 13	70	3.24	21	Avg = 19	2.13
M35SFB20	4.52	10		3.77	3.19	8		2.76	72	16		53	2.62	9		2.25
M35SFB15	4.48	4		4.17	2.24	16		1.65	50	14		39	1.87	24		1.14
M35SFB10	4.51	9		3.85	1.90	11		1.56	42	10		35	1.46	21		0.97
M35SFC45	4.91	12	Avg = 12	3.98	3.55	17	Avg = 19	2.53	72	11	Avg = 20	59	2.13	30	Avg = 39	1.08
M35SFC35	4.47	14		3.45	2.44	15		1.83	55	13		43	1.51	35		0.64
M35SFC25	4.48	8		3.87	2.39	18		1.70	54	22		35	1.53	39		0.55
M35SFC15	4.68	15		3.52	1.55	26		0.89	34	34		15	0.51	51		0.08
M35SFD45	4.90	3	Avg = 9	4.63	3.01	16	Avg = 21	2.23	61	16	Avg = 21	46	1.72	20	Avg = 30	1.16
M35SFD35	4.89	12		3.95	2.48	29		1.30	51	23		32	1.65	20		1.09
M35SFD25	5.02	12		4.01	1.82	23		1.13	37	27		21	0.67	52		0.10
M35SFD15	5.11	10		4.28	2.17	17		1.56	43	17		31	1.68	28		0.89
M35SF0	3.99	13	-	3.12	0.22	26	-	0.12	6	16		4	0	-	-	0

In the absence of test data, the characteristic equivalent flexural strength of FRC is often taken as 70% of the mean value (e.g., TR34), which corresponds to a CoV of 18%, if  $k = 1.64$  (see Equation 4.1). From the values in Table 4.5, it can be seen that this assumption is acceptable for the hooked-ended fibres but is unconservative for the undulated fibres; a better assumption for the undulated fibres would be a characteristic equivalent flexural strength that is 65% of the mean value). On the other hand, the characteristic residual strength value can be as low as 65% for the undulated fibres and 36% for hooked-ended fibres with respect to the mean values.

#### **4.4 Guidelines for flexural toughness characterization**

Based on the tests performed in this study and other experience, the following are recommended for consideration in an Indian test standard that could be brought out in the near future:

- The test shall be performed on unnotched prisms of  $150 \times 150 \times 700$  mm under four point bending with a span of 450 mm. These dimensions are valid for concretes having aggregates with maximum grain size of up to 25 mm and fibres of up to 60 mm in length.
- The loads are to be applied at thirds of the span. The supports should be such that the rollers are able to freely rotate on their axes with no restraints; i.e., they should not be placed in grooves. Three rollers, as shown in Figure 3.2, including the two upper ones, shall be capable of being inclined in a plane perpendicular to the longitudinal axis of the specimen.
- Since a high amount of energy could be released upon cracking, which could destabilize the test, a very stiff testing frame is an essential requirement. Further, the test is to be performed at a prescribed deflection rate, which necessitates the use of a servo-controlled hydraulic system. The operator should be familiar with closed-loop or feedback loop testing and the adjustment of the control (PID) parameters to ensure stable testing.
- For toughness characterization, it is recommended that the flexural strength and the equivalent flexural strengths  $f_{e,n}$ , with  $n = 150$  and 300, be specified. The residual strengths have been found to exhibit high scatter and the equivalent strength ratios could be misleading when used as the only FRC parameter, and are, therefore, not recommended.

[Note: The guidelines have been the basis for a FRC guideline in India, published under the onus of Indian Concrete Institute as a technical recommendation -ICI TC/01.1 (2014), Test Method for the Flexural Strength and Flexural Toughness Parameters of Fibre Reinforced Concrete.]

#### 4.5 Characterization of FRC with glass fibres as per the suggested testing guidelines

In compliance with the guidelines developed for flexural toughness characterization, testing was also done for FRC with macro-glass fibres in order to assess the performance. The details of the fibres are given in Table 4.6.

Table 4.6 Details of the glass fibres used (properties as reported by the manufacturer)

Fibre designation	Type	Shape of fibre	Length of fibre (mm)	Aspect ratio	Tensile strength of fibres (MPa)
GF	Glass	Monofilament	36	67	1700

The mix was prepared by incorporating various dosages of glass fibres in M35 grade concrete having the same mix proportions as that used for the steel fibre mixes. The mix designations and the dosages are shown in Table 4.7. Four mixes including the plain concrete mix were prepared and tested as discussed in the guidelines (Section 4.4). The fresh concrete properties and the compressive strengths at 28 days are reported in Table 4.7.

Table 4.7 Mix designations and details of various GFRC used including fresh concrete properties and compressive strength (mean±std. deviation)

Mix ID	Fibre dosage	% volume fraction	Super-plasticizer dosage (%)	Unit weight of fresh concrete	Slump (mm)	Compressive strength (MPa) at 28 days
M35GF15	15	0.6	0.49	2470	55	44.9 ±3.1
M35GF10	10	0.4	0.35	2420	70	44.5 ±2.5
M35GF5	5	0.2	0.19	2440	75	45.8 ±2.4
M35GF0	0	0	0.05	2450	105	42.4±4.0

### 4.5.1 Fresh properties

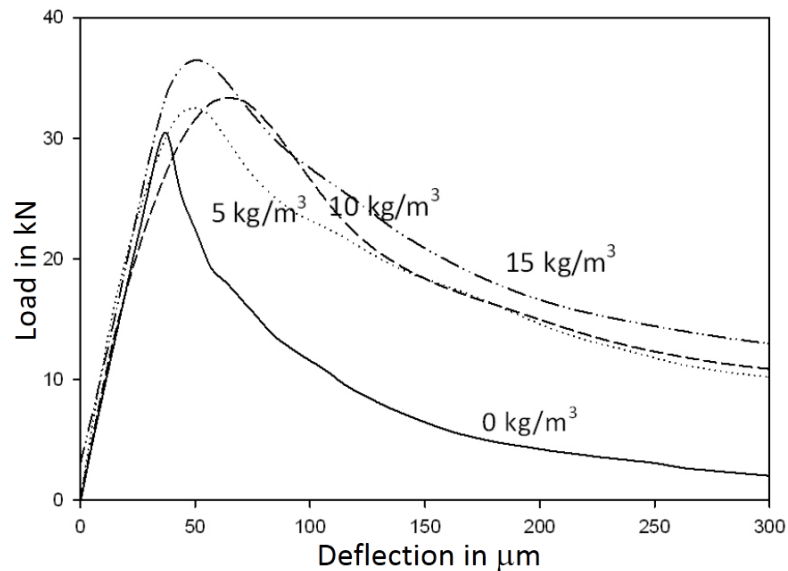
The target slump was 100 mm and superplasticizer (SP) was added to attain the slump. It can be seen that the dosages of superplasticizer used is higher for the fibre mixes since the loss of workability due to fibre addition had to be compensated (especially at dosages of 10 kg/m<sup>3</sup> and 15 kg/m<sup>3</sup>). However, even with high SP dosages (beyond which the mixes segregated), the target slump was not achieved (see Table 4.7). Nevertheless, all the mixes were uniform and had enough workability to be handled during fabrication and so further attempts to increase the slump by modifying the matrix was not done. The unit weight of all mixes is in the range of 2400 – 2500 kg/m<sup>3</sup>, suggesting that the mixes were uniform.

### 4.5.2 Compressive strength

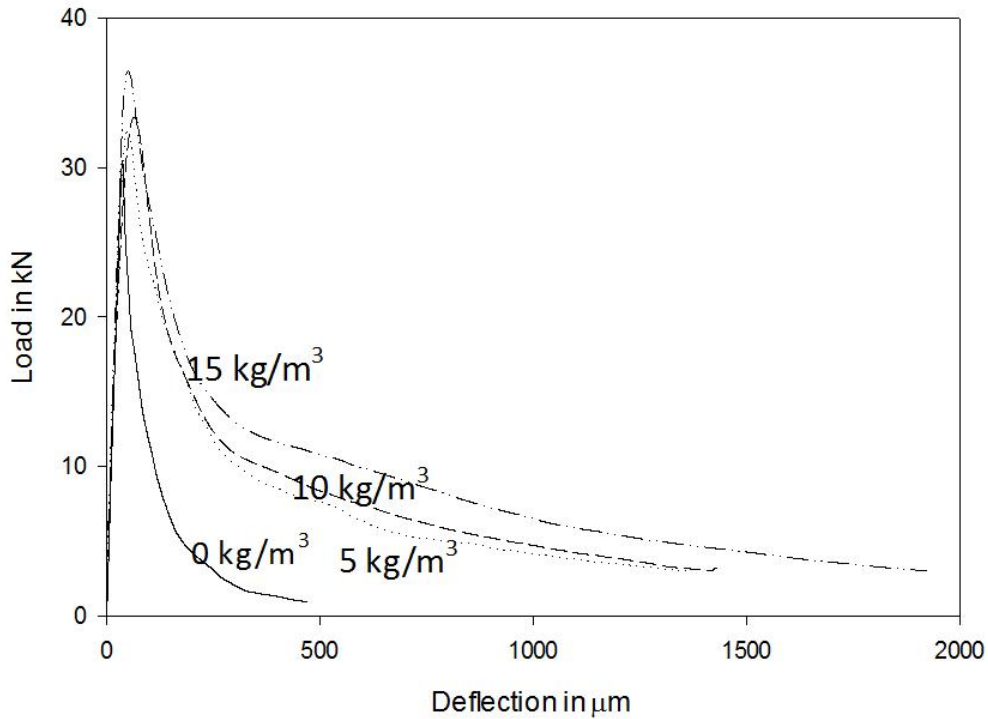
The compressive strength values in Table 4.7 indicates that the fibre incorporation has no influence on the values and the variability is similar to that of the steel fibre concretes (see Section 4.3.2).

### 4.5.3 Flexural behavior

Typical load-deflection curves of the various mixes are shown in Figure 4.3. The curves corresponding to the individual specimens are reported in Appendix B.



(a)



(b)

Figure 4.3 Typical load-deflection curves for M35 concrete with different dosages of glass fibres (a) up to 300  $\mu\text{m}$  deflection (b) up to 2000  $\mu\text{m}$  deflection

One observation from the load-deflection response is that the effect of fibres in post peak regime is negligible at larger deflections ( $>1000 \mu\text{m}$ ). However, the presence of fibres slightly enhances the load carrying capacity at and immediately after the peak load, at smaller deflections. Another striking feature, is the low influence of the increase in fibre dosage on the performance unlike in steel fibres. The curves are close to each other suggesting that an increase in dosage of  $5 \text{ kg/m}^3$  does not cause any significant increase in the residual capacity after cracking.

#### 4.5.4 Flexural toughness evaluation

The flexural toughness parameters were calculated, as in the case of steel fibre concrete, and are reported in Table 4.8. The values suggest an increase in the flexural strength with an increase in the dosage of glass fibres, the maximum increase being about 40% with reference to the

strength of plain concrete, as seen in Table 4.8. However, as far as the post-peak performance is concerned, the results reiterate the relative ineffectiveness of glass fibres, incorporated in the mixes in this study, in enhancing the flexural capacity especially at higher deflections.

Table 4.8 Flexural strengths and equivalent flexural strengths of FRC with glass fibres

Concrete	Fibre type and dosage in kg/m <sup>3</sup>		$f_{ct}$ (MPa)	$f_{e,300}$ (MPa)	$R_{e,300}$ as %	$f_{e,150}$ (MPa)	$R_{e,150}$ as %
M35GF15	GF	15	5.08	1.27	25	0.70	14
M35GF10		10	4.73	1.23	26	0.63	13
M35GF5		5	4.63	1.05	23	0.54	12
M35F0	0		3.60	0.44	12	0.22	6

Another observation is that there is no improvement in any of the parameters with an increase in dosage. The residual strength values shown in Table 4.9 indicate that even at lower deflections of 0.75 mm (i.e., span/600) the residual strengths are not significant, even at high dosages, which contradicts the results reported in literature. The glass fibres seem to yield toughening at lower deflections (of up to about 1.5 mm), after which fibre pullout occurs. It is possible that the lower performance of these fibres in the current study could be due to the use of crushed granitic aggregates, as opposed to rounded aggregates.

Table 4.9 Residual flexural strengths of FRC with glass fibres.

Concrete	Fibre type and dosage in kg/m <sup>3</sup>		$f_{r,600}$ (MPa)	$f_{r,300}$ (MPa)	$f_{r,150}$ (MPa)
M35GF15	GF	15	0.92	0.39	0.00
M35GF10		10	0.92	0.30	0.00
M35GF5		5	0.77	0.26	0
M35F0	0		0	0	0

In Table 4.10, the variability of results has been assessed and it is observed that the variability of all parameters is lower than that of the steel fibre mixes. This could be attributed to

the mechanism of pullout through slipping that dominates the fibre behavior leading to less variability.

Table 4.10 Variability in the flexural toughness parameters for glass fibre reinforced concrete

Concrete	$f_{ct}$ (MPa)			$f_{e,150}$ (MPa)				$R_{e,3}$ (%)				
	mean	CoV (%)		Charact- eristic value	Mean	CoV (%)		Charact- eristic value	mean	CoV (%)		Charact- eristic value
M35GF15	5.08	8	Avg = 6	4.5	0.70	14	Avg = 17	0.54	14	11	Avg = 16	12
M35GF10	4.73	7		4.2	0.63	18		0.44	13	17		11
M35GF5	4.63	3		4.4	0.54	18		0.38	12	19		9

#### 4.6 Summary

The chapter discusses the results obtained from the characterization programme on steel and glass fibre reinforced concrete. Various dosages of each fibre were incorporated in M35 grade concrete, and their fresh concrete and hardened concrete properties were discussed. The parameters included compressive strengths and flexural strength, along with the flexural toughness parameters. The results contribute to a material database to facilitate incorporation in design models developed in later chapters. The specific conclusions drawn from the study are:

- Toughness testing should essentially be done under stable deflection control so as to adequately capture the post-peak response. It is recommended that nine specimens be prepared for testing to ensure that at least six reliable test results are obtained since specimens could fail suddenly due to loss of control just after the peak load.
- The compressive strength of the concrete is not affected by the incorporation of the steel fibres considered here at dosages up to 0.6% (by volume of concrete).
- The incorporation of hooked-ended steel fibres does not influence the peak load in the flexural tests significantly. On the otherhand, the peak load and the cracking response are altered by the undulated steel fibres. However, for volume fractions of up to 0.6%, the incorporation of steel fibres can only enhance the flexural strength slightly, say up to 10%, and cannot be accounted for in design.

- From the load-deflection behavior, it can be concluded that at large deflections the hooked-ended steel fibres are more efficient in comparison to the undulated fibres and vice versa at smaller deflections. Such behavior can be attributed to the different mechanisms of pull out in the two types of fibres that include elongation and then pull out for hooked end fibres, and straightening of undulated fibres with subsequent cracking and crushing of the concrete without substantial straining of the fibres.
- The equivalent flexural strengths, i.e., the  $f_{e,n}$ -values, increase with an increase in dosage of the hooked-ended steel fibres and an increase in the aspect ratio, as expected. However, the equivalent flexural strengths for undulated fibres do not show a clear trend.
- Comparison of the values of the equivalent flexural strength for different steel fibres show that  $f_{e,150}$  is slightly higher than or practically equal to  $f_{e,300}$  for the hooked-ended fibres but is lower than  $f_{e,300}$  for the undulated fibres, reflecting the softening-type response of concretes with the latter fibres. Consequently, in all the concretes with the hooked-ended fibres,  $R_{e,150}$  is almost the same or slightly higher than  $R_{e,300}$ , whereas in the concretes with the undulated fibres,  $R_{e,150}$  is much lower than  $R_{e,300}$ , indicating a drop in load-carrying capacity as the crack widens. Also, the residual strength at the deflection of  $l/150$  mm for the undulated fibres is on an average less than 40% of the residual strength at  $l/600$  mm as compared to a maximum drop of 20 % for straight hooked-ended fibres. These results indicate that the hooked-ended steel fibres are more efficient in retaining the post-cracking load-carrying capacity than the undulated fibres.
- It has been illustrated that different combinations of steel fibre type and dosage can have similar toughness values, and different fibres at the same dosage can give different toughness values, which has important implications for design.
- On average, the scatter in the values of the residual strength is much higher than in the equivalent strength, which implies that the latter is a more reliable parameter than the former. Further, the lowest scatter is observed for the SFB fibre, which has the least variability in the cross-section dimension and shape.

- From the analysis of test results, the characteristic value of the equivalent flexural strength of hooked-ended steel fibre concrete can be conservatively considered to be 0.7 times the mean value, and for undulated fibres a lower value of 0.65 may be used.
- The flexural toughness parameters of the glass fibre reinforced concrete indicate a limited influence on the post-cracking behaviour especially at higher deflections (above 0.5 mm) though there is some enhancement of the flexural strength.
- Based on the experience gained from the test programme on steel fibre concrete, detailed guidelines have been prepared for flexural toughness characterization of FRC. The guidelines have paved the way for an FRC guideline in India, published under the onus of Indian Concrete Institute as a technical recommendation ICI TC/01.1 (2014), Test Method for the flexural strength and Flexural Toughness Parameters of Fibre Reinforced Concrete.



# 5 CHARACTERIZATION OF CONCRETES WITH HYBRID COMBINATION OF AMORPHOUS METALLIC AND STEEL FIBRES

## 5.1 Introduction

From the discussion in Chapter 2 on different types of fibres, it is evident that the shorter (micro) fibers used in larger quantities enhance the resistance against crack initiation and/or delay damage localization, resulting in a substantial increase in the tensile or flexural strength. On the contrary, longer macro-fibers improve the toughness, after crack localization, as illustrated by the results of tests discussed in Chapter 4.

Amorphous metallic fibers (AMF), such as those fabricated with an iron-chromium alloy, are an interesting family of fibers, because of the corrosion resistance and high tensile strength (Choi et al. 2014). Tests on concretes with AMFs, as reported in literature, suggest that there is enhancement in the resistance to crack initiation, resulting in the significant increase in the flexural and tensile strengths. Consequently, several researchers have proposed the incorporation of AMFs in structural concrete, as supplementary reinforcement (Rossi 1992, Casanova and Rossi 1996, Hameed et al. 2009a, 2013). However, the influence of these fibers at larger crack widths does not seem to be encouraging (Rossi 1992, Pons et al. 2007, Hameed et al. 2009b, 2010).

In FRC applications, where a certain amount of cracking can be allowed under service conditions (e.g., in slabs-on-grade and pavements), the loss of load-carrying capacity due to the corrosion of fibers is a matter of concern. The use of AMFs in combination with conventional hooked-ended cold-drawn steel fibers (SF) may be a suitable solution to mitigate the loss in load-carrying capacity over time since conventional steel macro fibers, at comparable dosages, improve ductility and the post-cracking performance, resulting in a long pseudo-ductile “tail” in the load-deflection response of the concrete as seen in Chapter 4. Consequently, the performance of the hybrid system has been investigated through a flexural toughness test programme lines as discussed in Chapters 3 and 4. Since the mechanisms of action of the AMF and SF enhance the

response at different stages of crack evolution, the suitability of combining them is assessed for a possible synergistic effect.

Initially a short discussion of AMF is presented in the chapter since these fibres are different in composition and behavior with respect to the conventional fibres. A discussion on the tests performed in order to assess the corrosion resistance followed by the flexural toughness testing, done as per the guidelines in Chapters 3 and 4, is presented. Based on the results of the flexural toughness on concrete mixes with single fibres, hybrid mixes have been designed and tested. The results are followed by a study of the synergistic response due to the fibre combination.

## 5.2 Amorphous metallic fibres

Amorphous metallic fibres (AMF), with the composition given by the manufacturer as (Fe,Cr)80 (P,C,Si)20, have been used in conjunction with collated hooked-ended cold-drawn steel fibers (SF); the properties of both fibers are given in Table 5.1. The incorporation of AMF in concrete has been shown to increase the flexural strength of concrete significantly (Rossi 1992, Pons et al. 2007, Hameed et al. 2010, Won et al. 2013, Choi and Ku 2014). The SF was chosen to represent fibers commonly used in applications such as flooring, pavements and structural elements. The effect of such hooked-ended steel fibers on improving the flexural toughness has been well established (e.g., Nayar et al. 2014). The amorphous nature of the AMF was verified through X-Ray diffraction analysis using a Panalytical X'pert-Pro apparatus, with Cu-Ka radiations, 20° to 90° sweep, 0.02° step size and 20s duration per step; the XRD spectrum shown in Figure 5.1 for AMF is devoid of peaks that are characteristic of crystalline phases, as evident in the SF spectrum.

Table 5.1 Fibres used and their properties (as given by the manufacturers)

Fibre type	Shape	Dimensions	Minimum tensile strength (MPa)	Density (kg/m <sup>3</sup> )
Amorphous metallic (AMF)	Straight, flat	length = 20 mm width = 1 mm thickness = 24 µm	1400	7200
Steel (SF)	Hooked-ended, round cross-section	length = 60 mm diameter = 0.8 mm	1225	7800

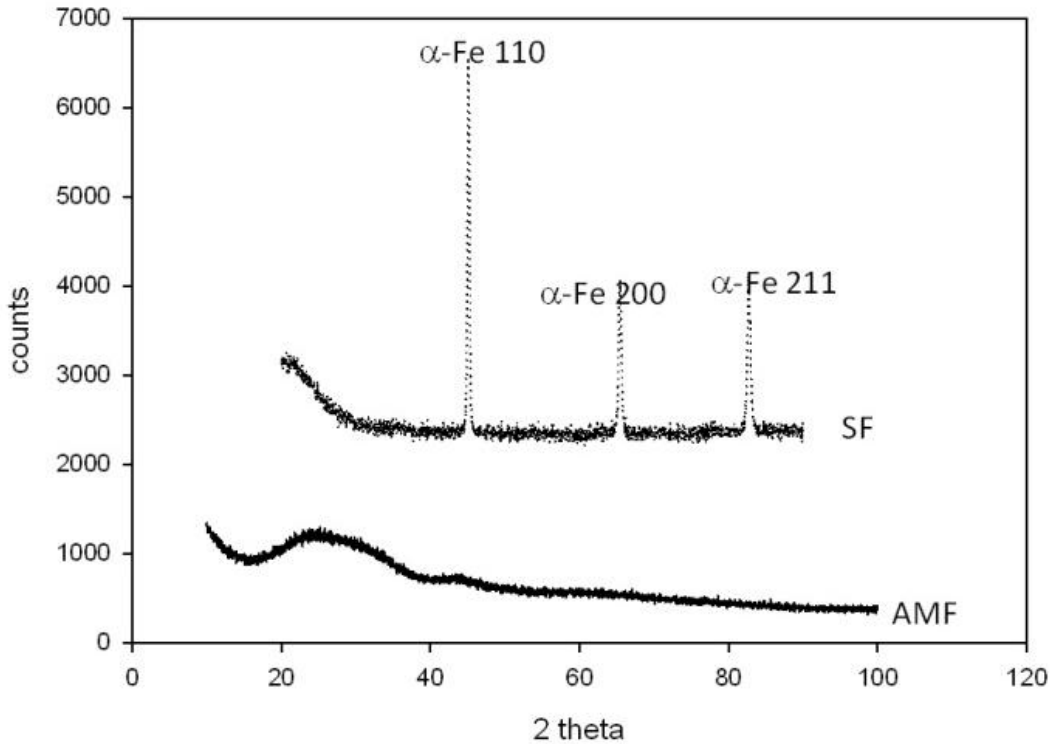


Figure 5.1 XRD spectra of AMF and SF

As mentioned earlier, one of the benefits of the AMF is the corrosion resistance (Redon and Chermant 1999, Hameed et al. 2010). In order to assess this, samples of SF and AMF were immersed in a solution of 3.5% NaCl in water for 4 weeks; SF showed significant rusting within a week and continued to corrode further whereas the AMF exhibited slight staining in a few fibers after 3 weeks (see photographs of the fibers before and after immersion in Figure 5.2 and 5.3).

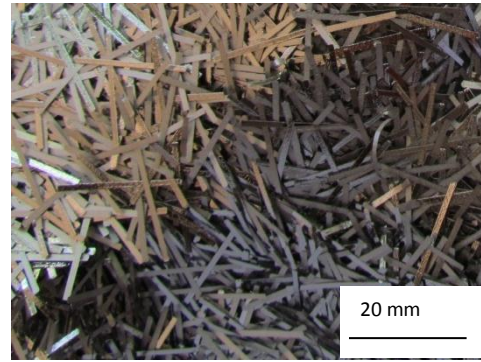
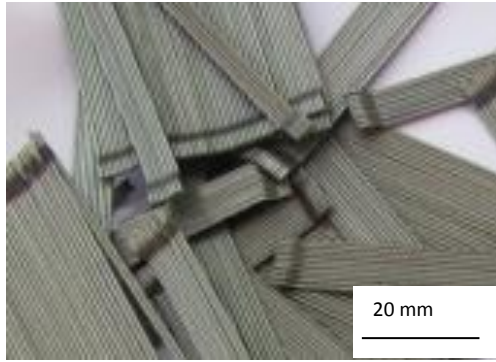


Figure 5.2 Fibres as received.



Figure 5.3 Fibres after 4 weeks of immersion in 3.5 % NaCl solution.

### 5.3 Experimental programme

Flexural toughness testing was done as discussed in Chapter 3 and follows the guidelines given in Section 4.4 of Chapter 4. The fibres were incorporated in M35 grade concrete with the mix proportions as in Table 3.8. The different dosages of fibres used are given in Table 5.2. Note that SF was incorporated at the minimum recommended dosage of  $15 \text{ kg/m}^3$ , based on performance obtained in the test programme as discussed in Chapter 4. Compressive strength tests were conducted at the ages of 3, 7 and 28 days, and flexural tests at the age of 28 days.

Table 5.2 .Concrete designation and fibre dosages

Concrete	Fibre type	Dosage kg/m <sup>3</sup>	Volume fraction, %
F0 (Control)	-	0	0
SF15	SF	15	0.20
AMF10	AMF	10	0.14
AMF20	AMF	20	0.28
AMF30	AMF	30	0.42
S15AMF10	SF	15	0.34
	AMF	10	
S15AMF20	SF	15	0.48
	AMF	20	

#### 5.4 Results and discussions

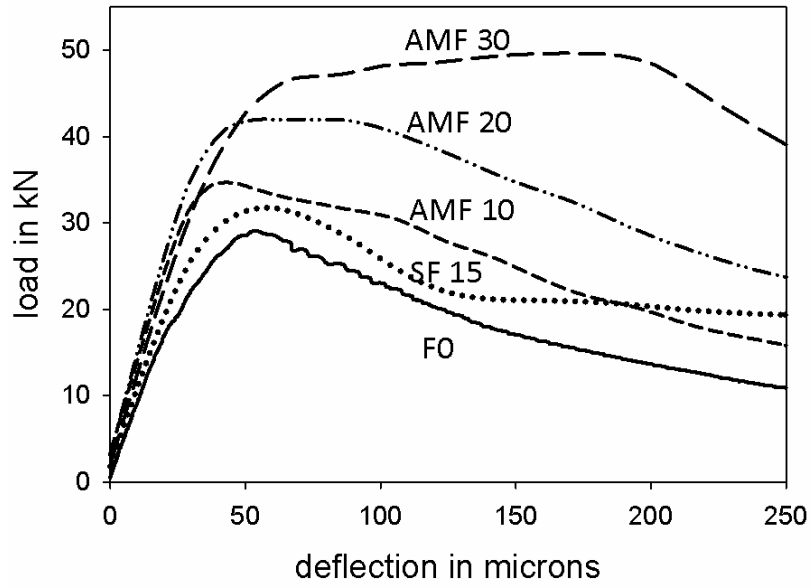
The fresh concrete properties and the compressive strength values at the ages of 3, 7 and 28 days are given in Table 5.3 for all the concretes. The slump values reflect the decrease in workability due to the incorporation of the AMF in spite of an increase in the superplasticizer dosage. This can be attributed to the large number of fibers added in the case of the AMF (i.e., in the order of 8.3 million/m<sup>3</sup> of concrete for a fiber dosage of 30 kg/m<sup>3</sup>), which restricts the flow of the concrete significantly (Pons et al. 2006). Nevertheless, the low variation among the unit weight values indicates that all the mixtures had uniform compaction suggesting that concretes with slump values as low as 40 mm could be used in practice.

The compressive strength values are slightly higher in the concretes with AMF. The evolution of compressive strength and its variability are within the usual range, and not influenced by the incorporation of fibers.

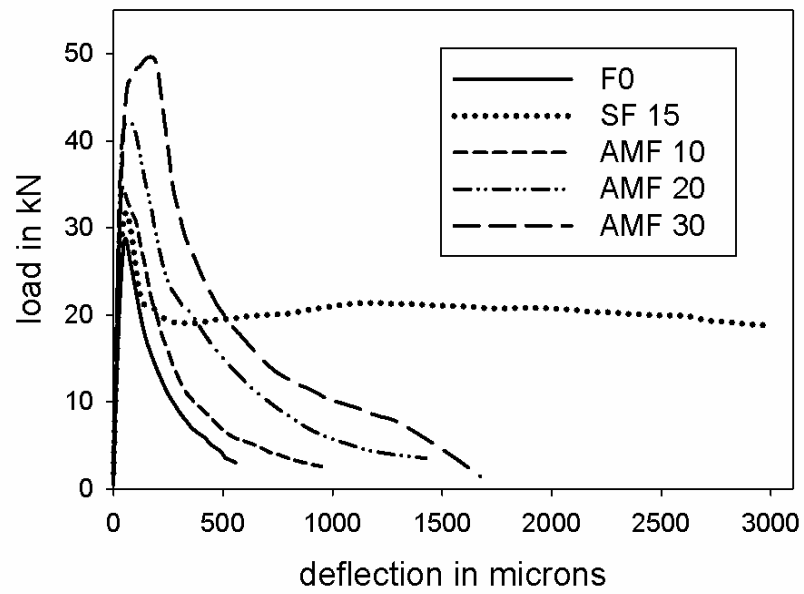
Table 5.3 Fresh concrete properties and compressive strengths

Concrete	Super-plasticizer dosage (% by weight of binder)	Slump mm	Unit weight of fresh concrete kg/m <sup>3</sup>	Compressive strength MPa (mean $\pm$ std. dev)		
				3-day	7-day	28-day
F0	0.05	105	2450	13.4 $\pm$ 2.1	20.2 $\pm$ 0.1	42.4 $\pm$ 4.0
SF15	0.15	130	2410	14.2 $\pm$ 0.7	21.5 $\pm$ 0.5	40.9 $\pm$ 2.6
AMF10	0.13	100	2470	14.7 $\pm$ 0.1	22.7 $\pm$ 0.4	43.0 $\pm$ 1.9
AMF20	0.26	70	2440	14.6 $\pm$ 0.3	22.7 $\pm$ 0.4	43.2 $\pm$ 1.5
AMF30	0.50	40	2415	14.2 $\pm$ 0.5	23.4 $\pm$ 1.1	43.2 $\pm$ 0.5
S15AMF10	0.15	110	2410	15.0 $\pm$ 0.6	24.0 $\pm$ 0.7	42.5 $\pm$ 0.7
S15AMF20	0.35	40	2405	16.3 $\pm$ 1.8	25.2 $\pm$ 0.6	45.2 $\pm$ 0.9

Figure 5.4 shows typical load-deflection curves for the different concretes studied. The curves corresponding to the individual specimens are reported in Appendix C. It can be observed that the incorporation of AMF increases the peak load significantly and leads to hardening-type behavior before the load-carrying capacity drops (Figure 5.4(a)). It can be seen in Figure 5.4(b) that the load decreases significantly in the AMF concrete after a displacement of about 0.3 mm and is almost zero beyond the deflection of about 2 mm. This is in accordance with earlier reports that only higher dosages of AMF (above 0.4 % volume fraction) result in any significant increase in flexural toughness (Won et al. 2013, Choi and Ku 2014). However, the SF concrete, even though the dosage is only 15 kg/m<sup>3</sup>, has a softening response with little effect of the fibers on the peak load but with considerable retention of load-carrying capacity, as expected (Nayar et al. 2014). The differences in the responses suggest that hybrid mixes of SF and AMF could result in superior performance, compared to that of concretes with the individual fibers. Accordingly, tests were performed on the hybrid S15AMF10 and S15AMF20 concretes (see Table 5.2); the typical load-deflection curves of these mixtures are shown in Figure 5.5, along with the curves for concretes with only AMF. The curves corresponding to individual specimens for each mix are given in Appendix C.

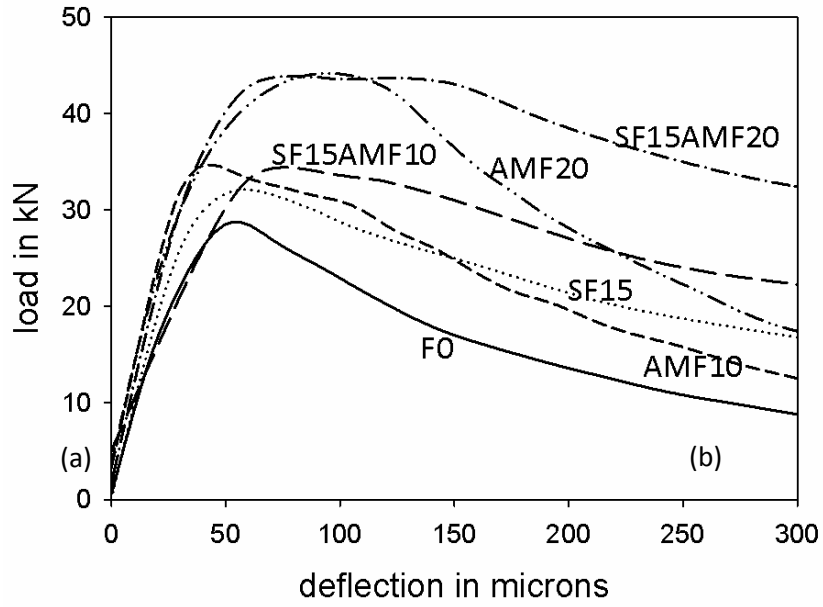


(a)

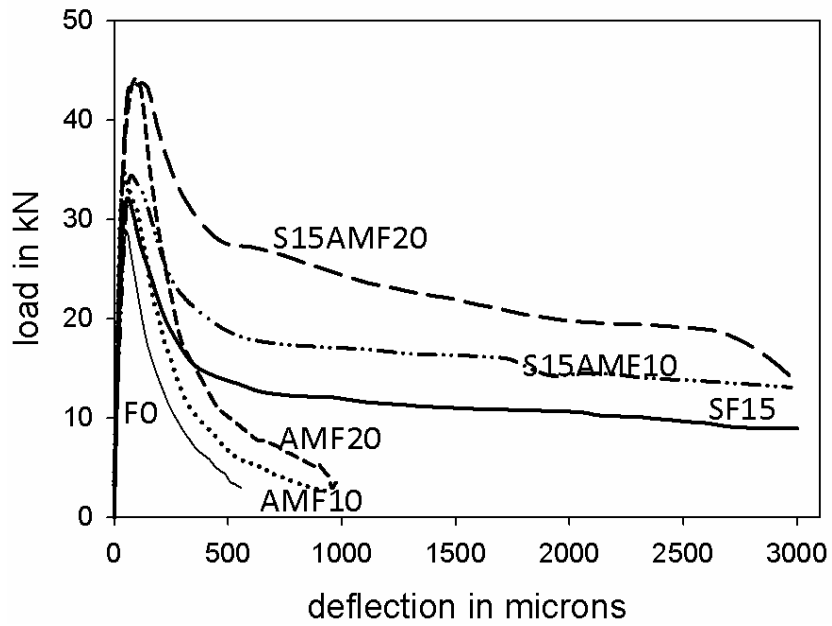


(b)

Figure 5.4 Typical curves for the different concretes shown (a) upto 250  $\mu\text{m}$  deflection, and (b) upto 3000  $\mu\text{m}$  deflection.



(a)



(b)

Figure 5.5 Typical curves of different mixtures including hybrid mixtures (a) upto 200  $\mu\text{m}$  deflection, and (b) upto 3000  $\mu\text{m}$  deflection.

The load-deflection curves of the hybrid mixtures indicate significant enhancement in the peak load, as well as appreciable post-peak load carrying capacity, even at larger deflections. It is

interesting to note that there is better post-peak performance in the hybrid mixtures than in the concretes with individual fibers confirming the synergistic response. For example, the load-deflection curve of SF15AMF10, at larger deflections, exhibits a much higher load-carrying capacity than SF15 though the AMF10 contribution (in isolation) is negligible. The results indicate that the longer fibers provide better synergy since results obtained earlier by Hameed et al. (2009b, 2010) using shorter fibers did not show any comparable synergistic enhancement of properties at lower dosages.

Using the load-deflection curves, the flexural toughness parameters were calculated as discussed in Chapter 2. The average values of the different toughness parameters, for all the mixtures, are shown in Table 5.4, along with the coefficients of variation. It is seen that there is higher scatter in the results obtained for concretes with lower dosages of AMF, while for other concretes the variations are similar to that seen in typical steel fiber reinforced concretes (e.g., Nayar et al. 2014).

From the comparison of results in Table 5.4, the most significant observation is the considerable increase in the flexural strength,  $f_{ct}$ , of the concrete with the addition of AMF fibers with respect to that of plain concrete; an increase of about 30% is obtained when the AMF dosage is  $10 \text{ kg/m}^3$  and of about 90% for a dosage of  $30 \text{ kg/m}^3$ . This can be attributed to the large number of fibers at the crack region that enhance the crack resistance, and to the good bond of these fibers with concrete due to a high specific surface area (Kawatama et al. 2003, Hameed et al. 2010, Won et al. 2013). However, the AMF fiber could be ineffective at larger deflections (beyond 0.5 mm), especially at lower dosages, due to the rupturing of fibers (Pons et al. 2007, Hameed et al. 2010, Won et al. 2012).

The flexural toughness of the hybrid mixtures is much better than that of the mixtures with a single type of fibers due to the synergistic effects. For example, the equivalent flexural and residual strength values at  $n=150$ ,  $f_{e,150}$  and  $f_{r,150}$ , are about 35% more in SF15AMF10 than the values for concrete with steel fiber alone, and the  $R_{e,150}$ -value is about 15% more. Similarly, synergistic behavior has been reported in literature for hybrid mixtures with longer AMF fibers (length = 30 mm) at higher dosages (Granju et al. 2004, Nehdi and Ladanchuk 2004, Pons et al. 2007, Hameed et al. 2009b, 2010). This can also be attributed to the improved anchorage of the macro-fibres due to the confining effect produced by the AMF reinforcement.

Table 5.4 Flexural toughness parameters (means and coefficients of variation)

Concrete	$f_{ct}$ MPa	$f_{e,300}$ (MPa)	$f_{e,150}$ (MPa)	$f_{r,600}$ (MPa)	$f_{r,300}$ (MPa)	$f_{r,150}$ (MPa)	$R_{e,150}$ (%)	$R_{e,300}$ (%)
F0	3.58 (±13.4%)	0.44 (±40.2%)	0.22 (±41.2%)	0	0	0	6 (±33%)	12 (±33%)
SF15	4.48 (±4.3%)	2.38 (±11.2%)	2.24 (±15.9%)	2.16 (±15.9%)	2.17 (±20.5%)	1.87 (±23.8%)	50 (±14%)	53 (±9%)
AMF10	4.56 (±13.6%)	0.92 (±29.8%)	0.46 (±29.8%)	0.40 (±99.0%)	0	0	10 (±23%)	21 (±23%)
AMF20	5.87 (±6.1%)	1.51 (±18.3%)	0.76 (±18.5%)	1.00 (±17.8%)	0	0	13 (±18%)	26 (±19%)
AMF30	6.85 (±4.4%)	2.76 (±11.0%)	1.44 (±15.5%)	2.09 (±19.4%)	0.57 (±80.1%)	0	21 (±12%)	40 (±8%)
S15AMF10	5.43 (±7.0%)	3.33 (±20.2%)	3.08 (±25.2%)	3.09 (±24.6%)	3.04 (±25.1%)	2.56 (±33.8%)	56 (±22%)	61 (±17%)
S15AMF20	6.37 (±7.1%)	3.95 (±15.1%)	3.36 (±16.7%)	3.66 (±17.7%)	3.03 (±22.1%)	2.48 (±21.4%)	53 (±11%)	62 (±9%)

## 5.5 Synergistic behaviour and its implications

It has been suggested that the behaviour of concrete with hybrid reinforcement can be predicted by the simple use of the rule of mixtures (Granju et al. 2004, Pons et al. 2007; Hameed et al. 2010). Consequently, the hybrid behaviour should correspond to:

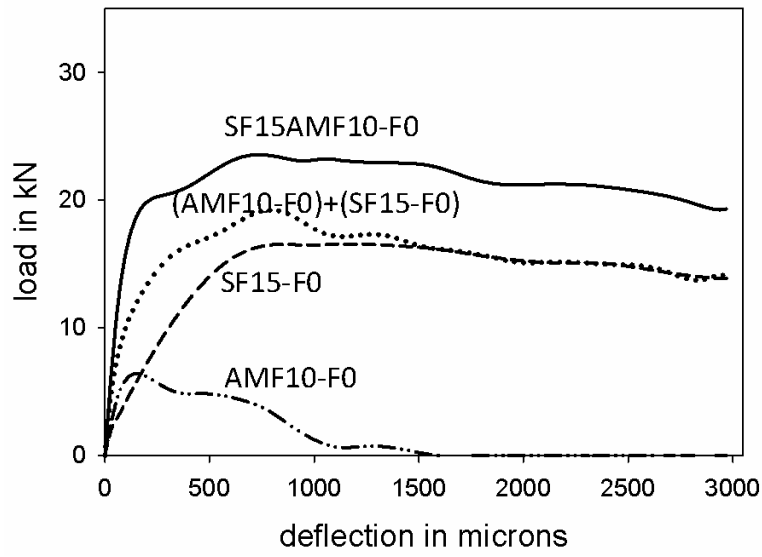
$$\text{FRC response} = \text{Matrix response} + \text{Sum of the fibre responses} \quad (5.1)$$

Accordingly, estimates of the toughness and strength properties of the hybrid fiber concretes were made from the properties obtained experimentally with a single type of fiber. The estimated and measured values of the parameters are shown in Table 5.5. From the comparison, it can be seen that except for the flexural strength, there is always a significant difference between the estimated and measured parameters, with the post-peak load-carrying capacity and toughness being under-estimated. This reflects the beneficial synergy due to the combined effect of the fibers.

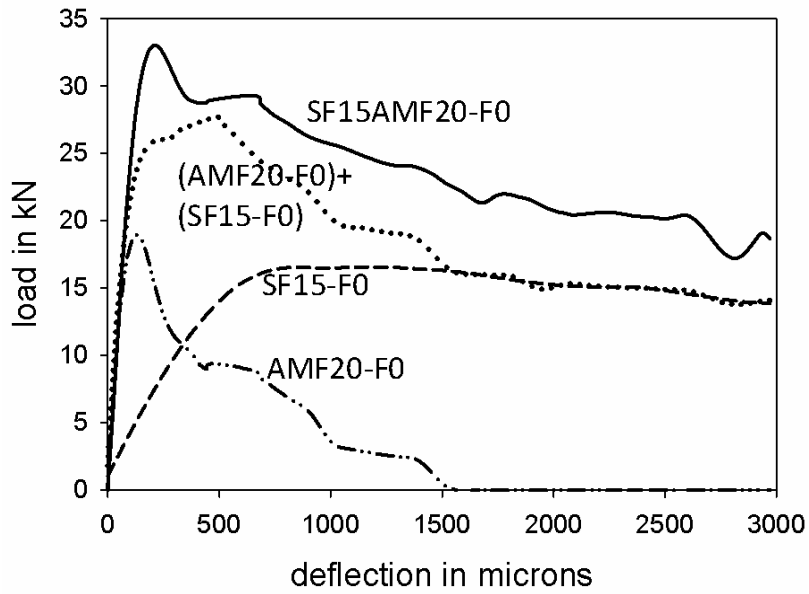
Table 5.5 Comparison of toughness parameters obtained from test results and estimated using the rule of mixtures

Concrete		$f_{ct}$ (MPa)	$f_{e,150}$ (MPa)	$f_{e,300}$ (MPa)	$f_{r,150}$ (MPa)	$f_{r,300}$ (MPa)	$R_{e,150}$ (%)	$R_{e,300}$ (%)
SF15AMF10	Estimated	5.47	2.48	2.86	1.87	2.17	45	52
	Measured	5.43	3.08	3.33	2.56	3.04	56	61
SF15AMF20	Estimated	6.78	2.78	3.45	1.87	2.27	41	50
	Measured	6.37	3.36	3.95	2.48	3.03	53	62

The synergistic effect was further studied by comparing the estimated load-deflection curves with the experimentally-obtained curves. The fiber contribution to the load-deflection response was estimated by subtracting the matrix contribution (F0), as done by Pons et al. (2007), from the average load-deflection curves of the fiber concretes (Figure 5.6); for example, the curve labeled as SF15AMF10-F0 is the curve obtained by subtracting the average load values from the tests on F0 from those of SF15AMF10 (see Figure 5.5) at different displacement values. It can be seen that curves AMF10-F0 and AMF20-F0 show negligible contributions beyond the displacement of about 1 mm whereas the contributions of the hybrid fibers (shown by the curves SF15AMF10-F0 and SF15AMF20-F0) are much more than that of the steel fiber alone (SF15-F0), as well as the sums of the individual contributions (given by the curves SF15-F0+AMF10-F0 and SF15-F0+AMF20-F0). Due to the synergistic effect, the rule of mixtures underestimates the response of the concretes with the hybrid fiber combinations. This is also evident in Figure 5.7, where the estimated load-deflection curves of the concretes with the hybrid fiber combinations (obtained as SF15+AMF10-F0 and SF15+AMF20-F0) are compared with the band of data from the tests on SF15AMF10 and SF15AMF20, respectively. It can clearly be seen that the most of the experimental data lie above the average response estimated with the rule of mixtures.

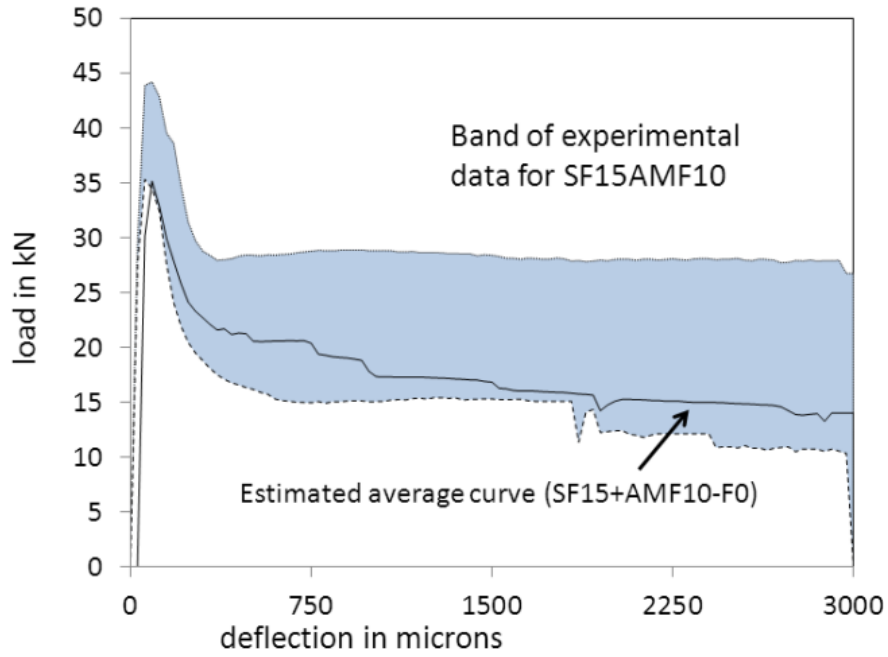


(a)

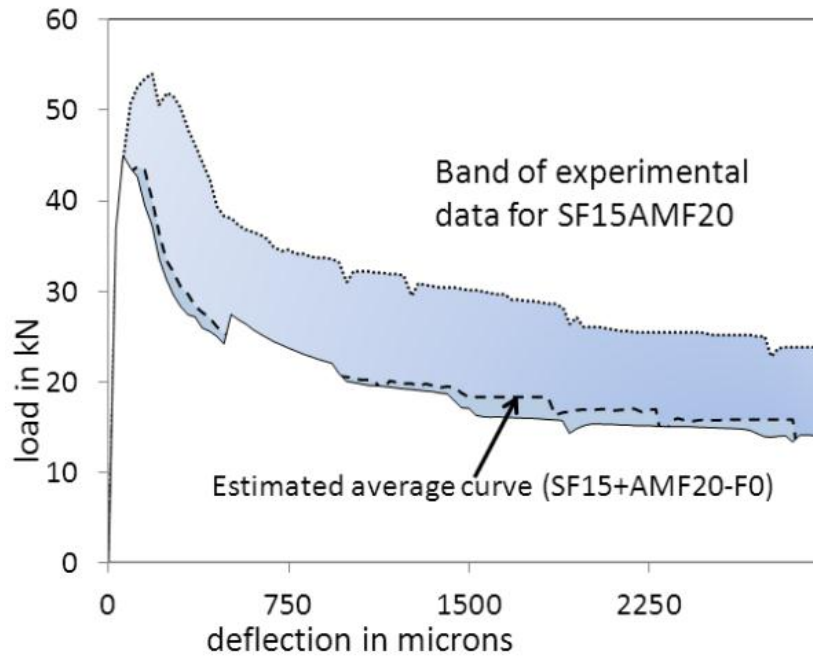


(b)

Figure 5.6 Comparison of fibre contributions to the load deflection behavior for (a) 10 kg/m³ of AMF and (b) 20 kg/m³ of AMF.



(a)



(b)

Figure 5.7 Estimated curve and band of measured load deflection curves (a) for SF15AMF10 mix (b) for SF15AMF20 mix

## 5.6 Summary

The experimental study shows that the contribution of amorphous metallic fibres (AMF) to concretes having hybrid combinations with conventional cold-drawn steel fibres (SF) is significant. The specific conclusions drawn, considering the parameters studied, are:

- From the experimental investigation, the corrosion resistance of AMF fibres in comparison to conventional steel fibres has been demonstrated
- Incorporation of AMF increases the flexural strength of concrete significantly; the increase is about 90 % when its dosage is  $30 \text{ kg/m}^3$ . The addition of SF does not alter the flexural strength considerably, as expected.
- In the post peak regime, the incorporation of AMF could be ineffective at larger deflections (beyond 0.5 mm), especially at lower dosages, due to rupturing of fibers.
- More importantly, the performance of concretes reinforced with the hybrid combinations is significantly enhanced due a synergistic effect between the AMF and SF. For example, the modulus of rupture or flexure strength and the equivalent flexural strength values increase by 21% and 35%, respectively, when  $10 \text{ kg/m}^3$  of AMF are incorporated in a concrete with  $15 \text{ kg/m}^3$  of SF.

# 6 DESIGN METHODOLOGY FOR FIBRE REINFORCED CONCRETE SLABS-ON-GRADE

## 6.1 Introduction

As has been discussed in Chapter 2, there is no standardization of the design and application methodologies for fibre reinforced concrete slabs-on-grade, especially in countries like India where the advent of this technology is relatively new. On a global level, a few guidelines are available, such as the Concrete Society Guidelines for Industrial floorings TR34 (1994, 2003, 2013), ACI 360 R, FIB Model CODE 2010 and DBV recommendations, which have been essentially developed based on the performance of concrete, climatic and usage requirements of the respective countries or regions. Consequently, the current work aims at developing and suggesting a comprehensive design methodology for slabs-on-grade with fibre reinforced concrete, including guidelines for design and application.

This chapter has a brief discussion stating the limitations identified in the existing methods for FRC slabs-on-grade design, followed by a detailed description of the design methodology and design equations. The suitability of the adopted material parameters is also demonstrated using comparisons with test/numerical analysis results from the literature. A parametric study is further discussed in order to identify the significance of each of the design variables. The chapter also presents a complete case of design done as per the suggested method. The design framework is followed by a comparison of the suggested method with existing design guidelines and methods.

## 6.2 Critical factors to be considered in design of slabs-on-grade

For the purpose of analysis it is essential to understand the actions on the slab that cause critical stress conditions. The major actions are discussed below.

### 6.2.1 External actions (wheel loads, rack loadings, line loads, etc.)

Major stresses occurring in the slabs are the tensile/bending stresses developed due to external point/patch loads, uniformly distributed loads and line loads. The most critical in this regard is the patch load, such as that caused by a wheel load or the load from a rack support base, which is

usually approximated as a point load (TR34 2003, Knapton 2005). In the case of industrial flooring, it is essential to consider the positioning of adjacent patch loads representing frames placed side-by-side and choose the load magnitude appropriately. The occurrence of line loads or uniformly distributed loads are also to be considered in design, in terms of stacking loads, fixed equipment loads, partition walls etc.

In addition to loading, an important consideration in the case of design is the position of the load with respect to the edges, joint and corners. From a review of the existing design techniques, it is understood that three loading conditions are critical:

- Load in the centre/interior of the slab (away from the edge of the slab)
- Loading on a free edge
- Loading at a free corner.

Most of the literature on the analysis of concrete slabs-on-grade has discussed the above three positions of loading and have suggested separate equations for the stresses, deflections or moments in the slab in each of these cases (Westergaard 1945, Losberg 1961, Meyerhoff 1962, Ringo and Anderson 1996, TR 34 2003, 2013, ACI 360 R 2010).

### **6.2.2 Thermal and shrinkage stresses**

Though normally not critical for slabs-on-grade, due to the small variations in the exposure conditions, thermal stresses and curling of the slab may occur in exterior slabs or cold storage warehouses due to high thermal gradients across the depth of the slab (Cachim 1999, Beckett 2000, Olesen and Stang 2000, Huang 2004). Shrinkage is a major action to be considered in design, especially in the design of joints and joint spacing, and is, consequently, one of the factors governing the dimensions of the slab in conjunction with the concrete properties and restraints posed by sub base.

### **6.2.3 Fatigue stresses**

Fatigue become important in industrial flooring where frequent and repeated loads occur causing cycling of stresses. However, the use of a dynamic load factor of 1.5 is generally recommended to account for such occurrences and is considered suitable since it is not as critical as in pavements (TR34 2003, Knapton 2005, ACI 360 R)

#### **6.2.4 Impact loading**

Sudden accidental loading could cause impact on the floor, which may be accounted for, if considered significant, by using a suitable factor of safety as suggested by ACI 360 R, though no specific values have been specified.

### **6.3 Limitations of existing approaches to the design of FRC slabs-on-grade**

A detailed review of the existing design methods for FRC slabs-on-grade has been done in Section 3 of Chapter 2. From the review it has been understood that the effective exploitation of the crack resisting potential of fibre reinforced concrete (FRC) by the inclusion of appropriate material parameters in design is a necessity for applications such as slabs-on-grade, where FRC with relatively low dosages of fibres may be employed as "stand-alone" reinforcement. Many design guidelines are available in this area, in addition to those provided by fibre manufacturers (TR34:2003, 2013, ACI 360 R-10, DBV recommendations, DRAMIX Manual, Maccaferri design solution, di Prisco and Mauri 2004). A detailed review of these methods brings out the following shortcomings:

- Most design methods use expressions from analysis done on infinitely large slabs, without considering the actual dimensions and behaviour of the finite slab (TR 34:2003, 2013, ACI 360 R-10), where the cracks interact with the boundaries. The consequent design solutions may underestimate the stresses generated.
- Many methods use material parameters that may not appropriately represent the material in the slab systems. For example, the use of a constant multiplier (e.g., 0.7) for obtaining the characteristic value from the mean value of toughness disregards variations in the fibres due to production quality differences (TR 34:2003, 2013, ACI 360 R-10, DRAMIX Manual). Further, the use of an equivalent flexural strength ratio (instead of the absolute strength) leads to the misinterpretation that the toughness is a multiple of the modulus of rupture (often calculated empirically from the compressive strength) (di Prisco and Mauri 2004, Elsaigh et al. 2005, Altoubat et al. 2008).

- Thermal and shrinkage stresses are not dealt with in detail though they could be significant when the joint spacing is large, and/or the slab is exposed to major environmental changes.

The current study attempts to address the above mentioned limitations, as discussed in the following sections.

## **6.4 Design philosophy**

Incorporating fibres in concrete is expected to impart sufficient rotation capacity to the slab-on-grade during cracking so that the plastic moment capacity of the slab is fully mobilized. The ultimate load may then be estimated with the yield lines forming a mechanism and the regions bounded by the yield lines behaving as rigid-plastic sections. However, the yield line patterns and the corresponding ultimate loads are dependent on the type of loading, slab dimensions and end conditions, as well as the soil pressure distribution (Losberg 1961, Meyehof 1962, Baumann and Weisberg 1983, Meda 2003).

### **6.4.1 Failure pattern**

Based on the various possible cases, the following critical failure patterns may be envisaged to occur for slabs-on-grade.

#### ***6.4.1.1 Case 1: D-cracking at the edges***

In cases where the dimensions of the slabs are not sufficiently large but more than 50% load transfer can be assumed at the joints (i.e., enough to prevent free lifting of slab edges) or the loading is on or near the edge of the slab, the D-shaped failure pattern will govern (Meyerhof 1962, Bauman and Weisberg 1983, Meda 2003). Radial cracks start from under the load location followed by circumferential cracking, limited by the edges of the slab (see Figure 6.1). The radial yield lines are taken to have fully plastic moments and the circumferential yield lines are subjected to negative moments.

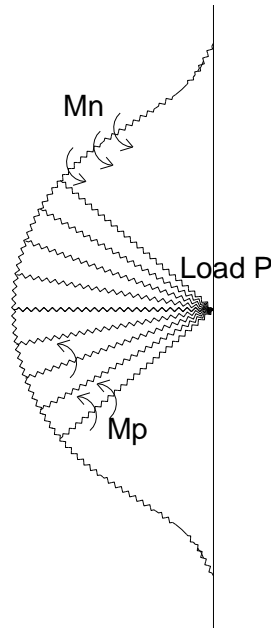


Figure 6.1 D-cracking at the edges

#### 6.4.1.2 Case 2: Circular fan type failure – for interior loading

Such failure has been typically considered in most design documents for FRC flooring, where radial cracks initially appear at the bottom of the slab and widen, followed by circumferential cracking (Figures 6.2 and 6.3). Eventually, the moments along the radial yield lines equal the plastic moment capacity ( $M_p$ ) of the concrete and the negative moment ( $M_n$ ) at the top of the slab reaches the flexural capacity (Losberg 1961, 1978, Meyerhof 1962, Bauman and Weisberg 1983, Rao and Singh 1986, TR34:2003, 2013, ACI 360 R). The appearance of cracking at the top is considered as the failure state. Such failure can occur only when the slab dimensions are large enough to allow the radial yield lines to develop followed by the circumferential yield lines. Meyerhof's solution (Meyerhof 1962), used by many design guidelines, for the ultimate collapse load, is based on the large slab assumption; the condition is that the load should be at least at a distance of  $5l$  from the edge where  $M_n/M_p = 1$ , with  $l$  being the radius of relative stiffness (see Eqn. 2.5). This implies that such failure will occur only when the slab width is at least  $10l$  (i.e., about 6 m for  $E = 3.2$  GPa,  $\mu = 0.15$ ,  $k = 0.1$  N/mm<sup>3</sup> and  $h = 150$  mm). Another possibility for this type of failure to occur is when the stress or load transfer mechanism between slabs is very efficient and the slabs together behave monolithically as a large continuous slab, which cannot normally be expected to happen.

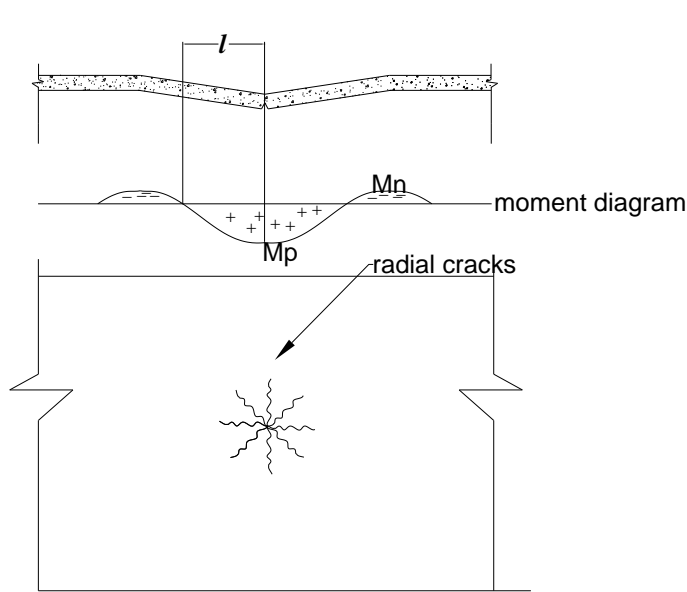


Figure 6.2 Crack initiation and appearance of radial yield lines

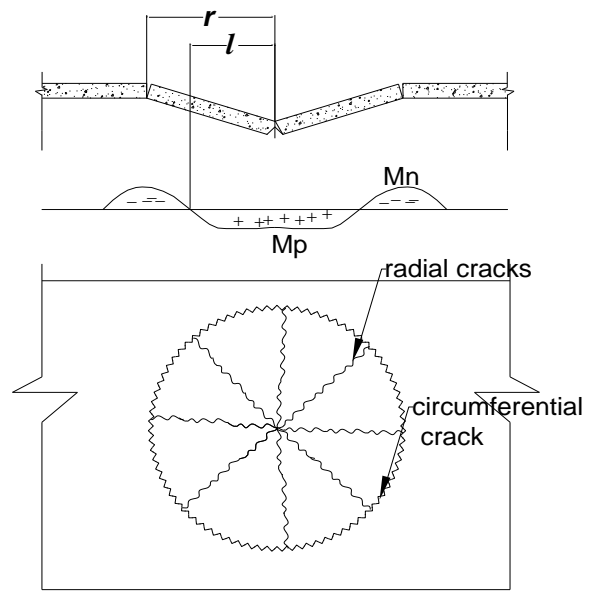


Figure 6.3 Collapse condition: appearance of radial yield lines

**6.4.1.3 Case 3: Centre line cracking – load in the interior of slab with free edges**

Centre line cracking, as shown in Figure 6.4, occurs when the slab is of finite dimensions ( $B \times L$ ) and the edges are free to lift. The moment along all the yield lines may be assumed to be plastic as the slab rotates about the yield lines simultaneously; collapse is governed only by the plastic moment capacity (Meda 2003).

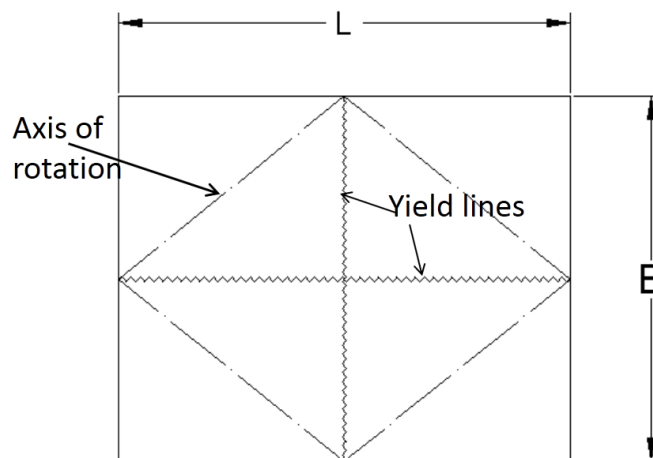


Figure 6.4 Yield line pattern for slabs-on-grade with free edges

## 6.5 Considerations for the choice of joint spacing and slab dimensions

As discussed in the previous section, the failure pattern depends on the dimensions and end conditions of the slab. It is recommended that the dimensions (other than thickness of the slab) and the joint spacing be chosen such that the failure occurs after cracking at the bottom, which will make the fibre reinforcement most advantageous. This implies that the failure pattern should be that of D- or circular-cracking.

Nevertheless, the choice of slab dimensions and joint spacing may at times be governed by temperature variation and shrinkage stresses, in order to restrict curling and transverse cracking. Contraction joints are then needed at appropriate spacing to limit the restraint on the slab, for which the following recommendations compiled from existing standards maybe considered:

- Length/width ratio of the slab = 1 - 1.5 (TR34:2003, TR34 2013)
- Largest dimension between joints to be restricted to 4.5-6 m depending upon the thickness  $h$ , with the smaller value for higher thickness (TR34:2003, TR34:2013, IRC 15, Delatte, 2014). A maximum joint spacing of  $L = 24 h$  has been suggested by Delatte (2014).
- Joints should normally be located along the column lines with intermediate joints located at equal spacing between them (ACI 360R).
- Typically, sawn joints are recommended with groove widths not less than 3 mm and depths of about  $1/3^{\text{rd}}$  to  $1/4^{\text{th}}$  of the thickness of the slab (IRC 15:2002).

Normally, expansion joints do not have to be provided. However, expansion should be permitted wherever the slab is in contact with elements like walls and columns to avoid the generation of lateral loads (TR34:2003, TR34:2013, ACI 360R).

## 6.6 Moment capacity based on equivalent flexural strength

### 6.6.1 Limiting moment capacity estimate

The plastic moment capacity in the FRC slab is taken as the post-cracking moment carrying capacity, which is a function of post-cracking flexural strength, such as the equivalent flexural strength as specified in JSCE SF4 or ICI/TC 01.1. Consequently, the plastic moment capacity per unit length of the slab is estimated as:

$$M_p = f_{e,nk} \frac{h^2}{6} \quad (6.1)$$

where  $f_{e,nk}$  is the characteristic equivalent flexural strength of concrete (obtained from the flexural test of an unnotched prism) until a specified deflection and  $h$  is the thickness of the slab. The equivalent flexural strength is used here instead of the residual strength (as specified in ASTM 1609) since the former represents an average response over a range of crack widths rather than at a specific width and has lower variability than the latter (Parmentier et al. 2008, Vandewalle et al. 2008, Merretz et al. 2011).

The negative moment capacity will be a function of the flexural strength (or modulus of rupture) of the concrete (obtained from the same flexural test) as:

$$M_n = f_{ct,k} \frac{h^2}{6} \quad (6.2)$$

where  $f_{ct,k}$  is the characteristic value of the flexural strength of the concrete.

### 6.6.2 Using equivalent flexural strength instead of the equivalent flexural strength ratio

The toughness parameter adopted in the proposed design method is the equivalent flexural strength,  $f_{e,n}$ , defined as per the Japanese standard JSCE SF4 (1984) and ICI TC/01.1(2014). The use of the strength based term is recommended here mainly due to the limitations identified in using other terms. For example, in many of the existing guidelines, the design is based on the use of equivalent flexural strength ratio,  $R_{e,n}$  as specified by JSCE SF4 (1984) and ASTM 1609 (2010). However, the use of  $R_{e,n}$  for representing the post-cracking capacity is deemed unsuitable due to the fact that normalizing the equivalent flexural strength with peak flexural strength results in the misleading interpretation of the residual capacity in cases where the post-peak

flexural strength enhancement is accompanied by a substantial increase in the flexural strength. This is illustrated in the following case where the load-deflection curves of two different fibres (SFB and SFC) have similar areas under the load deflection curve, as shown in Figure 6.5, at different dosages (30 and 45 kg/m<sup>3</sup>, respectively)

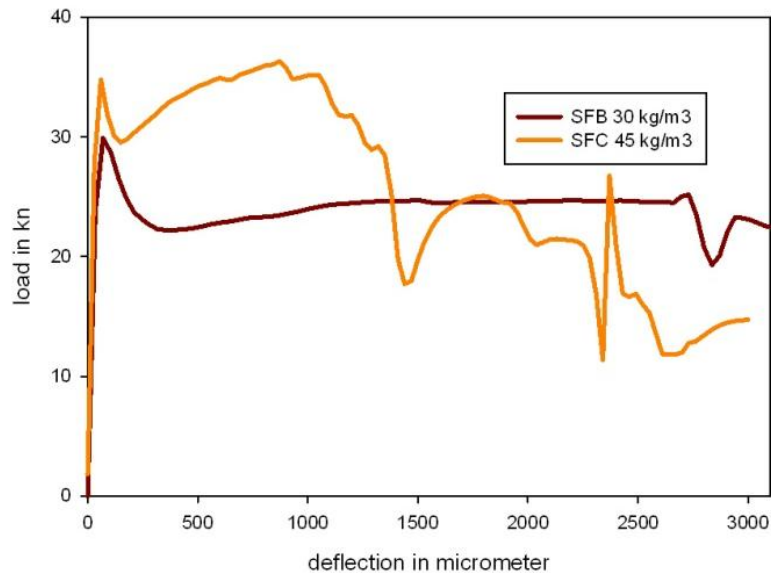


Figure 6.5 Load deflection curves of FRC with two fibres having comparable areas under curve

From the evaluation of the toughness parameters (see Table 6.1), it can be seen that both concretes have comparable equivalent flexural strength  $f_{e,150}$  and so have comparable post-cracking capacity. However, the  $R_{e,150}$  values do not capture this similarity in performance since the peak flexural strength of SFC is higher than that of SFB. On normalization of  $f_{e,150}$  with  $f_{ct}$ , the  $R_{e,150}$  value of SFC works out to be only 71%, which is considerably lower than the  $R_{e,150}$  value of SFB (88%). Suppose we had a requirements of  $f_{ct} > 3.8$  MPa and  $R_{e,150} > 75\%$ , SFC would be rejected even though it shows better performance than SFB. However, if the requirements are  $f_{ct} > 3.8$  MPa and  $f_{e,150} > 2.85$  MPa (i.e.,  $0.75f_{ct}$ ), both the concretes would comply. Concretes with high values of both  $f_{ct}$  and  $f_{e,150}$  are penalised if  $R_{e,150}$  is given as a requirement instead of  $f_{e,150}$ .

Table 6.1. Toughness parameters of FRC having similar area under the load – deflection curve

Fibre type	Area under $P-\delta$ curve (kN mm)	$P_{max}$ (kN)	$P_{e,150}$ (kN)	$f_{ct}$ (MPa)	$f_{e,150}$ (MPa)	$R_{e,150}$ (%)
SFB	77200	29.2	25.8	3.89	3.43	88
SFC	77400	36.5	25.8	4.85	3.44	71

Consider another case of the hybrid mix as shown in Table 6.2. If the values of  $f_{e,150}$  are compared, the value for the hybrid mix SF15AMF20 is about 33% higher than the SF15 mix thus showing a significant enhancement of the post peak flexural capacity. However, if the  $R_{e,150}$  values are compared, the improvement is only 6 %, which is clearly an underestimation of the post-peak capacity. The contradiction occurs since the  $f_{ct}$  of the hybrid mix is higher than the SF15 mix by about 42% thereby camouflaging the advantage of having a higher  $f_{e,150}$  value when normalized with  $f_{ct}$ .

Table 6.2 Toughness parameters of mixes having misrepresentation of post-peak capacity

Concrete	$f_{ct}$ (MPa)	$f_{e,150}$ (MPa)	$R_{e,150}$ (%)
SF15	4.48	2.24	50
S15AMF20	6.37	3.36	53

Consequent to the above discussions, the flexural toughness parameter chosen for the proposed design procedure is the equivalent flexural strength.

### 6.6.3 Justification for deflection limit of $l_s/150$

The design of a slabs-on-grade, as seen in the above section, is based on the values of the flexural strength and equivalent flexural strength of fibre reinforced concrete of the chosen mix. The deflection limit ( $l_s/n$ ), where  $l_s$  is the span of the test beam, for the evaluation of toughness parameter from the four point bending test on unnotched prism specimens is commonly specified as 3 mm, which corresponds to  $l_s/150$  for a span of 450 mm (see Section 2.4.1 in Chapter 2). This deflection limit seems to have been chosen arbitrarily without any relevance to serviceability requirements (Tatnall 2006). The use of the equivalent flexural strength obtained

from the beam test for the deflection limit of  $l_s/150$  implies that the rotation capacity of the slab at the design load should be less than or equal to the rotation of the beam used for determining the toughness parameter at this deflection limit (Vandewalle et al. 2008, Merretz et al. 2011). The following discussion examines whether this condition is realistic in the case of slabs-on-grade designed through the yield line approach.

As discussed in detail in Section 6.4.1.2, circular cracking in FRC slabs-on-grade could occur with the radial yield lines formed along the lines corresponding to the maximum positive moment  $M_p$  and circumferential yield lines corresponding to the maximum negative moment  $M_n$ . Assuming the circular yield lines to occur at a radius of  $r$ , the relation between the maximum yield line rotation  $\theta$  and the displacement of the slab under the load can be written as  $\Delta = r\theta$ . The total maximum crack rotation is given by  $\alpha = 2\theta$ , considering the portions of the slab between the yield lines to be rigid, as shown in Figure 6.6.

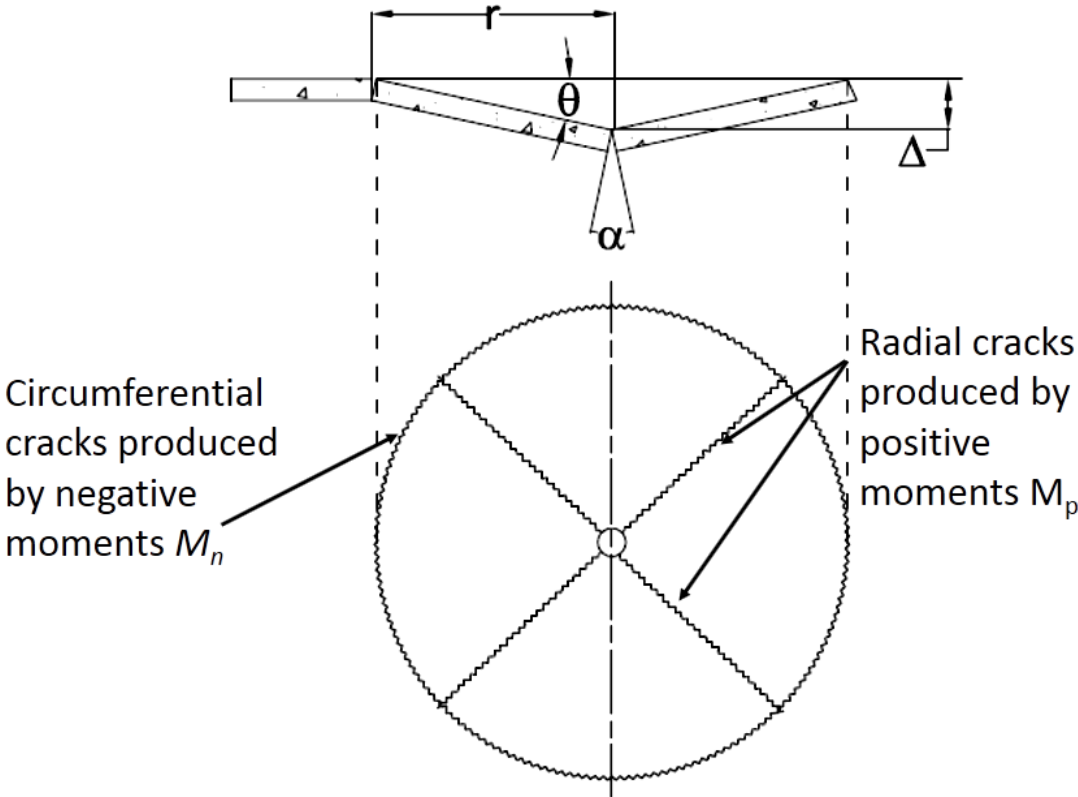


Figure 6.6 Relation between the crack rotation and the slab geometry at collapse

In the case of the prism used in the flexural test for toughness, the rotation at the crack corresponding to the deflection limit, denoted as  $\alpha_b$ , can also be calculated assuming the portions of the beam between the crack and support to be rigid. For a beam of  $150 \times 150$  mm cross-section and 450 mm span, the deflection limit is 3 mm (i.e.,  $l_s/150$ ). For this limiting deflection, the rotation at the crack is obtained as  $\alpha_b = 0.0267$  rad, from a similar analysis as used for the slabs:

$$\frac{\alpha_b}{2} = \frac{l_s/150}{l_s/2} = 0.0133 \text{ rad} \quad (6.3)$$

If we were to calculate the displacement in the slab for the condition  $\alpha = \alpha_b$ , the maximum allowable deflection at the design loading can be found by substituting  $\theta = \alpha_b/2$  (see Figure 6.6):

$$\Delta_{\max} = r\theta = 0.0133r \quad (6.4)$$

For predicting the rotation at limiting moment, we write the virtual work equation for the slab portion as:

$$WD_{\text{internal}} + WD_{\text{ext,soil}} = WD_{\text{ext,load}} \quad (6.5)$$

where  $WD_{\text{internal}}$ ,  $WD_{\text{ext,soil}}$  and  $WD_{\text{ext,load}}$  are the work done internally, by the soil and by the loading, respectively. From yield line analysis for a point load, the following expression can be used for work done due to virtual displacement  $\delta$  at the yield lines (Baumann and Weisberg 1983):

$$2\pi(M_p + M_n) + \frac{k\pi\Delta r^2}{6} = P - 2P \frac{c}{3r} \quad (6.6)$$

where,  $c$  is the contact radius of the loading plate. Rearranging the terms, we get the deflection at failure as:

$$\Delta = \frac{6}{k\pi r^2} \left[ P \left( 1 - \frac{2c}{3r} \right) - 2\pi(M_p + M_n) \right] \quad (6.7)$$

The deflection  $\Delta$  at failure can be calculated from the Equation 6.7 and checked if it is less than or equal to the  $\Delta_{max}$  (i.e.,  $0.0133r$ ) in order to satisfy the limit imposed by the rotation capacity. For the calculation of deflection, the value of  $r$  can be taken as  $2l$ , where  $l$  is the radius of relative stiffness (Timoshenko and Kriger 1959, Meyerhof 1962, Baumann and Weisberg 1983, Falkner and Teutsch 1993, TR34:2003).

In order to assess whether the rotation capacity implied by the beam deflection limit is reasonable, the deflection was calculated for a case corresponding to the test data of Alani et al. (2012), the details of which are given in Table 6.3, where the applied load is taken as 493 kN. Maximum allowable  $M_p$  and  $M_n$  values of 10400 Nmm and 11400 Nmm, respectively, were obtained for the M35 grade concrete with  $40 \text{ kg/m}^3$  of hooked ended steel fibres (see Table 4.3 in Chapter 4), using  $f_{ctk} = 3.04 \text{ MPa}$  and  $f_{e,150} = 2.78 \text{ MPa}$  (see Chapter 4). Also, we obtain  $l = 665.6 \text{ mm}$  and  $c = 6.42 \text{ mm}$ .

Table 6.3 Parameters from the tests by Alani et al. (2012)

Parameters	Values
Slab dimension	6.0 m×6.0 m×0.15 m
Loading plate dimensions	100 mm×100 mm
Strength class	C32/40
Fibre type used	Hooked ended steel fibres
Fibre dosage	40 kg/m <sup>3</sup>
Subgrade modulus, $k$	0.05 N/mm <sup>3</sup>
Elastic modulus of concrete	33500 MPa
Flexural strength of concrete $f_{ctk,fl}$	3.04 MPa
Equivalent flexural strength $f_{e,150k}$	2.78 MPa

From Equation 6.7, the theoretical deflection at the assumed collapse condition is obtained as 7.4 mm. From Equation 6.4,  $\Delta_{max}$  for the corresponding value of  $r$  (i.e.,  $= 2l = 2 \times 665.6 \text{ mm}$ ) is 17.7 mm, which is much higher than the theoretical maximum deflection. The test results of Alani et al. (2012), show a maximum deflection at the centre of the slab of approximately 18 mm at failure, which matches the calculated limiting deflection well (Alani et al. 2012, Alani and Beckett 2013). Since the theoretical deflection at the assumed collapse condition is much lower than the allowable maximum deflection, it is concluded that the use of a toughness parameter

calculated at a deflection limit of 3 mm is acceptable as it provides for more rotation capacity than required before failure occurs in slab.

#### 6.6.4 Design equations

For cases where the limiting moments is given by the sum of the plastic and negative moment capacities (i.e., the circular and D-cracking cases) as  $M_{limit} = M_n + M_p$ , the design equation is formulated in terms of the required flexural and equivalent flexural strengths as:

$$f_{e,150krequired} = \left[ \frac{6M_{applied}}{h^2} - \frac{f_{ct,k}}{\gamma_c} \right] \gamma_c \quad (6.8)$$

where  $\gamma_c$  is the material safety factor. The value of  $\gamma_c$  specified in various existing design guidelines varies from 1.2 – 1.5 (TR34 2003, 2013, ACI 360R-10). However, since the material behaviour is pseudo-ductile and allows for stress redistribution, it is suggested, for slabs-on-grade and pavements, that  $\gamma_c$  be taken as 1.0 -1.2, considering the level of reliability needed.

For cases where the limiting moment is only the plastic moment capacity (i.e., for centre line cracking), the design equation is:

$$f_{e,150krequired} = \left[ \frac{6M_{applied}}{h^2} \right] \gamma_c \quad (6.9)$$

$M_{applied}$  is obtained for each loading condition from yield line or other inelastic analysis as:

$$M_{applied} = f\left(P, \frac{c}{l}\right) \quad (6.10)$$

where  $P$  is the factored applied load,  $c$  is the contact radius of the load application, and  $l$  is the radius of relative stiffness.

Based on the suggested methodology, the design equations for some loading cases are discussed below. Expressions for various cases of loading based on the expected failure pattern are framed here by modifying the moment equations available in literature and presented later in Table 6.4.

##### 6.6.4.1 Single Point load

*D-cracking – load at the edge of slab with significant load transfer along joints*

These expressions are modified forms of Meyerhof's equation for a large slab on Winkler foundation (Meyerhof 1962, TR34 2003):

For  $c/l = 0$ ,

$$f_{e,150k} = \frac{2}{\pi} \left[ \frac{6P}{h^2} - \left( \frac{\pi}{2} + 2 \right) \frac{f_{ctk}}{\gamma_c} \right] \gamma_c \quad (6.11)$$

For  $c/l > 0.2$ ,

$$f_{e,150k} = \left[ \frac{6}{\pi h^2} \left[ 1 - \frac{2c}{3l} \right] P - \left( 1 + \frac{4}{\pi} \right) \frac{f_{ctk}}{\gamma_c} \right] \gamma_c \quad (6.12)$$

*Circular type failure – load at the interior of a large slab (see Section 6.4.1.2)*

These expressions are also modified forms of Meyerhof's equation for a large slab on Winkler foundation:

For  $c/l = 0$ ,

$$f_{e,150k} = \left[ \frac{6P}{2\pi h^2} - \frac{f_{ctk}}{\gamma_c} \right] \gamma_c \quad (6.13)$$

For  $c/l > 0.2$ ,

$$f_{e,150k} = \left( \left[ \frac{6P}{4\pi h^2} \left[ 1 - \frac{c}{3l} \right] \right] - \frac{f_{ctk}}{\gamma_c} \right) \gamma_c \quad (6.14)$$

*Centre line failure – for square slabs with finite dimensions and true free edges*

In case of square slabs, for the failure pattern as shown in Figure 6.4 the expressions of yield line solutions given by Meda (2003) are considered as they are based on the plastic rotation capacity along the central yield lines. The expression for the design criteria is adapted from Meda (2003) and presented as:

$$f_{e,150k} = \gamma_c \frac{3P}{4h^2} \left[ 1 + \left( \frac{k}{6 \left( \frac{K_s}{b^2} \right)} \right) \right]^{-1} \quad (6.15)$$

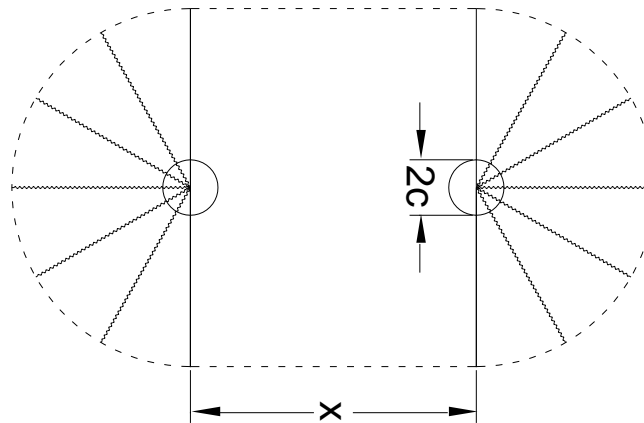
where  $K_s$  is the slab stiffness given by  $K_s = \frac{86D}{\left(b \times \frac{\sqrt{2}}{2}\right)^2}$  and  $D=kl^4$ , with  $b$  = width of the square

slab (Meda 2003).

For a rectangular slab, similar expressions have to be derived for the possible yield pattern since the yield line locations and the axis of rotation will be different.

#### 6.6.4.2 Multiple point loads

When many point loads have to be considered and the adjacent point loads are close enough ( $x < 2h$ ) to assume the action to be concurrent with each other, where  $x$  is the centre to centre distance between the loads and  $h$  is the slab thickness, Meyerhof suggests the use of an equivalent contact radius to combine the action of two point loads as a single point load.



However, if the loads are at considerable distance from each other (i.e.,  $x \geq 2h$ ), then the following design equations based on Meyerhof's analysis will be valid.

For dual point loads at an interior location, we can use the following expressions as (Meyerhof 1962):

For  $c/l = 0$ ,

$$f_{e,150k} = \left[ \frac{6P}{h^2 \left(2\pi + 1.8 \frac{x}{l}\right)} - \frac{f_{ctk}}{\gamma_c} \right] \gamma_c \quad (6.16)$$

For  $c/l > 0.2$ ,

$$f_{e,150k} = \left[ \frac{6P}{h^2 \left[ \frac{4\pi}{(1-3c/l)} + \frac{1.8x}{(l-c/2)} \right]} - \frac{f_{ctk}}{\gamma_c} \right] \gamma_c \quad (6.17)$$

In the case of multiple point loads at the edge, an estimate of the required flexural strength could be made following the recommendation in TR34 2003 that the collapse load at the edge is approximately 50% of that for interior position. Accordingly, the required equivalent flexural strength expressions for edge load would be:

For  $c/l = 0$ ,

$$f_{e,150k} = \left[ \frac{12P}{h^2 (2\pi + 1.8x/l)} - \frac{f_{ctk}}{\gamma_c} \right] \gamma_c \quad (6.18)$$

For  $c/l > 0.2$ ,

$$f_{e,150k} = \left[ \frac{12P}{h^2 \left[ \frac{4\pi}{(1-3c/l)} + \frac{1.8x}{(l-c/2)} \right]} - \frac{f_{ctk}}{\gamma_c} \right] \gamma_c \quad (6.19)$$

In the case of quadruple point loads at interior locations, we can use the following expressions: (Meyerhof 1962)

For  $c/l = 0$ ,

$$f_{e,150k} = \left[ \frac{6P}{h^2 \left[ 2\pi + \frac{1.8(x+y)}{l} \right]} - \frac{f_{ctk}}{\gamma_c} \right] \gamma_c \quad (6.20)$$

For  $c/l > 0.2$ ,

$$f_{e,150k} = \left[ \frac{6P}{h^2 \left[ \frac{4\pi}{(1-c/3l)} + \frac{1.8(x+y)}{(l-c/2)} \right]} - \frac{f_{ctk}}{\gamma_c} \right] \gamma_c \quad (6.21)$$

For the edge loading position, the same assumptions as for dual point loads can be made leading to the following expressions (Meyerhof 1962, TR34:2003, 2013):

For  $c/l = 0$ ,

$$f_{e,150k} = \left[ \frac{12P}{h^2 \left[ 2\pi + \frac{1.8(x+y)}{l} \right]} - \frac{f_{ctk}}{\gamma_c} \right] \gamma_c \quad (6.22)$$

For  $c/l > 0.2, c$

$$f_{e,150k} = \left[ \frac{12P}{h^2 \left[ \frac{4\pi}{(1-c/3l)} + \frac{1.8(x+y)}{(l-c/2)} \right]} - \frac{f_{ctk}}{\gamma_c} \right] \gamma_c \quad (6.23)$$

For values between  $c/l > 0$  and  $c/l = 0.2$ , linear interpolation of values may be used.

#### ***6.6.4.3 Line loads and uniformly distributed load***

Owing to limited inelastic analysis and design techniques available in the form suitable for slabs-on-grade, the classical Hetenyi's elastic analysis is recommended for line loads and uniformly distributed loads, as suggested in TR34 (2003, 2013). Since the method basically assumes elastic stresses in the section, post-cracking residual flexural strength capacity cannot be used in the design (TR34:2003, 2013).

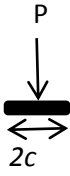
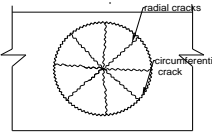
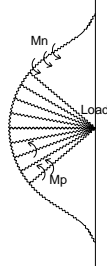
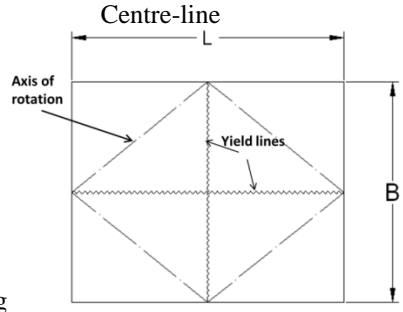
#### ***6.6.4.4 Load at a corner of the slab***

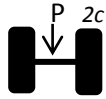
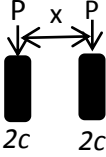
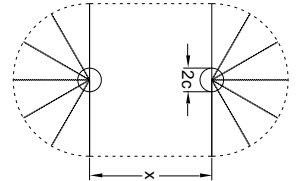
It is understood that the transfer mechanism at the corners should be designed with proper detailing so as to ensure 100% load transfer. Therefore, in the design, corner loads will not be considered to govern. In the undesirable case of inadequate load transfer, positive sagging moments will not be mobilized due to the cantilever action and the design has to be based on the elastic flexural capacity.

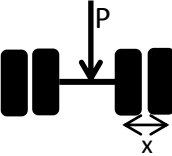
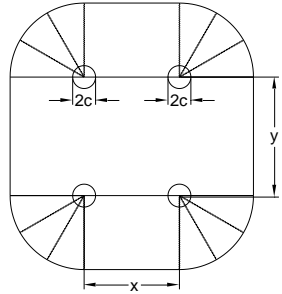
#### **6.6.5 Summary of the design expressions**

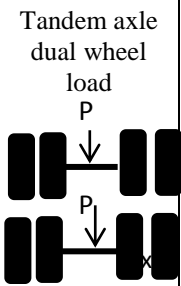
Various cases of loading and positions of loading as applicable to slabs-on-grade have been addressed. In general, the design expressions have been formulated to determine the characteristic value of the required equivalent flexural strength based on inelastic/elastic moment equations. The design expressions applicable for each case are presented in Table 6.4.

Table 6.4. Design expressions for each loading case as per the suggested method

Load type	Load approximation	Load magnitude	Position of load	Failure pattern	Design expression
Rack or Post loads,  	Point load	P	Interior	Circular 	$\text{for } c/l = 0 \quad f_{e,150k} = \left[ \frac{6P}{2\pi\pi^2} - \frac{f_{ctk}}{\gamma_c} \right] \gamma_c$ $\text{for } c/l > 0.2 \quad f_{e,150k} = \left[ \frac{6P}{4\pi h^2} \left[ 1 - \frac{c}{3l} \right] - \frac{f_{ctk}}{\gamma_c} \right] \gamma_c$
			Edge/Interior		$\text{for } c/l = 0 \quad f_{e,150k} = \frac{2}{\pi} \left[ \frac{6P}{h^2} - \left( \frac{\pi}{2} + 2 \right) \frac{f_{ctk}}{\gamma_c} \right] \gamma_c$ $\text{for } c/l > 0.2 \quad f_{e,150k} = \frac{6}{\pi h^2} \left[ \left[ 1 - \frac{2c}{3l} \right] P - \left( 1 + \frac{4}{\pi} \right) \frac{f_{ctk}}{\gamma_c} \right] \gamma_c$
			Interior		$f_{e,150k} = \frac{3P}{4h^2} \left[ 1 + \left( \frac{k}{6 \left( \frac{K_s}{B^2} \right)} \right) \right]^{-1} \gamma_c$ $K_s = \frac{86D}{\left( B \times \frac{\sqrt{2}}{2} \right)^2} \quad D = kl^4$

Load type	Load approximation	Load magnitude	Position of load	Failure pattern	Design expression
Axle load 	Point load	P/2		Design approach is same as point load at various locations and failure patterns	
Dual post loads 	Dual point loads	P	Interior	Circular/Semi-circular 	for $c/l = 0$ $f_{e,150k} = \left[ \frac{6P}{h^2(2\pi + 1.8x/l)} - \frac{f_{ctk}}{\gamma_c} \right] \gamma_c$  for $c/l > 0.2$ $f_{e,150k} = \left[ \frac{6P}{h^2 \left[ \frac{4\pi}{(1 - 3c/l)} + \frac{1.8x}{(l - c/2)} \right]} - \frac{f_{ctk}}{\gamma_c} \right] \gamma_c$
Edge			-	for $c/l = 0$ $f_{e,150k} = \left[ \frac{12P}{h^2(2\pi + 1.8x/l)} - \frac{f_{ctk}}{\gamma_c} \right] \gamma_c$  for $c/l > 0.2$ $f_{e,150k} = \left[ \frac{12P}{h^2 \left[ \frac{4\pi}{(1 - 3c/l)} + \frac{1.8x}{(l - c/2)} \right]} - \frac{f_{ctk}}{\gamma_c} \right] \gamma_c$	

<p>Single axle dual wheel load</p> 	<p>Dual point load</p>	<p>P/4</p>	<p>Design approach is same as dual point load at various locations and failure patterns</p>		
<p>Quadruple point load</p>	<p>Four point loads with <math>x &lt; 2h</math></p>	<p>P</p>	<p>Interior</p>		<p>Load at interior point in slab</p> <p>for <math>c/l=0</math></p> $f_{e,150k} = \left[ \frac{6P}{h^2 \left[ 2\pi + \frac{1.8(x+y)}{l} \right]} - \frac{f_{ctk}}{\gamma_c} \right] \gamma_c$ <p>for <math>c/l &gt; 0.2</math></p> $f_{e,150k} = \left[ \frac{6P}{h^2 \left[ \frac{4\pi}{(1-3c/l)} + \frac{1.8x}{(l-c/2)} \right]} - \frac{f_{ctk}}{\gamma_c} \right] \gamma_c$

			Edge	<p>for <math>c/l = 0</math></p> $f_{e,150k} = \left[ \frac{12P}{h^2 \left[ 2\pi + \frac{1.8(x+y)}{l} \right]} - \frac{f_{ctk}}{\gamma_c} \right] \gamma_c$ <p>for <math>c/l &gt; 0.2</math></p> $f_{e,nk} = \left[ \frac{6P}{h^2 \left[ \frac{4\pi}{(1-3c/l)} + \frac{1.8x}{(l-c/2)} \right]} - \frac{f_{ctk}}{\gamma_c} \right] \gamma_c$
<p>Tandem axle dual wheel load</p> 	Quadruple point load	P/4	Design approach is same as quadruple point load at various locations and failure patterns	

## 6.7 Validation of design equations in terms of load-carrying capacity

In order to validate the proposed methodology, the allowable loads obtained as per the suggested design expressions have been compared with results available in the literature.

### 6.7.1.1 Case 1: D-cracking due to load at edge

The allowable load as per Equation 6.12 was determined and compared with the results of Belletti et al. from slab tests on FRC slabs with edge loading (Belletti et al. 2008, Sorelli et al. 2006). The tests were performed on a 3 m × 3 m slab of 150 mm thickness made with M25 concrete. Steel fibres of 50 mm length and aspect ratio of 50 were incorporated in the concrete at a dosage of 0.38 % volume fraction. The slabs were supported at the bottom on steel supports (similar to springs) at constant spacing to reproduce a Winkler foundation and the loading was done using a hydraulic jack with a loading plate of dimension 200 mm square (Belletti et al. 2008, Sorelli et al. 2006). The ultimate load was defined as the load at collapse of the slab. The test parameters used in the design are listed in Table 6.5.

Table 6.5 Parameters from the tests by Belletti et al. (2008)

Parameter	Value
Strength class	C25/30
Thickness of slab (mm)	150
Subgrade modulus, $k$ (N/mm <sup>3</sup> )	0.08
E – modulus of concrete (MPa)	21000
Poisson's ratio	0.15
Dimension of loading plate (mm)	200 × 200

In order to estimate the flexural toughness parameters to be input in the design, the mean tensile strength value of 1.79 MPa reported in the experimental programme was converted to flexural strength using the expression given in TR34 (2003, 2013):

$$f_{ct} = f_{tensile} \left( 1.6 - \frac{h}{1000} \right) \quad (6.24)$$

and the flexural strength was obtained as 2.6 MPa.

From the data obtained from Bekaert for 50 mm length hooked ended steel fibres, the  $R_{e,150}$  value of 65% was used to convert the flexural strength to equivalent flexural strength for the given dosage of 0.38 % (30 kg/m<sup>3</sup>) as  $f_{e,150} = 0.65 \times 2.6 = 1.7$  MPa

The derived design parameters are  $l = 450$  mm and  $c = 112.4$ .mm, and stresses due to temperature and shrinkage are neglected. The load obtained from Equation 6.12 is 108 kN, which is lower than the experimental value of 120 kN. So, the design equation can be considered as conservative in this case.

#### ***6.7.1.2 Case 2: Circular cracking due to load at the interior position***

The allowable load as per Equations 6.13 and 6.14 was validated using the experimental work done on large slabs by Alani et al. (2012), which has been already discussed in Section 6.6.3. The tests were done on 6 m  $\times$  6 m slabs with 150 mm thickness. The slab with concrete of strength class C32/40 and 40 kg/m<sup>3</sup> of 60 mm length hooked-ended fibres has been considered. The details of the test parameters have already been given in Table 6.3. The failure has been reported to be due to punching and it has been mentioned that no cracks were visible at the top of the slab at failure (Alani et al. 2012, Alani and Beckett 2013).

The derived design parameters are  $l = 665$  mm and  $c = 56.4$  mm. In order to determine the moment carrying capacity, the reported flexural strength of 4.2 MPa was used to obtain the equivalent flexural strength, using the reported  $R_{e,150}$  value (48%), as  $0.48 \times 4.2 = 2.0$  MPa. From the obtained material parameters, the maximum allowable load for the case where  $c/l = 0.085$  is obtained, by interpolating the design values for  $c/l = 0$  (Equation 6.13) and  $c/l = 0.2$  (Equation 6.14), and works out to be 218 kN, which is much lower than the reported failure load of 493 kN. Thus, the proposed method gives a conservative result for the case studied.

Another result chosen here for validating the case of circular cracking is from the numerical analysis of infinite slabs on Winkler foundation by Shentu et al. (1997). The study uses finite element analysis of a circular slab, which is modeled as part of an infinite slab by providing restriction to horizontal movement of the circular slab and allowing for vertical movement. Though the case reported in the work is with plain concrete (without fibres), the study was chosen for validation since Meyerhof's method is also applicable for such a case, with the limiting moment equation being governed by the negative moment capacity (Meyerhof 1962); the plastic moment capacity is taken as zero in the design equation.

The slab parameters used in the study and relevant to the design are reported in Table 6.6. The calculations are done neglecting the stresses due to temperature and shrinkage. As per the

suggested method, the maximum allowable load from Equations 6.13 and 6.14 (for  $c/l < 0.2$ ) is 85 kN, which is much lower than the reported load of 240 kN at first visible cracking at the top of the slab.

Table 6.6 Parameters from Shentu et al. (1997)

Parameter	Value
Compressive strength	25.5 MPa
Concrete tensile strength (MPa)	2.17
Thickness of slab (mm)	160
Subgrade modulus, $k$ (N/mm <sup>3</sup> )	0.02
E – modulus of concrete (MPa)	26000
Poisson's ratio	0.2
Contact radius of load (mm)	100

### 6.7.1.3 Case 3: Centre line cracking validation

The maximum allowable load obtained as per the suggested method using the Equation 6.15 has been compared to the results of tests on FRC slabs by Falkner and Teutsch (1993); the test parameters are given in Table 6.7. The tests were done on a 3 m square slab resting on cork subbase to simulate Winkler foundation. The loading was done until complete collapse (due to punching), and the loads at the occurrence of cracking at the slab edge and at failure have been reported. The test report indicates the failure pattern to be centre-line cracking. This confirms the present criteria as the slab dimensions do not meet the conditions for circular cracking to occur, and the free edge conditions, which permit the uplift of the slab rule out D-cracking. The terms needed for applying Equation 6.14 were calculated as  $l = 720$  mm and  $K_s = 129$  kN/mm using the parameters in Table 6.7. The material parameters needed were taken from the results of the tests on M35 grade concrete done at IITM for similar fibres and same dosage (see Table 4.3). The calculated load capacity is 124 kN, which falls below the reported fracture load of 165 kN from the test results. Thus the design equation is, in this case, conservative.

Table 6.7 Parameters from the tests of Falkner and Teutsch (1993)

Parameters	Values
Slab dimension	3.0 m × 3.0 m × 0.15 m
Loading plate dimensions	120 mm × 120 mm
Grade of concrete	C30/37
Fibre type used	Steel fibres, 60 mm long, diameter of 0.75 mm (Dramix RC 80/60 fibres)
Fibre dosage	20 kg/m <sup>3</sup>
Bedding type	Cork with k = 0.025 N/mm <sup>3</sup>
Elastic modulus of concrete	23400 N/mm <sup>2</sup>
Mean flexural strength of concrete $f_{ct}$	4.52 MPa*
Mean equivalent flexural strength $f_{e,150}$	3.19 MPa*

\*Estimated from tests performed on similar FRC with same grade of concrete, fibre type and fibre dosage at IIT

Madras (see Table 4.3)

## 6.8 Design for thermal stresses

In cases where the temperature variations are significant, the design has to account for thermal stresses. Axial tensile forces could occur if the temperature change is uniform over the depth (which usually occurs in thinner slabs). A conservative estimate of the consequent axial stresses has been suggested by Ghosh and Dinakaran (1970), and Yoder and Witzack (1975), as:

$$\sigma_{\Delta T_{axial}} = 24 \frac{wLf}{h} \quad (6.25)$$

where  $w$  = weight of slab, in N/m<sup>2</sup>,  $L$  = length of slab in m,  $f$  = coefficient of subgrade restraint (<1.0), and  $h$  = thickness of slab, in m. However, these stresses are generally negligible and are, consequently, not taken into account in practice.

Flexural stresses could be generated when there are substantial temperature gradients (Losberg 1978, Gettu et al. 2000, TR34: 2003), which can reduce the negative moment capacity to resist applied loads, affecting the failure occurring with circular and D-cracking:

$$M_{limit} = M_p + (M_n - M_{\Delta T}) \quad (6.26)$$

Therefore, the required equivalent flexural strength is to be modified to account for this, as:

$$f_{e,nkrequired} = \frac{6P}{h^2} f\left(\frac{c}{l}\right) - f_{ctk} + f_{\Delta T} \quad (6.27)$$

where  $f_{\Delta T}$  is the flexural stress due to the temperature differential ( $\Delta T$ ) in the slab, which can be estimated using the classical Bradbury's equation, as:

$$f_{\Delta T} = \frac{E\alpha\Delta T}{2(1-\nu^2)} (C_1 + \nu C_2) \quad (6.28)$$

where  $\alpha$  is the coefficient of thermal expansion, and  $C_1$  and  $C_2$  are the Bradbury's correction factors for curling in a finite slab, which are obtained from charts prepared for various values of  $B/l$ , where  $B$  is the joint spacing (Yoder and Witzack 1975).

## 6.9 Design for shrinkage stresses

Proper concrete mix design and good construction practices are key to reducing shrinkage stresses in concrete especially in the plastic stage. In the hardened concrete, the shrinkage stresses can be considerably reduced by providing friction relief layers, such as polyethylene sheets, so as to reduce the restraint against slab movement due to shrinkage and by providing joints at adequate intervals.

Though a few researchers have reported a qualitative link between restrained shrinkage stress and the cracking potential obtained from the restrained ring test, no models are available to predict the stresses in the slab from the test parameters (Weiss and Shah 1998, See et al. 2004, Hossain and Weiss 2004). Here, an approach similar to that used for curling stresses is recommended, in line with the method suggested in TR 34:2003, to account for the shrinkage stresses. The shrinkage stresses estimated from ultimate (free) shrinkage strain values ( $\epsilon_{sh}$ ) is reduced from the total negative moment capacity, as:

$$M_{limit} = M_p + (M_n - M_{\Delta T} - M_{sh}) \quad (6.29)$$

and the flexural stress associated with the moment due to shrinkage strain is calculated as:

$$f_{sh} = E\epsilon_{sh} \quad (6.30)$$

where  $E$  is the modulus of elasticity of concrete and  $\epsilon_{sh}$  is the ultimate shrinkage strain.

In the absence of  $\varepsilon_{sh}$  data for the concrete used in the slab, a value between 300–500 microstrains may be assumed. Further, a restraint factor of 0.2 can be taken when a friction release layer is used, following TR34 (2003), and the reduced shrinkage stresses is then given as:

$$f_{sh} = 0.2E_{cm}\varepsilon_{sh} \quad (6.31)$$

Thus, the generalised design equation, including the shrinkage stresses and temperature stresses, can be written as:

$$f_{e,nkrequired} = \left[ \frac{6P}{h^2} f(c/l) - A \frac{f_{ctk}}{\gamma_c} + f_{\Delta T} + f_{sh} \right] \gamma_c \quad (6.32)$$

where A represents a constant that depends on the moment function used in the inelastic analysis. For the cases discussed in Section 6.6.5 the value of A is listed in Table 6.8 below

Table 6.8 Values of constant A to be used in Eqn. 6.32 for various load cases

Load approximation	Position of load	Expected failure pattern	Value of A
Point load	Interior	Circular cracking	1
	Edge/Interior	D-cracking	$(\pi/2)+2$
	Interior	Center line cracking	0
Dual point load	Interior	Circular/Semi-circular	1
	Edge	D-cracking	1
Quadruple point loads	Interior	Circular/Semi-circular	1
	Edge	D-cracking	1

## 6.10 Design check

Once the critical equivalent flexural strength value is determined by considering all possible loading and failure patterns, this can be specified as the performance requirement for choosing

the fibre type, dosage and concrete mix, for a specified slab thickness. The choice can be made using any existing material database or test data.

From the actual parameters corresponding to the fibre type, dosage and concrete mix to be used in the slab, preferably from test data, a final design check is recommended. The maximum allowable load should be calculated using the relevant inelastic design equations (e.g., Equation 6.32), and it should be ensured that the following is satisfied:

$$P_{allowable} > P_{actual} \quad (6.33)$$

## 6.11 Parametric study for the suggested method

In order to understand the influence of various parameters on the design method, a parametric study was done by taking three variables, viz., load, thickness and subgrade modulus. Though the grade of concrete is also a variable, this has been taken as M35 throughout the study due the availability of test data for various fibres in that grade.

### 6.11.1 Parametric study 1 – Influence of load magnitude on the design solutions

Variable parameter – Load  $P$

Constant parameters – Thickness  $h$ , Modulus of subgrade  $k$ , Grade of concrete

Types of fibres used – SFA, SFB, SFC, SFD

The design was done for values of axle loads, as shown in Table 6.9, and solutions were obtained in terms of the minimum required fibre dosage, for given slab thickness and modulus of subgrade.

The required dosages were obtained assuming different steel fibres for which material parameters were available (from Table 4.3). From the results given in Table 6.8, it can be seen that for higher loads, the use of fibres with very high variability, i.e., SFC and SFD (as seen from Table 4.5), will require much higher dosages than those used in the experimental programme discussed in Chapter 4. Further, for the chosen thickness and subgrade modulus, each fibre will require a different dosage for the same load. So, a lower dosage of a particular fibre could give the same or better performance than another fibre at a higher dosage of (say, 10 kg/m<sup>3</sup> of SFB gives better performance than 15 kg/m<sup>3</sup> of SFA). Thus, arbitrarily specifying a dosage applicable

to all fibre brands in design/contractual specifications could be unconservative, and rather a minimum required  $f_{e,150}$  should be specified.

Table 6.9 Results of parametric study of suggested method with load as variable

Fibre type	Load (kN)	Minimum required dosage (kg/m <sup>3</sup> )
SFA	40	15
	60	15
	70	28
	80	>45
SFB	40	10
	60	10
	70	18
	80	30
SFC	40	15
	60	15
	70	>45
	80	>45
SFD	40	25
	60	25
	70	>45
	80	>45

### 6.11.2 Parametric study 2 – Influence of thickness of slab on the design solutions

Variable parameter – Thickness  $h$

Constant parameters – Load  $P$ , Modulus of subgrade  $k$ , Grade of concrete

Types of fibres – SFA, SFB, SFC, SFD

In the second study, with load and  $k$  constant, the design was done for various slab thicknesses. It is seen that the minimum required thickness for the fibres with higher variability (SFC and SFD) for the same load (say, 80 kN) is about 30% more than for the fibre types SFA and SFB, as can be seen in Figure 6.7. Thus, it can be concluded that the type of fibre has significant influence on

the design, and that the proposed design method accounts for the variability in the performance of fibres.

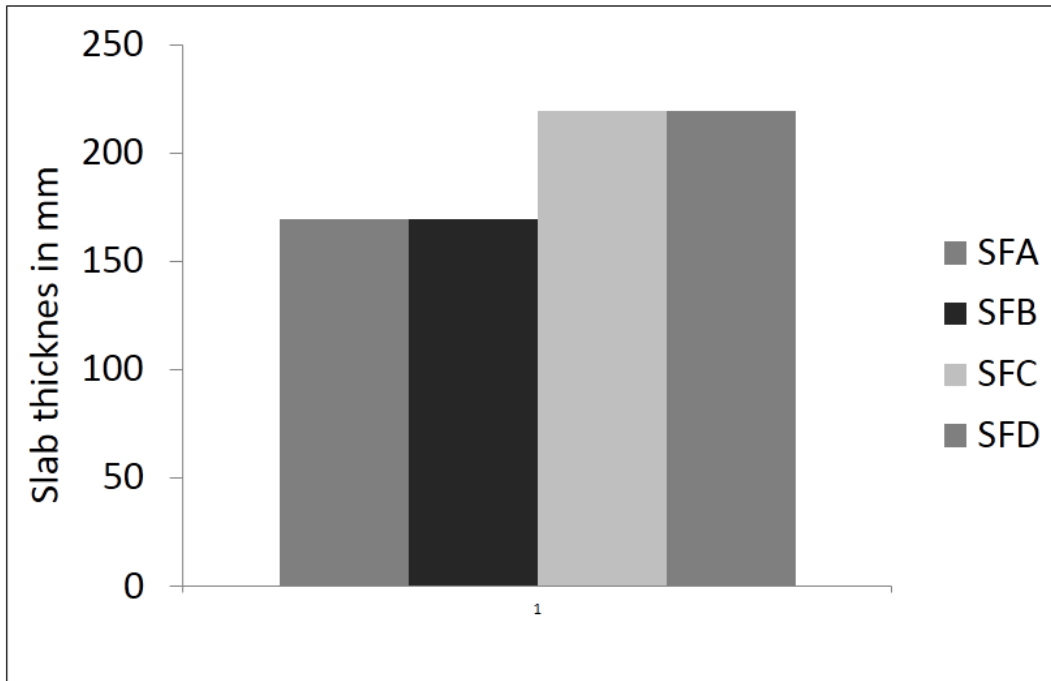


Figure 6.7 Minimum required thickness for 80 kN load on FRC with four types of steel fibres

The same calculations were done for various loads and a single fibre type, and the minimum required dosages obtained for various thicknesses and loads are plotted in Figure 6.8. It can be observed that the dosage reduction with respect to thickness increase is lower at higher loads; for example, at lower loads, say  $P = 40$  kN, a 16 % increase in thickness resulted in a decrease in the dosage of fibres by  $20 \text{ kg/m}^3$  but at higher loads, say 120 kN, an 18 % increase in thickness gives a decrease in the required dosage of only about  $15 \text{ kg/m}^3$ . This indicates that at higher loads, the thickness of the slab is more critical than the fibre dosage.

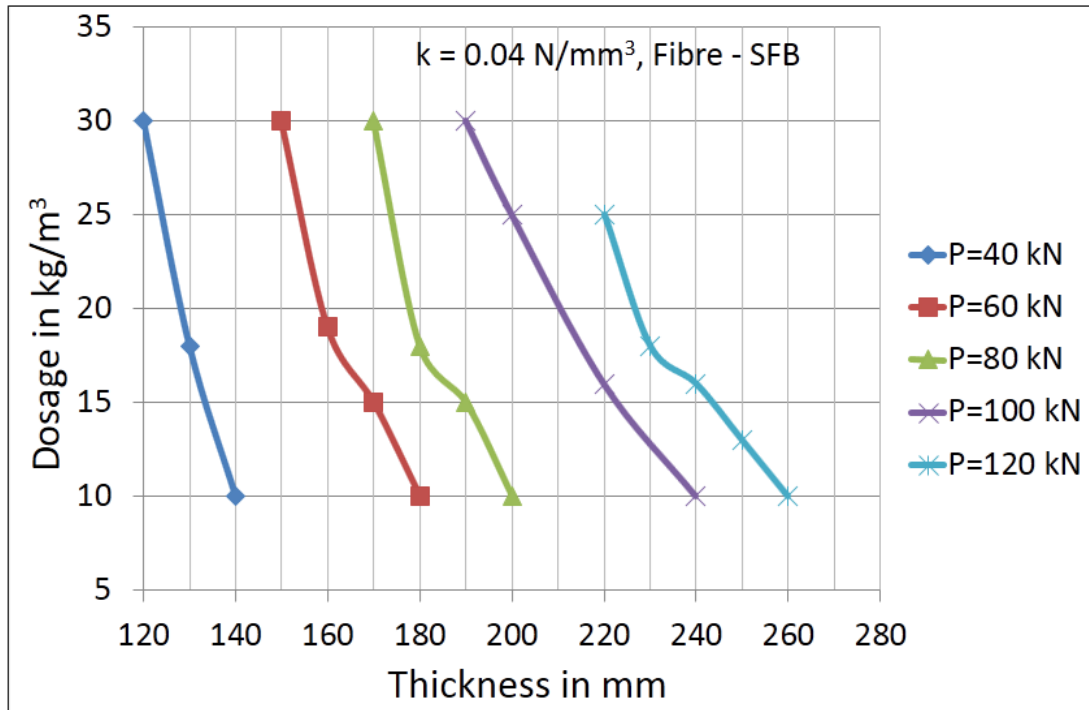


Figure 6.8 Variation of minimum required dosage of SFB fibre with thickness for different load

### 6.11.3 Parametric study 3 - Influence of the material parameters on the design

Owing to the presence of the constant  $A$  in the generalised design equation as shown in Equation 6.32 and Table 6.8, it is understood that the influence of the FRC material parameters, viz., flexural strength  $f_{ctk}$ , and equivalent flexural strength  $f_{en,k}$ , on the design solutions, may not be to the same extent in all cases. Therefore, a parametric study was done to clarify the influence of material parameters, by design trials. For this study, hypothetical cases were considered by keeping one parameter constant and varying the other within reasonable ranges. The design solutions obtained were compared based on the minimum required slab thickness. The design was done for two cases, single point loading assuming both edge loading with D-cracking and interior loading with circular cracking with the following parameters,:

Point load  $P$  – 80 kN

Area of base plate - 100 mm×100 mm

$k$  - 0.04 N/mm<sup>3</sup>

E modulus = 21 GPa

In the first trial, the flexural strength was varied from 3.0 MPa to 5.5 MPa with increments of 0.5 MPa keeping  $f_{en,k}$  at 3.0 MPa. In the second trial, the  $f_{en,k}$ -value was varied from 3.0 MPa to 5.0 MPa keeping  $f_{ct,k}$  at 4.0 MPa. The results from the two studies are plotted in Figure 6.9. The plots point to the fact that in the case of edge loading, where  $A = (\pi/2+2)$ , the design is more sensitive to the change in flexural strength than the equivalent flexural strength. This is evident since the slope of the plot for constant  $f_{ct,k}$  is steeper, indicating lower influence of change in  $f_{en,k}$  on the maximum allowable load, as well as the minimum required thickness. This can be further reinforced from the data presented in Tables 6.9 and 6.10; e.g., for an increase of about 42% in  $f_{ct,k}$ , the reduction in thickness is about 17% as opposed to only 8% reduction with the same % increase in  $f_{en,k}$ .

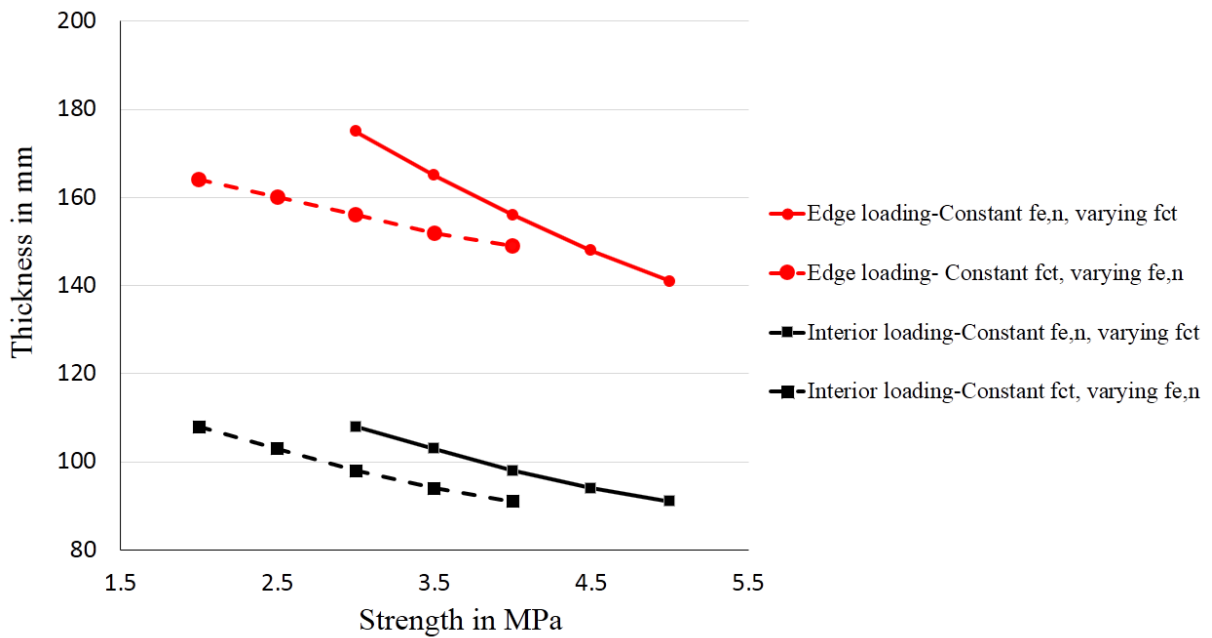


Figure 6.9 Variation of minimum required thickness with toughness parameters

Table 6.10 Variation of minimum required slab thickness with flexural strength for edge-loading of single point load

$f_{en,k}$ (MPa)	$f_{ct,k}$ (MPa)	Minimum required thickness, $h$ (mm)
3.0	3.5	174
	4.0	162
	4.5	151
	5.0	143
	5.5	136

Table 6.11 Variation of minimum required slab thickness with equivalent flexural strength for edge-loading of single point load

$f_{en,k}$ (MPa)	$f_{ct,k}$ (MPa)	Minimum required thickness, $h$ (mm)
3.0	4.0	162
3.5		157
4.0		153
4.5		149
5.0		145

In the case of interior loading since  $A=1.0$ , the extent of influence of both parameters are the same, indicating that the optimum solution will be when both  $f_{ctk}$  and  $f_{e,nk}$  are increased to the same extent.”

Mostly, the critical case of failure is D-cracking due to edge loading. For such failure, the design is more sensitive to changes in the flexural strength, and therefore, fibres that improve this parameter, such as the AMF discussed in Chapter 5, will be beneficial, as long as significant post-cracking capacity is ensured (such as in the hybrid mixes discussed in Chapter 5). In cases where the load is high and slab thickness is to be reduced, the hybrid mixes with AMF and SF could give better performance than the single fibre mixes. As an example, two design trials were done to compare the benefits of using a hybrid mix of AMF and steel fibres (SF) instead of only steel fibres (SF). The first trial was done for a point load of 80 kN applied with a base plate of 100 mm × 100 mm. The second trial was done for a loading case of 250 kN point load applied through a base plate of 150 mm × 150 mm. The design solutions for M35 grade FRC having only

steel fibres (Mix 1) and FRC with hybrid combination of AMF and SF (Mix 2 and Mix 3) have been compared in Table 6.12 and 6.13 below.

Table 6.12 Details of design trial 1

Design parameter	Mix 1	Mix 2	Mix 3
Load (kN)	80		
Subgrade Modulus, $k(\text{N}/\text{mm}^3)$	0.04		
Elastic modulus (MPa)	21000		
Poisson's ratio	0.15		
Base plate dimension (mm)	150 × 150		
Dosage of fibres ( $\text{kg}/\text{m}^3$ )	SF - 17	SF - 15 AMF - 10	SF - 15 AMF - 20
Characteristic flexural strength $f_{ct,k}$ (MPa)	3.8	4.8	5.6
Characteristic equivalent flexural strength $f_{e,150k}$ (MPa)	2.0	1.8	2.4
Minimum design thickness (kN)	200	170	160
Maximum allowable load (kN)	100	100	116

Table 6.13 Details of design trial 2

Design parameter	Mix 1	Mix 2	Mix 3
Load (kN)	250		
Subgrade Modulus ( $\text{N}/\text{mm}^3$ )	0.17		
Elastic modulus (MPa)	34000		
Poisson's ratio	0.15		
Base plate dimension (mm)	100 × 100		
Dosage of fibres ( $\text{kg}/\text{m}^3$ )	SF - 30	SF - 15 AMF - 10	SF - 15 AMF - 20
Characteristic flexural strength $f_{ct,k}$ (MPa)	3.9	4.8	5.6
Characteristic equivalent flexural strength $f_{e,150k}$ (MPa)	3.0	1.8	2.4
Minimum design thickness (kN)	300	280	260
Maximum allowable load (kN)	305	302	340

From the two trial designs, it can be clearly understood that by using FRC with hybrid combination of fibres (AMF+SF), which has higher flexural strength and similar post-cracking capacity as FRC with only steel fibres, a significant reduction in thickness of slab can be attained. For an increase in flexural strength of about 45 %, the reduction in thickness is about 13 – 20 %. This could be a major benefit in construction and will also give better performance due to the more pronounced crack resistance, as has been already discussed in Chapter 5.

## 6.12 Design example

In order to illustrate the complete design method, an example has been worked out below in detail

Table 6.14 Design input

Design input	Value
Type of slab	Container yard
Load details	Number of Containers Stacked: 4, Maximum Weight of each Container : 25 Tons Load Calculation: Total Load [4 × 25 Tons ] = 100 Tons Distributed Through Base Plate = 150 × 150 mm No. of Base Plate Points = 4 Load / Point = 25 Tons
Subgrade modulus	0.17 N/mm <sup>3</sup>
Minimum thickness of slab	300 mm
Slab dimension	6000 mm × 6000 mm
Assumed maximum temperature differential in slab	10°C
Grade of concrete	M35
Elastic modulus	34 GPa
Poisson's ratio	0.15
Coefficient of thermal expansion	0.00001 /°C

Table 6.15 Assumed and derived design parameters

Parameter	Value
Load factor*	1.2
Load transfer at joints*	60 %
Radius of relative stiffness, $l$ (Eqn 2.5)	824.2 mm
Contact radius, $c = \sqrt{\frac{150 \times 150}{\pi}}$	84.6 mm
$c/l$	0.102

\*Assumed parameter

*Dimension check for ascertaining failure pattern*

$L = 6000$  mm

$10l = 10 \times 824.2 = 8242$  mm.

$L < 10l$  – Circular fan type failure is not possible (see section 6.4.1.2)

Since load transfer assumed is  $>50\%$  and the slab is large enough to rule out centre-line cracking, the possible failure pattern is D-cracking at the edges (see section 6.4.1)

Maximum width allowable for neglecting shrinkage =  $24 \times 300$  mm = 7200 mm (see Section 6.5). The actual width is 6000 mm  $<$  7200 mm so the shrinkage stresses maybe considered as negligible.

Table 6.16 Curling stresses due to temperature differential

$\alpha$	0.00001/ $^{\circ}\text{C}$
$\Delta T$	10 $^{\circ}\text{C}$
$L/l$	7.28
$C$	1.043
$f_{\Delta T}$ (Eqn 6.28)	1.8 MPa

*Design equations*

Since the value of  $c/l$  is  $<$  0.2, the design solution has to be obtained for the case  $c = 0$  and  $c/l = 0.2$  as shown below:

For  $c/l=0$

$$f_{e,150k} = \frac{2}{\pi} \left[ \frac{6P}{h^2} - \left( \frac{\pi}{2} + 2 \right) \frac{f_{ctk}}{\gamma_c} + f_{\Delta T} \right] \gamma_c \quad (6.34)$$

For  $c/l=0.2$

$$f_{e,150k} = \left[ \frac{6}{\pi h^2} \left[ 1 - \frac{2c}{3l} \right] P - \left( 1 + \frac{4}{\pi} \right) \frac{f_{ctk}}{\gamma_c} + f_{\Delta T} \right] \gamma_c \quad (6.35)$$

For factored load of  $P_u = 1.2 \times P = 300$  kN.

Estimated flexural strength of concrete  $f_{ctk}$  (as per TR34:2003, for M35 grade concrete and 300 mm thickness) = 3.55 MPa.

The material safety factor  $\gamma_c$  has been taken as 1.0 (see Section 6.6.4).

From interpolation  $f_{e150k}$ , required = 2.8 MPa

From the material database, the possible choice of fibres can be made. In this case, the requirements are satisfied by use of 30 kg/m<sup>3</sup> of the SFB fibre ( $f_{ct,k} = 3.8$ MPa,  $f_{e150,k} = 3.0$  MPa).

The final design is summarised in Table 6.16.

Table 6.17 Final design for the case study

Thickness of slab	300 mm
Grade of concrete	M35
Min. Required flexural strength $f_{ct,k}$	3.55 MPa
Min. Required equivalent flexural strength, $f_{en,k}$	2.80 MPa

### 6.13 Comparison of the suggested method with existing design methods.

The suggested method is compared in this section with design solutions obtained from various existing guidelines in terms of slab thickness and fibre dosage; comparisons are made with TR34 2003, TR34 2013, ACI 360 R-10 and the Losberg yield line method (TR34:2003, 2013, ACI 360

R-10, Losberg 1961). The parameters that are significant for each method are shown in Table 6.17.

TR34:2003 uses the Meyerhof's equation wherein the equivalent flexural strength ratio is used to calculate the plastic moment capacity and the flexural strength is used for the negative moment capacity estimate to arrive at the allowable load. The TR34:2013 method uses the residual flexural strength (from a notched beam test) as the material parameter, and neglects thermal and shrinkage stresses in the design equations, which results in an underestimation of stresses resulting in a less conservative design. ACI 360R uses approximate equations suggested in Meyerhof's analysis for a slab on elastic foundation, with the assumption that the contact radius of the load ( $c$ ) is equal to or greater than the thickness of the slab, which leads to an underestimation of the stresses. In Losberg's yield line analysis, the soil pressure distribution curves developed based on the elastic theories for the infinite elastic slab lead to more conservative estimates than the Meyerhof's analysis.

Table 6.18 Details of the design parameters for each method used for numerical comparison

Design method	Input variables	Input material parameters	Dependent material parameters	Design output
TR 34:2003	Load ( $P$ ) Subgrade modulus ( $k$ ) Thickness ( $h$ )	$R_{e,150}$ Grade of concrete	Type of fibre Dosage of fibre $f_{ctk}$ $f_{e,150k}$	$P_{all}$
TR34:2013		$f_{r1}/f_{r4}$ Grade of concrete	Type of fibre Dosage of fibre $f_{ctk}$	$P_{all}$
ACI 360		Grade of concrete	Type of fibre Dosage of fibre $f_{ctk}$	$R_{e,150}$ $P_{all}$
Losberg		$f_{e,150mean}$ Grade of concrete	Type of fibre Dosage of fibre $f_{ctk}$	$P_{all}$
Suggested method		Grade of concrete	$f_{ctk}$	$f_{e,150k}$ $f_{ctk}$ $P_{all}$

The maximum allowable loads considering edge cracking due to a single point load (see section 6.6.4.1) were obtained here using the above-mentioned methods, for different slab thicknesses and for an M35 grade concrete having 20 kg/m<sup>3</sup> hooked ended steel (SFB) fibres of length 60 mm and aspect ratio of 80. The material parameters for this combination were obtained from tests performed on notched and unnotched prism specimens, as listed in Table 6.19. The stress due to thermal and shrinkage strains was taken as 1.5 MPa, based on TR34:2003 recommendations. The material safety factor  $\gamma_c$  has been assumed as 1.0 for all methods in order to maintain uniformity.

Table 6.19 Parameters used in the design trials for comparison of methods (mean and characteristic values)

$f_{ct}$ , MPa		$f_{e,150}$ MPa		$f_{r1}$ MPa		$f_{r4}$ MPa		$R_{e,150}$ %		Assumed stress due to thermal and shrinkage strains, MPa
<i>Mean</i>	<i>Char</i>	<i>Mean</i>	<i>Char</i>	<i>Mean</i>	<i>Char</i>	<i>Mean</i>	<i>Char</i>	<i>Mean</i>	<i>Char</i>	
5.80	4.87	3.72	2.8	3.96	2.86	4.17	3.26	64	64	1.50

From Figure 6.9, it can be seen that the maximum allowable load calculated as per the suggested method is higher than those obtained from the Losberg's yield line method and TR 34:2003, while it is lower than that given by TR34:2013 and ACI-360 R. For the case considered, the suggested method gives a higher capacity than TR34:2003 (even though the basic equations are same) and Losberg yield line methods since it takes into account the characteristic value of the mechanical parameters from actual test results rather than taking the characteristic value as 0.7×mean value; in this case, the actual characteristic strengths are higher than those obtained with the factor of 0.7 as can be seen from Table 6.19. However, the suggested design method would give a lower estimate than TR34 2003 and Losberg's methods if the characteristic values had been lower. It is, therefore, more realistic to take the actual characteristic values in the design rather than factored mean values.

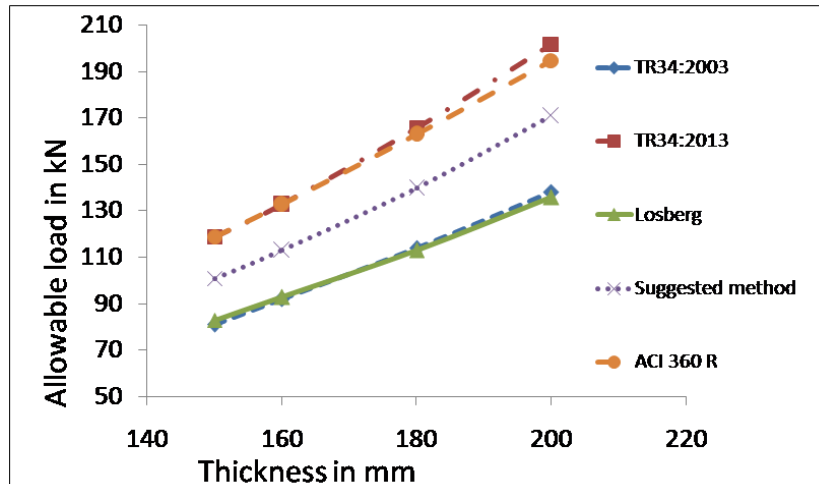


Figure 6.9 Comparison of allowable loads for different slab thickness as calculated using different design methods

Since the TR34:2013 and the ACI 360R methods are consistently less conservative than the other three methods, the next comparison only considers the suggested method, and the TR34:2003 and Losberg’s yield line methods. The minimum required fibre dosage (for the same fibre type considered earlier) for a tyre load = 80 kN, slab thickness = 120 mm and  $k = 0.02 \text{ N/mm}^3$  is calculated for each method and reported in Table 6.20, assuming that the failure occurs by D-cracking. The results suggest that for the same design parameters, the dosage of fibres required as per the suggested method is lowest, providing the most economical design.

Table 6.20 Minimum fibre dosage required for 80 kN tyre load

Design method	Minimum required $f_{e,150k}$ MPa	Corresponding minimum dosage $\text{kg/m}^3$
TR34:2003	1.7	16
Losberg method	2.5	27
Suggested method	1.5	10

Another comparison of the required dosage for the three methods, viz., TR34:2003, Losberg yield line method, and the suggested method was done for two cases. In the first case, the applied load, subgrade modulus and type of fibre were kept constant and design was done by varying the thickness, as shown in Table 6.21. In the second case, the load was varied keeping other

parameters constant. The minimum required dosages for each design run for the below-mentioned set of parameters were determined as shown in Tables 6.21 and 6.22 for the three methods, and compared in Figure 6.10 and 6.13.

Table 6.21 Design parameters for the comparison study of required dosages

Design parameter	Case 1	Case 2
Load (kN)	100	Variable
Modulus of subgrade, $k$ (N/mm <sup>3</sup> )	0.02	
Design thickness (mm)	Variable	150
Grade of concrete	M35	
Type of fibre	Hooked-ended steel fibres length = 60 mm, aspect ratio = 80 mm	
Modulus of elasticity (assumed) (GPa)	3.4	3.4

Table 6.22 Design solutions as per each method for case 1 (load 100 kN constant)

Design method	$h$ (mm)	Minimum required dosage (kg/m <sup>3</sup> )	Corresponding $f_{ctk}$ (MPa)	Corresponding $f_{enk}$ (MPa)
TR34:2003	130	19	3.8	2.4
	140	10	3.8	1.5
	150	10	3.8	1.5
Losberg	130	30	3.82	3.0
	140	17	3.8	2.1
	150	10	3.8	1.5
Suggested	130	16	3.8	1.9
	140	10	3.8	1.5
	150	10	3.8	1.5

Table 6.23 Design solutions as per each method for case 2 (thickness 150 mm constant)

Design method	Load (kN)	Minimum required dosage (kg/m <sup>3</sup> )	Corresponding $f_{ctk}$ (MPa)	Corresponding $f_{enk}$ (MPa)
TR34:2003	80	10	3.8	1.5
	100	10	3.8	1.5
	120	10	3.8	1.5
	140	24	3.8	2.7
	145	30	3.8	3.0
Losberg	80	10	3.8	1.5
	100	10	3.8	1.5
	120	18	3.8	2.22
	140	27	3.8	2.9
	145	30	3.8	3.0
Suggested	80	10	3.8	1.5
	100	10	3.8	1.5
	120	10	3.8	1.5
	140	19	3.8	2.4
	145	26	3.8	2.8

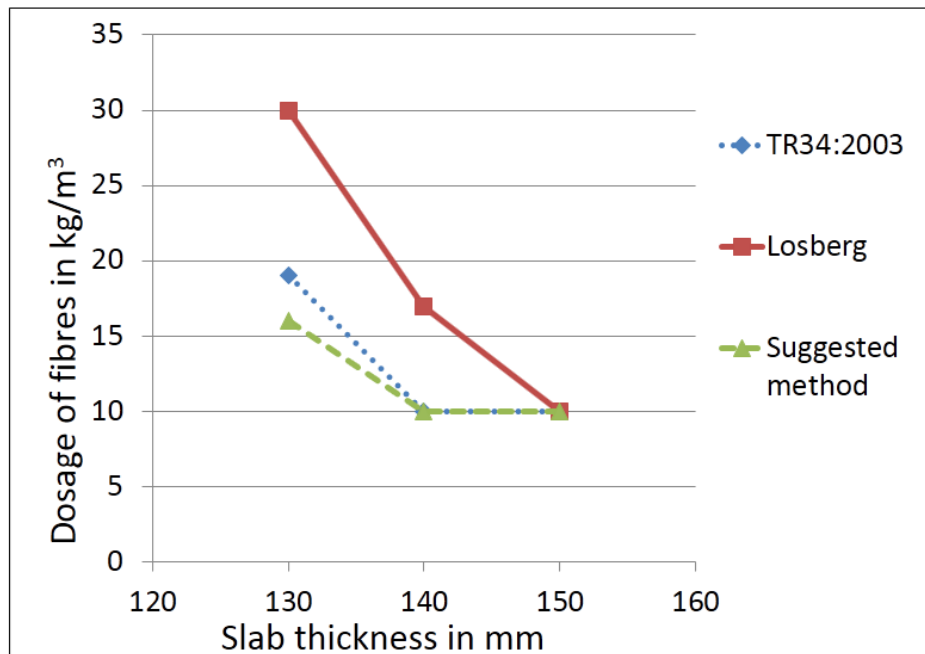


Figure 6.10 Comparison of required dosage for varying thickness

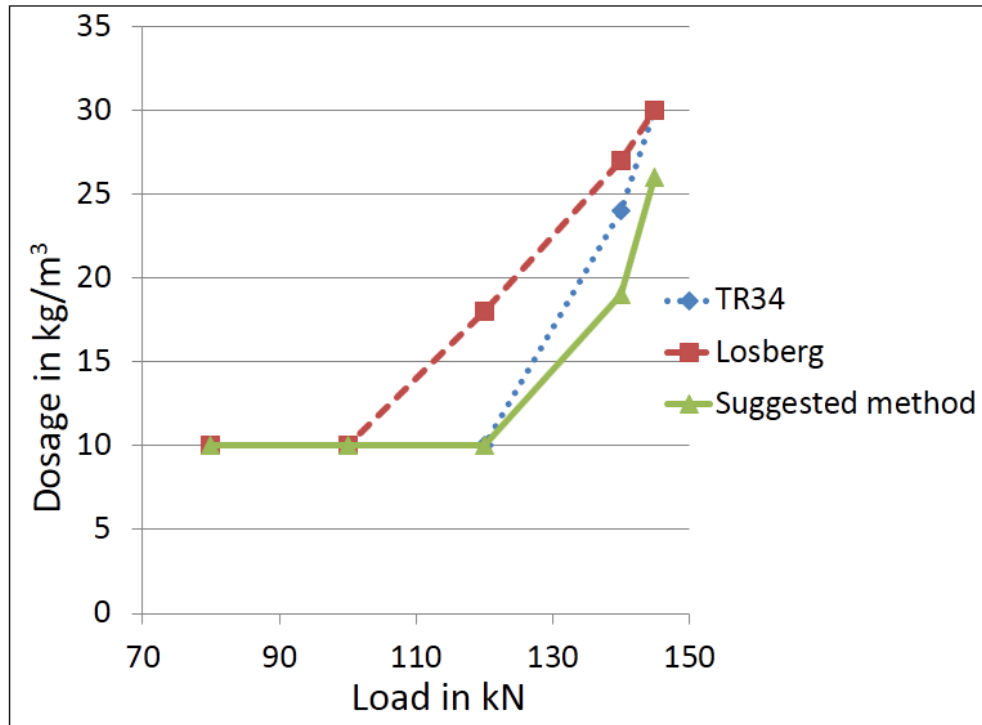


Figure 6.11 Comparison of required dosages for varying load

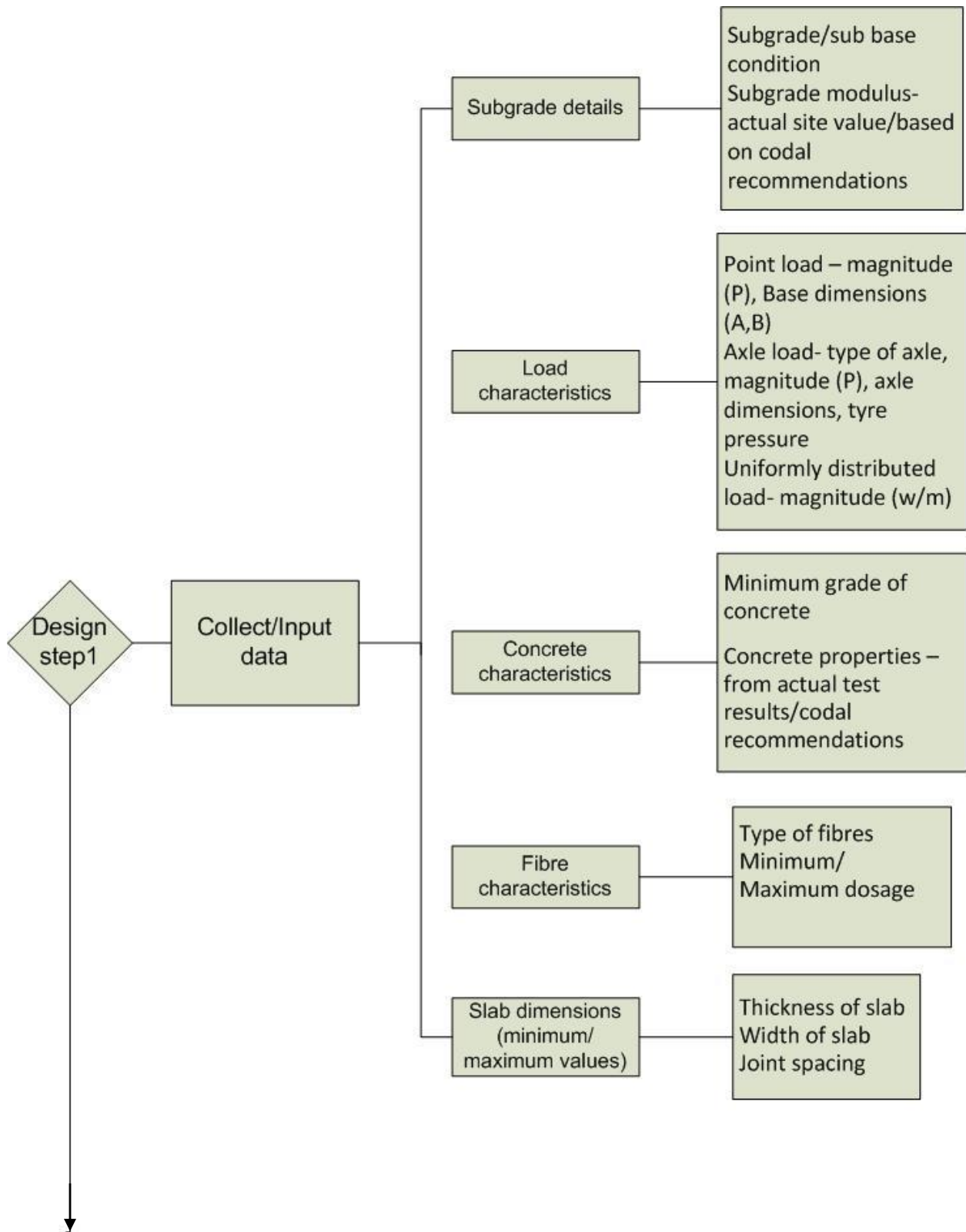
From both comparisons, it can be seen that the TR34:2003 method and the suggested method have similar trends since both are governed by the same design equations. However, the suggested method gives more economical solutions owing to a more effective treatment of the material performance (as has been discussed earlier in the Section 6.11). Note that the Losberg's yield line method clearly gives a much more conservative design.

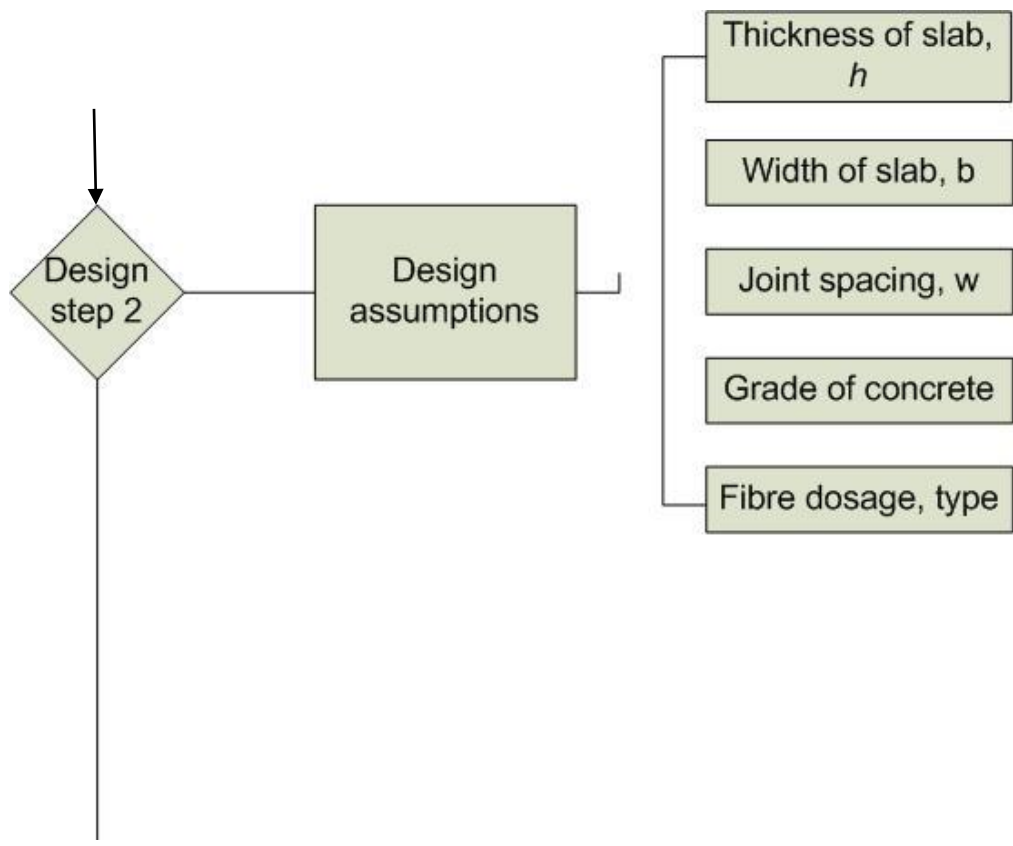
#### 6.14 Design framework and summary

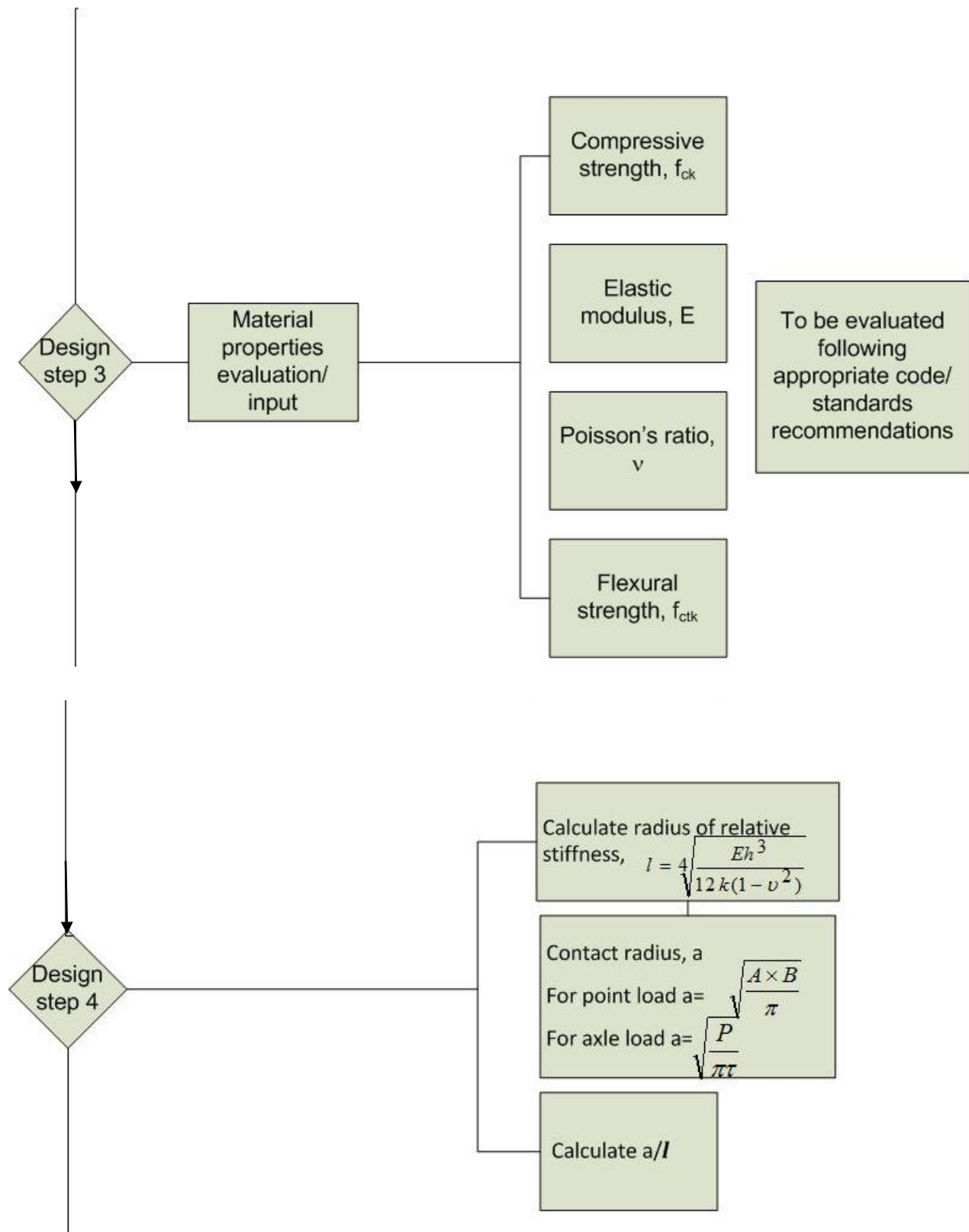
Based on the justification of the design equations of the suggested methodology, it can be deemed to be suitable for FRC slab-on-grade. A list of the assumptions/hypotheses valid to the method are given below:

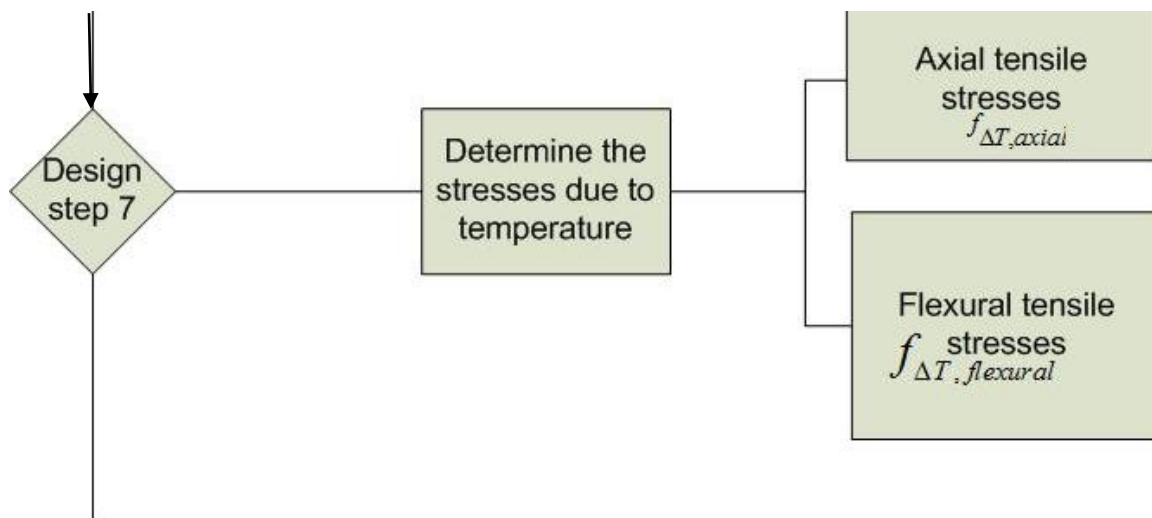
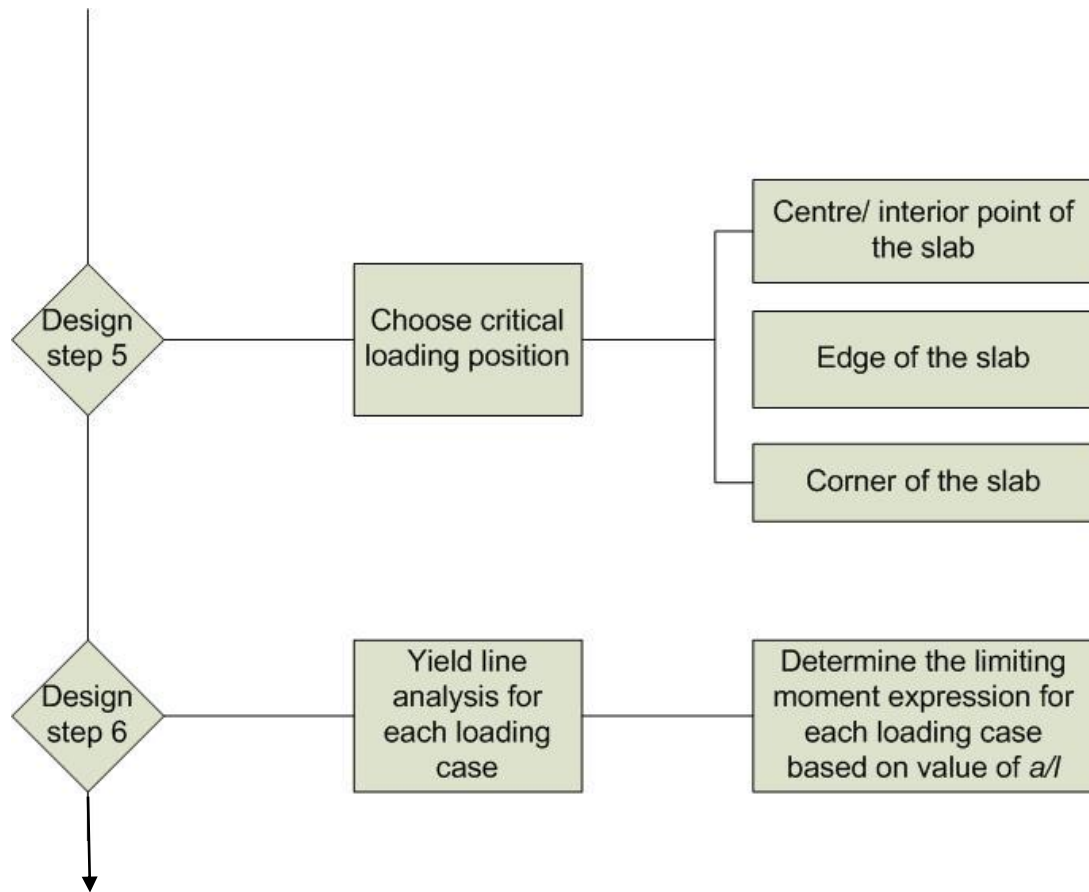
- Winkler model is acceptable for the subgrade
- Fibres are uniformly and isotropically distributed in the concrete.
- Rotation at the crack at failure load does not exceed 0.0267 rad.

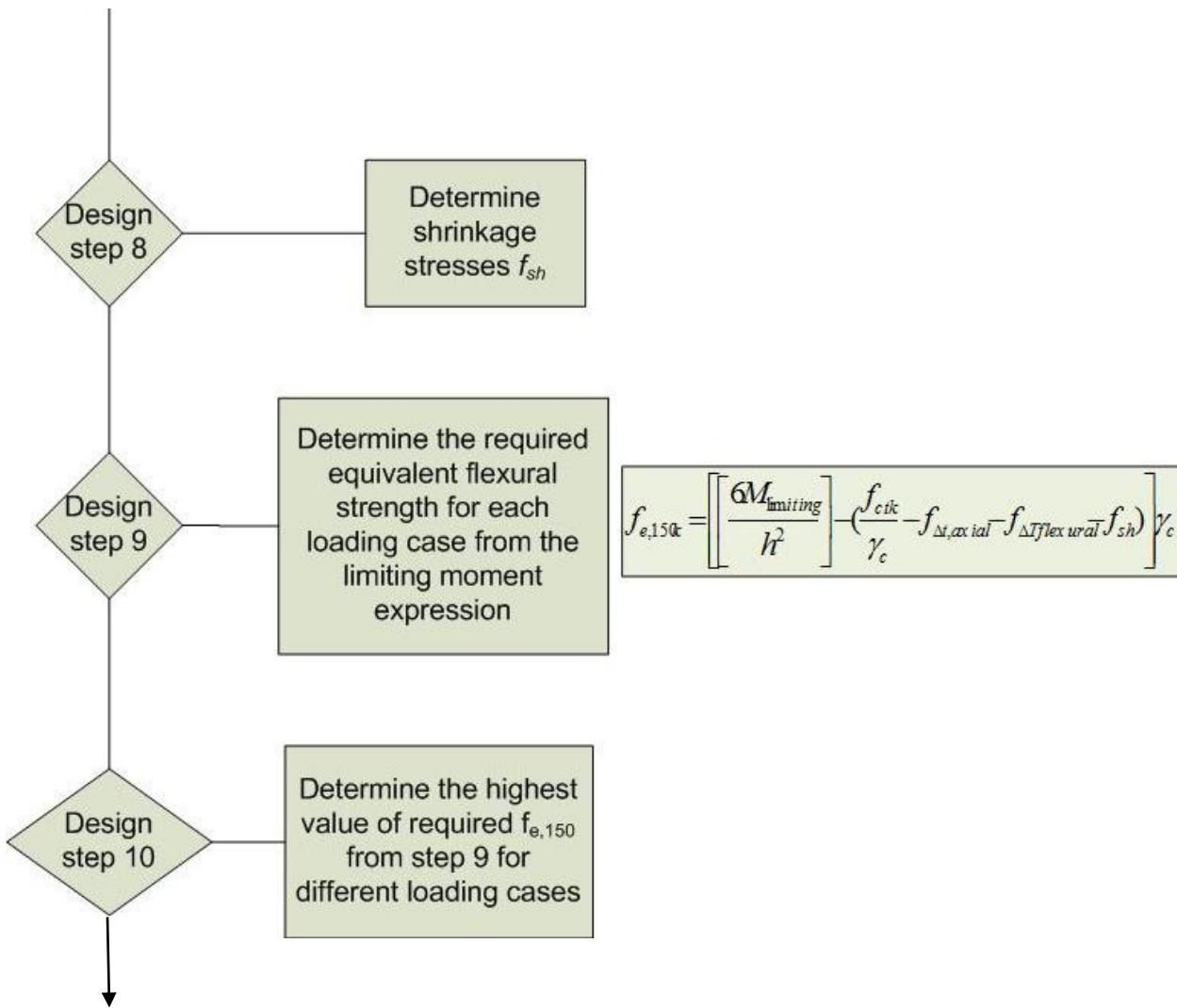
The complete method is now presented as the framework shown below.

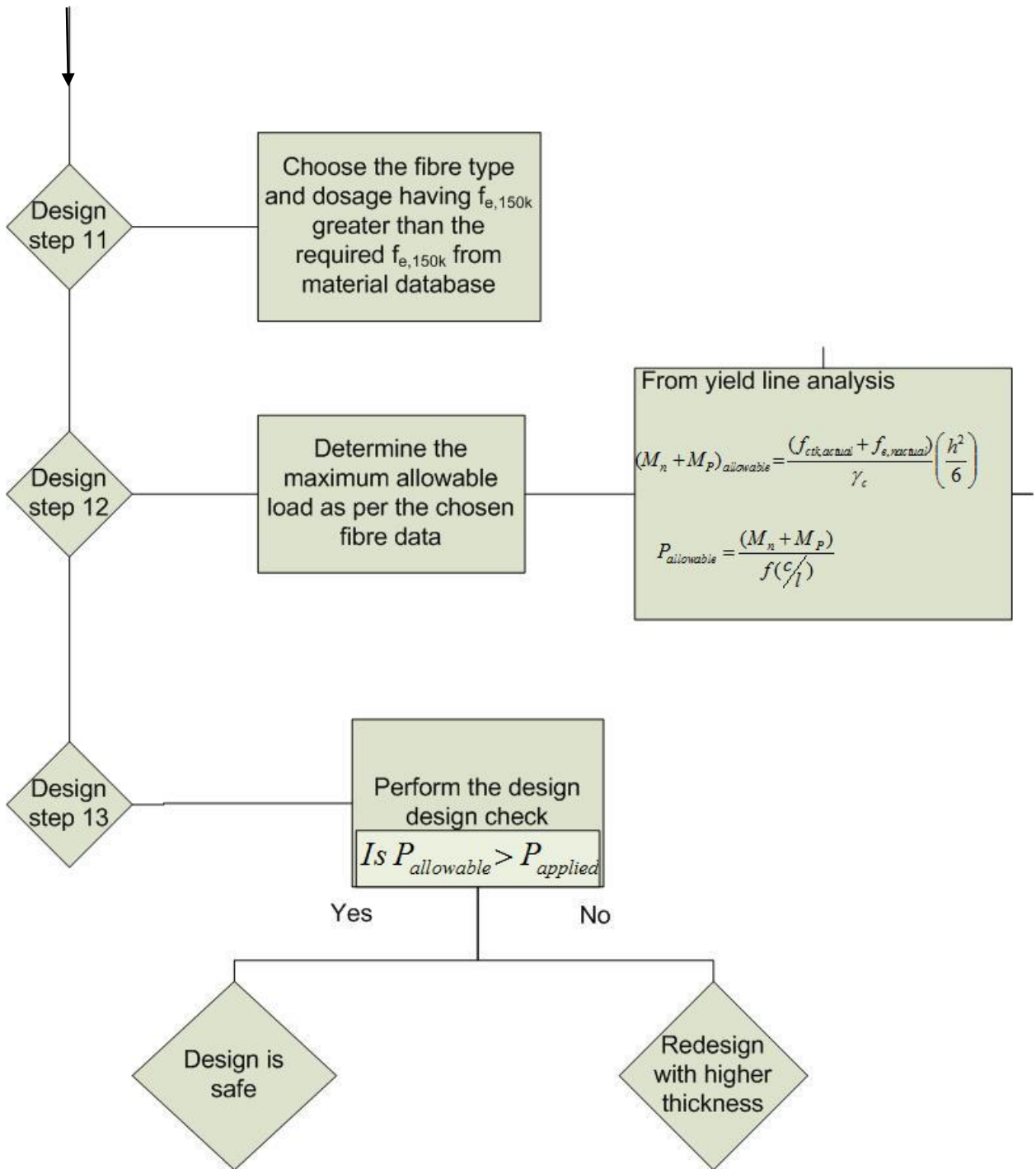












This Chapter discusses the design methodology developed for FRC slabs-on-grade based on in-elastic analysis. The design incorporates the flexural toughness parameter in the inelastic

design expressions based on each possible failure pattern to provide conservative as well as economical design. The specific conclusions from the discussions are:

- Equivalent flexural strength is a parameter that is a more realistic estimate of the post cracking capacity of the slabs-on-grade.
- The design equation estimates the required equivalent flexural strength for the given loading condition leading to a performance requirement for concrete.
- The governing design equations are dependent on the yield pattern that occurs based on the dimensions and end conditions of the slab.
- The design check allows for incorporating the actual material test data along with the variability since the characteristic value of the parameters have to be input.
- The design has been validated using the data from the literature based on experimental or numerical results.
- Parametric studies have shown that the design is more sensitive to variations in flexural strength than in the equivalent flexural strength, and therefore, mixes with fibres enhancing both flexural strength and flexural toughness perform better in terms of crack resistance even at lower slab thicknesses.
- The design solutions of the suggested method are compared with existing design methods and found, in general to be conservative.

## 7 DESIGN METHODOLOGY FOR PAVEMENTS

### 7.1 Introduction

Maximizing design life with minimum maintenance warrants the use of materials and technologies that have superior performance in comparison to traditional ones, especially in pavement systems, where a large part of the investment is used up in maintenance. Though flexible pavement systems are still the most popular technology adopted, there has been a shift to rigid pavement systems due to the comparatively lower maintenance requirements.

As discussed in Section 2.6, low flexural capacity added to the crack intolerance of concrete slabs lead to rigid pavement design being mostly guided by conservative elastic approaches. The adoption of fibre reinforced concrete (FRC), having better performance with respect to resistance to cracking, allows for design that is less conservative than that used for plain concrete (IRC SP 46:2013, TR34:2003, 2010, Roesler et al. 2006). In addition, the use of FRC in pavement systems can be considered more appropriate due to better performance with respect to fatigue, which is the most probable failure loading on pavements.

The current chapter presents a design methodology developed for FRC pavements based on inelastic analysis incorporating fatigue models in the moment calculation. A discussion of the possible causes and patterns of failure causes for pavements is given, followed by the description of the suggested methodology, which is later compared with existing design methods for FRC pavements. A parametric study follows in order to assess the influence of each variable on the design solutions, and finally the design framework is presented.

### 7.2 Failure patterns and conditions in rigid pavements

The phenomenon of curling influences the failure pattern in pavements significantly. As it is well understood, the two curling modes, viz., downward curling during day time and upward curling during night time, could lead to transverse cracking when the wheel passes over the slab, as shown in Figure 7.1 (Ghosh and Dinakaran 1970, Pandey 2005, Huang 2008, IRC 58:2010). However, in both cases, the design has to be governed by pure bending since the slab will lose contact with the subgrade, and the failure would be controlled by the flexural strength of concrete alone.

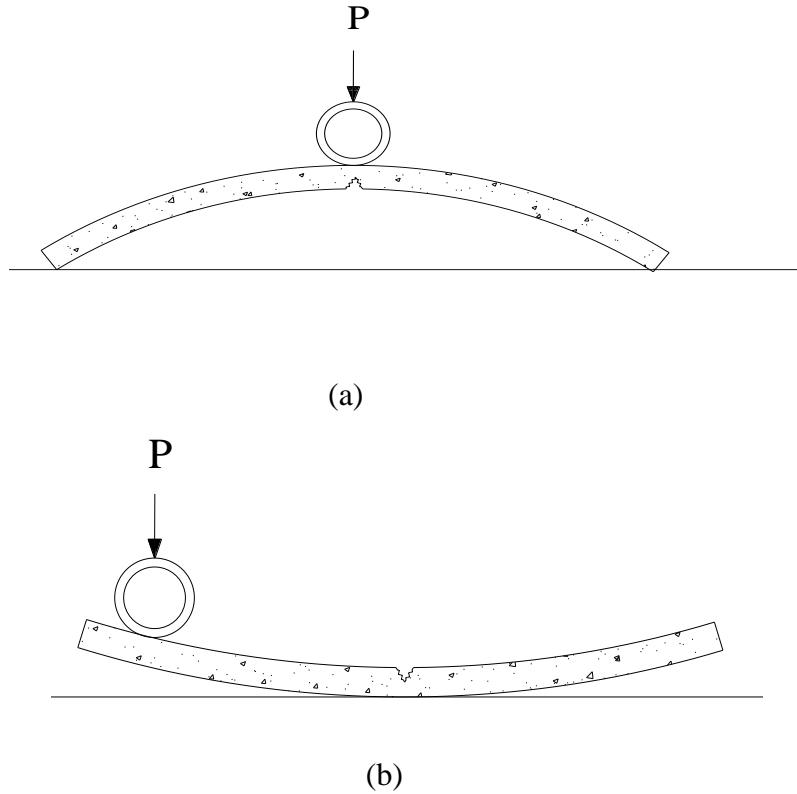


Figure 7.1 Cracking pattern in pavements (a) bottom-up cracking due to downward curling during day time (b) top-down cracking due to upward curling during night time

In case there is such loss of contact due to curling, the use of FRC may be less advantageous since design cannot be extended beyond the elastic limit or first-crack load. For the same exposure conditions, loss of contact may be completely prevented if the weight of the slab is significant. Such a situation occurs when the slab is long enough so that curling is completely neutralized by the weight of the slab (Ghosh and Dinakaran 1970). Thereby, in this case, the slab is in contact with the subgrade throughout the loading history and thus inelastic design based on plastic moment capacity, such as used in IRC SP:46 (2013), would be suitable.

The condition for completely neutralized curling is given in Equation 7.1:

$$\delta_{curling} + \delta_{self-weight} + \delta_{soil\ pr} = 0 \quad (7.1)$$

where each  $\delta$  term indicates the deformation of the slab due to one of the three effects, namely, curling, self-weight and soil pressure, respectively. Based on this condition, expressions have

been suggested by Ghosh and Dinakaran (1970) for calculating the minimum length of slab required for neutralizing curling:

$$\text{Self weight / m} - \text{foundation reaction / m} = \frac{0.8\alpha\Delta TEh^2}{L} \quad (7.2)$$

where  $\alpha$  is the coefficient of thermal expansion of concrete,  $\Delta T$  is the temperature differential between the top and bottom of slab,  $E$  is the elastic modulus of concrete,  $h$  is the thickness of the slab and  $L$  is the length of slab. The minimum required value for  $L$  works out to be  $8l$ , based on the study by Ghosh and Dinakaran (1970), where  $l$  is the radius of relative stiffness.

Consequently, by performing an initial dimension check, the failure mode of the pavement can be contemplated with respect to curling and a suitable design approach can be adopted, as discussed in the following sections.

### **7.2.1 Case 1: Curling of slab is significant leading to the loss of contact with the subgrade**

Condition: length of slab  $< 8l$

#### **7.2.1.1 Case 1a: Bottom-up cracking**

This is the classical crack pattern encountered when upward curling occurs during daytime, which is addressed in most rigid pavement design methods (Figure 7.1(a)). The cracks are usually transverse across the slab width and the design is governed by pure bending stresses, since the slab is mostly separated from the sub grade. Elastic design techniques, such as IRC 58:2010, can be used irrespective of whether the concrete being reinforced with fibres or not. The design will be based on the first-crack strength, which is generally not affected by fibres at the commonly used dosages; thus, the benefit of fibre action cannot be exploited in an elastic design. The exception is the case of FRC with AMF where there is an increase in the  $f_{ct}$  due to the incorporation of such fibres.

#### **7.2.1.2 Case 1b: Top-down cracking**

Similar to the previous case, the design is governed by elastic stresses since transverse cracks occur when the wheel passes over the edges of the slab that has curled upwards during the night

(Figure 7.1 (b)). Elastic design as per IRC 58:2010 is suggested as the first-crack limits the capacity.

**7.2.2 Case 2: Curling of the slab is completely neutralized by self-weight and there is no loss of contact with the sub-grade**

Condition: length of slab  $L \geq 8l$

**7.2.2.1 Case 2a: D-cracking/Circular cracking of slab**

A case of circular cracking due to load at an interior position or D-cracking due to loads on edge may occur if the slab dimensions are large enough (both width and length). The case is ideal for the use of FRC since the behavior is similar to that of slabs-on-grade, and inelastic design techniques, such as IRC SP 46:2013, will be suitable (see 2.6.1 and Section 6.4.1). In order for such a failure pattern to occur, the condition to be satisfied is given in Equation 7.3 (taken from Ghosh and Dinakaran (1970)):

$$b \geq \left[ \frac{P}{\pi(2l - c/3)} (M_p - 0.1\alpha\Delta TEh^2) \right] \quad 7.3$$

where  $M_p$  is the plastic moment capacity of FRC,  $b$  is the width of the slab,  $c$  is the contact radius of the load  $P$ . Thus, if the value of  $b$  is greater than or equal to the value obtained from the above equation, then the slab is expected to fail by circular/ D-cracking. The limiting moment obtained from Meyerhof's inelastic analysis for each loading case may be adopted in the design and the full potential of FRC can be exploited by using the equivalent flexural strength and flexural strength to represent the positive (plastic) and negative moment capacity respectively. Thus, the design equation would be represented by the limiting moment expression  $M_{limit} = M_p + M_n$ , as is further elaborated in Section 7.4.

**7.2.2.2 Case 2b: Cracking due to transverse yield lines**

In this case, the crack pattern is transverse across the slab but the failure is caused by the formation of yield lines, as shown in Figure 7.2. The condition for this type of failure is that the slab has limited width in comparison to the length, which makes transverse cracking more probable (Ghosh and Dinakaran, 1970). The limiting width for this condition is such that  $b$  is less

than that required for Equation 7.3 to be satisfied. In this case, the limiting moment is governed by the plastic moment capacity as the slabs rotate about the two boundary cracks simultaneously. Expressions for the limiting moment and slab stresses have been given in the study by Ghosh and Dinakaran (1970).

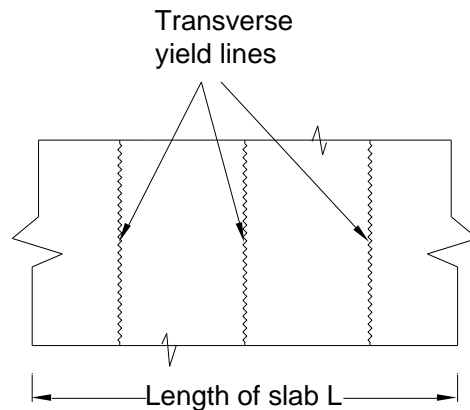


Figure 7.2 Formation of transverse yield lines on a slab with low width and high slenderness

The above discussion considers the possible failure patterns in pavements and the approach to be used for design. However, it is not sufficient for a design method for pavements to address only the tyre (static) loading conditions as it is well established that failure of pavements occurs mainly due to fatigue (MEPDG 2004, Fwa 2006, Huang 2008), which is addressed in the following sections.

### 7.3 Fatigue based design

Though there are design methods that adopt fatigue based procedures for pavements, some of which are relevant in the context of FRC, there are a few drawbacks that can be identified in these approaches as listed below;

- Many design techniques address the issue of fatigue loading through the consideration of a dynamic factor converting the cyclic load to an equivalent static load (TR34 2003, TR34 2013, Dramix Manual 2001, di Prisco and Mauri 2004, ACI 360R 2010). However, such an approximation, though widely accepted, has its drawbacks in that it is not possible to accommodate the performance characteristics of the material since the

dynamic factor is not specific with respect to material. In a case such as FRC, this becomes a significant drawback as FRC has a better fatigue response than plain concrete.

- Though the design methods for FRC pavements are based on inelastic analysis for static loading, the design for fatigue is based on elastic stresses and thus the design is always governed by the elastic analysis rendering the inelastic analysis ineffective for optimising the design (IRC SP 46:2013).
- Some methods use a modified flexural strength for FRC, denoted as the design flexural strength, given as a factored value of the actual flexural strength, often related to the equivalent flexural strength ratio (Roesler 2006, Elsaigh et al. 2005, IRC SP 46:1997). Such an approach is unsuitable as in cases where the design moments are governed only by the plastic moment capacity or the negative moment capacity, the use of such a design flexural strength is erroneous.

Keeping in view the requirements of performance and rationality, a design method has been developed, where it is attempted to overcome the limitations mentioned above and is presented in the following sections.

#### **7.4 Proposed design method for FRC pavements**

Once the dimensions of the slabs are obtained as per the requirements, the design is initiated by checking the length and width of the slab, to decide the design case, as suggested in Section 7.2, with respect to the failure patterns. If the dimensions satisfy the conditions for fully neutralized curling with circular/D-cracking, then the design can be done as discussed below (which is generally the case in pavements). The design is based on the collapse condition being taken as the appearance of cracking at the top of the slab, as discussed in Section 2.5.3.

At this condition as discussed for slabs-on-grade in Section 6.4.1, the plastic moment capacity due to the FRC is fully mobilized at the bottom of the slab since the crack is open and the negative moment capacity at the top of the slab corresponds to the flexural strength of concrete. Thus, the limiting moment is the sum of the positive plastic moment  $M_p$  and the negative moment  $M_n$ :

$$M_o = M_n + M_p \quad (7.4)$$

As per the stress condition, the allowable moment per unit width of the slab is:

$$M_{all} = (f_{ctk} + f_{e,150k}) \frac{h^2}{6} \quad (7.5)$$

where  $f_{e,150k}$  is the characteristic equivalent flexural strength of FRC up to a deflection of span/150,  $f_{ctk}$  is the characteristic flexural strength of the FRC and  $h$  is the thickness of slab.

In the case of FRC pavements, the section capacity will be affected by fatigue loading. The challenge is to estimate the material response parameters, such as flexural strength, endurance limit and toughness, for incorporation in the inelastic methodologies. In the present approach, reduction factors based on the fatigue models from literature are applied to the strength parameters used in the design of the section. Equation 7.5 is then modified for the moment carrying capacity under fatigue loading, as

$$M_{all} = \left( X \frac{f_{ctk,k}}{\gamma_c} + Y \frac{f_{e,150k}}{\gamma_c} \right) \frac{h^2}{6} \quad (7.6)$$

where  $X$  and  $Y$  are the reduction factors for the negative moment carrying capacity (i.e., at crack initiation) and the positive moment carrying capacity (i.e., post-cracking regime – crack opening), respectively. The values of  $X$  and  $Y$  are to be obtained from suitable fatigue models (e.g.,  $S-N$  curves) considering the fibre type and dosage used, and the specified grade of concrete, as explained in the next section.

#### 7.4.1 Determination of fatigue reduction factors

In the case of pavement design, the starting point of the design should be the axle load spectra from the traffic data. Also, the expected number of repetitions for each axle load class has to be obtained, as in typical rigid pavement design. For each load class, the corresponding maximum expected number of load repetitions,  $n_i$ , has to be used when determining the reduction factor from the fatigue model. Appropriate fatigue models have to be chosen for both uncracked and post-cracked stages of the FRC and the safe stress ratio corresponding to the assumed  $N$ -value has to be determined. This is illustrated in Figure 7.3 where  $S-N$  curves for uncracked and pre-cracked concrete are used to obtain the reduction factors; e.g., for a required  $N = 1000$  (i.e.,  $\log N = 3$ ), the safe stress ratio limits for FRC are, in the uncracked state,  $X = 0.91$  from curve of uncracked FRC, and for the cracked state,  $Y = 0.84$  from curve of pre-cracked FRC.

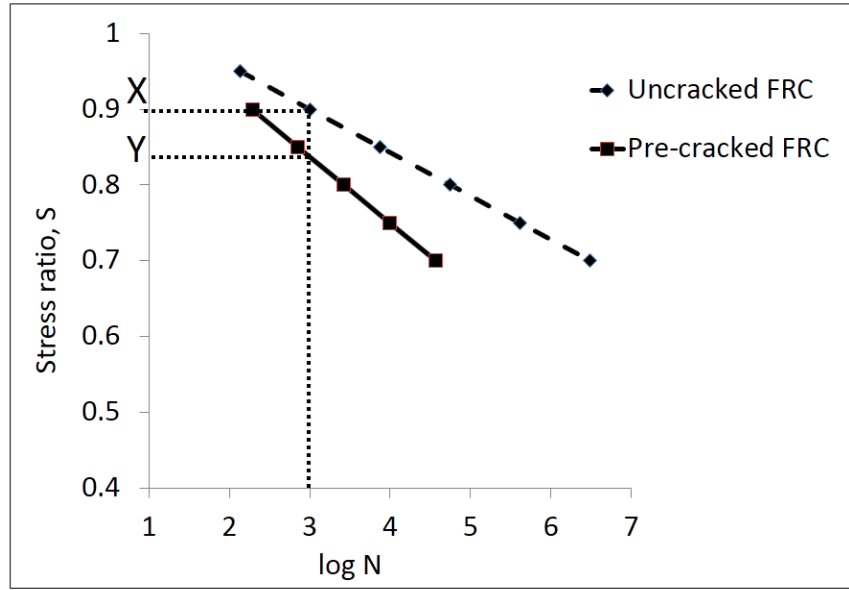


Figure 7.3 Fatigue reduction factors from S-N curves

From a review of existing studies on fatigue testing of plain and fibre reinforced concrete, it is understood that the fatigue models based on S-N curves, for same material, may differ with the amplitude of loading. It has been suggested by some researchers that the number of cycles to failure reduces with an increase in the amplitude of loading (Germano and Plizzari, 2012, Germano et al. 2015). Consequently, with respect to design, in order to have a conservative solution, it is suggested that the S-N model used, should pertain to a fatigue test with load amplitude as high as possible (for e.g., cycling up to near-zero load level as the lower limit).

#### 7.4.2 Thermal stresses

Since the major assumption for the inelastic design is that there is no loss of contact of the slab with the sub-grade since curling is completely neutralized by self-weight, the curling stresses developed will have to be accounted for in the design. An approach similar to that discussed in the design methodology for slabs-on-grade is suggested wherein the negative moment carrying capacity is reduced based on the flexural stresses developed due to temperature gradients in the slab:

$$M_{all} = M_p + (M_n - M_{\Delta T}) \quad (7.7)$$

Therefore, the design moment equation will be modified to account for this, as:

$$M_{all} = \left[ Y \frac{f_{e,150k}}{\gamma_c} + \left( X \frac{f_{ctk}}{\gamma_c} - f_{\Delta T} \right) \right] \frac{h^2}{6} \quad (7.8)$$

where  $f_{\Delta T}$  is the flexural stress due to the temperature differential ( $\Delta T$ ) in the slab.

Table 7.1 Results of the temperature differential testing on model slabs (avg. of two cycles).

Locations for diurnal temperature profile	Month with extreme max. and min. temp. (diurnal temperature difference)	Mean Maximum temp in °C /Relative humidity	Slab thickness in mm	Max positive temp. diff. between top and bottom of slab in °C	Max negative temp diff between top and bottom of slab in °C
Chennai	May (10°C)	37.4/62%	100	3.65	-1.95
			200	4.30	-1.85
			300	5.10	-1.70
Delhi	May (13.2°C)	39.8/33%	100	5.95	-3.95
			200	6.00	-4.15
			300	6.65	-4.10
	November (15.2°C)	28/55%	100	6.25	-1.20
			200	6.05	-2.30
			300	5.95	-3.20
Nagpur	May (14.5°C)	42.5/27%	100	9.85	-4.05
			200	11.00	-3.40
			300	11.55	-2.95
Jodhpur	January (15.6° C)	25/53%	100	4.50	-2.35
			200	4.35	-3.80
			300	5.00	-4.95
Hypothetical cycle 1	15 °C	20/30%	100	3.87	-2.02
			200	3.19	-3.34
			300	2.93	-4.48
Hypothetical cycle 2	10 °C	45/70%	100	4.18	-1.06
			200	3.99	-1.94
			300	3.76	-2.94

Since the thermal stresses in pavements are critical with respect to slab behavior, an experimental study was designed and tests were done on slab models under various diurnal temperature conditions to measure the temperature difference. The details of the tests and results

are discussed in Appendix D. The main results are given in Table 7.1 showing the maximum temperature differentials for various diurnal environmental conditions. The results give ranges and typical values that can be adopted for stress calculations in case actual data are not available. On comparison with the temperature considered in IRC 58 (2010), it is seen that these values are generally less conservative.

### 7.4.3 Shrinkage stress

As discussed in Section 6.5, the joint spacing of the slab could be decided so as to minimise the stresses due to shrinkage. In addition, the use of a friction relief layer is recommended for pavements so as to minimise the stresses due to shrinkage. In spite of this, if the shrinkage stresses are significant, an approach similar to that adopted for slabs-on-grade is suitable, where the estimated shrinkage stresses, from the measured/predicted strain values ( $\epsilon_{sh}$ ), given by:

$$f_{sh} = E_{cm} \times \epsilon_{sh}, \quad (7.9)$$

can be reduced from the total hogging moment capacity, as:

$$M_{limit} = M_p + (M_n - M_{\Delta T} - M_{sh}) \quad (7.10)$$

Thus, the design equation will be modified as:

$$M_{all} = \left[ Y \frac{f_{e,nk}}{\gamma_c} + \left( X \frac{f_{ctk}}{\gamma_c} - f_{\Delta T} - f_{sh} \right) \right] \frac{h^2}{6} \quad (7.11)$$

### 7.4.4 Design steps

From the assumed thickness and FRC material properties, the allowable moment is calculated as per the design expression in Equation 7.11. From the inelastic yield line expressions corresponding to each load condition (Meyerhof 1962, TR34 2003, 2014), the maximum allowable load corresponding to the maximum allowable moment is calculated as:

$$P_{all} = M_{all} f\left(\frac{c}{l}\right) \quad (7.12)$$

where  $f(a/l)$  depends on the load position and failure pattern assumed, and the corresponding expressions are obtained from Meyerhof's analysis, as discussed in Chapter 2 and given in TR34 (2003, 2014). If the allowable load is higher than the maximum applied load, then the

combination of thickness, grade of concrete and dosage of fibres is sufficient with respect to the inelastic design.

#### **7.4.5 Fatigue damage check**

Since a separate serviceability check for fatigue has to be performed, fatigue damage analysis is suggested along lines similar to IRC SP:46 and IRC SP:58, by determining the cumulative fatigue damage (CFD) and applying the Palmgren-Miner's rule. For determining the CFD, stress ratio on the slab is obtained as the ratio of elastic stress due to the applied load to the first crack strength. In order to obtain the allowable number of repetitions ( $N_i$ ), the fatigue model used for determination of  $X$ , as described in Section 7.4.1 is used. From the allowable and actual expected number of load repetitions for each load class ( $i$ ), the CFD is obtained as:

$$CFD = \frac{\sum n_i}{\sum N_i}.$$

As per the Palmgren-Miner's rule, the design is safe if  $CFD < 1$ .

The elastic stress due to the applied load maybe obtained using appropriate analytical solutions such as Westergaard's equations (see Equation 2.6) or numerical solutions (e.g., FEA based). In India, IRC 58 is a commonly adopted standard for rigid pavement design based on elastic stress analysis, and it is suggested that, in the absence of other solutions, the stress equations provided in Section 5.3 of IRC 58:2010 (reproduced in Appendix E) be used.

#### **7.5 Design example**

For the purpose of illustration, the design is worked out for the example given in IRC SP:46 2013, with the axles load spectrum given in Table 7.2.

Table 7.2 Axle load spectrum

P <sub>axle</sub> (kN)	No. of repetitions
190	362191
180	347823
170	364586
150	259022
140	59467
130	32328
120	52283
110	52882
100	64855
90	282369

***Input variables***

Grade of concrete – M35

Modulus of subgrade reaction,  $k = 0.225 \text{ N/mm}^3$

Tyre pressure =  $0.8 \text{ N/mm}^2$

***Assumed parameters***

Thickness of pavement = 265 mm

Width of slab = 3.5 m

Fibre type and dosage - hooked-ended cold-drawn steel fibres,  $30 \text{ kg/m}^3$

*From test data (see section 4.3.4)*

Expected characteristic flexural strength ( $f_{ctk}$ ) = 3.82 MPa

Expected characteristic equivalent flexural strength ( $f_{e,nk}$ ) = 3.0 MPa

Material safety factor  $\gamma_c$  assumed as 1.0 (see Section 6.6.4)

The radius of relative stiffness  $l$  can be obtained as,  $l = \sqrt[4]{\frac{Eh^3}{12(1-\mu^2)k}} = 730 \text{ mm}$

Based on the dimension check, the minimum length of slab required for curling to be neutralized

$$= 8 \times 730 = 5.8 \text{ m (see Section 7.2.1)}$$

The minimum width for circular/D-cracking to occur (from Equation 7.3) = 2 m

Since  $B$  assumed is  $3.5 \text{ m} > 2\text{m}$ , inelastic design will govern based on Circular/D-cracking. Therefore, the panel dimensions are taken as  $6 \text{ m} \times 3.5 \text{ m}$ .

The sources and values of X and Y are shown in Table 7.3.

Table 7.3 Values of X and Y used

Determination of strength reduction factors for $N = 2 \times 10^6$ cycles (assumed)					
		Parameters for $f_{ct}$ (first crack)		Parameters for $f_{e,n}$ (post cracking)	
S-N relation		<b>log N = -17.4 S + 18.66</b> (Lee and Barr 2004)		<b>log N = -11.4 S + 12.55</b> (Germano and Plizzari 2012)	
Strength reduction factors	X	<b>0.71</b>	Y	<b>0.55</b>	

Stresses due to a temperature differential of 8°C (from Bradbury's expressions: see Eqn 6.28) = 1.5 MPa

$$\text{Allowable } M_p = Y \times f_{en,k} h^2 / 6 = 19.3 \text{ kNmm/mm}$$

$$\text{Allowable } M_n = X \times (f_{ctk} - f_{\Delta T} - f_{sh}) h^2 / 6 = 19.3 \text{ kNmm/mm}$$

*Critical load position – Edge of slab*

for  $a/l = 0$

$$P_{all} = (\pi(M_p + M_n)/2) + 2M_n = 99.2 \text{ kN}$$

for  $a/l = 0.2$

$$P_{all} = (\pi(M_p + M_n) + 4M_n) / (1 - (2a/3l)) = 22.9 \text{ kN}$$

Maximum allowable load = 99 kN (lower of the above two critical cases)

As per the axle load spectrum, the maximum applied load = 190/2 = 95 kN < Maximum allowable load.

*Fatigue damage check*

In order to determine the elastic stress due to single axle loading condition the expression adopted from IRC 58:2010 is:

$$\sigma = -0.238 - 7.02 \left( \frac{\rho h^2}{kl^2} \right) + 2.41 \frac{Ph}{kl^4} + 0.0585(\Delta T)$$

where  $\rho$  is the unit weight of concrete assumed as 24 kN/m<sup>3</sup> as specified in IRC 58:2010.

Table 7.4 Fatigue damage analysis for the load spectrum

Axle load category (kN)	Expected repetitions (n)	Stress * (based on elastic analysis)	Stress ratio, S	N (from the S-N relation $\log N = -17.4 S + 18.66$ )	$(n_i/N_i)$
190	362191	2.85	0.75	495283	0.73
180	347823	2.72	0.71	1851655	0.19
170	364586	2.60	0.68	6922554	0.05
150	259022	2.34	0.61	96756197	0
140	59467	2.22	0.58	361730395	0
130	32328	2.09	0.55	1352356571	0
120	52283	1.97	0.51	52156237122	0
110	52882	1.84	0.48	159935822635	0
100	64855	1.72	0.45	490439279631	0
90	282369	1.59	0.42	1503920028928	0
				CFD=	0.97

\*Taken from expressions in IRC 58:2010 for elastic stresses on plain concrete slab

Thus, the design is safe both in terms of inelastic moment capacity and fatigue life. The final design is summarized in Table 7.4.

Table 7.5 Final design solution

Slab thickness	265 mm
Slab dimension	6 m $\times$ 3.5 m
Grade of concrete	M35
Fibre type and dosages	Hooked ended steel fibres of length 60 mm, aspect ratio 80 at 30 kg/m <sup>3</sup> , $f_{ctk} = 3.82$ MPa , $f_{en,k} = 3.0$ MPa

## 7.6 Parametric study

A parametric study is done in order to understand the design solutions with respect to the various variables. The axle load spectrum for which the designs were performed is the same as in Section 7.5 (see Table 7.2). The minimum thickness has been obtained for 10, 20 and 30 kg/m<sup>3</sup> of hooked-ended steel fibres and different subgrade moduli, and reported in Table 7.6, along with the expected failure pattern or mode.

Table 7.6 Results of the parametric study of the design methodology

Dosage of steel fibres in kg/m <sup>3</sup>	Subgrade modulus, $k$ in N/mm <sup>3</sup>	Required minimum thickness, $h$ in mm	Expected failure pattern or mode
10	0.08	290	D/Edge cracking
10	0.14	290	D/Edge cracking
10	0.225	290	D/Edge cracking
20	0.08	290	Fatigue cracking
20	0.14	280	Both D/Cracking and Fatigue cracking
20	0.225	270	Both D/Cracking and Fatigue cracking
30	0.08	285	Fatigue cracking
30	0.14	275	Fatigue cracking
30	0.225	265	Fatigue cracking

As discussed earlier, there are two design checks: the first check for the maximum allowable load as per the inelastic moment capacity and the second check for the serviceability based on fatigue damage. It can be seen that for FRC with a low dosage of fibres (10 kg/m<sup>3</sup>), where the post cracking flexural strength is low, the slab possesses limited rotation capacity and yield lines develop, causing the slab to crack before fatigue cracking can occur. On the other hand, at higher fibre dosages, the design is essentially governed by fatigue failure; the higher flexural toughness renders the design to be safe with respect to the inelastic design moment (as seen in Table 7) even at lower thicknesses but a higher slab thickness is required to satisfy the CFD check for fatigue damage based on the elastic stress.

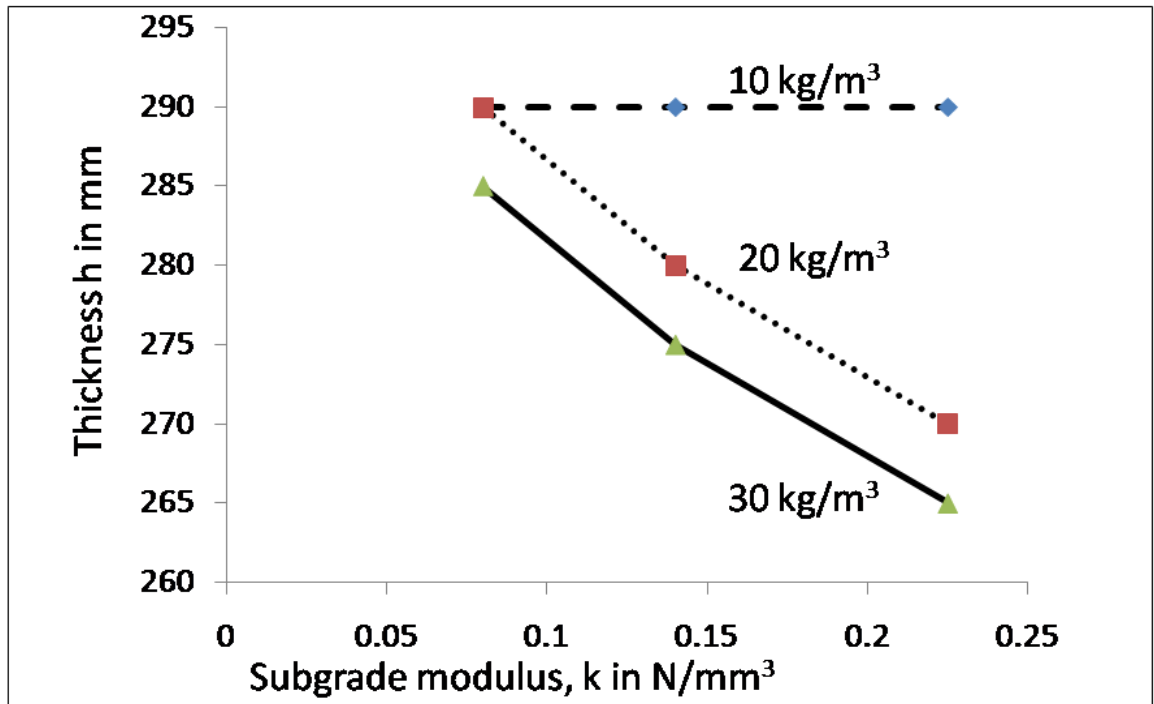


Figure 7.4 Variation of minimum required thickness with subgrade modulus for slab of M35 grade concrete having different dosages of hooked ended steel fibres.

### 7.7 Comparison with existing design methods

As has been discussed in detail in Sections 2.6.2 and 7.3, there are few design methods available for FRC pavements, and they have certain shortcomings and limitations. The suggested design methodology tries to overcome most of these limitations, which can be illustrated through a comparative study. Two design methods have been identified for this comparative study as they incorporate inelastic and fatigue analysis in the design: the IRC SP 46:2013 method for FRC pavements and the FHWA research report method (Roesler et al. 2008) for the design of Ultra-thin white toppings (overlays) with FRC.

In the first comparison, for the axle load spectrum taken from IRC 46:2013 (see Table 7.2), the design thickness is evaluated using all the three methods. Two concrete mixes were adopted of grade M35 with 10 kg/m<sup>3</sup> (Mix 1) and 20 kg/m<sup>3</sup> (Mix 2) of hooked-ended steel fibres with length 60 mm and aspect ratio 80. The material parameters used for the design are listed in Table

7.7 and the material safety factor has been assumed as 1.0 in all methods for uniformity. The minimum required thickness was obtained for different  $k$  values.

Table 7.7 Material parameters used for the design trial for comparison

Parameter	Mix 1	Mix 2
Grade of concrete	M35	
Dosage of fibres $\text{kg/m}^3$	10	20
$f_{ct,k}$ (MPa)	3.8	3.8
$f_{e,150k}$ (MPa)	1.5	2.52

From the comparative illustration in Figure 7.5 and 7.6, it can be seen that the design thickness as per the suggested method is lowest for both cases. It is evident that the IRC SP 46:2013 method is insensitive to the change in dosage. This is because the design is highly conservative as it is similar to that of plain concrete. The FHWA method design, though sensitive to the dosage of fibres, gives conservative results mainly because the fatigue model used is more conservative, as shown in Figure 7.7, where the fatigue models for first crack as used in each method have been plotted.

Thus, it could be concluded that the suggested method, though less conservative than the other two methods, is more suitable since both possible types of failure are accounted for in the design.

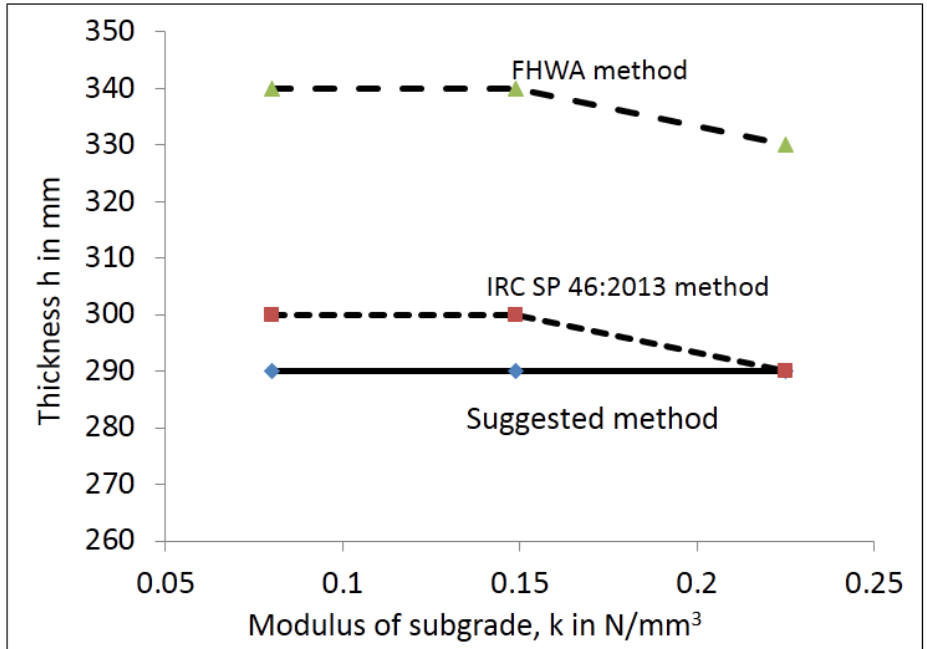


Figure 7.5 Comparison of design solutions for FRC with 10 kg/m<sup>3</sup> of steel fibres

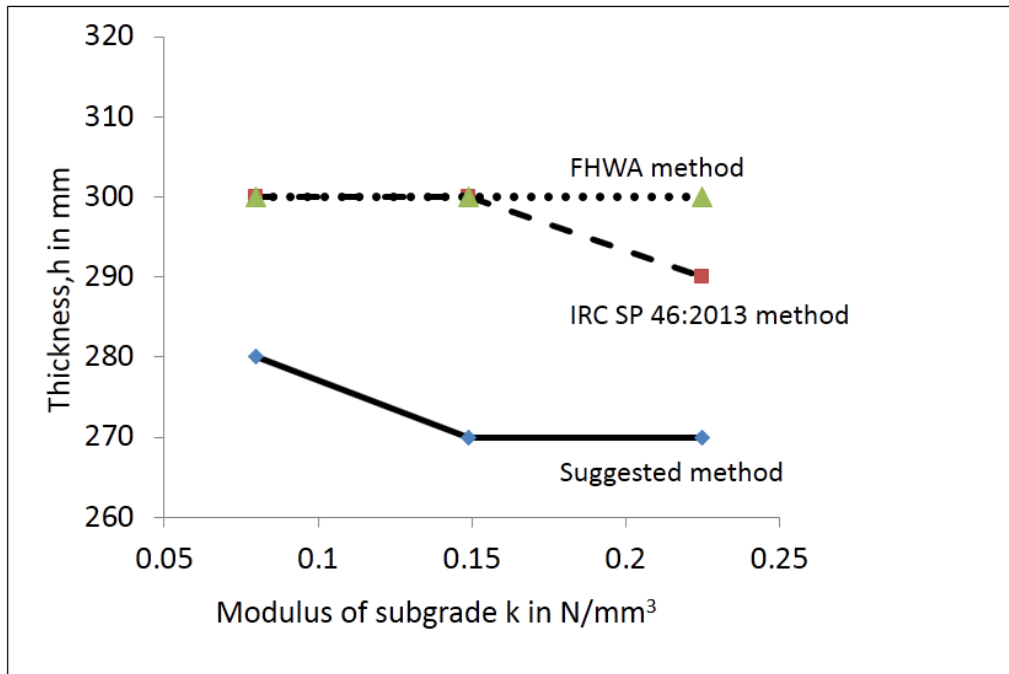


Figure 7.6 Comparison of design solutions for FRC with 20 kg/m<sup>3</sup> of steel fibres

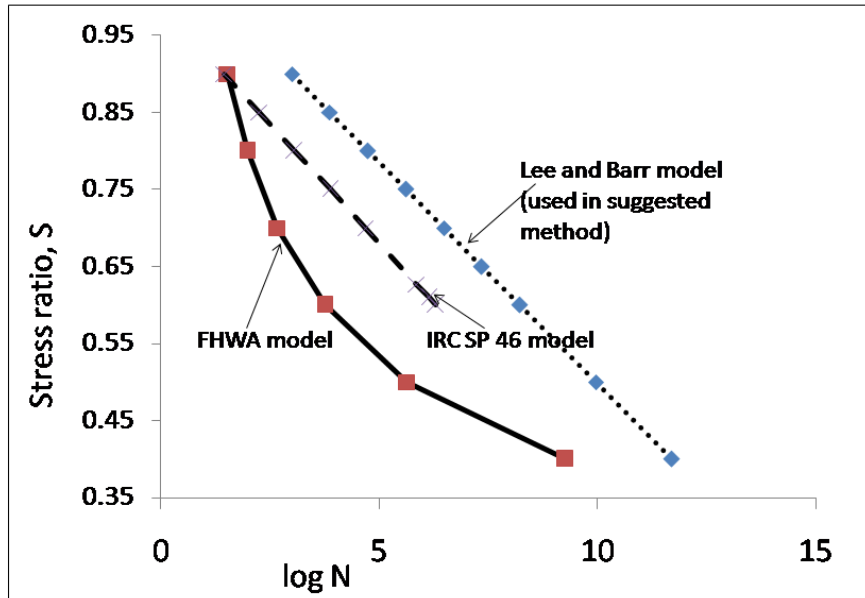
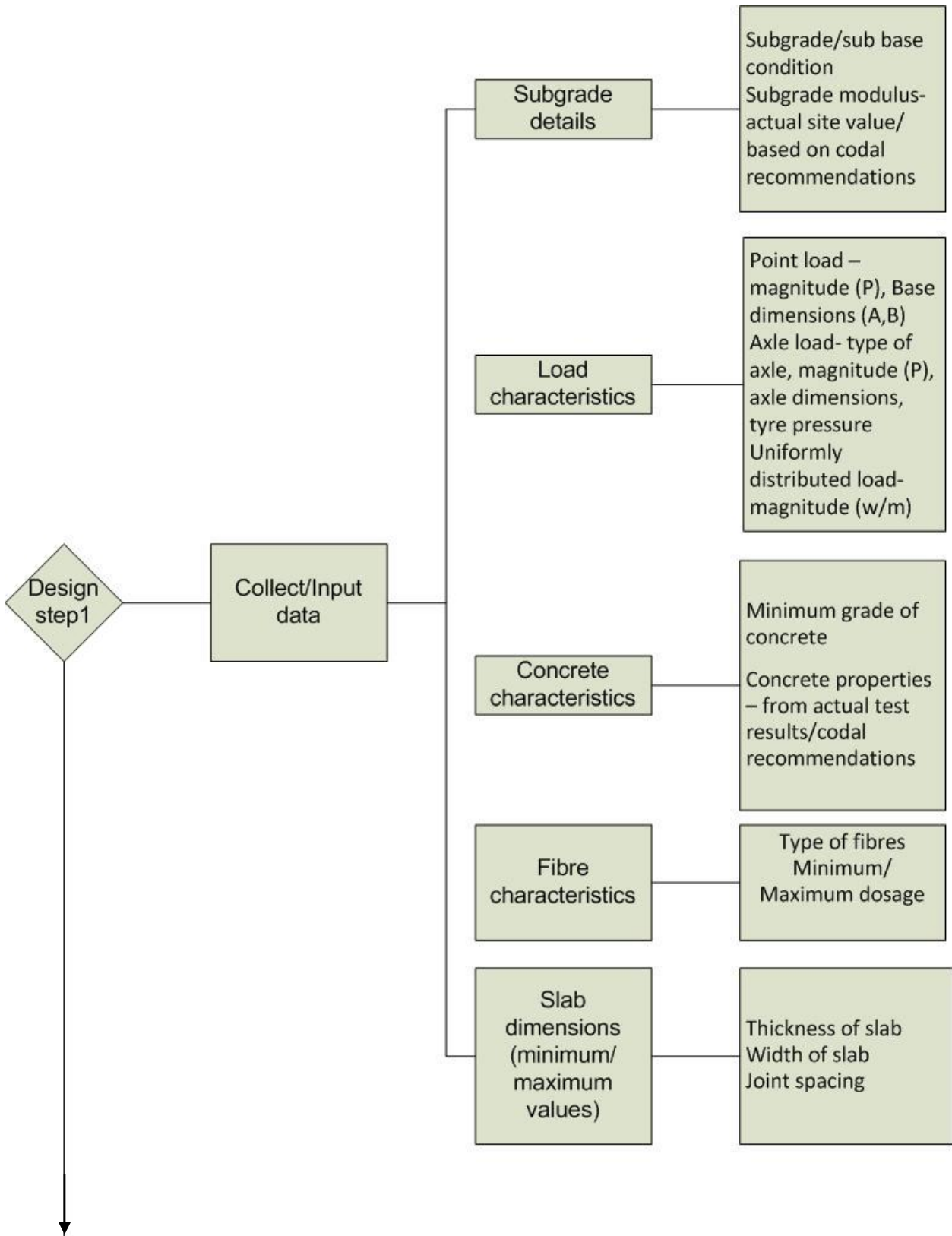
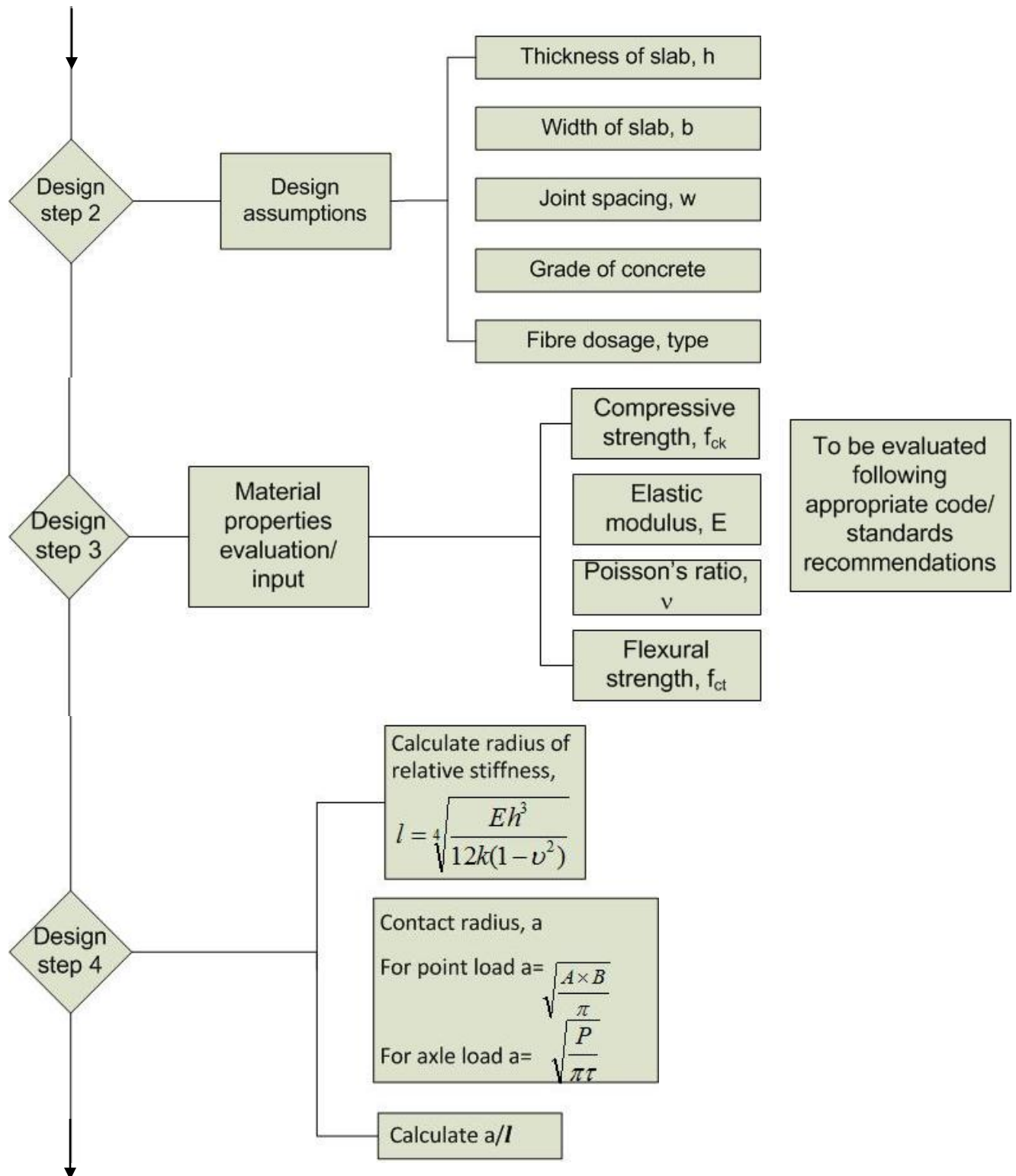


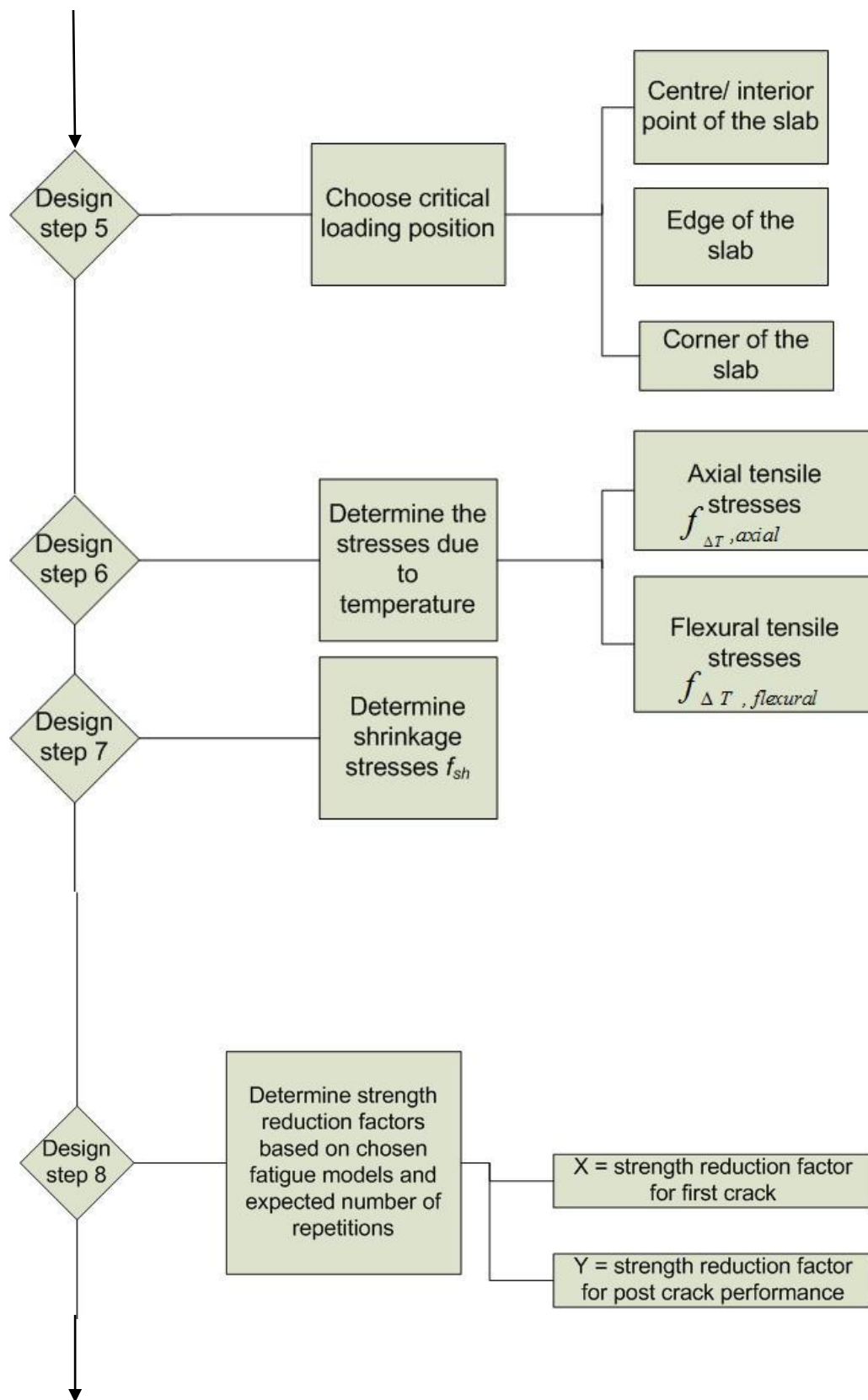
Figure 7.7 Fatigue models for first crack strength used in the three design methods in the comparative study

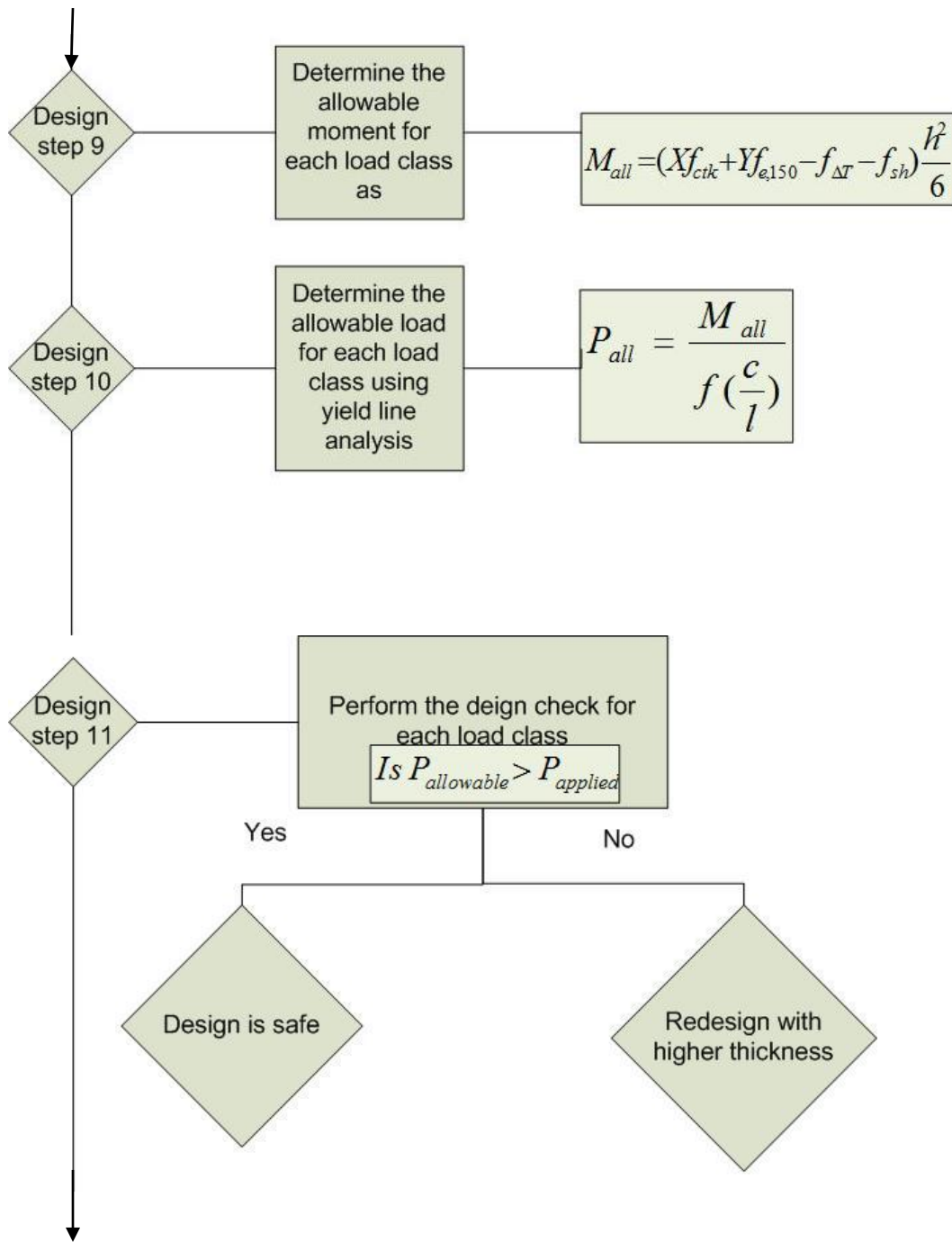
## 7.8 Design framework

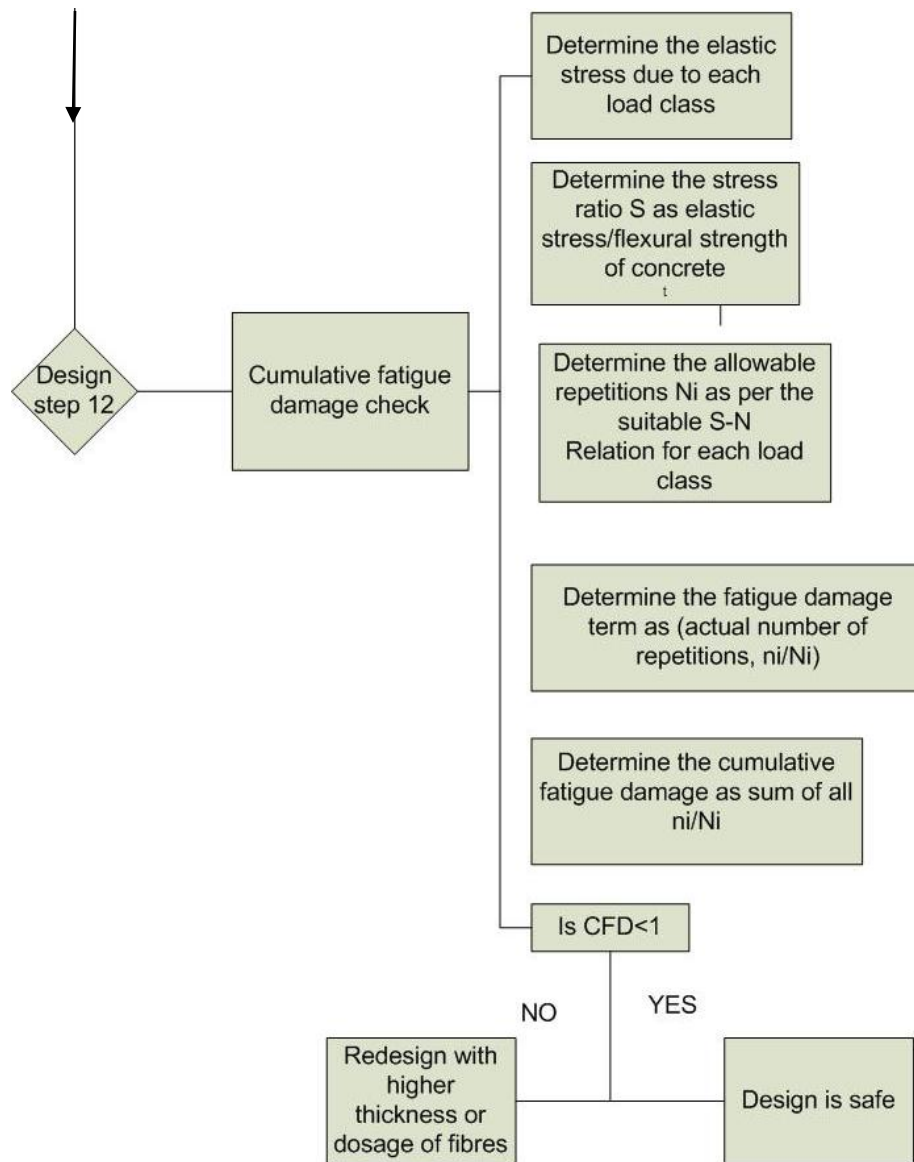
For illustration of the methodology, the design framework is presented below.











## 7.9 Case studies

### 7.9.1 Compilation of trial stretches laid in the IIT Madras Campus

Seven stretches of FRC pavements were laid with various thicknesses and dosage of fibres in the IIT Madras campus over the past five years. The details of these projects are given in Table 7.8, and discussed further in the following sections.

Table 7.8 Details of trial stretches of FRC pavements laid within IIT Madras campus until November 2015

Details	Trial stretch 1 (GATE office)	Trial stretch 2 (Structural Engg. lab)	Trial stretch 3 (Taramani Guest house entrance)	Trial stretch 4 (Border road)	Trial stretch 5 (Biotechnology entrance)	Trial stretches 6-8 (Krishna gate, Hospital and KV school approach roads)	Trial stretch 9 (BSB lab approach road)
Period of casting	April 2009	November 2009	December 2009	February 2011	March 2012	August 2011	April 2012
Length×width of pavement	60 m×5 m	69m×3.5m	60 m×6.5 m	218 m ×4 m	50m×5 m	145m ×4m	70 m×4m
Joint spacing	3 m	3 m	4 m	4 m	2.5 m	2.5 m	3 m
Thickness in mm	150	150	150	120	100	150	150
Grade of concrete	M30	Not known	M35	M35	M40	M35	M35
Fibre type; see Table 4.1 for details	SFB	Not known	SFA	SFB	SFB	SFB	SFB
Fibre dosage/m <sup>3</sup>	15	Not known	25	15	30	20	20

### 7.9.2 Details of Trial stretch 4

A stretch of 218 m of (4.0 m wide) pavement within IIT Madras campus was laid with SFRC during the month of February 2011, in two phases: 124 m in Phase 1 and remaining 94 m in Phase 2. The initial stretch of about 25 m in Phase 1 was laid on ground that had been prepared by removing an old asphalt pavement, which was highly distressed due to the sinking of the ground below, laying water bound macadam compacted by rolling with drum-type rollers, overlaying with quarry dust, and covering with high density polyethylene (HDPE) sheets (see Figure 7.8). The remaining stretch of 100 m of Phase 1 was laid directly on the existing asphalt overlay as it was in good condition. The casting for the first phase commenced at around midday on 2<sup>nd</sup> February 2011, and the full stretch was completed including finishing within 20 hours. The site temperature was around 33°C. A total of 13 trucks of RMC, each carrying 6 m<sup>3</sup> of concrete, were used for the construction.

An average thickness for the concrete slab of 150 mm and minimum thickness of 120 mm was ensured. The concrete was placed and vibrated using screed vibrators (see Figures 7.9 and 7.10). The slump of the concrete was stipulated as 100±20mm, since less workable concrete resulted in the deformation of the fibres. For finishing the surface, power toweling was done followed by brooming with metal wire brush (see Figures 7.11 and 7.12). The curing commenced after 4 hours of casting and was done by ponding (see Figure 7.13). Within 24 hours, saw cutting was done at a groove spacing of 4 m using a disc cutter (see Figure 7.14).



Figure 7.8 Prepared surface of the existing pavement to receive the new concrete (a) leveled surface, (b) HDPE sheet on the prepared surface



Figure 7.9 Concrete being poured and spread on the prepared surface



Figure 7.10 Screed vibration and manual screeding



Figure 7.11 Power trowelling of freshly laid concrete surface



Figure 7.12 Wire brush finishing for final surface texturing



Figure 7.13 Curing of pavement surface by ponding



Figure 7.14 Saw cutting of grooves

Sampling of concrete for compression tests and counting of fibres was done, and the corresponding tests were conducted in the laboratory. The fibre counting was done on both fresh concrete and hardened concrete as per EN 14488 - 7. In the fresh concrete, a sample was washed with water to remove the mortar, and fibres were separated manually using a magnet from the remaining material and weighed. In the dry concrete, the cube used for compression testing was completely crushed, and the fibres were separated out using a magnet and weighed. The results indicated that the samples contained an average dosage of  $14 \text{ kg/m}^3$  of fibres and had an average compressive strength of  $43 \pm 3.1 \text{ N/mm}^2$  at 28 days.

Phase 2 of the trial stretch was laid 2 days after Phase 1 and completed within 16 hours mostly during the night. Due to the delay in saw cutting of the grooves, one crack occurred within 48 hours of casting, running across the pavement, as seen in Figure 7.15.

The pavement was opened for traffic when the compressive strength had reached a value of  $17 \text{ N/mm}^2$ , 3 days after laying the Phase 2 stretch. The pavement performance till date (after about 4.5 years) has been satisfactory with respect to comfort. The traffic density is very low (less than 10 passes of four wheelers per day). However, there is some ready mix concrete truck traffic making the axle loads higher than other similar roads in IIT Madras campus (about 75 passes in a year). Two cracks have been observed in the slabs till date.



Figure 7.15 Crack occurred within 48 hours after casting during the second phase

### **7.9.3 Trial stretch 3**

The FRC pavement was laid at the entrance of the Taramani guest house. The traffic density is moderate (about 30 passes of four wheelers per day), with the highest possible load from water

tankers. The laying of the slab was similar to trial stretch 4. The joint cutting was done after 4 weeks of casting the slab. No cracks have appeared on the slab.



Figure 7.16 Trial stretch 3

#### **7.9.4 Trial stretch 5**

A stretch of 50 m of FRC pavement was laid at the entrance of the Department of Biotechnology in IIT Madras. The pavement is mostly used by two wheelers or four wheelers and has very low traffic density (less than 10 passes of critical loads per day).

#### **7.9.5 Trial stretch 6-8**

Three stretches of FRC pavements were laid having the same design thickness and fibre dosages. Trial stretch 4 is an approach road to the exit gate (for two wheelers only) near the boys' hostel, trial stretch 5 is an approach road to a school on campus, trial 6 is an approach road to the hospital on campus. All three pavements have the same traffic pattern with maximum load corresponding to four wheelers with frequent movement (more than 100 passes of critical loads per day).

#### **7.9.6 Trial stretch 9**

A stretch of FRC pavement has been laid as an approach road to the Construction Materials Testing Laboratory. The stretch was laid prior to receiving a consignment of heavy machinery to

be installed in the laboratory, during which period the axle load on the road was high but with very few passes.

### **7.9.7 Comparison with the design**

For each of the trial stretches (see Table 7.8), the traffic was assessed through observation and discussion with the engineers of IIT Madras, and consequently the corresponding critical loading configurations were identified and reported in Table 7.9, in terms of type of traffic and axle configuration. Further, the current (2015) condition, with respect to cracking and any other visible damage, of each stretch has been given in Table 7.9, along with the estimated repetitions of the critical load till date.

It is assumed that the stretches should have an expected life to be 20 years. Consequently, the load repetitions during the design life has been estimated and given in Table 7.9.

Considering the pavement thickness, grade of concrete, and fibre type and dosage used in each trial stretch laid in the campus (see Table 7.8), the maximum allowable load for the corresponding critical loading configuration was determined according to the suggested design method, and the results are reported in Table 7.9 below. By comparing the calculated maximum loads to observed traffic load, we can see that, with the exception of Stretch 4, the calculated values are more than the actual loading. Considering that only Stretch 4 has experienced cracking, it can be concluded that the observations from the trial stretches support the proposed design method for pavements. For the Stretch 4, as per the suggested method, the minimum required slab thickness, for the critical axle load condition, is 150 mm which is higher than the actual slab thickness.

Table 7.9 Assessment of the design as per the suggested method for trial stretches in IIT Madras

Parameter	Trial stretch 3	Trial stretch 4	Trial stretch 5	Trial stretch 6-8	Trial stretch 9
Critical traffic condition	Moderate traffic density and moderate axle loads	Low traffic density and moderate axle loads	Low density low axle loads	High density low axle loads	Low density high axle loads
Critical axle configuration and corresponding wheel load	Single axle, single wheel 20 kN	Front – Single axle single wheel, Rear – Tandem axle single wheel 30 kN	Single axle, single wheel 20 kN	Single axle, single wheel 20 kN	Front – Single axle, single wheel Rear – Tandem axle, single wheel 30 kN
Estimated load repetitions till date	$10^4$	300	$10^3$	$10^4$	10
Current condition	No cracks	2 major transverse cracks and few narrow longitudinal cracks	No cracks	No cracks	No cracks
Repetitions of critical load taken for the design	$1 \times 10^6$	$1 \times 10^3$	$1 \times 10^6$	$2 \times 10^6$	$1 \times 10^2$
Maximum allowable wheel load for the critical axle configuration as per the design	30 kN	25 kN	15 kN	30 kN	40 kN
Remarks	Satisfactory	Serviceability is satisfactory but thickness is inadequate for preventing cracking	Satisfactory	Satisfactory	Satisfactory

## 7.10 Conclusions

The chapter discusses a design procedure for fibre reinforced concrete pavements considering various failure conditions and criteria. The major conclusions are:

- The design gives specific checks to ascertain the failure pattern and the consequent design strategy to be adopted.
- If the design is governed by material behaviour in the inelastic state then the ultimate load analysis is used to derive full advantage of the FRC potential.
- The limiting moment is obtained assuming the failure condition to be the initiation of cracking at the top of the slab thus making the limiting moment to be the sum of the positive moment at the bottom cracked part of the slab and negative moment at the top of the slab.
- The design method directly incorporates the equivalent flexural strength in the evaluation of the moment carrying capacity.
- Fatigue failure criteria are incorporated in the design by assigning reduction factors for the flexural and equivalent flexural strengths in the calculation of section capacity.
- Thermal and shrinkage stresses are incorporated in the design by reducing the moment capacity by taking into account the estimated stresses.
- Cumulative fatigue damage analysis is done as serviceability check
- A parametric study done on the design illustrates that the design accounts for the critical failure mode (multiple cracking or fatigue cracking) due to the two level check on inelastic moment capacity and cumulative fatigue damage. The design solutions indicate that use of very low dosage (like 10 kg/m<sup>3</sup> of hooked ended steel fibres) results in the failure of slab under much lower stresses by inelastic cracking before fatigue cracking occurs.

- The design according to the proposed method has been compared to the designs as per IRC SP 46:2013 and FHWA, and the solutions obtained are found to give lower thickness and fibre dosage, which could result in more economical solutions.
- Trial stretches of FRC pavement laid on IIT Campus has been compared with the design results for the validation of the methodology.

## 8 CONCLUSIONS AND SCOPE FOR FUTURE WORK

### 8.1 General conclusions

In general, the work has resulted in development of design methodologies for FRC slabs-on-grade and pavements. The work had two facets in which M35 concrete with various types of fibres were characterized and then the results were incorporated in the design for both slabs-on-grade and pavements. The salient conclusions that correspond to the fulfilment of the principle objectives of this work are given below.

- The material characterization programme on M35 grade concrete with various types of fibres demonstrates that the equivalent flexural strength  $f_{e,150}$  is a suitable flexural toughness estimate to be adopted as material parameter in design methods owing to its sensitivity to the type of fibre and the dosage of fibres. The equivalent flexural strength in conjunction with the flexural strength furnish appropriate performance characteristics indicative of the influence of fibres in the crack development in the concrete.
- The results of the flexural toughness tests indicate that the performance of concrete with same dosage of different fibres will vary based on the material, shape and size of fibres. Thus, arbitrarily specifying a dosage applicable to all fibre brands in design/contractual specifications could be unconservative, and the specification of a minimum required  $f_{e,150}$  should be done.
- From the characterization of FRC with various types of steel fibres it was understood that hooked-ended steel fibres does not influence the peak load whereas the peak load and the cracking response are altered by the undulated steel fibres. At the same time, at large deflections the hooked-ended steel fibres are more efficient in comparison to the undulated fibres and vice versa at smaller deflections.
- The flexural toughness characterization of FRC with AMF and steel fibres indicate that the hybrid combination results in significant synergy in the behavior causing an increase in flexural strength as well as post peak capacity. It was later demonstrated that the use of

such mixes in the design of FRC slabs-on-grade and pavements would be beneficial since this leads to significant reduction in thickness requirements.

- The pre-normative proposal for flexural toughness characterization based on the experimental programme can be suitably incorporated in design standards for both FRC slabs-on-grade and pavements as the applicability of the tests have been verified for FRC with most types of fibres available in Indian market. The test configuration, test procedure and reporting methods are described in the guidelines, which have been the basis for the Indian Concrete Institute technical recommendation ICI TC/01.1 (2014)- Test Method for the Flexural Strength and Flexural Toughness Parameters of Fibre Reinforced Concrete.
- The design methodology developed for FRC slabs-on-grade based on inelastic analysis addresses various failure patterns, depending on the dimensions and end conditions of the slab. The expressions for lead to a performance requirement in terms of required equivalent flexural strength for a minimum thickness and chosen grade of concrete. The design allows the use of any fibre and dosage that meets the performance requirement. The methodology considers various failure patterns due to loading and integrates stresses due to temperature variation and restraint to shrinkage.
- The design methodology developed for FRC pavements addresses various critical conditions causing pavement failure based on the dimensions of the slab. Through a dimension check, the governing failure mechanism is categorised into elastic (since pavements are more susceptible to curling, resulting in loss of contact of slab with subbase and fatigue failure) or inelastic. The expressions for inelastic design considers the fatigue response of the material by the use of strength reduction factors in the moment capacity estimate. The design also includes a fatigue damage-accumulation based check thereby ensuring the required performance of the pavement throughout the design life.

## 8.2 Specific conclusions

### 8.2.1 Flexural behaviour of FRC with different fibres and fibre combinations

- Based on the experience gained from the test programme it can be concluded that toughness testing done with the four point bending configuration under stable deflection control is an appropriate characterization technique for qualifying FRC for slabs-on-grade and pavement application.
- In order to ensure proper quality control, it is recommended that nine specimens be prepared for testing to ensure that at least six reliable test results are obtained, since specimens could fail suddenly due to loss of control just after the peak load.
- From the results of the flexural toughness tests it can be concluded that fibres of different materials and shape differ in their influence on the flexural behavior of FRC. Some fibres like undulated steel fibres, glass fibres and amorphous metallic fibres affect the peak load and cracking response but have low influence in the post-cracking capacity especially at large deflections. Hooked-ended steel fibres are more efficient at large deflections and impart significant post-cracking capacity as well as the retention of post-cracking capacity upto large deflections.
- Different combinations of fibre type and dosage can have similar toughness values, and different fibres at the same dosage can give different toughness values, which has important implications for design.
- It has been illustrated from the tests on FRC with hybrid combination of amorphous metallic fibre and steel fibres, that combining the two types of fibres that influence the cracking behavior at different levels of deflection/crack (at first crack and at large crack widths) results in a synergistic effect leading to better performance. Such mixes can be better adopted in cases where the design is significantly affected by the first crack strength even when the design is governed by post-cracking capacity, for example, FRC pavement design.
- Based on the current study, the use of the strength based toughness parameter, equivalent flexural strength  $f_{e,150}$ , is recommended in design methodologies to represent post-

cracking capacity rather than the widely used non-dimensional toughness parameters such as equivalent flexural strength ratio,  $R_{e,150}$ . This is so since normalizing the equivalent flexural strength with peak flexural strength might result in misleading interpretation of the residual capacity, in cases where the post-peak flexural strength enhancement is accompanied by a substantial increase in the flexural strength.

- From the analysis of test results, it can be observed that the characteristic values of strength based toughness parameters (depending on the variability in results) are significantly influenced by the material, size and shape of the fibres used. Consequently, the conversion of mean strength to characteristic strength for FRC, with each type of fibres should be based on the corresponding statistical variation and not on a common factor, e.g., the characteristic value of the equivalent flexural strength of straight hooked-ended steel fibre concrete can be conservatively considered to be 0.7 times the mean value, and for undulated fibres a lower value of 0.65 may be used.
- On an average, the scatter in the values of the residual strength is much higher than in the equivalent strength, which implies that the latter is a more reliable parameter than the former.

### 8.2.2 Inelastic design method for FRC slabs-on-grade

- The developed design procedure considers separate expressions for each possible failure pattern for various combinations of load and load positions. Consequent to the identification of the possible failure patterns, the design incorporates various limiting moment expressions based on yield line theory.
- In all design expressions, the limiting moment capacity is related to either the plastic moment capacity (post-cracking moment capacity)  $M_p$  or the negative moment capacity  $M_n$  or the sum of both capacities based on the failure pattern. The plastic moment capacity/m is estimated as  $M_p = f_{e,150k} \frac{h^2}{6}$  and the negative moment capacity/m is related to the first crack flexural strength as  $M_n = f_{ct,k} \frac{h^2}{6}$ .

- The design equation includes the flexural stresses due to restraint of shrinkage and temperature differentials as an additional stress.
- The design equation estimates the required equivalent flexural strength for the given loading condition, leading to a performance requirement for concrete, and the final design check allows for incorporating the actual material test data along with the variability since the characteristic value of the material parameters have to be provided as input.
- The design methodology has been validated by comparing with data from the literature and it is found that the maximum allowable load is less than the reported collapse load in all cases. In addition, the method has been compared to design solutions of existing design methods relevant to this context.
- Parametric studies of the design method suggest that it is sensitive to the variability in the material parameters, accounting for the performance of the fibres in the concrete mix. The required dosage of fibres increase with high variability of material parameter since the design uses the characteristic values of the material parameters.
- Parametric study also leads to the conclusion that the design is more sensitive to variations in flexural strength than the equivalent flexural strength, once the minimum required post-cracking capacity is ensured, therefore, mixes with fibres enhancing both flexural strength and flexural toughness would perform better.

### **8.2.3 Design methodology developed for FRC pavements**

- The suggested design methodology for FRC pavements addresses various possible failure conditions, based on the dimensions and the temperature profiles in the slab and recommends either elastic or inelastic design, for each case of slab boundary condition.
- As the design incorporates fatigue life, both in the inelastic analysis and the serviceability check, it is governed by either of the two criteria, depending on the fibre dosage, material parameters and thickness of the slab. The most suitable solution is when the design satisfies both the criteria (i.e., inelastic moment capacity check and fatigue damage accumulation check).

- The effect of fatigue on the section capacity of the FRC pavement has been incorporated in the design by applying strength reduction factors to both the materials strength parameters viz., flexural strength and equivalent flexural strength.
- The difference in fatigue response of FRC with respect to first cracking and post cracking is brought in by choosing separate fatigue models for first crack strength and equivalent flexural strength.

### **8.3 Recommendations for future work**

The thesis presents design methodologies for FRC slabs-on-grade and pavements with approaches to address the various failure conditions specific to each application with an underlying commonality in the inelastic principle adopted for design. Though the design methods are quite comprehensive, further studies would give better understanding and suitable models for improving the design efficiency. Some recommendations are:

- A more detailed study of the actual shrinkage characteristics of FRC at the material level and the structural level can be carried out so as to develop suitable models to be incorporated in the design expressions for more realistic values of stresses.
- Numerical modelling and analysis of the slab using appropriate material models for FRC can be performed so as to simulate the response under various loading conditions in order to extend the scope of the design to various fibre combinations and grades of concrete. It will also help in further validating the design procedure.
- An extensive experimental study on the flexural fatigue behaviour of FRC is needed so as to validate existing models and to formulate more efficient models to be incorporated in the design. The study has to be done with respect to the first-crack fatigue characteristics, as well as the post-cracking fatigue characteristic.
- The temperature differential testing method presented in the Appendix D can be extended to FRC slabs with different boundary conditions for various temperature profiles to better understand the response of slab to temperature variation. Numerical modelling and analysis of the test will be needed to validate the results and also to develop a model to be adopted in the design procedure.

- Most significant, especially in the case of FRC pavement design, would be prototype applications with proper instrumentation in order to validate the design methodology. This may require the laying of trial stretches with elaborate instrumentation.



## 9 REFERENCES

**AASHTO** (1993) Guide for Design of Pavement Structures, *American Association of State Highway and Transportation Officials*, USA

**Abbas, A. A., Syed Mohsin, S. M., & Cotsovos, D. M.**, (2014) Seismic Response of Steel Fibre Reinforced Concrete Beam-Column Joints, *Engineering Structures*, Vol. 59, pp 261–283

**ACI 360R** (2010) Guide to Design of Slab-on-Ground, *American Concrete Institute*, Detroit, USA.

**ACI 544.2R** (2009) Measurement of Properties of Fiber Reinforced Concrete, *American Concrete Institute*, USA.

**ACI 544.3R-08** (2008). Guide for Specifying, Proportioning and Production of Fibre-Reinforced Concrete, *American Concrete Institute*, USA.

**Alani, A. M., Beckett, D., & Khosrowshahi, F.** (2012) Mechanical Behaviour of a Steel Fibre Reinforced Concrete Ground Slab, *Magazine of Concrete Research*, Vol. 2, No. 7, 12 p.

**Alani, A. M., & Beckett, D.** (2013) Mechanical Properties of a Large Scale Synthetic Fibre Reinforced Concrete Ground Slab, *Construction and Building Materials*, Vol. 41, pp 335–344.

**Altoubat, S. A., Roesler, J. R., Lange, D. A., & Alexander, K. R.** (2008) Simplified Method for Concrete Pavement Design with Discreet Structural Fibres, *Construction and Building Materials*, Vol. 22, pp 384-393.

**ASTM C1018-97** (1997) Standard Test Method for Flexure Toughness and First Crack Strength of Fibre – Reinforced Concrete (Using Beam with Third- Point Loading), *American Society of Testing and Materials*, USA.

**ASTM C1399/C 1399 M-10** (2010) Standard Test Method for Obtaining Average Residual-Strength of Steel Fibre Reinforced Concrete, *American Society of Testing and Materials*, Philadelphia, USA.

**ASTM C1550-08 (2008)** Standard Test Method for Flexural Toughness of Fibre Reinforced Concrete (Using Centrally Loaded Round Panel), *American Society of Testing and Materials*, USA.

**ASTM C1609/C1609M-10** (2010) Standard Test Method for Flexural Performance of Fiber Reinforced Concrete (Using Beam with Third-Point Loading), *American Society of Testing and Materials*, USA.

**Balaguru, P. and Shah, S. P.** (1992) *Fibre Reinforced Cement Composites*, McGraw-Hill, New York.

**Banthia, N. and Trottier, J. F.** (1995) Test Methods for flexural toughness characterization of fibre reinforced concrete: Some concerns and proposition, *ACI Materials Journal*, Vol. 92, No. 1, pp 48-57.

**Banthia, N., & Mindess, S.** (2004). Toughness Characterization of Fiber-Reinforced Concrete: Which Standard to Use?, *Journal of Testing and Evaluation*, Vol. 32, No. 2, 5 p.

**Banthia, N., & Mindess, S.** (2012) Polymer Fibres as Concrete Reinforcement: a Second Look, *Proc. of the Conference on Fibre Reinforced Concrete – Global Developments, FIBCON 2012*, Nagpur, pp 49-73

**Barr, B., Gettu, R., Al-Oraimi, S. K. A. & Bryars, L. S.** (1996) Toughness Measurement - The Need to Think Again, *Cement and Concrete Composites*, Elsevier, Vol. 18, pp 281-297.

**Barr, B. I. G., Lee, M. K., Barragán, B., Dupont, D., Gettu, R., Olesen, J. F., Stang, H. & Vandewalle, L.** (2003) Round-Robin Analysis of The RILEM TC 162-TDF Uni-Axial Tensile Test: Part 1, Test Method Evaluation, *Materials and Structures*, Vol. 36, pp 265-274.

**Barragan, B., Gettu, R., Zalochi, R.F., Martin, M.A. & Agullo, L.** (2000) A Comparative Study of the Toughness of Steel Fibre Reinforced Concrete in Tension, Flexure and Shear,

*Proc. of Fifth International RILEM symposium on Fibre-Reinforced Concrete (Lyon, France)*, Eds. Rossi, P., & Chanvillard, G., RILEM Publications S.A.R.L., France, pp 441-450.

**Barragan, B., Gettu, R. and Zerbino, R.** (2003) Uniaxial Tension Test for Steel Fibre Reinforced Concrete – A Parametric Study, *Cement & Concrete Composites*, Vol. 25, No. 7 , pp 767-777.

**Barragán, B., Gettu, R., Ramos, G., Garcia, T., Fernández, C., & Oliver, R.** (2004) Potential Use of Steel Fiber Reinforced Concrete for the Barcelona Metro Tunnel Lining, *Proc. of International. Conference on Concrete and Construction*, Eds. Jagannadha Rao, P., Ramakrishnan, V., & Parameswaran, V. S., Allied Publishers, Vol. II, Hyderabad, pp 603-614.

**Barragan, B., Gettu, R., Agullo, L., & Zerbino, R.** (2006) Shear Failure of Steel Fibre Reinforced Concrete Based on Push-Off Tests, *ACI Materials Journal*, Vol. 103, No. 4, pp 251-257.

**Barros, J.** (1999) Analysis of Concrete Slabs Supported on Soil, Métodos Numéricos en Ingeniería, SEMNI, Spain, Eds. Abascal, R., Domínguez, G., & Bugada, J., pp 1–21.

**Barros, J. A. O., & Figueiras, J. A.** (2001) Model for the Analysis of Steel Fibre Reinforced Concrete Slabs on Grade, *Composites and Structures*, Vol. 79, No. 1, pp 97–106.

**Batson, G., Ball, C., Bailey, L., Landers, E., & Hooks, J.** (1972) Flexural Fatigue Strength of Steel Fibre Reinforced Concrete Beams, *ACI Journal*, Vol. 69, No. 11, pp 673-677.

**Baumann, R. A., & Weisberg, F. E.** (1983) Yield-Line Analysis of Slabs-on-Grade, *Journal of Structural engineering, ASCE*, Vol. 109, No 7, July, pp 1153-1568.

**Bayasi, Z., & Gebman, M.** (2002), Reduction of Lateral Reinforcement in Seismic Beam-Column Connection Via Application of Steel Fibers, *ACI Structural Journal*, Vol. 99, No. 6, pp 772–780.

**Beckett, D.** (1991) Report for Fibre Systems International (FSI) on the Load Testing of Wirand Steel Fibre Reinforced Ground Slabs, Report No: TP/FS1/2, Thames Polytechnic, Dartford, UK.

**Belletti, B., Bernardi, P., Meda, A., & Plizzari, G.** (2008) A NLFM Method for the Prediction of Slabs on Grade Behavior, Article, Department of Engineering Design and Technologies, University of Bergamo, Italy, 6 p.

**Belletti, B., Cerioni, R., Meda, A., & Plizzari, G.** (2009) Design Aspects on Steel Fiber-Reinforced Concrete Pavements. *ASCE Journal of Materials in Civil*, Vol. 20, No. 9, pp 599–607.

**Bekaert** (2001) Steel Fibre Reinforced Industrial Floors – Design in Accordance with Concrete Society TR 34 (2001), Bekaert Dramix Manual.

**Belletti, B., Cerioni, R., & Iori, I.** (2001) Physical Approach for Reinforced-Concrete (PARC) Membrane Elements. *ASCE Journal of Structural Engineering*, Vol. 127 No. 12, pp 1412–1426.

**Bharatkumar, B. H., Udhayakumar, V., Balasubramanian, K., Krishnamoorthy, T. S., Lakshmanan, N., Sharma, A., & Reddy, G. R.** (2008) Investigations on the Lead – Steel Hybrid Fibre Reinforced Concrete, *Proc. of the Seventh International RILEM Symposium on FRC: Design and Applications, BEFIB 2008* (Chennai, India), Ed. Gettu. R, RILEM Publications, pp. 173-182.

B.H. Bharatkumar, V. Udhayakumar, K. Balasubramanian, T.S. Krishnamoorthy, N. Lakshmanan, A. Sharma, G.R. Reddy

**Cachim, P. B.** (1999) *Experimental and Numerical Analysis of the Behaviour of Structural Concrete Under Fatigue Loading With Applications to Concrete Pavements*, Doctoral thesis, Faculty of Engineering, University of Porto, Portugal.

**Casanova, P., & Rossi, P.** (1996) Analysis of Metallic Fiber-Reinforced Concrete Beams Submitted to Bending, *Materials and Structures*, Vol. 29, No. 6, pp 354–361.

**Chang, D. I., & Chai, W.** (1995) Flexural Fracture and Fatigue Behaviour of Steel-Fibre-Reinforced Concrete Structures, *Nuclear Engineering and Design, Elsevier*, Vol. 156, No. 1-2, pp 201-207.

- Chen, L., Mindess, S. & Morgan, D. R.** (1994) Specimen Geometry and Toughness of Steel Fibre Reinforced Concrete, *Journal of Materials in Civil Engineering*, Vol. 6, No. 4, November, pp 529-541.
- Choi, K., & Ku, D.** (2014) Flexural Behaviour of Amorphous Metal-Fiber-Reinforced Concrete, *Structures and Buildings*, Proc. of Institution of Civil Engineers, Korea, 11 p.
- Choi, S. J., Hong, B. T., Lee, S. J., & Won, J. P.** (2014) Shrinkage and Corrosion Resistance of Amorphous Metallic-Fiber-Reinforced Cement Composites, *Composite Structures*, Vol. 107, pp 537–543.
- Choubane, B., & Tia, M.** (1995). Analysis and Verification of Thermal Gradient Effects on Concrete Pavement, *Journal of Transportation Engineering*, Vol. 121, No. 1, pp 75–81.
- Delatte, N. J.** (2014) Concrete Pavement Design, Construction and Performance, Second edition, CRC Press Publications, Taylor & Francis Group.
- di Prisco, M., & Mauri, M.** (2004) Fibre-Reinforced Concrete Industrial Flooring Slabs, FIBERFIX-BADESSI, A-Fibres Technology Pvt. Ltd.
- Elsaigh, W. A., Kearsley, E. P. & Robberts, J. M.** (2005) Steel Fibre Reinforced Concrete for Road Pavement Applications, *Proc. of 24th Southern African Transport Conference (Pretoria)*, South Africa, pp 191-200,
- Elsaigh, W. A.** (2007) *Modelling the Behavior of Steel Fibre Reinforced Concrete Pavements*, Doctoral Thesis, Faculty of Engineering, University of Pretoria.
- EN14488-3** (2006) Testing Sprayed Concrete Part-3: Flexural Strengths (first peak, ultimate and residual) of Fibre Reinforced Beam Specimens, *European Standard Norme Européenne Européische Norm*, CEN, Brussels, 2006.
- EN 14889-2** (2006). Fibres for Concrete - Part 1: Polymer Fibres - Definitions, Specifications and Conformity, *European Standard Norme Européenne Européische Norm*, CEN Brussels.

**EN14488-5** (2006) Test on Sprayed Concrete- Part-5: Determination of Energy Absorption Capacity of Fibre Reinforced Slab Specimens, *European Standard Norme Européenne Européische Norm*, CEN, Brussels.

**EN14488-7** (2006) Testing sprayed concrete - Part 7: Fibre content of fibre-reinforced concrete, *European Standard Norme Européenne Européische Norm*, CEN, Brussels.

**EN 14651** (2005) Test Method for Metallic Fibered Concrete – Measuring the Flexural Tensile Strength (Limit of Proportionality (LOP), Residual), *European Standard Norme Européenne Européische Norm*, CEN, Brussels.

**EFNARC ENC 371 FTC V1.1\_1** (2011) Testing Sprayed Concrete – EFNARC Three Point Bending Test on Square Panel with Notch, *Experts for Specialised Construction and Concrete Systems*.

**Falkner, H & Teutsch, M.** (1993) Comparative Investigations of Plain and Steel Fibre Reinforced Industrial Ground Slabs, Project report, No. 102, INSTITUT FÜR BAUSTOFFE, MASSIBAU UND BRANDSCHUTZ, Brunswick (D).

**Falkner, H., Huang, Z. & Teutsch, M.** (1995) Comparative Study of Plain and Steel Fibre Reinforced Concrete Ground Slabs, *Concrete International*, American Concrete Institute (ACI), Vol. 17, No. 1, pp 45-51.

**fib Model Code for Concrete Structures** (2010) *fib CEB-FIP* publication, 434 p.

**Fwa, T. F.,** (2006) Handbook of Highway engineering, CRC press, FL, USA, 888 p.

**Ganesan, N., Indira, P. V. & Santhoshkumar, P. T.** (2008) Strength and Behavior of Steel Fibre Reinforced Self Compacting Concrete Columns, *Proc. of the Seventh International RILEM Symposium on FRC: Design and Applications*, BEFIB 2008 (Chennai, India), Ed. Gettu, R., pp 173-182.

**Germano, F., & Plizzari, G. A.** (2013) Fatigue Behaviour of SFRC Under Bending, *Proc. of Eighth RILEM International Conference on Fibre Reinforced Concrete*, Eds, J. Barros et al., Portugal, 12 p.

**Gettu, R., Mobasher, B., Carmona, S., & Jansen, C. D.** (1996) Testing of Concrete Under Closed-Loop Control, *Advanced Cement Based Material Journal*, Elsevier, Vol. 3, No.2, pp 54-71.

**Gettu, R., Saldívar, H., Zerbino, R. L., & Mateos, M.** (1998) On the Characterization of the Toughness of Steel Fiber Reinforced Concretes, *Proc. of 1st Int. Congress of Concrete Technology (Buenos Aires)*, Asociación Argentina de Tecnología del Hormigón, Buenos Aires, Argentina, pp 47-60.

**Gettu, R., Schnütgen, B., Erdem, E., & Stang, H.** (2000) Design Methods for Steel Fiber Reinforced Concrete: A State-of-the-Art Report, Report of Sub-task 1.2 - Test and Design Methods for Steel Fiber Reinforced Concrete Brite-EuRam Project BRPR-CT98-0813 (DG12-BRPR).

**Ghosh, R. K., & Dinakaran, M.** (1970) Breaking Load for Rigid Pavement, *Transportation Engineering Journal, Proc. of ASCE*, Vol. 96, No 1, February, pp 87-107

**Gopalaratnam, V. S., & Gettu, R.** (1995) On the Characterization of Flexural Toughness in Fibre Reinforced Concretes, *Cement and Concrete Composites*, Vol. 17, No. 3, pp 239-254.

**Granju, J. L., Sabathier, V., Alcantara, M., Pons, G., & Mouret, M.** (2004) Hybrid Fiber Reinforcement of Ordinary or Self-Compacting Concrete, *Proc. of 6th RILEM Symp. on Fiber reinforced concrete*, BEFIB 2004 (Varenna, Italy), Eds. di Prisco, M., Felicetti, R., and Plizzari, G. A., Vol. 2, pp 1311-1330.

**Hameed, R., Duprat, F., Turatsinze, A., & Sellier, A.** (2009) Mechanical Properties of Fibrous Concrete Beams Under Reverse Cyclic Loading, *Proc. of 1st International Conference on Sustainable Built Environment Infrastructures in Developing Countries*, SBEIDCO, ENSET, Oran (Algeria), pp 271–278.

**Hameed, R., Turatsinze, A., Duprat, F., & Sellier, A.** (2009) Metallic Fiber Reinforced Concrete: Effect of Fiber Aspect Ratio on the Flexural Properties, *ARPN Journal of Engineering and Applied Sciences*, Vol. 4, No. 5, pp 67–72.

**Hameed, R., Turatsinze, A., Duprat, F., & Sellier, A.** (2010) Study on the Flexural Properties of Metallic-Hybrid-Fiber-Reinforced Concrete, *Maejo International Journal of Science and Technology*, Vol. 4, No. 2, pp 169–184.

**Hameed, R., Sellier, A., Turatsinze, A., & Duprat, F.** (2013) Flexural Behaviour of Reinforced Fibrous Concrete Beams: Experiments and Analytical Modeling, *Pak Journal of Engineering and Applied Science*, Vol. 13, pp 19–28.

**Holschemacher, K. & Müller, T.** (2007) Influence of Fibre Type on Hardened Properties of Steel Fibre Reinforced Concrete, *Proc. of 9th International Conference on Modern Building Materials, Structures and Techniques*, Vilnius Gediminas Technical University, Lithuania, May 16-18, , [http://leidykla.vgtu.lt/conferences/MBM\\_2007/](http://leidykla.vgtu.lt/conferences/MBM_2007/), accessed 1st August 2013.

**Hossain, A. B., & Weiss, W. J.** (2004) Assessing Residual Stress Development and Stress Relaxation in Restrained Concrete Ring Specimen, *Cement and Concrete Composites*, Elsevier, Vol 26, No. 5, pp 531-540.

**Huang, Y. H.** (2004), *Pavement Analysis and Design*, Second Edition, Pearson.

**ICI-TC/01.1** (2014) Test Methods for the Flexural Strength and Toughness Parameters of Fiber Reinforced Concrete, *Indian Concrete Institute Technical Committee Recommendation*, Indian Concrete Institute Journal, Vol. 15, No. 2, pp 39–43.

**Ioannides, A. M.** (2006) Concrete Pavement Analysis : the First Eighty Years,. *International Journal of Pavement Engineering*, Vol. 7, No. 4, pp 233–249.

**IRC: 58** (1988) Code for Design of Plain Jointed Rigid Pavements, *Indian Road Congress*, New Delhi.

**IRC 58** (2010) Guidelines for Design of Plain Jointed Rigid Pavements for Highways, *Indian Road Congress*, New Delhi.

**IRC SP 46** (1994) Steel Fibre Reinforced Concrete for Pavements, *Indian Road Congress*, New Delhi.

**IRC SP 46** (2013) Steel Fibre Reinforced Concrete for Pavements, *Indian Road Congress*, New Delhi.

**IRC 15** (1988) Standards, Specifications and Code of Practice for Construction of Concrete Roads, *Indian Road Congress*, New Delhi, India, 1988.

**IS 1489 Part 1** (2005) Portland-Pozzolana Cement — Specification Part 1 Fly Ash based, *Bureau of Indian Standards*, New Delhi

**IS 3812 (1999)** Specification for Fly Ash for Use as Pozzolana and Admixture., *Bureau of Indian Standards*, New Delhi.

**IS 383** (2007) Specification for Coarse and Fine Aggregates From Natural Sources for Concrete, *Bureau of Indian Standards*, New Delhi.

**IS 2386 – Part 1** (2007) Methods of Test for Aggregates for Concrete Part I Particle Size and Shape, *Bureau of Indian Standards*, New Delhi.

**IS : 2386 (Part III)** (1963) Methods of Test for Aggregates for Concrete, *Bureau of Indian Standards*, New Delhi.

**IS 10262** (2009) Concrete Mix Proportioning – Guidelines, *Bureau of Indian Standards*, New Delhi.

**Irving, J.** (1996). *Soil Structure Interaction of Fibre Reinforced Concrete Floor Slabs on Grade*, M S thesis, University of New Brunswick, Canada.

**ISO 13270** (2013), Steel Fibres for Concrete - Definitions and Specifications, *International Organisation for Standardisation*, Geneva, Switzerland.

**Jain, K., & Singh, B.** (2013) Flexural Performance Criteria for Steel Fibre Reinforced Concrete – and Experimental Investigation, *Journal of Structural Engineering*, Vol. 40, No. 5, pp 486-495.

**Jamet, D., Gettu, R., Gopalaratnam, V. S. and Aguado, A.** (1995) Toughness of High-Strength Concrete from Notched Beam Tests, *Testing Of Fibre Reinforced Concrete-ACI:SP155*, Eds. D, J. Stevens et al., American Concrete Institute, Detroit, USA, pp 23-39.

**Jafarifar, N., Pilakoutas, K., & Neocleous, K.** (2009) Steel-Fibre-Reinforcement and Increasing the Load-Bearing Capacity of Concrete Pavements, *Intersections/Intersectii*, Vol. 6, No. 7, pp 53–61.

**Jansson, A., Löfgren, I., Concrete, T., & Ab, G.** (2008) Design Methods for Fibre-Reinforced Concrete : A State-of-the-Art Review, *Nordik Concrete Research*, No. 38, pp 31–46.

**Johnston, C. D., & Zemp, R. W.,** (1991) Flexural Fatigue Performance of Steel Fibre Reinforced Concrete – Influence of Fibre Content, Aspect Ratio and Type, *ACI Materials Journal*, Vol. 88, No. 4, pp 374-383.

**JSCE Part III-2 (SF1–SF4)** (1984) Method of Tests for Steel Fiber Reinforced Concrete, *Concrete Library of JSCE*, Japan Society of Civil Engineers.

**JSCE-SF5 Part III** (1984) Method of Tests for Compressive Strength and Compressive Toughness of Steel Fibre Reinforced Concrete, *Concrete Library of JSCE*, The Japan Society of Civil Engineers.

**Kawamata, A., Mihashi, H., & Fukuyama, H.** (2003) Properties of Hybrid Fiber Reinforced Cement-based Composites, *Journal of Advanced Concrete Technology*, Vol. 1, No. 3, pp 283–290.

**Knapton, J.** (2005) Design of ground bearing concrete slabs, *Proc. of African Concrete Code Symposium*, pp 156–188.

**Kim, K. S., Lee, D. H., Hwang, J. H., & Kuchma, D. A.** (2012) Shear Behavior Model for Steel Fiber-Reinforced Concrete Members Without Transverse Reinforcements, *Composites Part B: Engineering*, Vol. 43, No. 5, pp 2324–2334.

**Kumar, S., & Prasad, M. M.** (2008) Flexural Behavior of Short Steel Fibre Reinforced Concrete Beams, BEFIB 2008, *Proc. of Seventh Intl. RILEM, Symp. on Fibre Reinforced Concrete: Design and Applications*, BEFIB, Ed. Gettu, R., pp 209–217.

**Kwak, Y., Eberhard, M. O., Kim, W., & Kim, J.** (2002) Shear Strength of Steel Fiber-Reinforced Concrete Beams without Stirrups, *ACI Structural Journal*, Vol. 99, No. 4, pp 530-538.

**Lee, M. K., & Barr, B. I. G.** (2004) An Overview of the Fatigue Behaviour of Plain and Fibre Reinforced Concrete, *Cement and Concrete Composites*, Elsevier, Vol. 26, No. 4, pp 299-305

**Losberg, A.** (1961) Design Methods for Structurally Reinforced Concrete Pavements, Transactions of Chalmers University of Technology, Sweden.

**Losberg, A.** (1978) Pavements and Slabs on Grade with Structurally Active Reinforcement, *ACI Journal proceedings*, Vol. 75, No. 12, pp 647-657.

**Meda, A.** (2003) On the Extension of the Yield-Line Method to the Design of SFRC Slabs-on-Grade, *Studies and Researches*, Graduate School of Concrete Structures, Politecnico di Milano, Italy, Vol. 24, pp 223-239.

**Meda, A., & Plizzari, G. A.** (2004) New Design Approach for Steel Fiber-Reinforced Concrete Slabs-on-Ground Based on Fracture Mechanics, *ACI Structural Journal*, Vol. 101, No. 3, pp 298–303.

**Meda, A., Minelli, F., Plizzari, G. A., & Riva, P.** (2005) Shear behaviour of steel fibre reinforced concrete beams, *Materials and Structures*, Vol. 38, No. 277, pp 343–351.

**MEPDG (2004)** Guide for Mechanistic Empirical Design of New and Rehabilitated Pavement Structures - Part 3 Design Analysis, Chapter 4-Design of New and Reconstructed Rigid Pavements, *NCHRP*, Illinois, USA.

**Meyerhof, G. G.** (1962) Load Carrying Capacity of Concrete Pavements, *Journal of the Soil Mechanics and Foundations Division*, Vol. 88, No. SM3, pp 89-116.

**Merretz, W., Borgert, J., Smith, G., & Baweja, D.** (2011) Steel Fibre Reinforced Concrete in Construction Contracts and the 3 Mm Residual Flexural Strength Beam Test, *Proc. of International. Conference on Concrete 2011- Building a Sustainable Future*, Perth, Concrete Institute of Australia, 12 p.

- Mindess, S., Chen, L., & Morgan, D. R.** (1994) Determination of First Crack Strength and Flexural Toughness of Steel Fibre - Reinforced Concrete, *Advanced Cement Based Materials*, Elsevier Science, Vol. 1, No. 5, pp 201-208.
- Molins, C., Aguado, A., & Saludes, S.** (2009) Double punch test to control energy dissipation in tension of FRC (Barcelona test), *Materials and Structures.*, Vol. 42, No. 4, pp 415-425.
- Moon, J. H., & Weiss, J.** (2006) Estimating Residual Stress in the Restrained Ring Test Under Circumferential Drying, *Cement and Concrete Composites*, Elsevier, Vol. 28, No. 5, pp 486-496.
- Naaman, A. E., & Hammoud, H.** (1998) Fatigue Characteristics of High Performance Fibre-Reinforced Concrete, *Cement and Concrete Composites*, Elsevier, Vol. 20, No. 5, pp 353-363.
- Narayanan, R., and Darwish, I. Y. S.** (1987) Use of Steel Fibers As Shear Reinforcement. *ACI Structural Journal*, Vol. 84, No. 3, pp 216–227.
- Nayar, S. K. and Gettu, R.** (2012) Characterization of Fibre Reinforced Concrete, *Proc. of Conference on Fibre Reinforced Concrete – Global Developments*, FIBCON, Indian Concrete Institute, Nagpur, pp 30-45.
- Nayar, S. K., Gettu, R., & Sreekrishnan, C.** (2014) Characterization of the Toughness of Fiber Reinforced Concrete – Revisited in the Indian context, *Indian Concrete Journal*, Vol. 88, No. 6, pp 8–23.
- Nataraja, M. C., Dhang, N., & Gupta, A. P.** (2000) Toughness Characterization of Steel Fibre Reinforced Concrete by JSCE Approach, *Cement and Concrete Research*, Vol. 30, No. 4, pp 593- 597.
- Nehdi, M., & Ladanchuk, J. D.** (2004) Fiber Synergy in Fiber-Reinforced Self-Consolidating Concrete, *ACI Materials Journal*, Vol. 101, No. 6, pp 508-517.
- Niranjana, G.** (2011) *Effect of Fibre Reinforcement in Cement Concrete Pavements*, Doctoral Thesis, Dept. of Civil Engineering, NIT Thiruchirapalli.

**Oh, B. H.** (1991) Fatigue Life Distributions of Concrete for Various Stress Levels, *ACI Materials Journal*, Vol. 88, No. 2, pp 122- 128.

**Olariu, I., Ioani, A. M., Poienar, N., & Cociardi, M.** (1992) Seismic Behaviour of Steel Fiber Concrete Beam Column, *Proc. of Tenth World Conference on Earthquake Engineering*, Balkema, Rotterdam.

**Pandey, B. B.,** (2005) Warping Stresses in Concrete Pavements – A Re-Examintaion, *Bulletin of Highway Research, Highway Research Board and Indian Road Congress*, No. 73, New Delhi, pp 49-58

**Parmentier, B., Vandewalle, L. & Rickstal, F.V.** (2008) Evaluation of Scatter of the Post Peak Behaviour of Fibre Reinforced Concrete in Bending: A Step Towards Reliability, *Proc. of Seventh International RILEM Symposium on FRC: Design and Applications*, BEFIB (Chennai, India), Ed. R. Gettu, RILEM Publications, Bagnaux, France, pp 133-144.

**Pasakova, T., & Meyer, C.** (1997) Low Cycle Fatigue of Plain and Fibre Reinforced Concrete, *ACI Materials Journal*, Vol. 94, No. 4, pp 273-286.

**PCA** (1984) Thickness Design for Concrete Highway and Street Pavement, Portland Cement Association, USA.

**Pons, G., Mouret, M., Alcantara, M., & Granju, J. L.** (2006) Mechanical Behaviour of Self-Compacting Concrete with Hybrid Fiber Reinforcement, *Materials and Structures*, Vol. 40, No. 2, 2006, pp 201–210.

**Rao, K. S. S., & Singh, S.** (1986) Concentrated Load Carrying Capacity of Concrete Slabs-on-Ground, *Journal of Structural Engineering*, ASCE, Vol. 112, No. 12, pp 2628-2642.

**Ravi, K., & Prakash, K. B.** (2008) An Experimental Investigation of Characteristic Properties of Hybrid Fibre Reinforced Concrete Subjected to Elevated Temperature, *Proc. of the Seventh International RILEM Symposium on FRC: Design and Applications*, BEFIB 2008 (Chennai, India), Ed. R. Gettu, RILEM Publications, pp. 173-182.

- Redon, C., & Chermant, J-L.** (1999) Damage Mechanisms Applied to Concrete Reinforced with Amorphous Cast Iron fibers, Concrete Subjected to Compression, *Cement and Concrete Composites*, Vol. 21, No. 3, pp 197-204.
- Reinhardt, H. W., & Cornelissen H. A. W.** (1984) Post-Peak Cyclic Behaviour of Concrete in Uniaxial Tensile and Alternating Tensile and Compressive Loading, *Cement and Concrete Research*, Vol. 14, No. 2, pp 263-270.
- Roesler, J. R., Altoubat, S. A., Lange, D. A., Rieder, K., & Ulreich, G. R.** (2006) Effect of Synthetic Fibers on Structural Behavior of Concrete Slabs-on-Ground, *ACI Materials Journal*, Vol. 103, No. 1, pp 3–10.
- Roesler, J., Bordelon, A., Ionnides, A., Beyer, M., & Wong, D.** (2008) A Report of the Findings of Design and Concrete Material Requirements for Ultra-Thin White Toppings, Research Report FHWA-ICT-08-016, Illinois Centre for Transportation, USA.
- Rossi, P., Acker, P., & Malier, Y.** (1987) Effect of Steel Fibres at Two Different Stages : The Material and the Structure, *Materials and Structures*, Vol. 20, No. 6, pp 436–439.
- Rossi, P.** (1992) Mechanical Behaviour of Metal-Fiber Reinforced Concretes, *Cement and Concrete Composites*, Vol. 14, No. 1, pp 3–16.
- RILEM TC 162-TDF** (2003) Test and Design Methods for Steel Fibre Reinforced Concrete – Final Recommendations for the  $\sigma$ - $\varepsilon$  Design Method, *Materials and Structures*, Vol. 36, pp 560-567.
- Ringo, B. C., & Anderson, R. B.** (1996) Designing floor slabs on grade- Step-by-step procedures, sample solutions and commentary, The Aberdeen Group Division of Hanley – Wood, Inc., Illinois, USA.
- Saldívar, H.** (1999) Flexural Toughness Characterization of Steel Fibre Reinforced Concrete - Study of Experimental Methods and Size Effects, Doctoral thesis, Universitat Politècnica de Catalunya, Barcelona, Spain.

**Sousa, J. L. A. O & Gettu, R.** (2006) Determining the Tensile Stress-Crack Opening Curve of Concrete by Inverse Analysis, *Journal of Engineering. Mechanics*, Vol. 132, No. 2, pp. 141-148.

**See, H. T., Attiogbe, E. K., & Miltenberger, M. A.** (2004) Potential for Restrained Shrinkage Cracking for Concrete and Mortar, *Cement, Concrete and Aggregates*, Vol. 26. No.2, pp 1-7.

**Shah, S. P., Brandt, A. M., Ouyang, C., Baggot, R., Eibl, J., Glinicki, M. A., Krenchel, H., Lambrechts, A., Li, V. C., Mobasher, B., and Taerwe, L.** (1996) Toughness Characterization and Toughening Mechanisms, Chapter 6, High Performance Fiber Reinforced Cement Composites 2, Eds. A. E. Naaman and H. W. Reinhardt, E&FN Spon, London, UK, pp 193-224.

**Sharma, H. K., Sharma, R. K., and Kant, S.** (2015) Behaviour of High Performance Fibre Reinforced Concrete Beam Column Joints, *Proc. of the International Conference on Transportation in Civil Engineering*, ICTCE, London, pp 108–115.

**Shentu, L., Jiang, D., & Cheng-Tzu Thomas Hsu.** (1997) Load-Carrying Capacity for Concrete Slabs on Grade, *ASCE Journal of Structural Engineering*, Vol. 123, No. 1, pp 95–103.

**Singh, S. P., & Kaushik, S. K.** (2003) Fatigue Strength of Steel Fibre Reinforced Concrete in Flexure, *Cement and Concrete Composites*, Elsevier, Vol. 25, No. 7, pp 779-786.

**Singh, S. P., Goel, S., Lal, R., & Kaushik, K.** (2004) Prediction of Mean and Design Fatigue Lives of Steel Fibrous Concrete Using S-N Relationships, *Asian Journal of Civil Engineering (Building and Housing)*, Vol. 5, Nos. 3-4, pp 175-190.

**Sivakumar, A., & Santhanam, M.** (2007) Mechanical Properties of High Strength Concrete Reinforced with Metallic and Non-Metallic Fibres, *Cement and Concrete Composites*, Elsevier, Vol. 29, No. 8, pp 603-608.

**Slowik, V., Plizzari, G. A., & Saouma, V. E.** (1996) Fracture of Concrete Under Variable Amplitude Fatigue Loading, *ACI Materials Journal*, Vol. 93, No. 3, pp 272-283.

- Soltanzadeh, F., Barros, J. A. O., & Santos, R. F. C.** (2015) High Performance Fiber Reinforced Concrete for the Shear Reinforcement: Experimental and Numerical Research, *Construction and Building Materials*, Vol. 77, pp 94–109.
- Soranakom, C., Yekani-Fard, M., & Mobasher, B.** (2008) Development of Design Guidelines For Strain Softening Fiber Reinforced Concrete, *Proc. of Seventh International RILEM Symposium on FRC: Design and Applications, BEFIB 2008* (Chennai, India), Ed. R. Gettu, RILEM Publications, Bagnaux, France, pp 513-523.
- Sorelli, L. G., Meda, A., & Plizzari, G. A.** (2006) Steel Fiber Concrete Slabs on Ground : A Structural Matter. *ACI Structural Journal*, Vol. 103, No. 4, pp 551–558.
- Soroushian, P., & Bayasi, Z.** (1991) Fibre Type Effects on the Performance of Steel Fibre Reinforced Concrete, *ACI Materials Journal*, Vol. 88, No. 2, pp 129-134.
- Swamy, R. N., Ed.** (1992) Fibre Reinforced Cement and Concrete, *Proc. of Fourth International. Symposium, RILEM*, University of Sheffield, U K.
- Tatnall, P. C.** (2006) Fibre Reinforced Concrete, Significance of Tests and Properties of Concrete and Concrete Making Materials, Eds. Lamond and Pielert, STP 169 D, ASTM International, USA, pp 578-590.
- Thomas, J., & Ramaswamy, A.** (2007) Mechanical Properties of Steel Fiber-Reinforced Concrete, *ASCE Journal of Materials in Civil Engineering*, Vol. 19, No. 5, pp 385–392.
- Trottier, J. F., & Banthia, N.** (1994) Toughness Characterization of Steel Fibre Reinforced Concrete, *Journal of Materials in Civil Engineering, ASCE*, Vol. 6, No. 2, pp 264-289.
- TR 34 (2003)** Concrete Industrial Ground floors: A Guide to Design and Construction, *The Concrete Society*, England.
- TR34 (2013)** Concrete Industrial Ground floors: A Guide to Design and Construction, *The Concrete Society*, England.

**UNE 83515 (2010)** Fibre Reinforced Concrete – Determination of Cracking Strength, Ductility and Residual Tensile Strength – Barcelona Test, *Asociacion Espanola de Normalizacion*, Madrid, Spain.

**Vandewalle, L., Rickstal, F.V., Heirman, G. & Parmentier, B.** (2008) On the Round Panel and 3-Point Bending Tests, *Proc. of Seventh International RILEM Symposium on FRC: Design and Applications, BEFIB 2008* (Chennai, India), Ed. R. Gettu, RILEM Publications, Bagneux, France, pp. 173-182.

**Wang, Y., Li, V.C. & Backer, S.** (1990) Experimental Determination of Tensile Behavior of Fiber Reinforced Concrete, *ACI Materials Journal.*, Vol. 87, No. 5, pp. 461-468.

**Wei, S., Jianming, G., & Yun, Y.** (1996) Study of Fatigue Performance and Damage Mechanism of Steel Fibre-Reinforced Concrete, *ACI Materials Journal*, Vol. 93, No. 3, pp 206-211.

**Weiss, J. W., & Shah, S. P.** (1998) Shrinkage Cracking of Restrained Concrete Slabs, *ASCE Journal of Engineering Mechanics*, Vol. 124, No. 7, pp 765–774.

**Weiss, J.** (1999) *Prediction of Early Age Shrinkage Cracking in Concrete*, Ph.D Thesis, Northwestern University , USA.

**Westergaard, H. M.** (1945) Technical Memorandum on- New Formulas for Stresses and Deflections in Concrete Airfields, Navy department bureau of standards, University of California, September.

**Won, J. P., Hong, B. T., Choi, T. J., Lee, S. J., & Kang, J. W.** (2012) Flexural Behaviour of Amorphous Micro-Steel Fiber-Reinforced Cement Composites, *Composite Structures*, Vol. 94, No. 4, pp 1443–1449.

**Won, J. P., Hong, B. T., Lee, S. J., & Choi, S. J.** (2013) Bonding Properties of Amorphous Micro-Steel Fiber-Reinforced Cementitious Composites, *Composite Structures*, Elsevier Ltd., Vol. 102, pp 101–109.

**Yoder, E. J., & Witczak, M. W.** (1975) Principles of Pavement Design, A Wiley Inter-Science publication, John Wiley and Sons, Canada.

**Zerbino, R. L., Giaccio, G. & Gettu, R.** (2006) Pseudo-Ductile Behavior of Steel Fibre Reinforced High-Strength Concretes, *The Indian Concrete Journal*, Vol. 80, No. 2, pp 37-43.

**Zhang, J., Stang, H., & Li, V. C.** (1999) Fatigue Life Prediction of Fibre Reinforced Concrete Under Flexural Load, *International Journal of Fatigue*, Elsevier, Vol. 21, No. 10, pp 1033-1049.

[http://www.researchgate.net/publication/267402014\\_A\\_nonlinear\\_FE\\_method\\_for\\_the\\_prediction\\_of\\_slabs\\_on\\_grade\\_behaviour](http://www.researchgate.net/publication/267402014_A_nonlinear_FE_method_for_the_prediction_of_slabs_on_grade_behaviour) last accessed 08.10.2015.

<http://repository.up.ac.za/bitstream/handle/2263/6329/021.pdf?sequence=1>; last accessed 31st July 2013.

[http://www.betong.net/ikbViewer/Content/779358/S89%20-%20Anette%20Jansson%20et%20al%202008-07-07\\_just%20af%20DB\\_FINAL.PDF](http://www.betong.net/ikbViewer/Content/779358/S89%20-%20Anette%20Jansson%20et%20al%202008-07-07_just%20af%20DB_FINAL.PDF)

[http://www.maccaferri.com.au/webfiles/MaccaferriAu/files/Industrial\\_Flooring\\_Brochure\\_2011.pdf](http://www.maccaferri.com.au/webfiles/MaccaferriAu/files/Industrial_Flooring_Brochure_2011.pdf), last accessed 12.02.15

[http://www.iitk.ac.in/nicee/wcee/article/10\\_vol6\\_3169.pdf](http://www.iitk.ac.in/nicee/wcee/article/10_vol6_3169.pdf)- last accessed 09-09-15

# APPENDIX A – LOAD DEFLECTION CURVES OF M35 GRADE CONCRETE WITH DIFFERENT STEEL FIBRES

## A.1 Fibre type – SFA

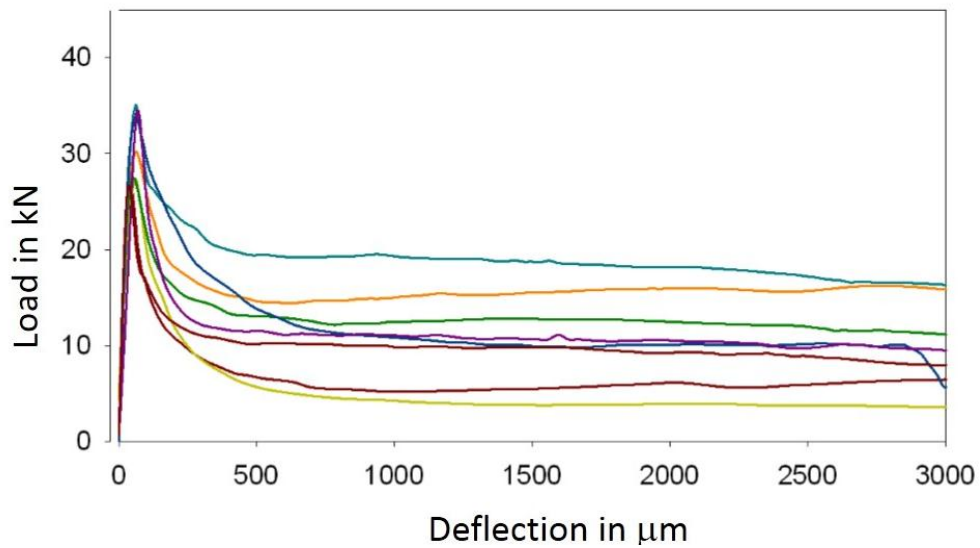


Figure A.1 Load deflection curves of all specimens of M35SFA15 mix

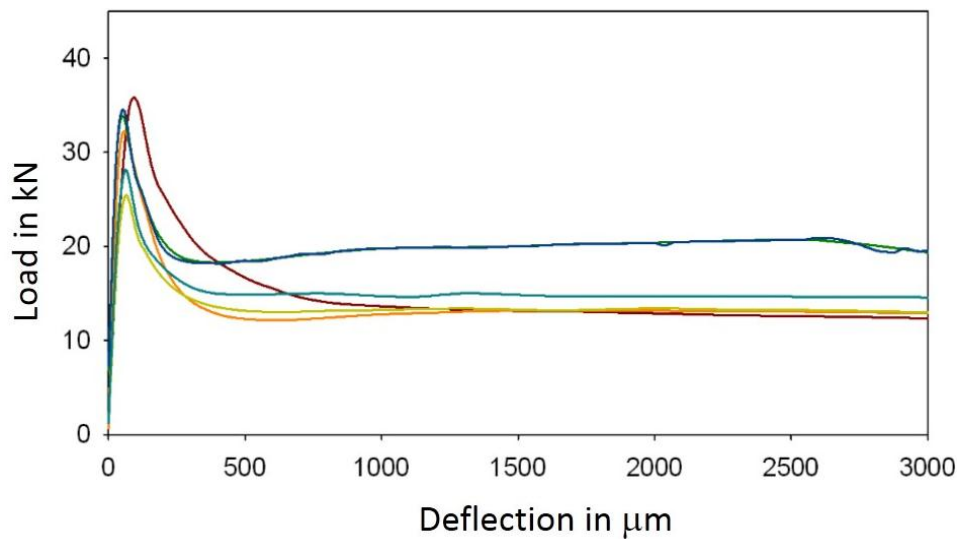


Figure A.2 Load deflection curves of all specimens of M35SFA25 mix

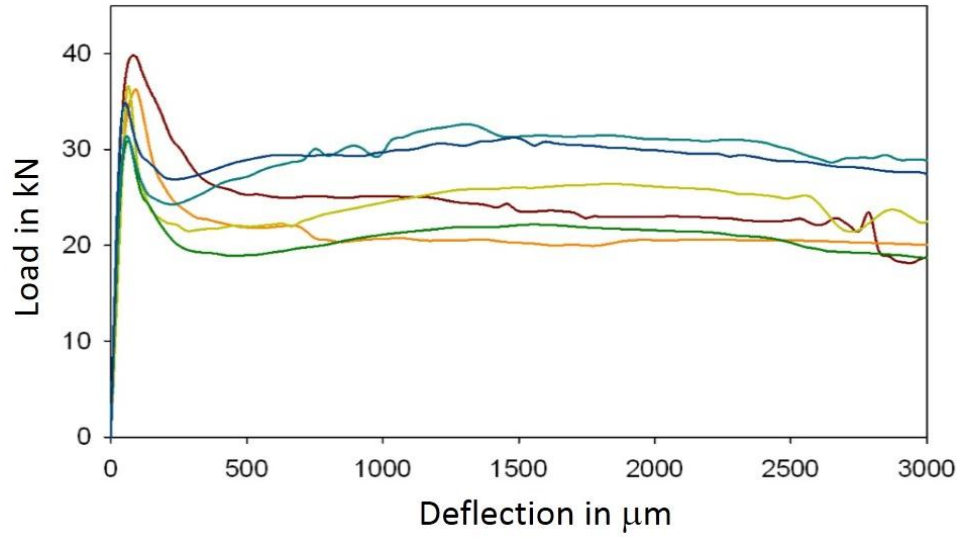


Figure A.3 Load deflection curves of all specimens of M35SFA35 mix

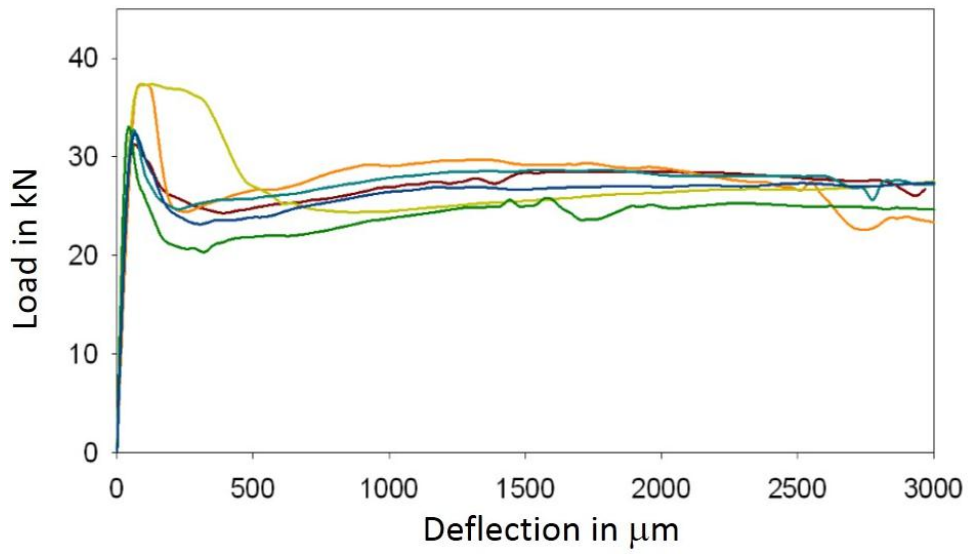


Figure A.4 Load deflection curves of all specimens of M35SFA45 mix

## A.2 Fibre type – SFB

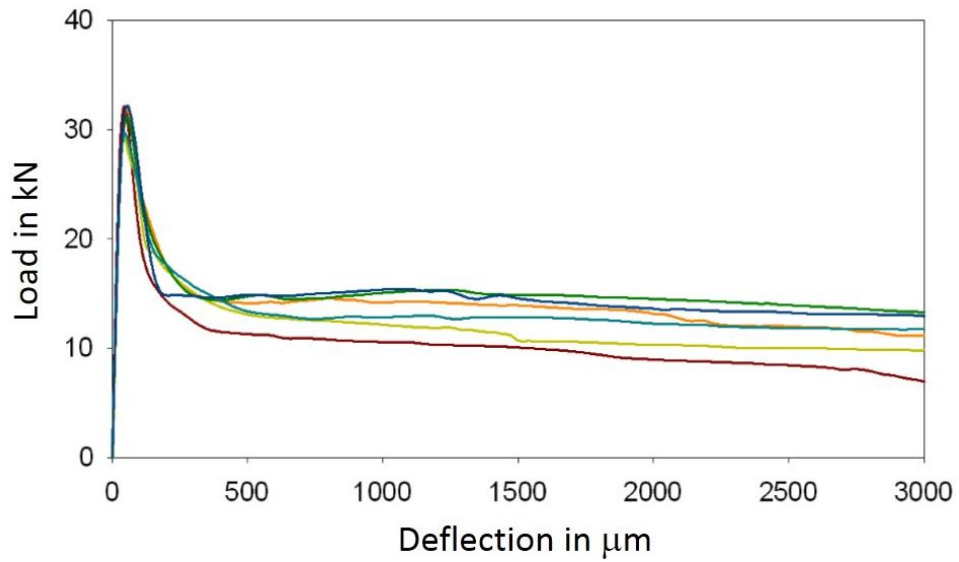


Figure A.5 Load deflection curves of all specimens of M35SFB10 mix

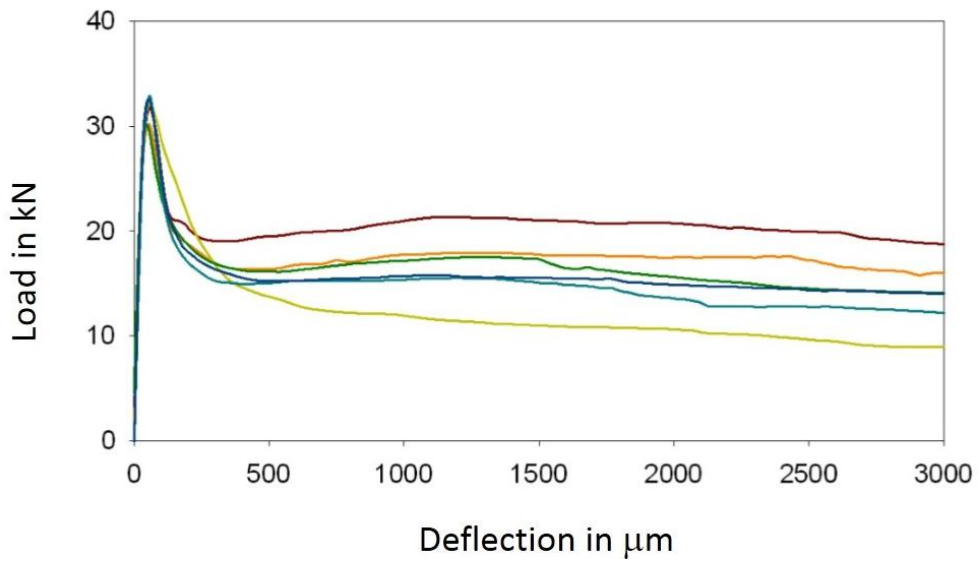


Figure A.6 Load deflection curves of all specimens of M35SFB15 mix

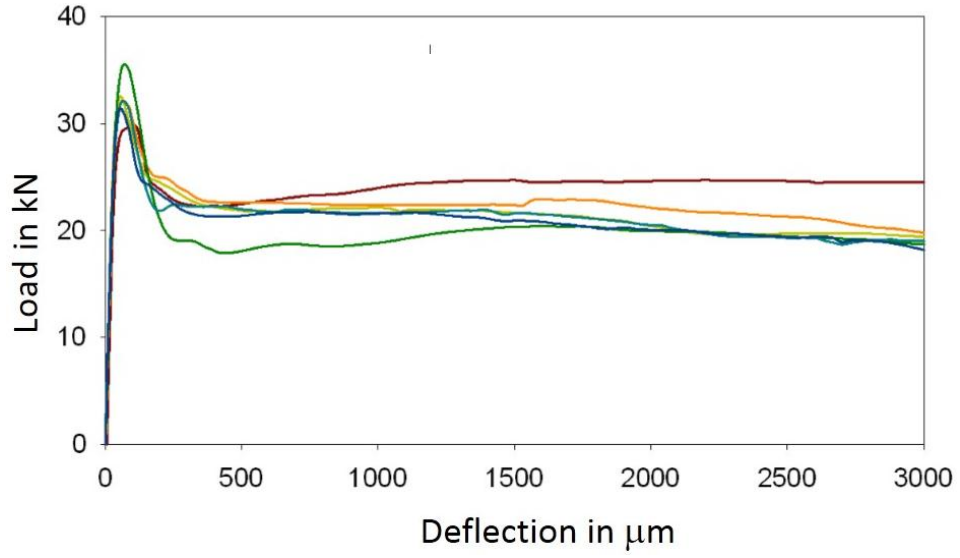


Figure A.7 Load deflection curves of all specimens of M35SFB20 mix

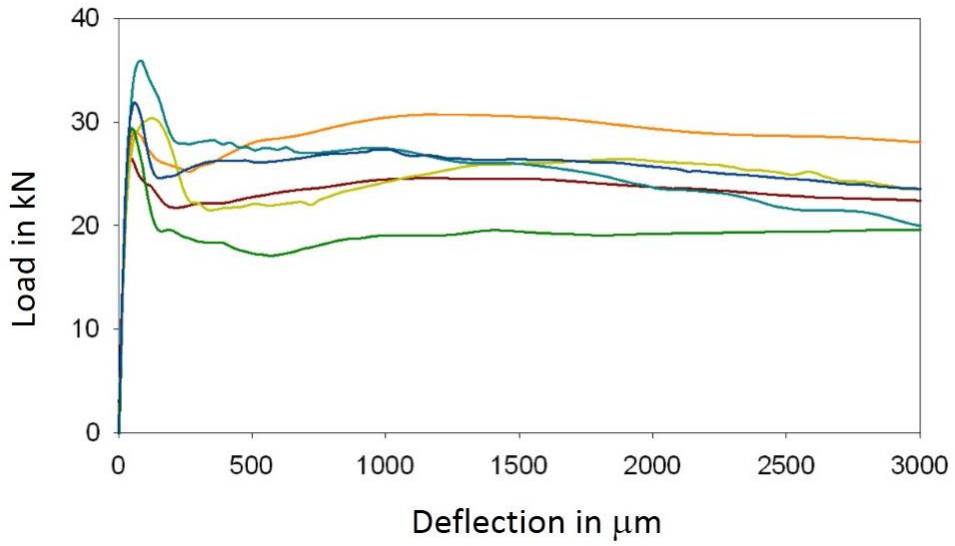


Figure A.8 Load deflection curves of all specimens of M35SFB30 mix

### A.3 Fibre type - SFC

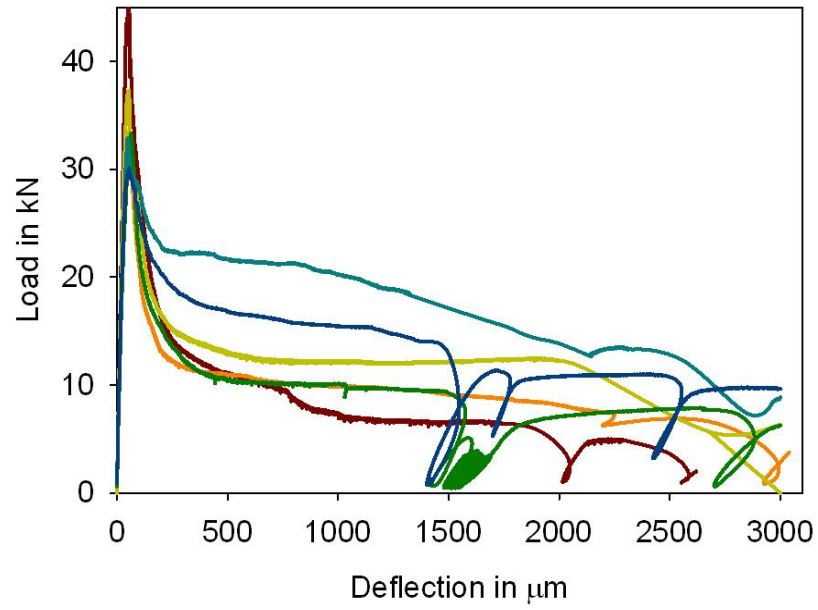


Figure A.9 Load deflection curves of all specimens of M35SFC15 mix

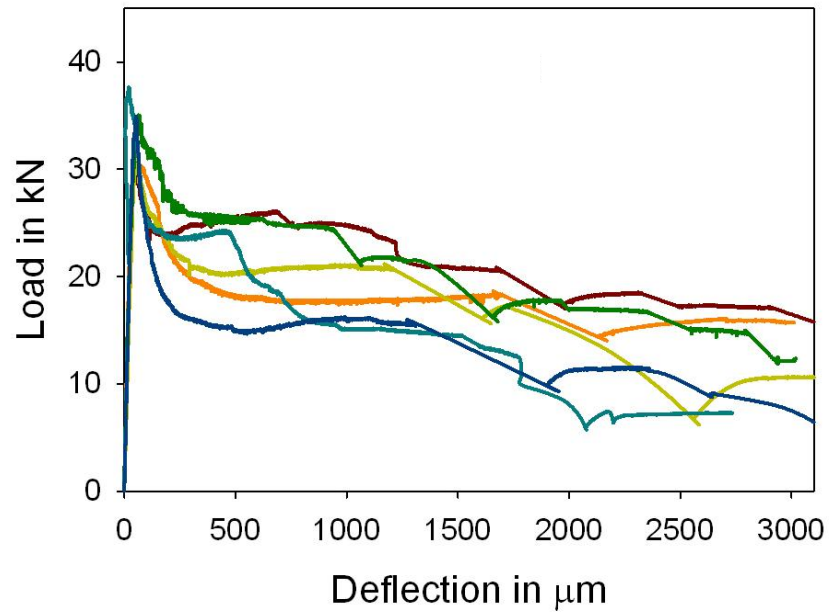


Figure A.10 Load deflection curves of all specimens of M35SFC25 mix

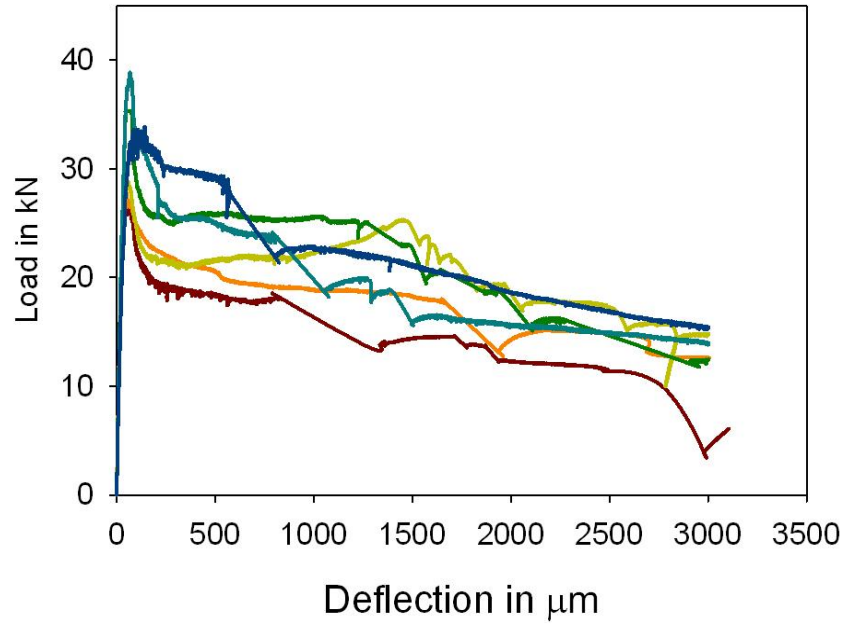


Figure A.11 Load deflection curves of all specimens of M35SFC35 mix

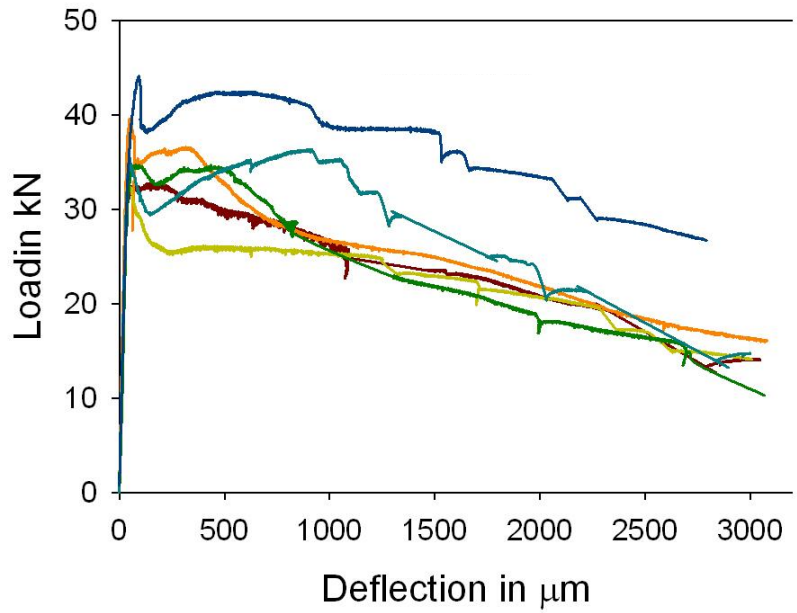


Figure A.12 Load deflection curves of all specimens of M35SFC45 mix

#### A.4 Fibre type – SFD

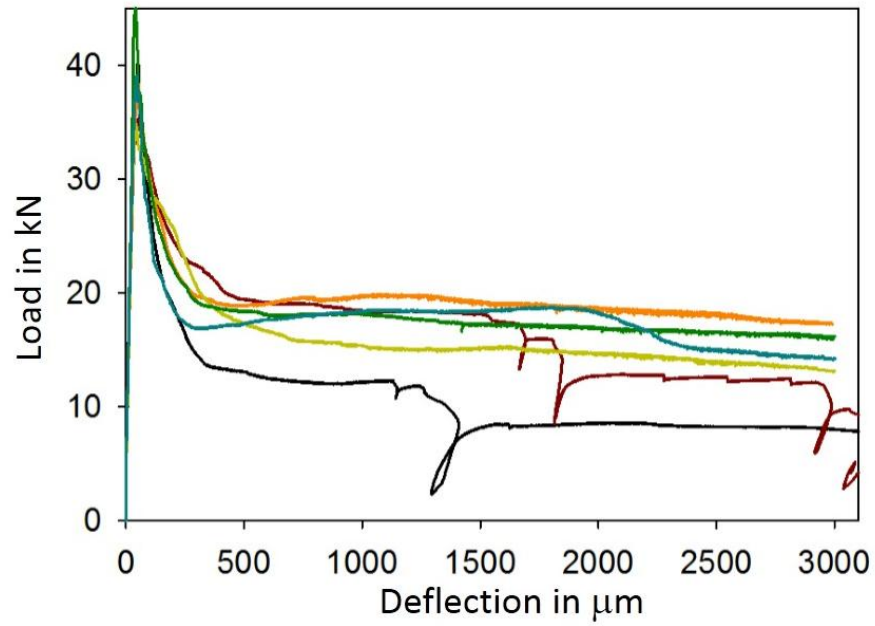


Figure A.13 Load deflection curves of all specimens of M35SFD15 mix

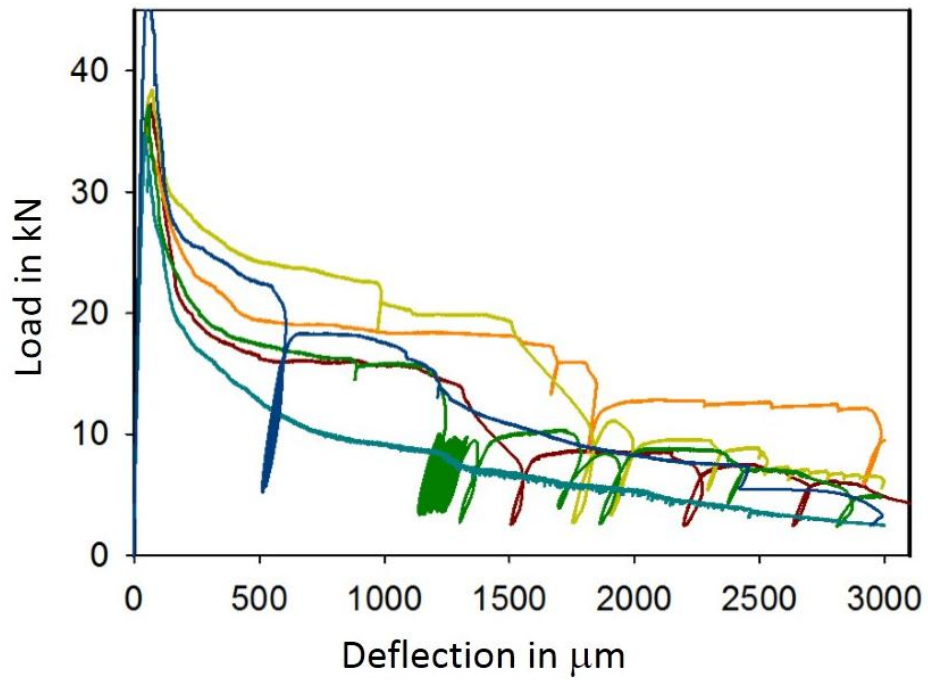


Figure A.14 Load deflection curves of all specimens of M35SFD25 mix

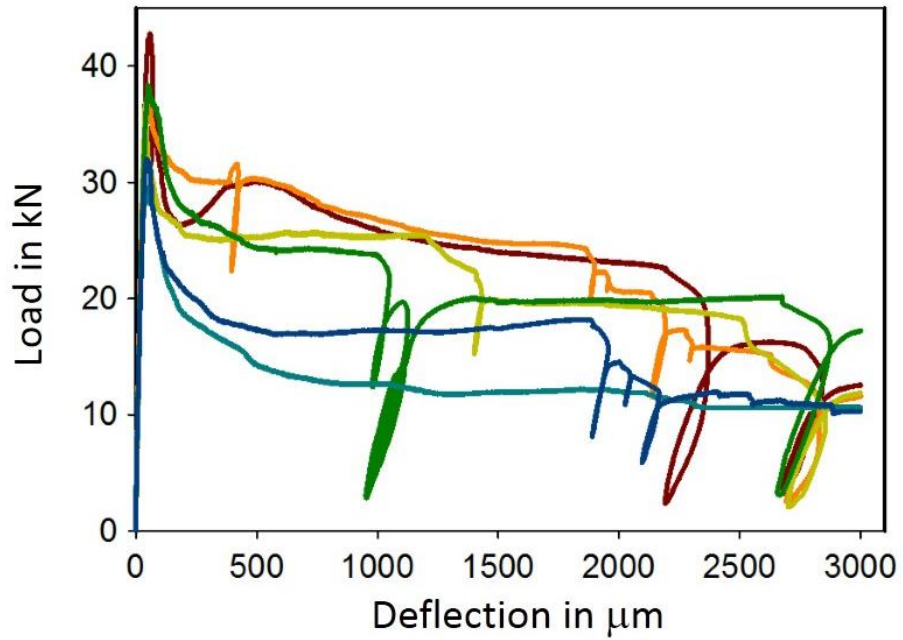


Figure A.15 Load deflection curves of all specimens of M35SFD35 mix

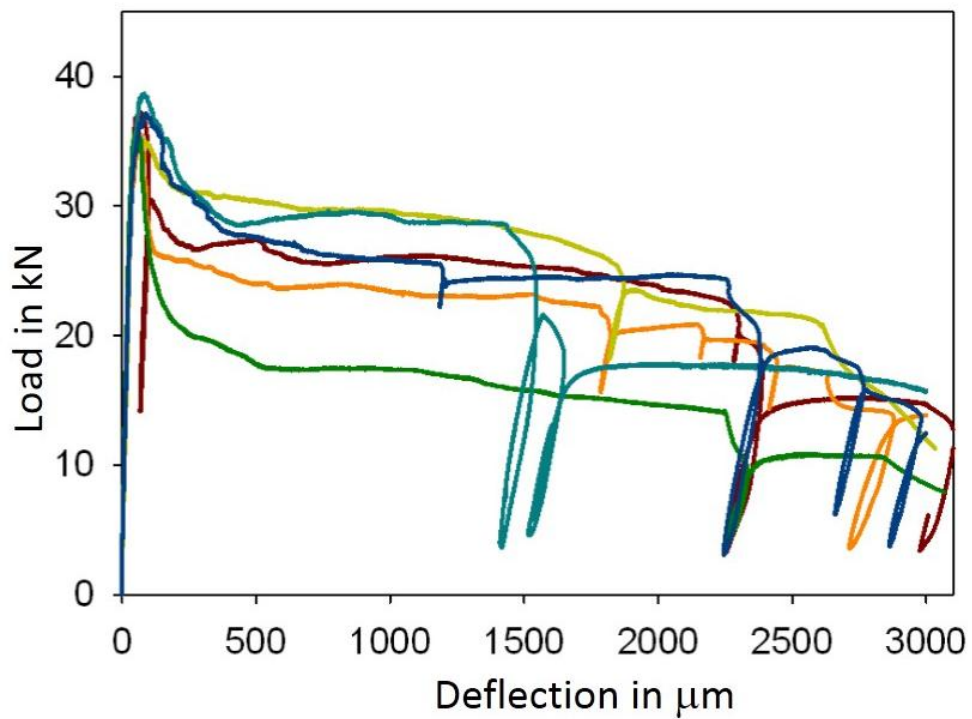


Figure A.16 Load deflection curves of all specimens of M35SFD45 mix

### A.5 Plain concrete mix

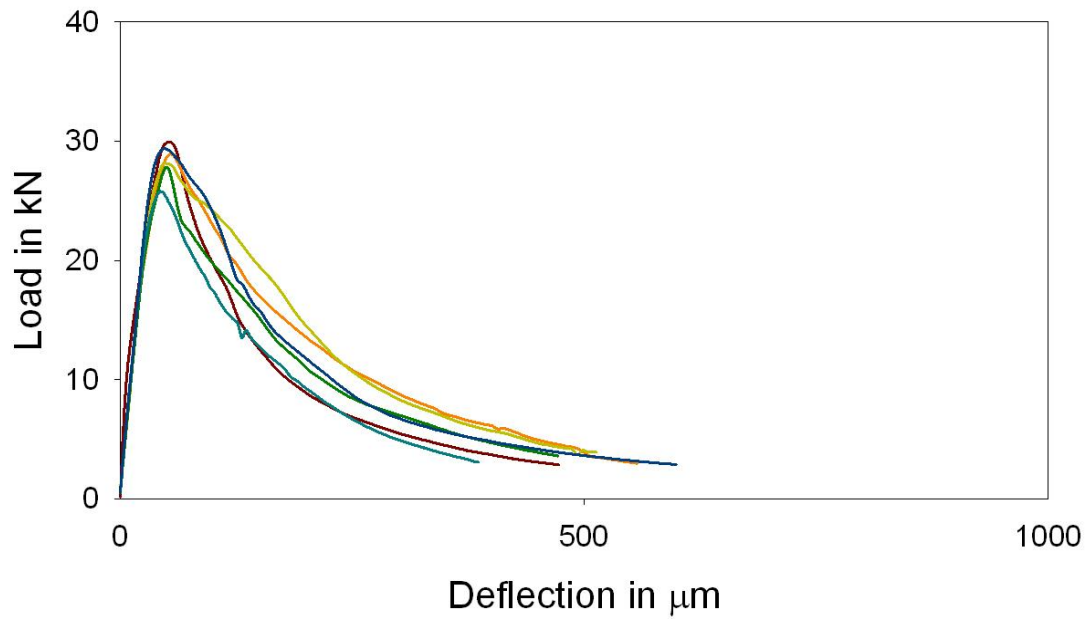


Figure A.17 Load deflection curves of all specimens of M35F0 mix



## APPENDIX B-LOAD DEFLECTION CURVES OF M35 GRADE CONCRETE WITH DIFFERENT GLASS FIBRES

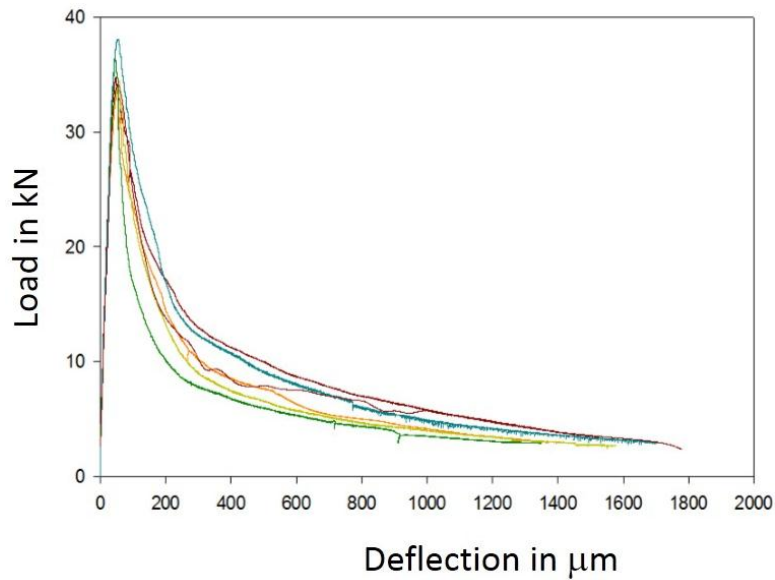


Figure B.1 Load deflection curves of all specimens of M35GF5 mix

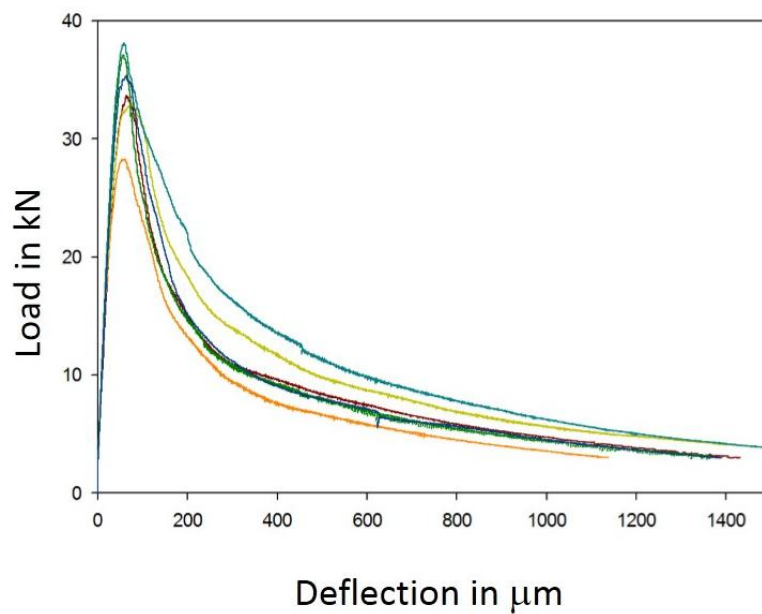


Figure B.2 Load deflection curves of all specimens of M35GF10 mix

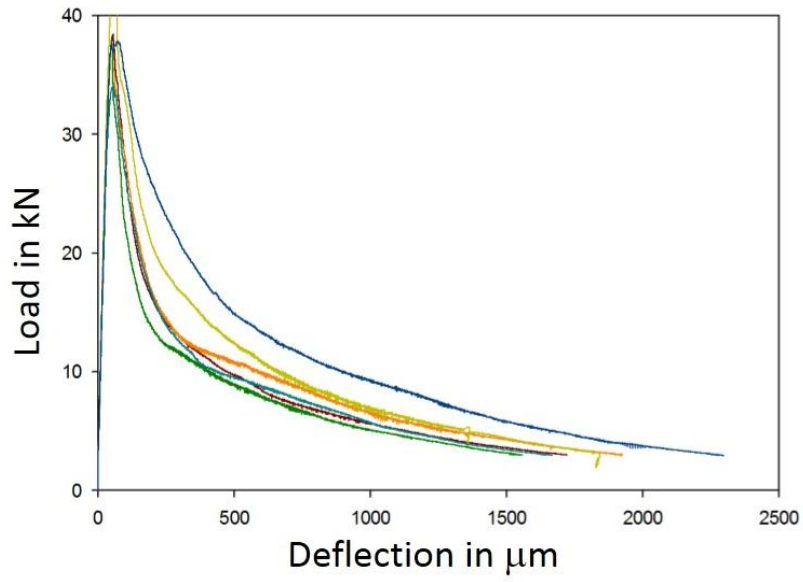


Figure B.3 Load deflection curves of all specimens of M35GF15 mix

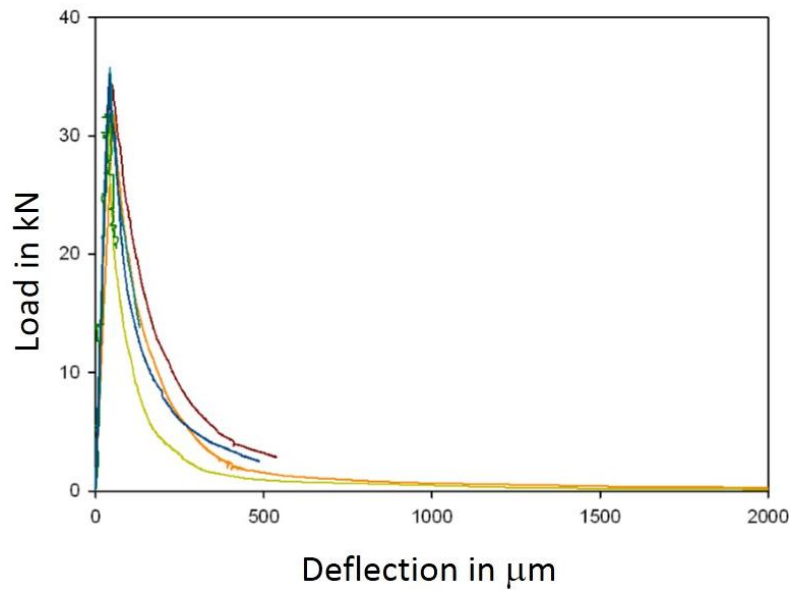


Figure B.4 Load deflection curves of all specimens of M35F0 mix

## APPENDIX C – LOAD DEFLECTION CURVES OF CONCRETE WITH AMF AND STEEL FIBRES

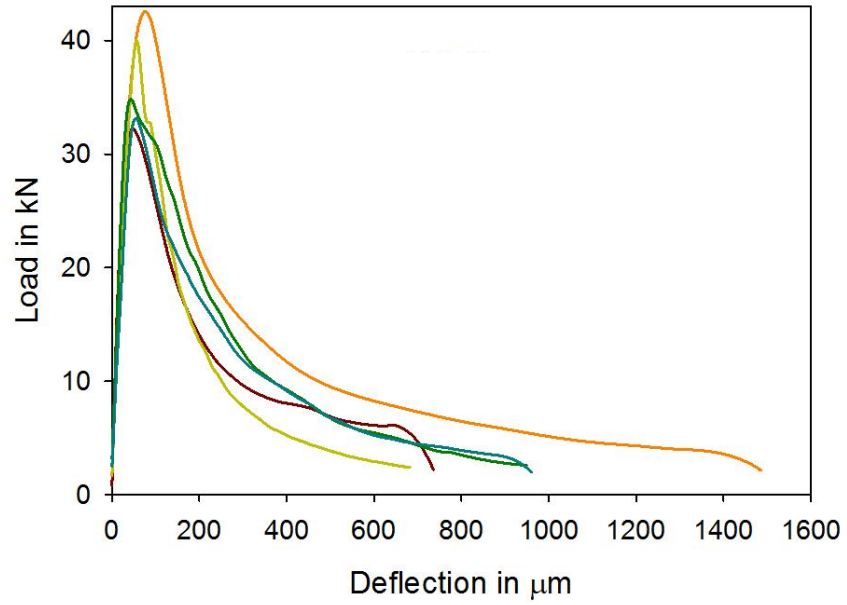


Figure C.1 Load-deflection curves of AMF10 mix.

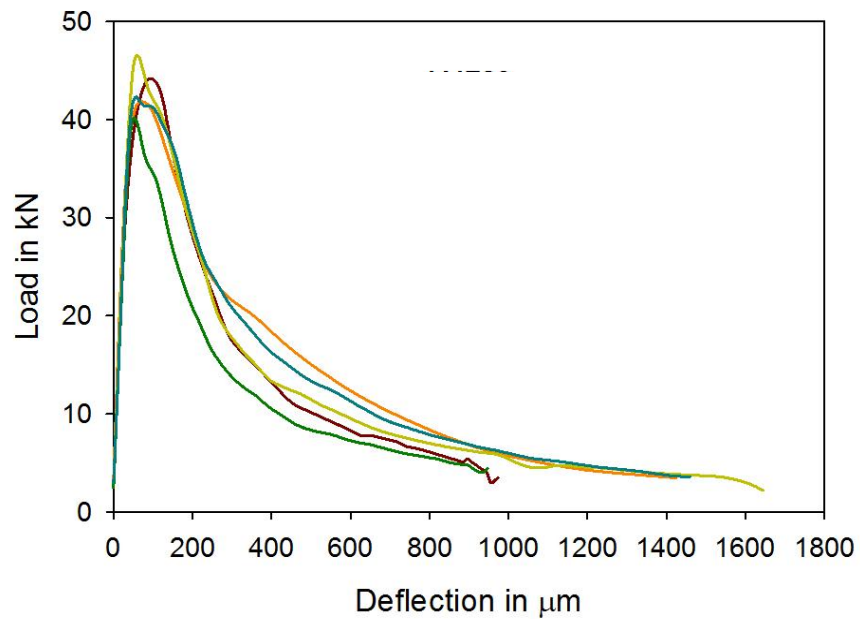


Figure C. 2 Load-deflection curves of AMF20 mix.

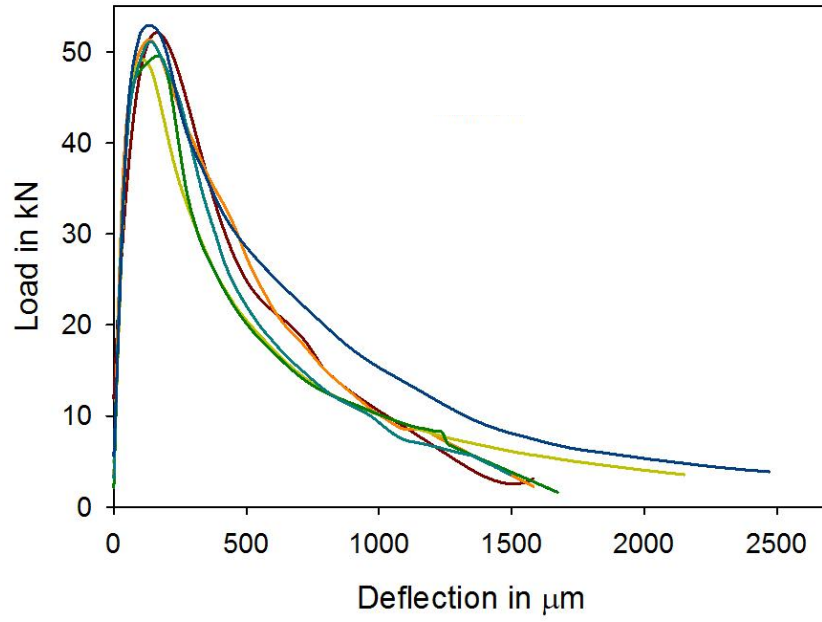


Figure C.3 Load-deflection curves of AMF30 mix.

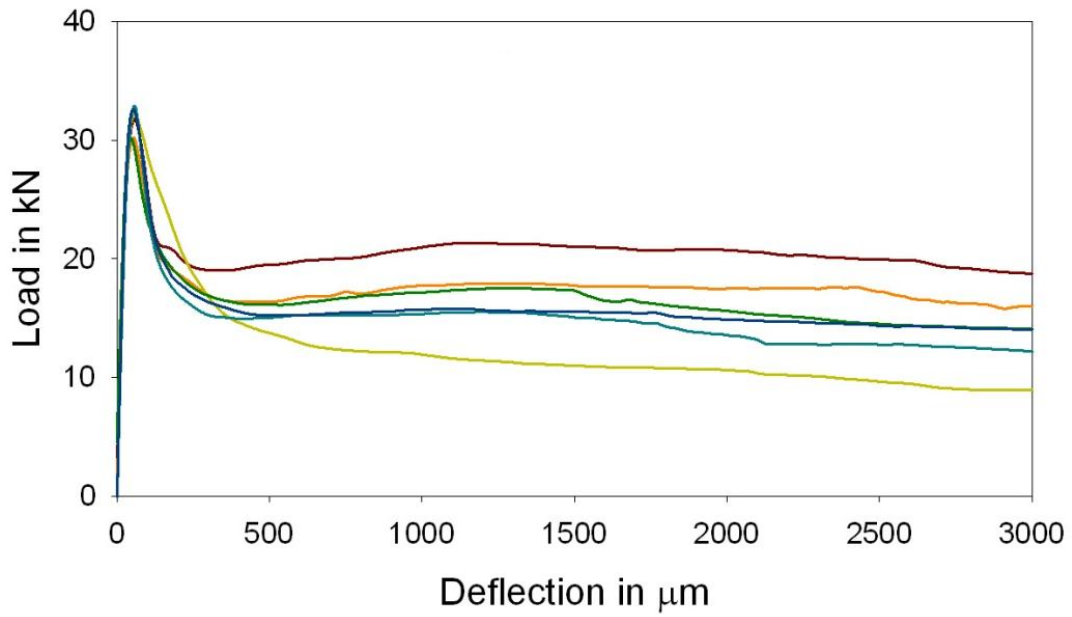


Figure C.4 Load-deflection curves of SF15 mix.

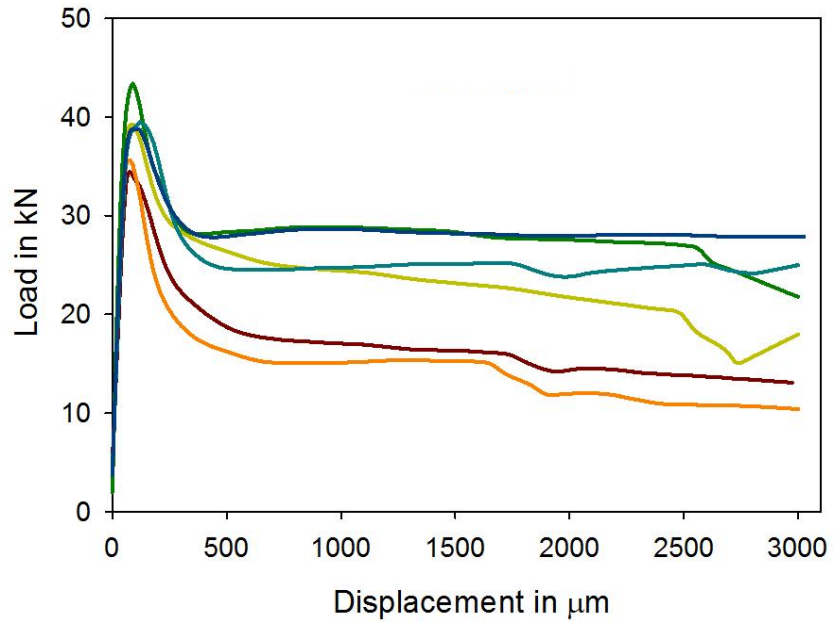


Figure C.5 Load-deflection curves of SF15AMF10 mix.

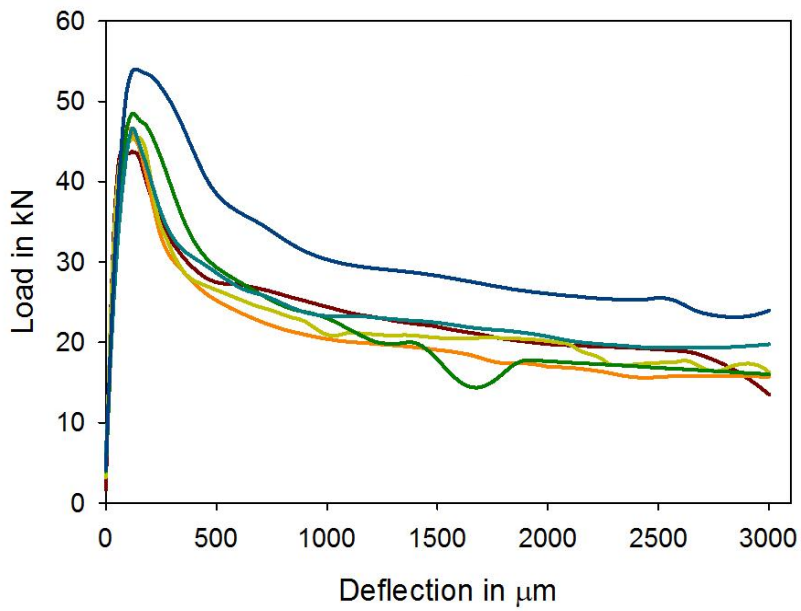


Figure C.6 Load-deflection curves SF15AMF20 mix.



## **APPENDIX D TEMPERATURE DIFFERENTIAL STUDIES**

### **D.1 Experimental study on the temperature differential in concrete slab**

The curling developed in concrete slab is significant when determining the critical moments and axial stresses in the slab. Most of the codes use either empirical relations like Bradbury's equation or numerical solutions based on FEA. In any case, the parameters influencing the stress calculations are the thermal properties of the concrete, such as the coefficient of expansion, specific heat capacity, and thermal conductivity, in addition to the temperature differential through the slab. In general, the thermal properties are either assumed or determined from testing. However, the differential temperature is a critical parameter that varies with location, maximum and minimum diurnal temperature, humidity, etc. In order to assess the possible temperature differentials within concrete for a range of ambient conditions a test programme was conducted as described below.

### **D.2 Experimental programme**

The tests were conducted on three concrete slabs with dimensions  $0.6 \text{ m} \times 0.6 \text{ m}$  and having depths 300 mm, 200 mm and 100 mm made with M35 grade concrete. The slabs were insulated on the four sides and bottom as shown in Figure D.1, so as to allow heat transfer only across the top surface in order to simulate the conditions of slab of large breadth and width. The insulation was done with polystyrene-based insulating foam with thermal conductivity value  $K = 0.041 \text{ W/mK}$ , for which the required thickness of the insulating foam to keep the temperature loss less than  $1^\circ \text{ C}$  within 24 hours was determined as 110 mm. Accordingly insulation comprising two layers of foam of 45 mm thickness separated by an air gap of about 45 mm was provided.

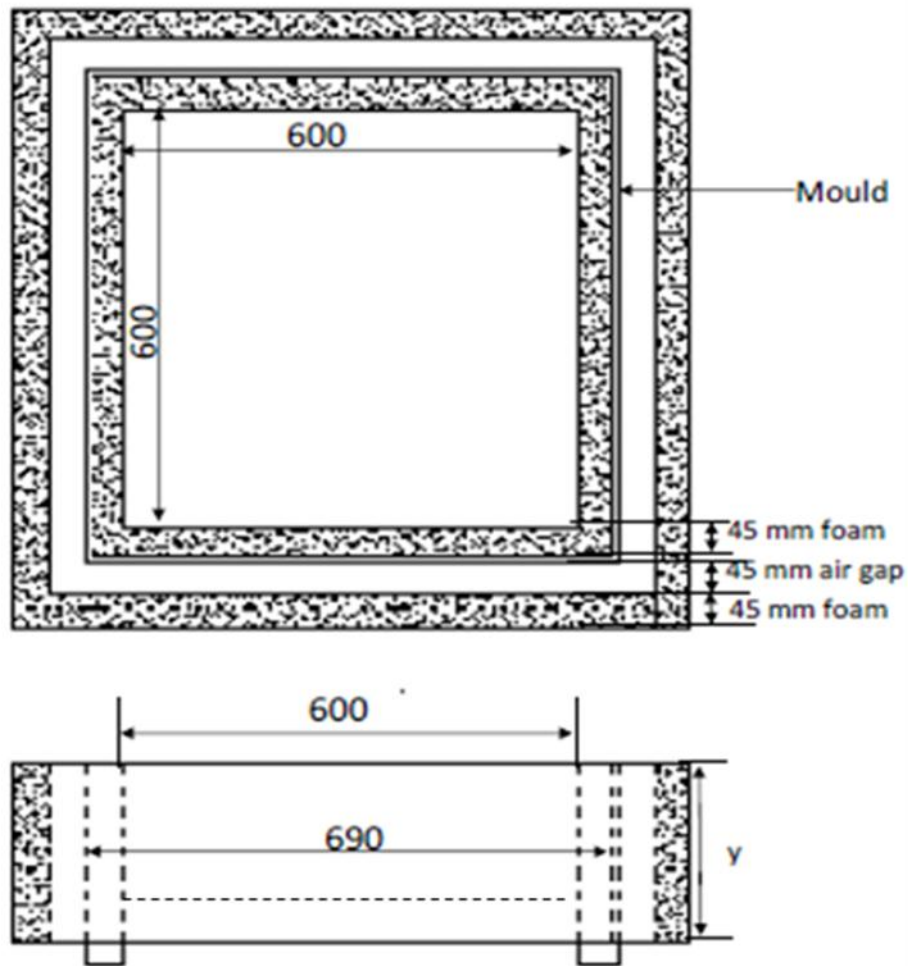


Figure D.1. Layout of the mould for the slab with the insulation

The slabs were instrumented with two resistance temperature detectors (RTDs) placed at the bottom and at the top of the specimen approximately at mid point in palm. The RTDs were connected to a six channel datalogger to provide accurate output at a frequency of 1 reading in 120 seconds. The slabs were moist cured in ambient conditions for 28 days and then shifted to the walk-in-environmental chamber in the laboratory as shown in Figure D.2. The slabs were preconditioned before performing each cycle at a temperature of 25°C and humidity of 50% for atleast 48 hours.



Figure D.2 Slabs placed inside the walk-in environmental chamber

### **D.2.1 Applied temperature profiles for testing.**

For the purpose of determining the temperature differentials, the slab was subjected to typical temperature and humidity cycles representative of critical diurnal variations in some of the locations within India. Four critical locations were chosen based on the seasonal variations and extreme climatic conditions expected at these locations and the corresponding climate data were analysed (from data available in web [www.wunderground.com](http://www.wunderground.com)), to determine the time of the year (i.e., month) during which the ambient temperature has the maximum difference between the maximum and minimum diurnal temperatures. Accordingly the climate data at these locations for past ten years during the critical month were analysed to arrive at the day during which the difference between minimum and maximum temperature was maximum. Two additional hypothetical temperature profiles were also generated to match a low-temperature low-humidity condition and a high-temperature high-humidity condition. The list of locations are shown in Table D.1 with the identified critical diurnal conditions.

Table D.1. List of locations and temperature details for generating temperature and humidity profile for testing

Locations for diurnal temperature profile	Area/ type of climate	Month with extreme max. and min. diurnal temp ( $\Delta T$ )	Mean max. temp./Relative humidity for the corresponding month
Chennai	Hot and humid conditions	May (10°C)	37.4/62%
Delhi	Summer	May (13.2°C)	39.8/33% 28/55%
	Winter	November (15.2°C)	
Nagpur	High summer temperature in central India	May (14.5°C)	42.5/27%
Jodhpur	Dry extreme temperatures	January(15.6°C)	25/ 53%
Hypothetical location 1	-	(15°C)	20/30%
Hypothetical location 2	-	(10°C)	45/70%

The diurnal temperature profiles were obtained from climate data (from the available database from the web) for these locations for the critical day and used as input for the temperature cycle imposed in the environmental chamber during test as given in Figures D. 3-9. The slabs were subjected to four diurnal cycles; the first two cycles were for conditioning and the temperature data was collected during the remaining two cycles.

The obtained output along with the applied temperature profiles are shown in Figures D.10 – D.30.

Location : Chennai

Month: May

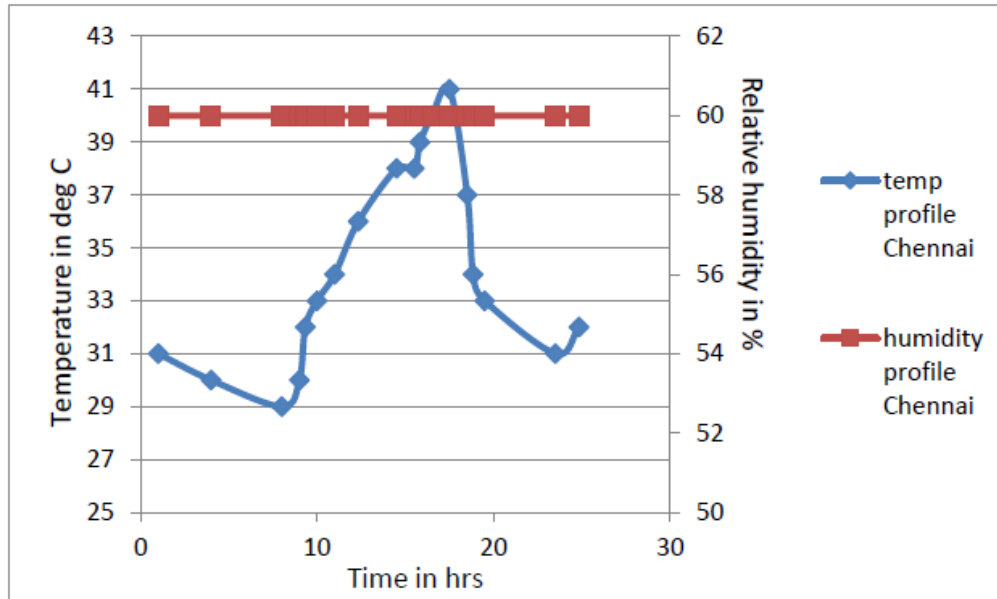


Figure D.3 Chennai – input temperature and humidity profile

Location : Delhi

Month: May

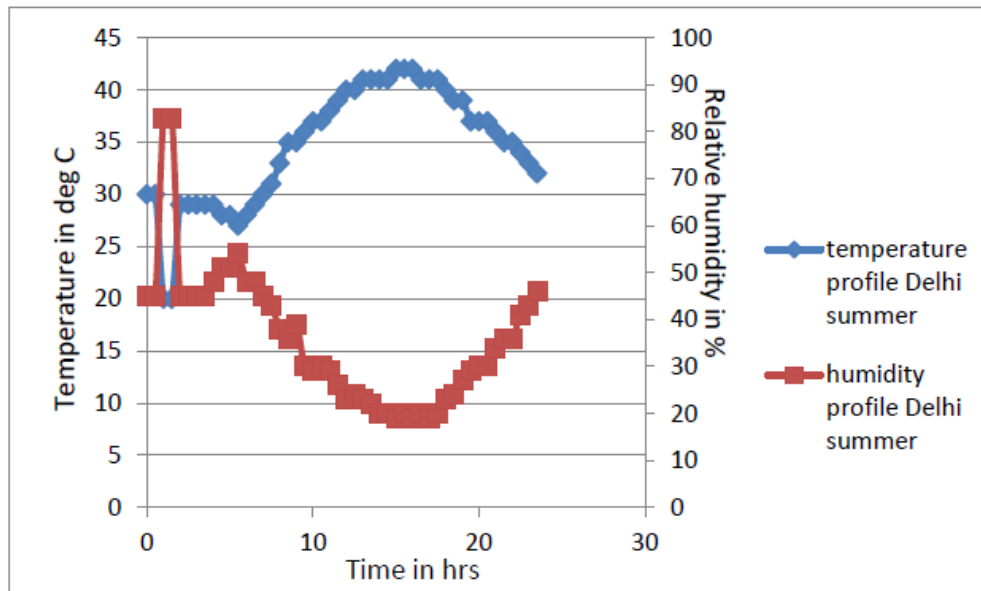


Figure D.4 Delhi summer – input temperature and humidity profile

Location : Delhi

Month: November

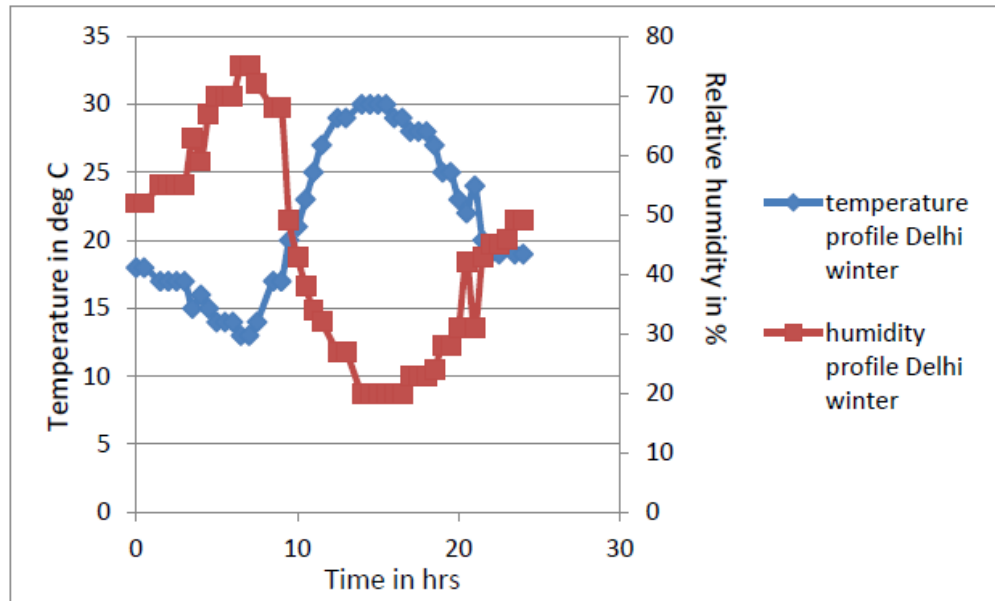


Figure D.5 Delhi winter – input temperature and humidity profile

Location : Nagpur

Month: May

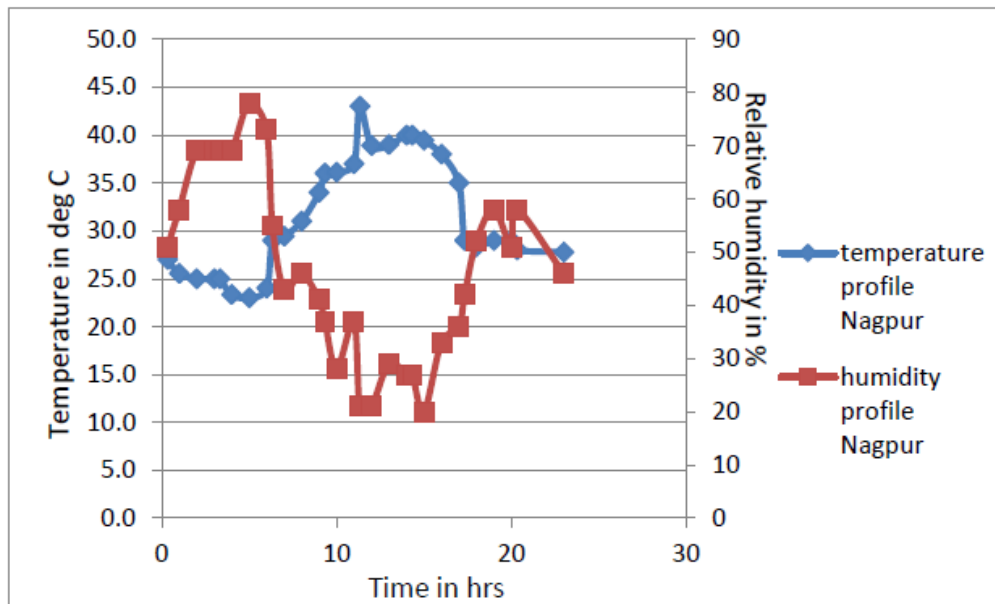


Figure D.6 Nagpur – input temperature and humidity profile

Location : Jodhpur

Month: January

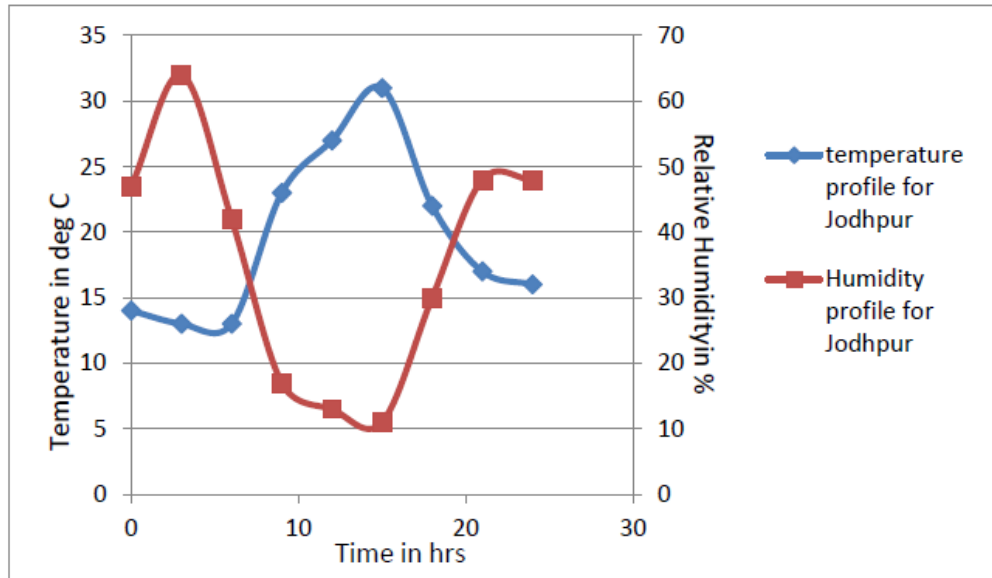


Figure D.7 Jodhpur – input temperature and humidity profile

Location : Hypothetical 1

Assumption:  $\Delta T = 15^\circ\text{C}$ , Max. Temp: =  $20^\circ\text{C}$ , Max. Humidity = 30%

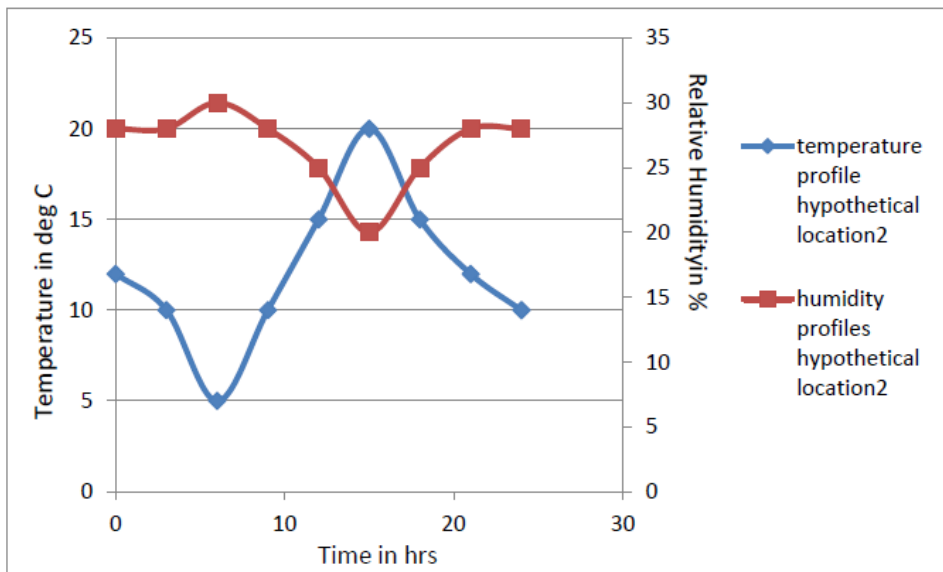


Figure D.8 Hypothetical location 1 – input temperature and humidity profile

Location : Hypothetical 2

Assumption:  $\Delta T = 10^\circ\text{C}$ , Max. Temp: =  $45^\circ\text{C}$ , Max. Humidity = 70%

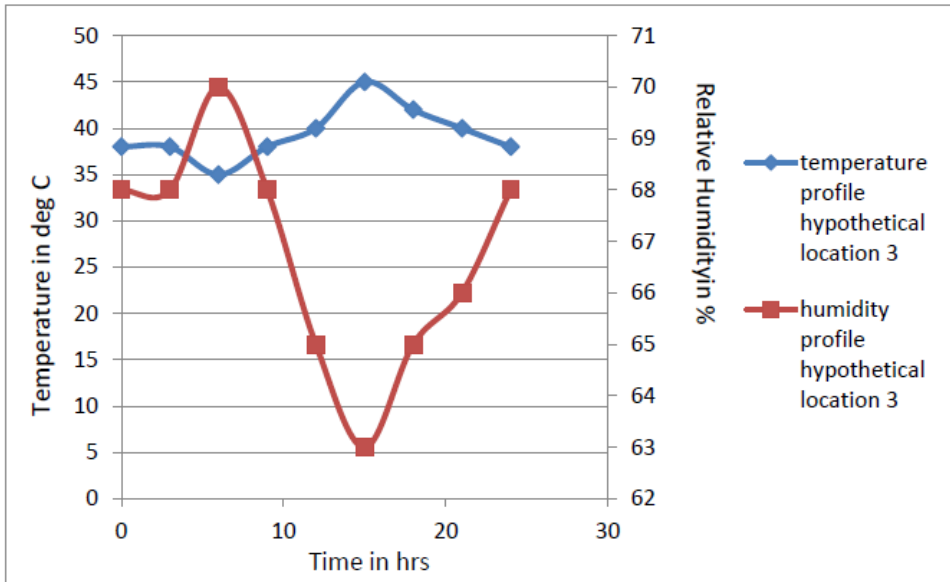


Figure D.9 Hypothetical location 1 – input temperature and humidity profile

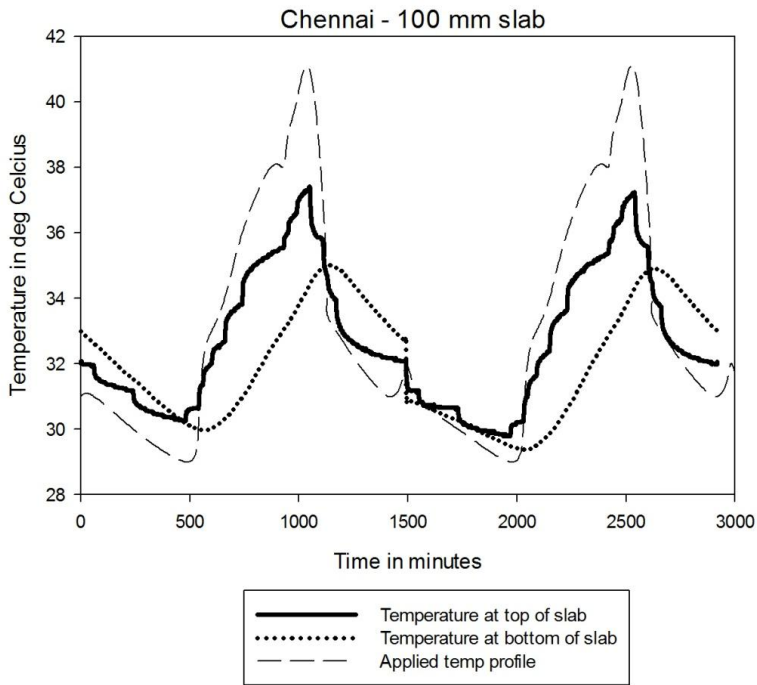


Figure D.10 Temperature output of 100 mm slab – location Chennai

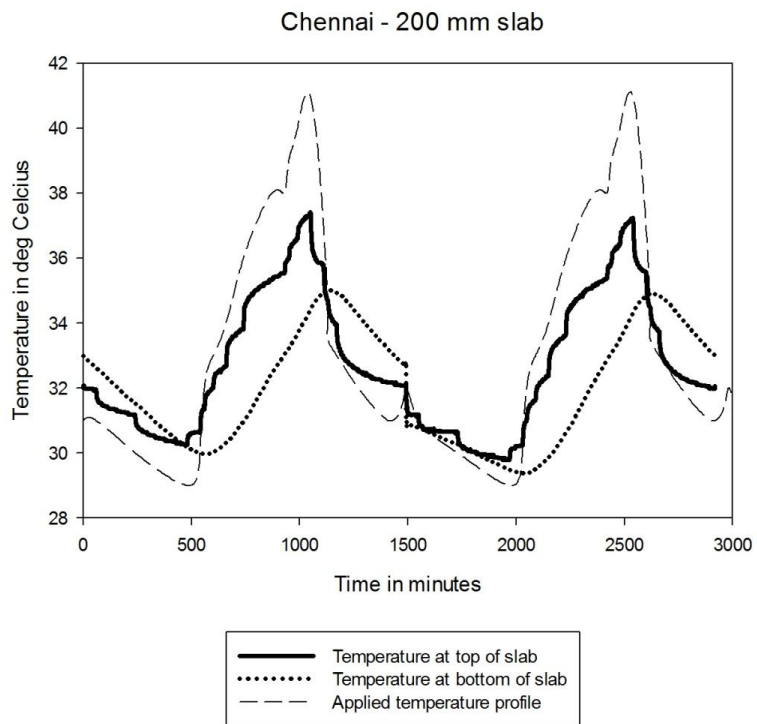


Figure D.11 Temperature output of 200 mm slab – location Chennai

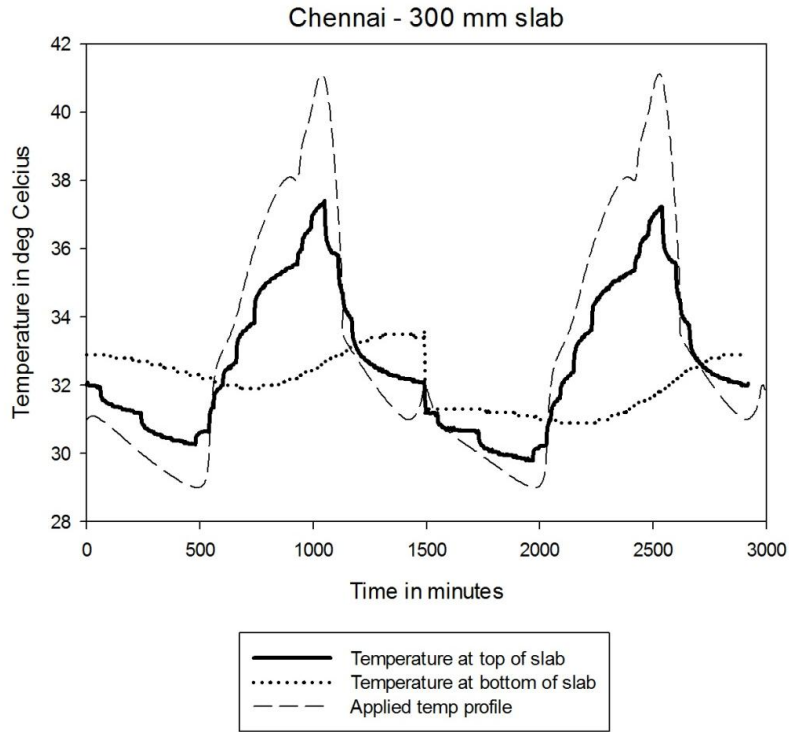


Figure D.12 Temperature output of 300 mm slab – location Chennai

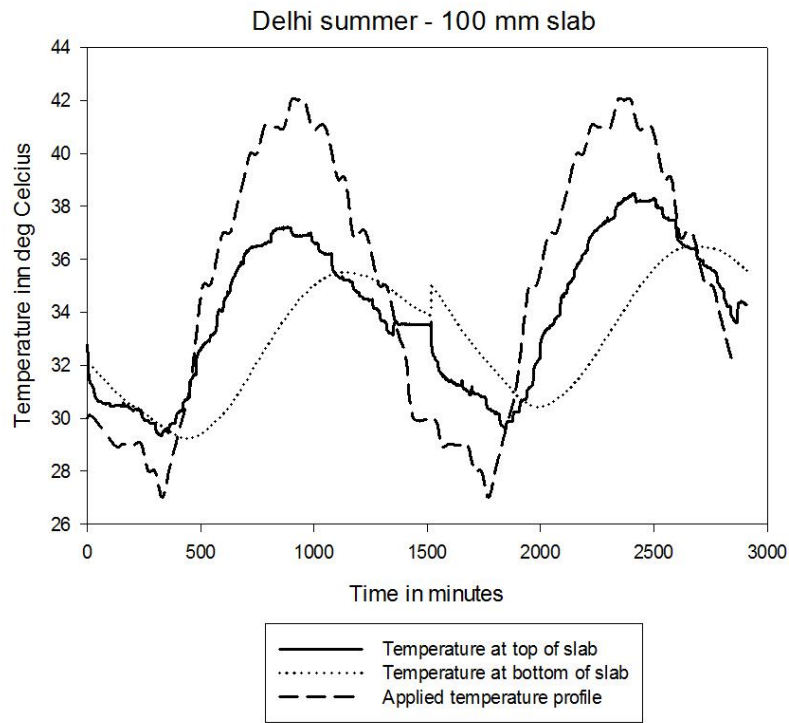


Figure D.13 Temperature output of 100 mm slab – location Delhi - summer

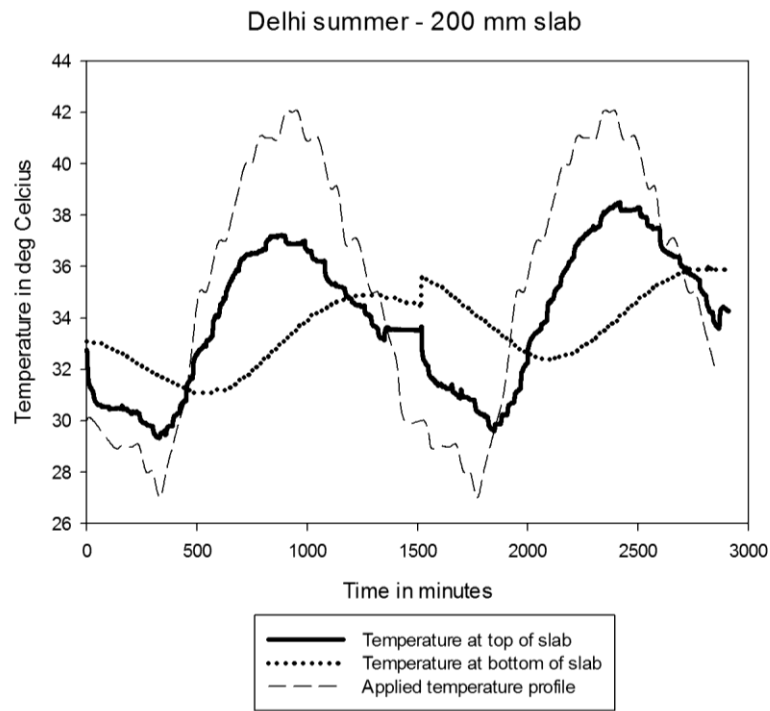


Figure D.14 Temperature output of 200 mm slab – location Delhi - summer

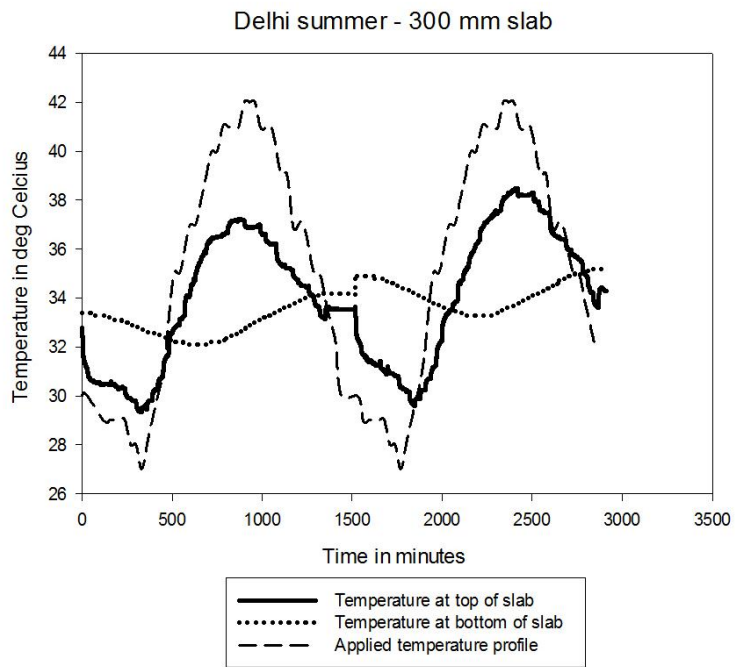


Figure D.15 Temperature output of 300 mm – location Delhi – summer

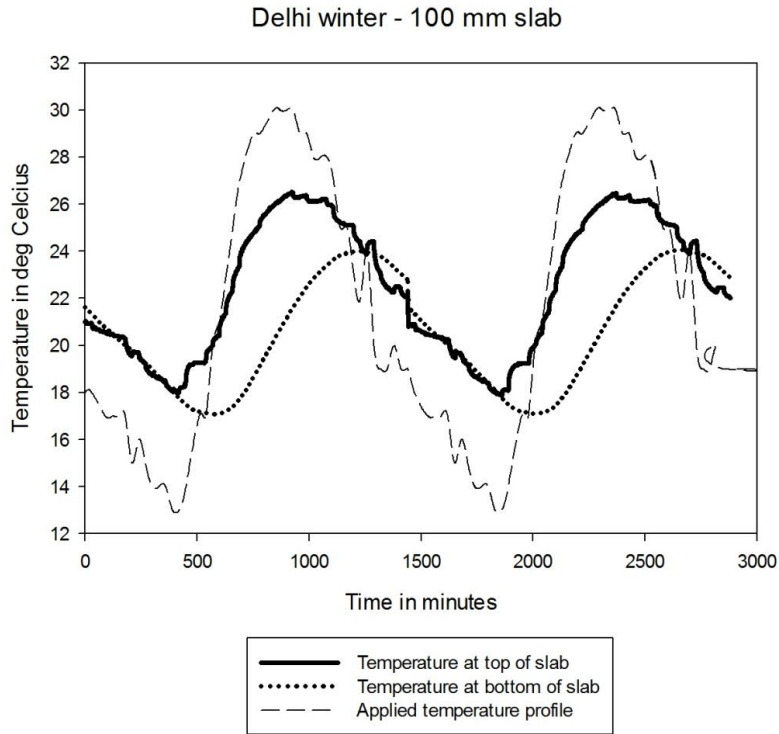


Figure D.16 Temperature output of 100 mm slab – location Delhi – winter

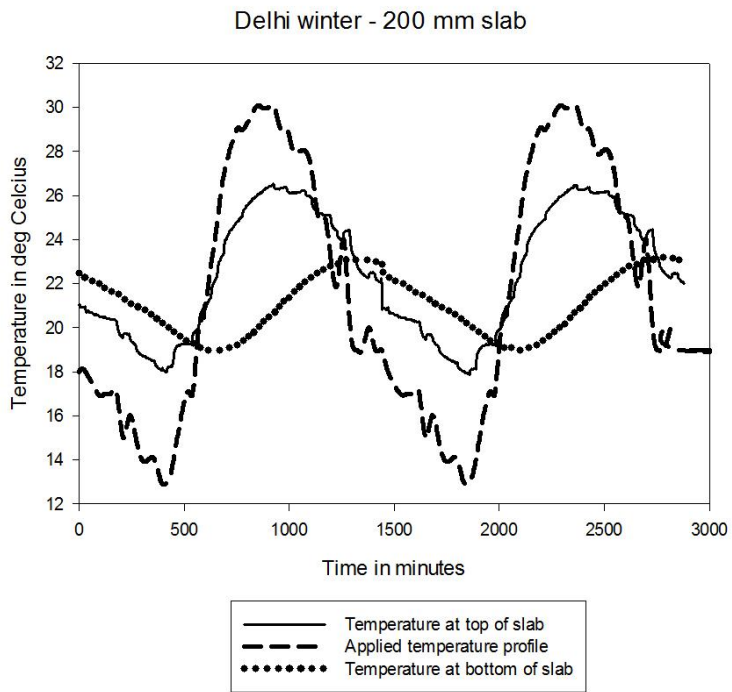


Figure D.17 Temperature output of 200 mm slab – location Delhi - winter

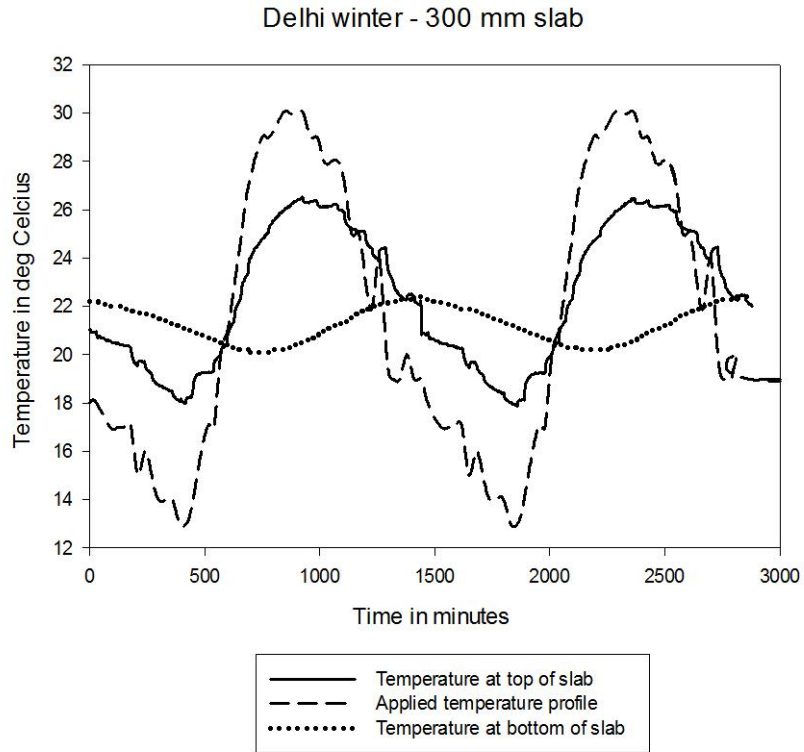


Figure D.18 Temperature output of 300 mm slab – location Delhi – winter

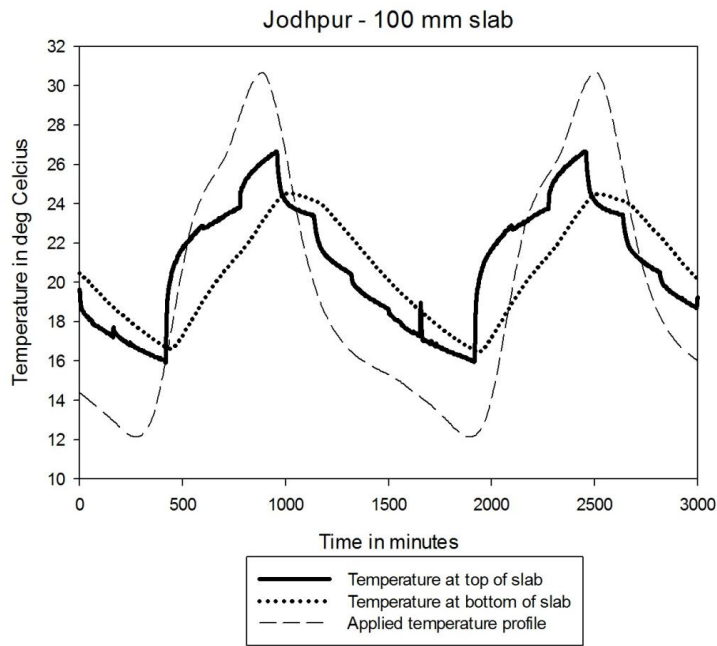


Figure D.19 Temperature output of 100 mm slab – location Jodhpur

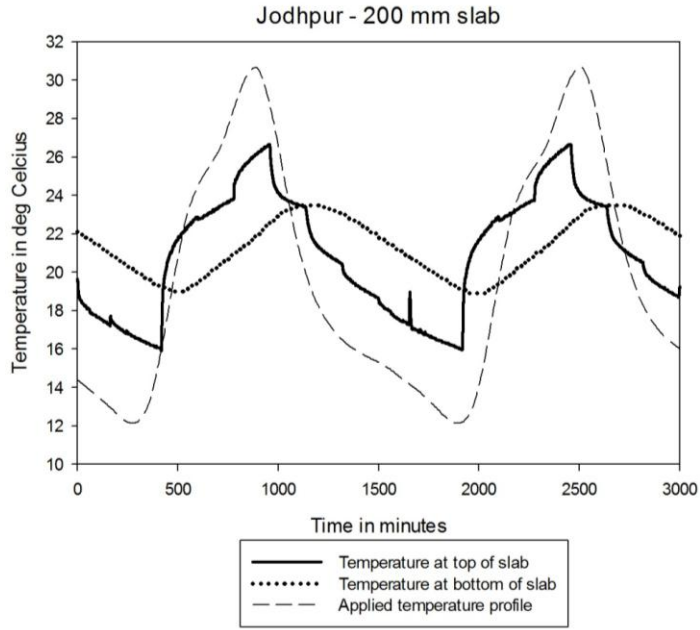


Figure D.20 Temperature output of 200 mm slab – location Jodhpur

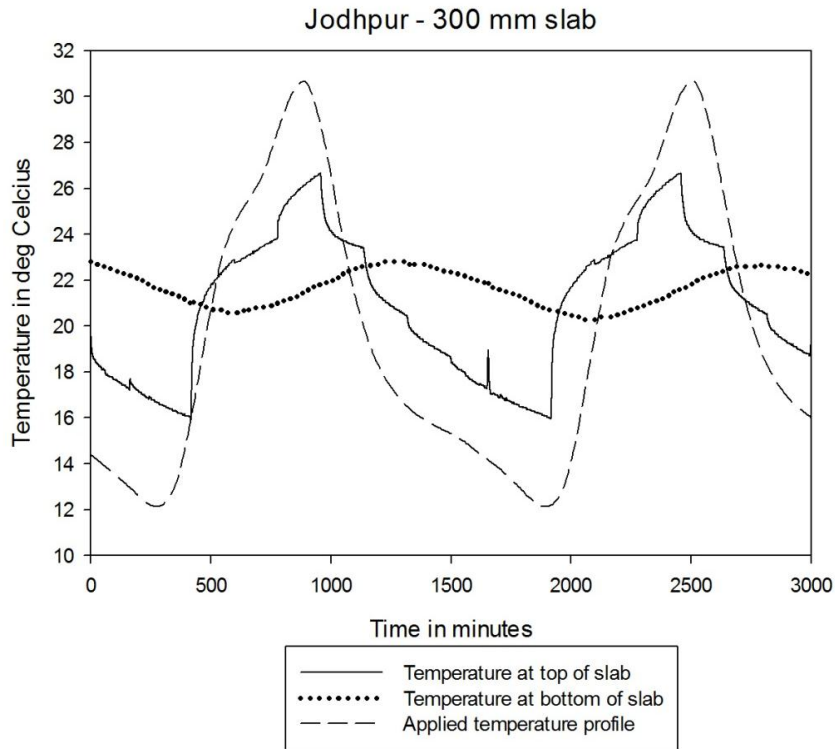


Figure D.21 Temperature output of 300 mm slab – location Jodhpur

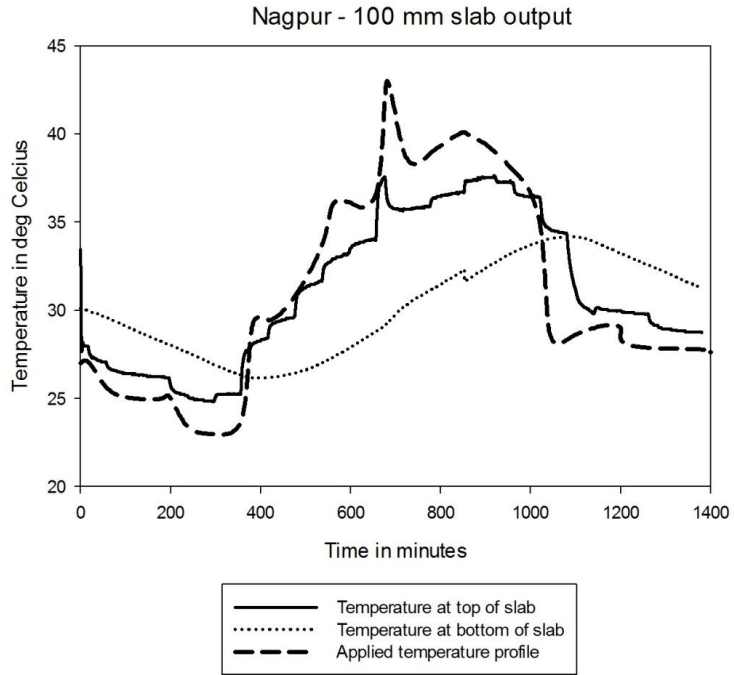


Figure D.22 Temperature output of 100 mm slab – location Nagpur

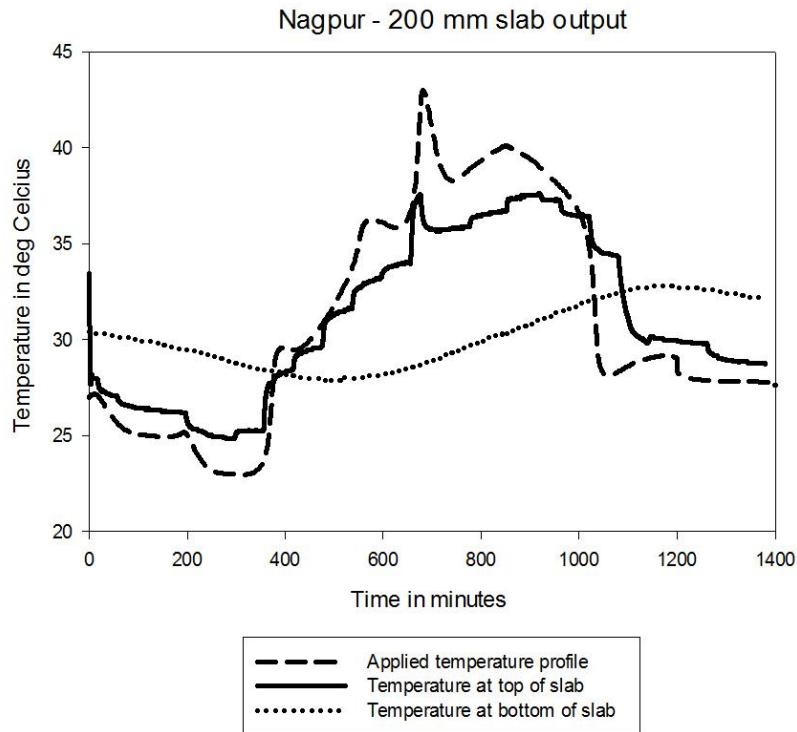


Figure D.23 Temperature output of 200 mm slab – location Nagpur

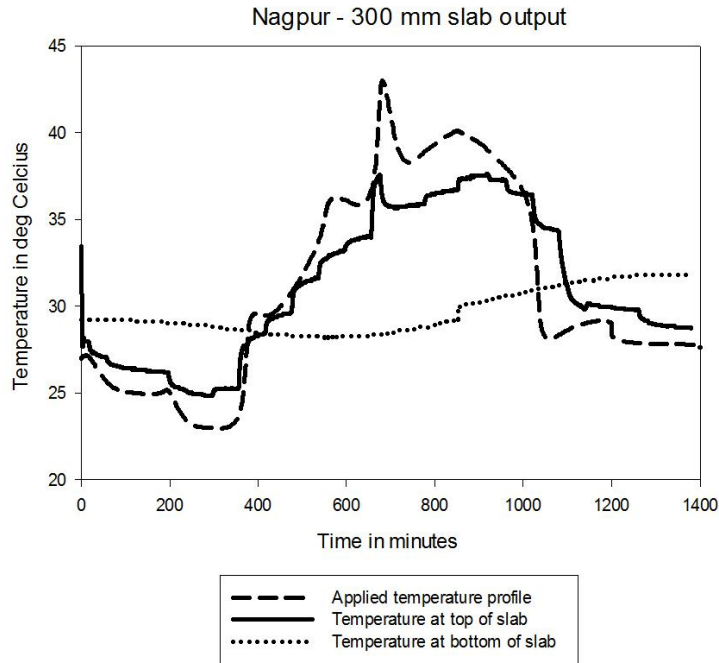


Figure D.24 Temperature output of 300 mm slab – location Nagpur

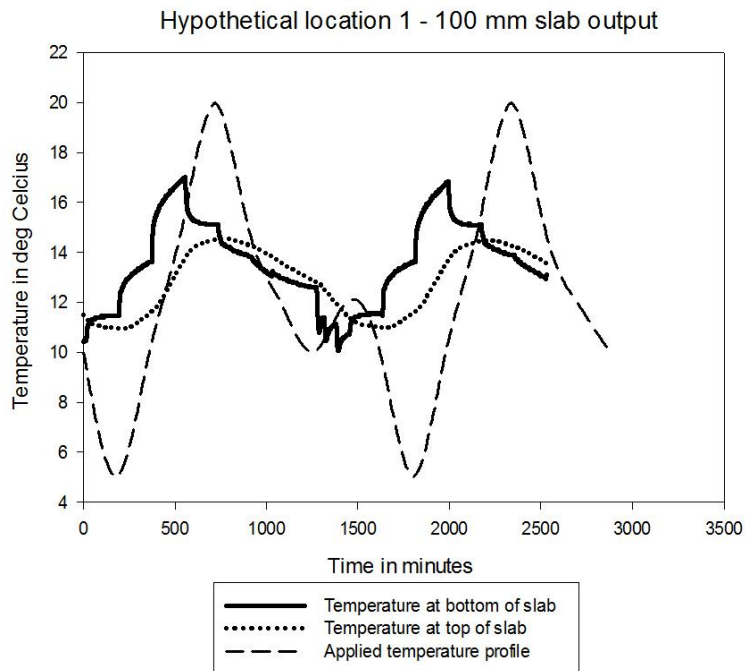


Figure D.25 Temperature output of 100 mm slab – hypothetical location 1

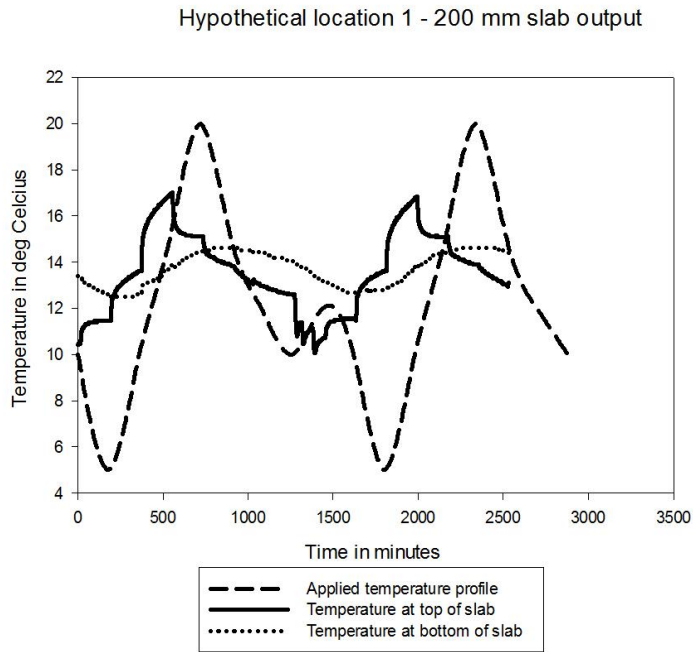


Figure D.26 Temperature output of 200 mm slab – hypothetical location

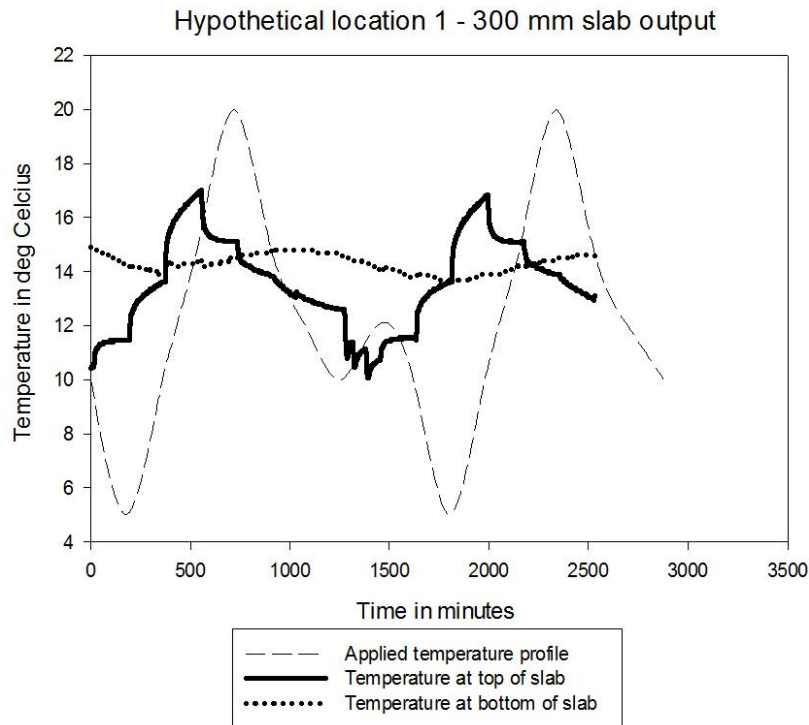


Figure D.27 Temperature output of 300 mm slab – Hypothetical location 1

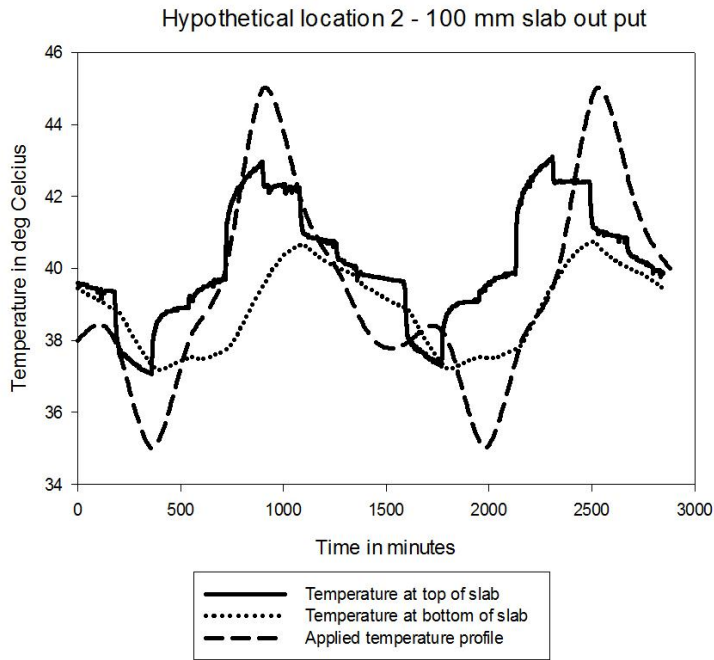


Figure D.28 Temperature output of 100 mm slab – Hypothetical location 2

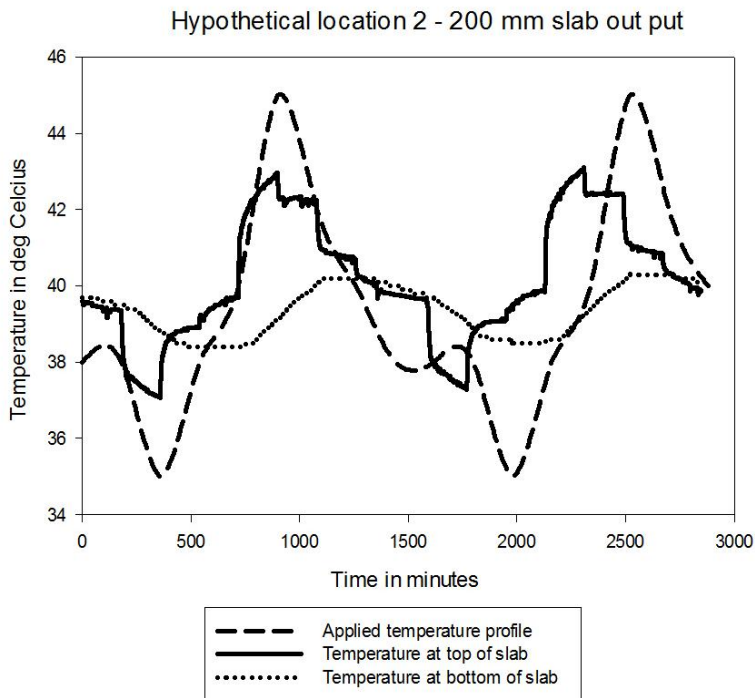


Figure D.29 Temperature output of 200 mm slab – Hypothetical location 2

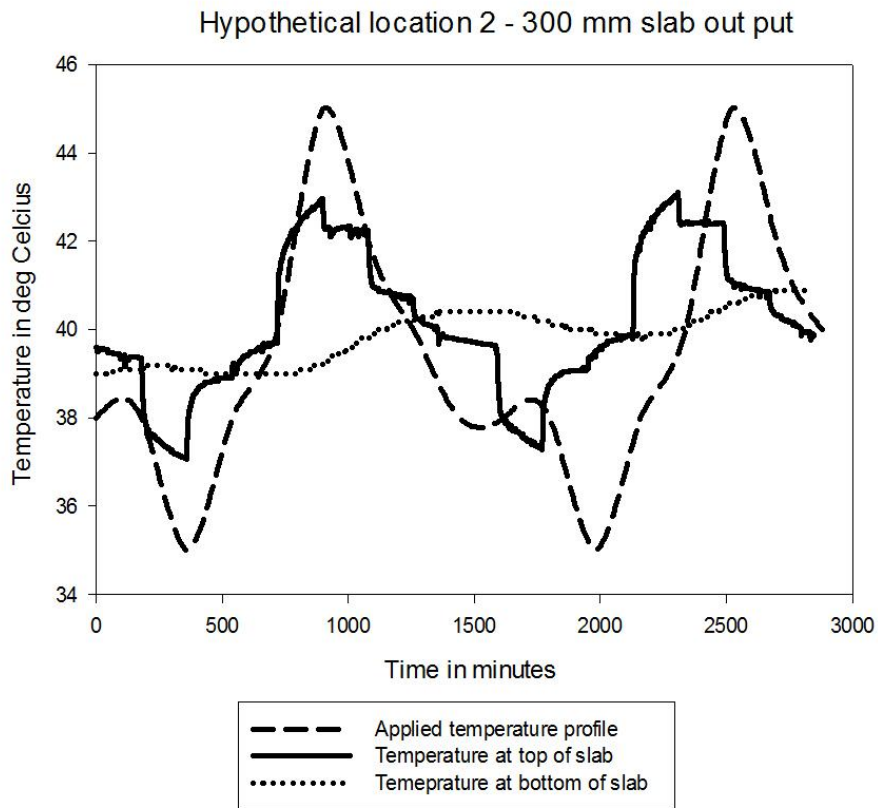


Figure D.30 Temperature output of 300 mm slab – Hypothetical location 2

From the obtained data the temperature differential between the top and bottom of the slabs were obtained as shown in Figures D.31- D.37.

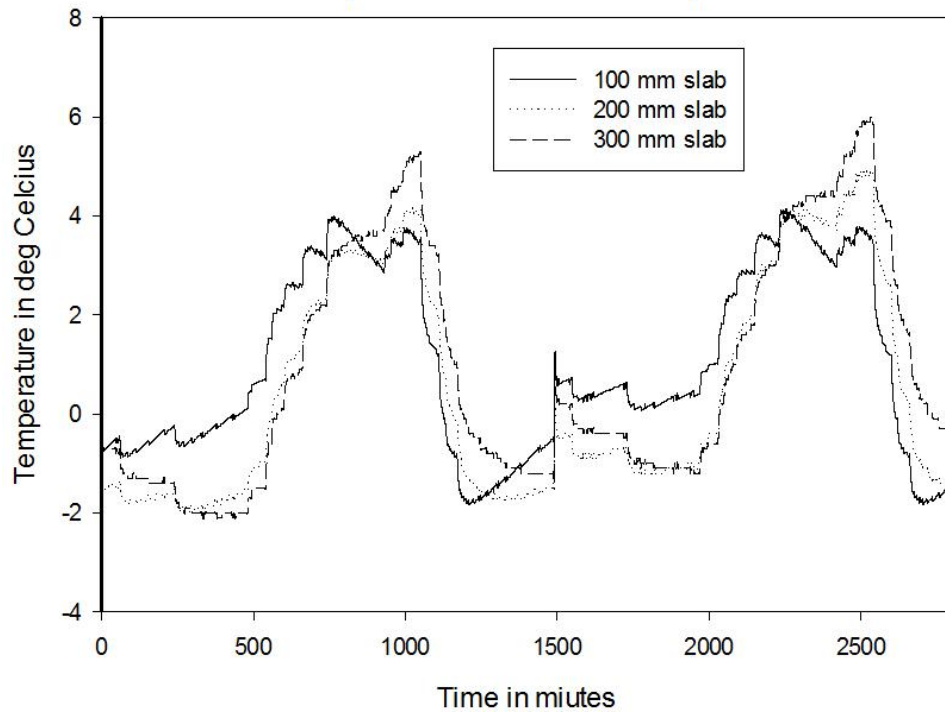


Figure D.31 Temperature differential between top and bottom of slab- Chennai profile

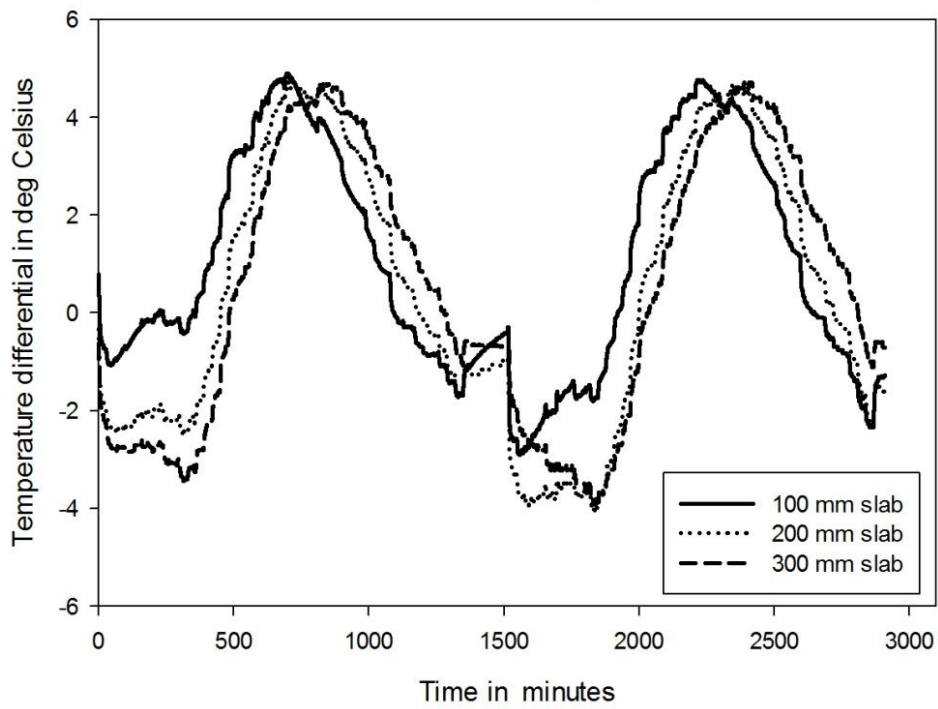


Figure D.32 Temperature differential between top and bottom of slab- Delhi summer profile

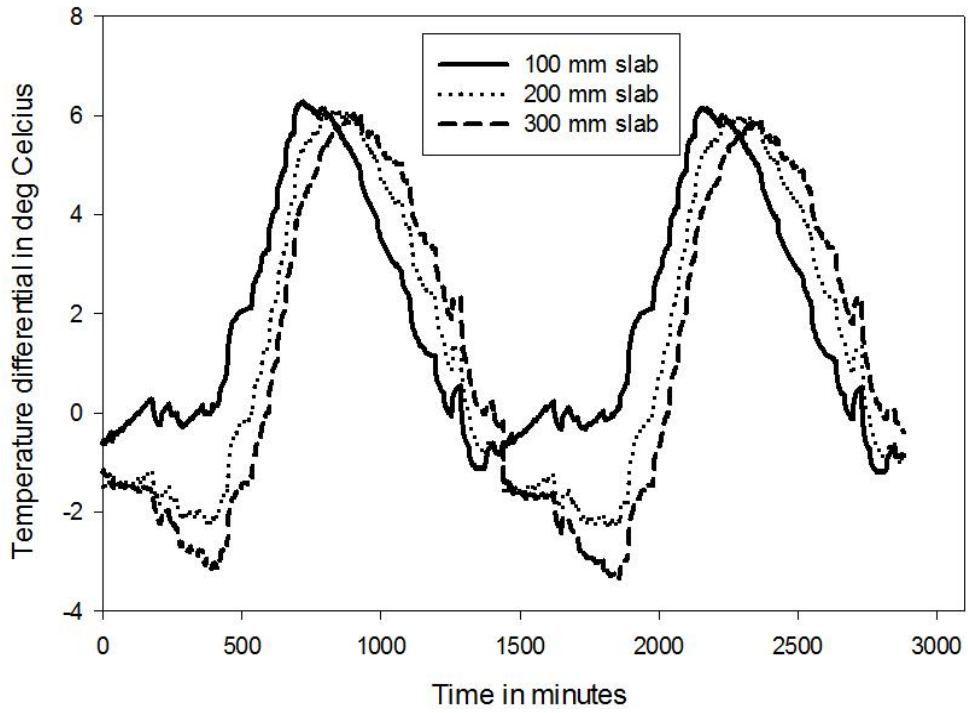


Figure D.33 Temperature differential between top and bottom of slab- Delhi winter profile

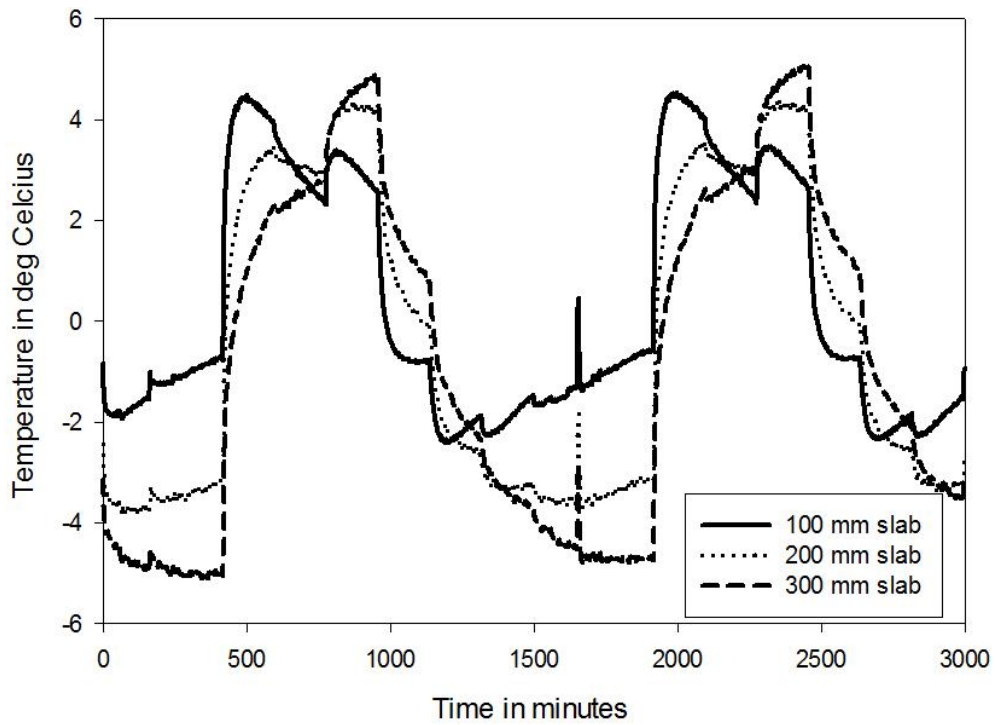


Figure D.34 Temperature differential between top and bottom of slab- Jodhpur profile

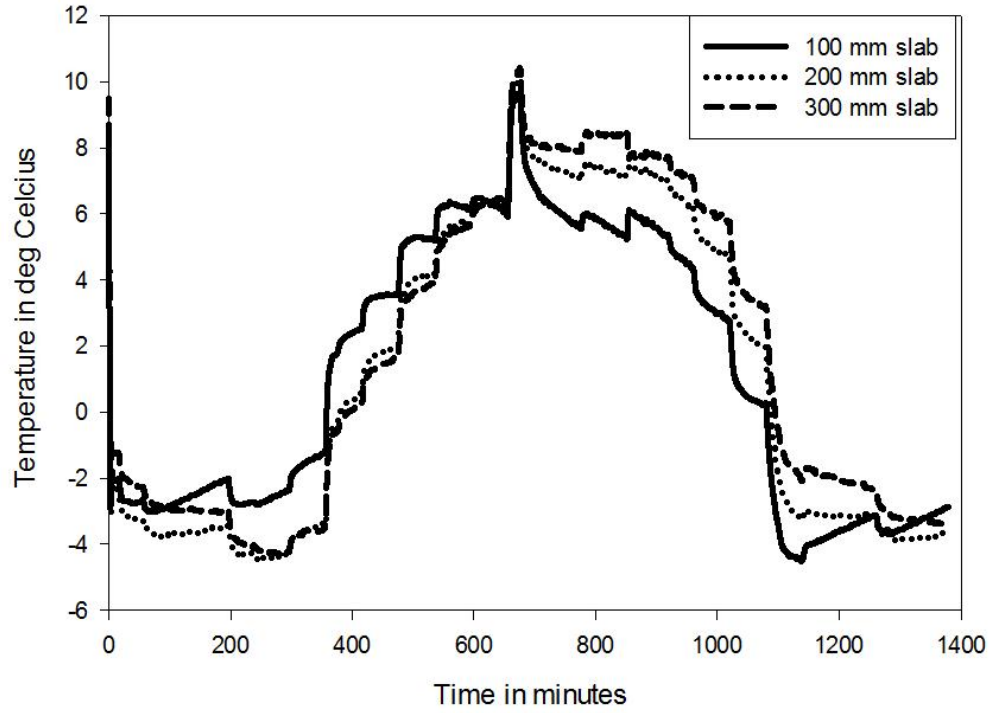


Figure D.35 Temperature differential between top and bottom of slab- Nagpur profile

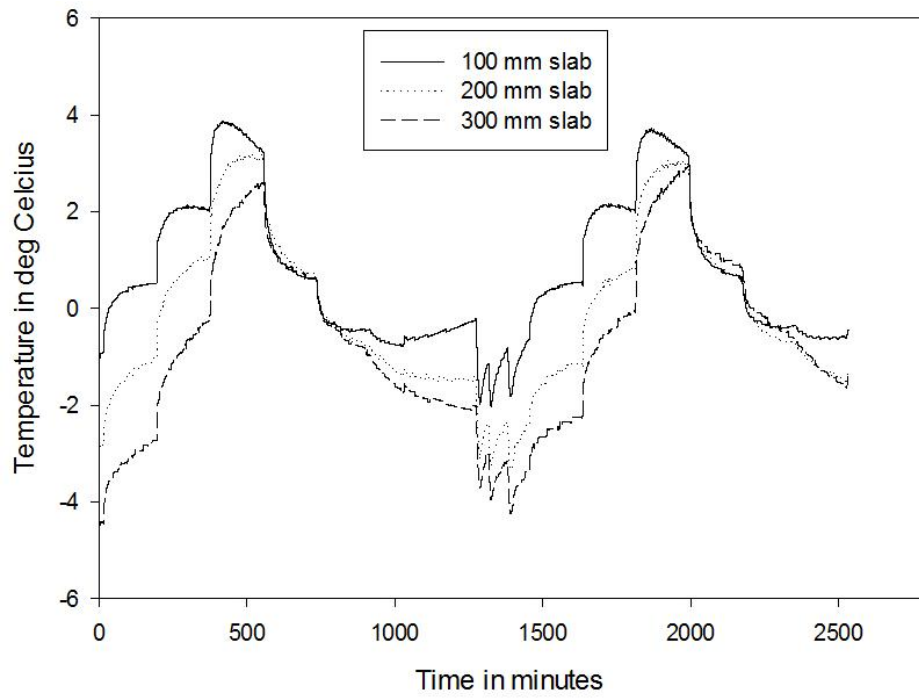


Figure D.36 Temperature differential between top and bottom of slab- Hypothetical location 1

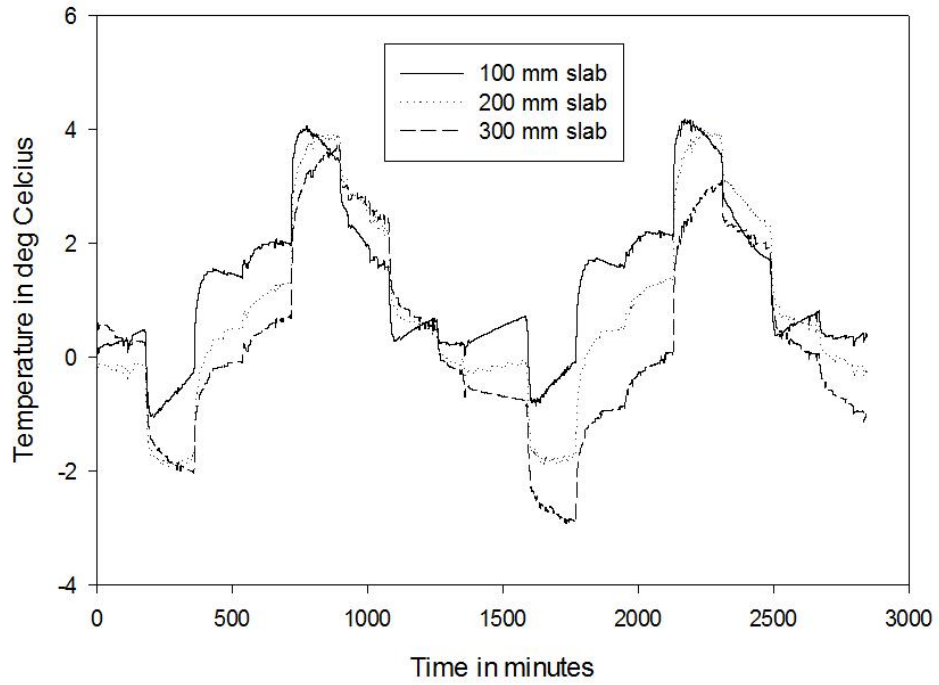


Figure D.37 Temperature differential between top and bottom of slab- Hypothetical location 2

From the data collected the maximum and minimum temperature differentials between the top and bottom of slab for each applied cycle, corresponding to the location, was obtained and is shown in Table 7.1 in Chapter 7.



## APPENDIX E

Flexural stresses based on elastic analysis of slabs due to various loading conditions, to be used for calculation of stress ratio (SR) in the cumulative fatigue damage analysis for FRC pavement (reproduced from IRC 58:2010) are given below:

### Case 1: Single axle with tied concrete shoulders with temperature differential

For  $k \leq 80$

$$\sigma = 0.008 - 6.12 \left( \frac{\gamma h^2}{kl^2} \right) + 2.36 \left( \frac{Ph}{kl^4} \right) + 0.0266(\Delta T)$$

For  $80 < k < 150$

$$\sigma = 0.008 - 9.69 \left( \frac{\gamma h^2}{kl^2} \right) + 2.09 \left( \frac{Ph}{kl^4} \right) + 0.0409(\Delta T)$$

For  $k > 150$

$$\sigma = 0.042 + 3.26 \left( \frac{\gamma h^2}{kl^2} \right) + 1.62 \left( \frac{Ph}{kl^4} \right) + 0.0522(\Delta T)$$

### Case 2: Single axle without tied shoulder with temperature differential

For  $k \leq 80$

$$\sigma = -0.149 - 2.60 \left( \frac{\gamma h^2}{kl^2} \right) + 3.13 \left( \frac{Ph}{kl^4} \right) + 0.0297(\Delta T)$$

For  $80 < k < 150$

$$\sigma = -0.119 - 2.99 \left( \frac{\gamma h^2}{kl^2} \right) + 2.78 \left( \frac{Ph}{kl^4} \right) + 0.0456(\Delta T)$$

For  $k > 150$

$$\sigma = -0.238 + 7.02 \left( \frac{\gamma h^2}{kl^2} \right) + 2.41 \left( \frac{Ph}{kl^4} \right) + 0.0585(\Delta T)$$

### Case 3: Tandem axle with tied concrete shoulders with temperature differential

For  $k \leq 80$

$$\sigma = -0.188 + 0.93 \left( \frac{\mathcal{H}^2}{kl^2} \right) + 1.025 \left( \frac{Ph}{kl^4} \right) + 0.0207(\Delta T)$$

For  $80 < k < 150$

$$\sigma = -0.174 + 1.21 \left( \frac{\mathcal{H}^2}{kl^2} \right) + 0.87 \left( \frac{Ph}{kl^4} \right) + 0.0364(\Delta T)$$

For  $k > 150$

$$\sigma = -0.210 + 3.88 \left( \frac{\mathcal{H}^2}{kl^2} \right) + 0.73 \left( \frac{Ph}{kl^4} \right) + 0.0506(\Delta T)$$

### Case 4: Tandem axle without ties shoulder with temperature differential

For  $k \leq 80$

$$\sigma = -0.223 + 2.73 \left( \frac{\mathcal{H}^2}{kl^2} \right) + 1.335 \left( \frac{Ph}{kl^4} \right) + 0.0229(\Delta T)$$

For  $80 < k < 150$

$$\sigma = -0.276 + 5.78 \left( \frac{\mathcal{H}^2}{kl^2} \right) + 1.14 \left( \frac{Ph}{kl^4} \right) + 0.0404(\Delta T)$$

For  $k > 150$

$$\sigma = -0.3 + 9.88 \left( \frac{\mathcal{H}^2}{kl^2} \right) + 0.965 \left( \frac{Ph}{kl^4} \right) + 0.0543(\Delta T)$$

## PUBLICATIONS BASED ON THE THESIS

### Journal publications:

- **Nayar, S. K., Gettu, R., and Krishnan, S.,** (2014), Characterisation of the Toughness of Fibre Reinforced Concrete - Revisited in the Indian Context, *Indian Concrete Journal*, Vol. 88, No. 2, pp 8–23.
- **Nayar, S. K., and Gettu, R.,** Synergy in Toughness by Incorporating Amorphous Metal and Steel Fibres, *ACI Materials Journal*, Accepted for publication on 16-04-15.

### Book Chapter:

- **Nayar, S. K., and Gettu, R.,** A Comprehensive Methodology for Design of Fibre Reinforced Concrete Pavements, *ACI/fib joint publication*, Accepted for publication on 03-06-15

### Conference publications:

- **Nayar, S. K., and Gettu, R.,** (2015), A Methodology for Designing Fibre Reinforced Concrete Pavements, *Proceedings of 3<sup>rd</sup> Conference of Transportation Research Group of India, CTRG 2015*, December 2015, Accepted for publication on 26.08.2015.
- **Nayar, S. K., and Gettu, R.,** (2015), Performance of Concrete Reinforced with Combinations of Amorphous Metallic and Conventional Steel Fibres, *Proceedings of 4<sup>th</sup> Asian conference on Ecstasy in concrete, ICI-ACECON 2015*, October 2015, Accepted for publication on 30-08-2015.
- **Gettu, R., and Nayar, S. K.,** (2015), A Design Methodology for Fibre Reinforced Concrete Slabs-on-Grade, *Proceedings of 27th Biennial National Conference of the Concrete Institute of Australia in conjunction with the 69<sup>th</sup> RILEM Week conference (Concrete 2015)*, Australia, pp 443-452.
- **Nayar, S. K and Gettu, R.,** (2014), A Design Methodology for Fibre Reinforced Concrete Pavements and Slabs-on-Grade, *Proceedings of 10<sup>th</sup> fib International Ph. D symposium*, Quebec, Canada, pp 51-56.
- **Nayar, S. K and Gettu, R.,** (2014), A Comprehensive Methodology for the Design of Fibre Reinforced Concrete Pavements, *Proceedings of Joint ACI-fib International*

*workshop on FRC: From design to structural applications, FRC 2014, Montreal, Canada, pp 453-464.*

- **Nayar, S. K., and Gettu, R.,** (2012), On the Design of Steel Fibre Reinforced Concrete Pavements and Slabs-on-Grade, *Proceedings of BEFIB 2012, Eighth RILEM International Conference on Fibre Reinforced Concrete.,* Guimarães, Portugal, 11 p.
- **Nayar, S. K., and Gettu, R.,** (2012), On the Design of Fibre Reinforced Concrete Slabs-on-Grade and Pavements, *Proceedings of the Conference on Fibre Reinforced Concrete – Global Developments, FIBCON 2012,* Nagpur, February, pp 85-92.
- **Nayar, S. K., and Gettu, R.,** (2012), Characterization of Fibre Reinforced Concrete, *Proceedings of the Conference on Fibre Reinforced Concrete – Global Developments, FIBCON 2012,* Nagpur, pp 30-47.
- **Nayar, S. K., and Gettu, R.,** (2011), On The Toughness-Based Design of Steel Fibre Reinforced Concrete Pavements, *Proceedings of 1<sup>st</sup> Conference of the transportation research group of India, CTRG,* Bangalore, India, 12 p.
- **D’costa, G., Nayar, S. K., and Gettu, R.,** (2011), Sustainability Assessment of Steel Fibre Reinforced Concrete Pavements, *Proceedings of the International conference on Structural engineering, Construction and Management, ICSECM 2011,* Kandy, Sri Lanka, 15 p.

#### **Technical Committee Recommendations (as committee member)**

- **ICI-TC/01.1,** “Test Methods for the Flexural Strength and Toughness Parameters of Fiber Reinforced Concrete”, ICI Technical Committee Recommendation, Indian Concrete Institute Journal, Vol. 15, No. 2, 2014, pp 39–43.
- **ICI-TC/01.2,** Specifications for Reference Concretes to be Used for Evaluating Fibres for Concrete Reinforcement, ICI Technical Committee Recommendation.
- **ICI-TC/01.3,** Definitions, Specifications and Conformity Requirements for Steel Fibres to be Used as Concrete Reinforcement, ICI Technical Committee Recommendation.
- **ICI-TC/01.4,** Definitions, Specifications and Conformity Requirements for Polymeric Fibres to be Used as Concrete Reinforcement, ICI Technical Committee Recommendation.

